The identification of cell-cycle related genes in response to antiretroviral drug treatment (ART) in lung cancer

By

Rahaba Makgotso Marima

A Thesis submitted to the Faculty of Health Sciences (Internal Medicine), University of the Witwatersrand, in fulfillment of the requirements for the degree of Doctor of Philosophy.

Johannesburg, 2017

Supervisor: Dr. Clem Penny

DECLARATION

I, Rahaba Makgotso Marima declare that this Thesis is my own, unaided work. It is being submitted for the Degree of Doctor of Philosophy in the University of the Witwatersrand, Johannesburg. It has not been submitted before for any degree or examination at any other University.

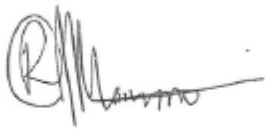

…… (Signature of Candidate)

DEDICATION

This Thesis is dedicated to Jesus Christ of Nazareth, The begotten Son of Jehovah The Most High God

To my husband, Owen Marima. Thank you for your love, support, patience, guidance, endurance, friendship, kindness and motivation, my best friend

To my sons, Omolemo and Siphiwesihle. Thank you boys for your love, care, warmth, fun and inspiration. You are a true blessing

To my parents, Mr and Mrs Mojakgomo. Thank you for your love, support encouragement throughout my studies, particularly towards my PhD. I love you Makonono le Montana

To my brother Raebi and my sister Malebelo for your love and support

To my nieces Lesego and Tshepiso for being there for me

To my extended family: The Marima family, Mojakgomo family and Makoro family

To my family at Rock of Salvation Church

I thank you all for your support and encouragement

He is before all things, and in Him all things hold together

For what shall it profit a man, if he shall gain the whole world, and lose his own soul?

Mark 8:36

CONFERENCE OUTPUTS

R. Marima, P. Ruff and C. Penny. The effects of Efavirenz and Lopinavir/ritonavir on lung cancer, a non-AIDs defining malignancy. Cancer Research Symposium, University of the Witwatersrand, February 2017-Poster.

R. Marima, P. Ruff and C. Penny. In silico bio-informatics analysis of cell-cycle related genes treated with efavirenz (EFV) and lopinavir/ritonavir (LPV/r) in human lung cancer cells. Molecular Biosciences Research Thrust (MBRT) Research Day, University of the Witwatersrand, December 2016-Poster.

R. Marima, P. Ruff and C Penny. Profiling of cell-cycle related gene expression in human non-small cell lung carcinoma treated with Efavirenz and Lopinavir/ritonavir. Health Sciences Research Day (HSRD), University of the Witwatersrand, September 2016-Oral.

R. Marima, P. Ruff and C. Penny. Effects of anti-retroviral drugs Efavirenz and Lopinavir/ritonavir on lung cancer. South African Society of Biochemistry and Molecular Biology (SASBMB) Congress, East London, July 2016-Poster.

R. Marima, P. Ruff and C. Penny. Investigating the role of antiretroviral treatment in lung cancer. Molecular Biosciences Research Thrust (MBRT) Research Day, University of the Witwatersrand, December 2014-Poster.

ACKNOWLEDGEMENTS

My sincere gratitude to:

My supervisor Dr. Clem Penny for his support, encouragement and intellectual input. Thank you for believing in me and affording me this valued opportunity

- Laboratory colleagues and Postdocs (in the Oncology lab)-Dr Rodney Hull for reading my thesis, to Dr Amber Khan, Dr Jeya and Dr Kumar for their support and encouragement
- The BD Biosciences application specialists, Sarika Vandayar and Ndavhe Tshikhudo for their assistance with flow cytometry
- The cytogenetics lab (Dr Pascal's Willem lab) for allowing me to use their ABI 7500 RT-qPCR instrument
- Prof. S. Weisse's lab in MCB for permitting me to use the Accuri C6 flow cytometer
- Mrs H. Ali and Mrs A. Mortimer (from Anatomy and Cell Biology), and Ms Therese Dix-Peek (Internal Medicine) for their assistance and support in times of need
- the National Research Foundation (NRF) for funding this project

ABSTRACT

South Africa has the largest ARV treatment programme in the world, wherein highly active antiretroviral treatment (HAART) has improved the health related quality of life (HRQoL) in HIV/AIDS patients. On the contrary, cancers not previously associated with HIV/AIDS (non-Aids defining cancers; NADCs) have been shown to be increasing, compared to the AIDS defining cancers (ADCs). Lung cancer, as a NADC has been documented in the HIV/AIDS population as a leading malignancy. The poor understanding of the association between ARV drugs and lung cancer places a burden on public health, both globally and in South Africa (SA). Furthermore, the deregulation of the cell-cycle is one of the hallmarks of cancer, including lung cancer. The main aim of this study was to elucidate the effects of HAART components Efavirenz (EFV) and Lopinavir/ritonavir (LPV/r) on cell-cycle related genes in an *in vitro* lung cancer model. To achieve this, cellular based, molecular and Bio-Informatics approaches were employed. First, the cytotoxic effects of EFV (at 4, 13, 26, 50 µM) and LPV/r (at 10, 32, 50, 80 µM), for 24h, 48h and 72h on normal lung fibroblasts (MRC-5) and lung adenocarcinoma (A549) cells, were evaluated using the Alamar Blue (AB) assay. This was then followed by cell-impedance "xCELLigence" real-time cell analysis (RTCA) assay. This was done to determine the effects of EFV (at 4, 13, 50 µM) and LPV/r (at 10, 32, 80 µM) on cell viability, cell death and proliferation. Cell-cycle analysis using propidium iodide (PI) by Fluorescence-activated cell sorting (FACS) was done to quantify DNA present at each of the cell-cycle stages of the cell-cycle in response to ARV treatment. Subsequently, an apoptosis assay using Annexin V FITC and Propidium iodide (PI) dual staining by FACS was carried out to confirm and quantify the ARVs potential apoptotic effects. Then, 4′,6-diamidino-2-phenylindole (DAPI) staining was used to assess changes in nuclear morphology exerted by the ARVs' effects. A more in depth interrogation of the cell-cycle was performed using a focussed gene array panel of some 84 human cell-cycle related genes. First, total RNA was isolated from both treated and untreated MRC-5 and A549 cells and reverse transcribed to cDNA for use as template in the PCR array reactions. From the array gene expression results, by convention a ±2 fold up-or-down-regulation was used as the basis of target selection. Following this, a real-time quantitative PCR (RT-qPCR) validation of selected genes of interest was done to quantify and confirm the PCR array results. This was followed

by *in-silico* Bio-informatics analysis to map the molecular pathways regulated by the identified targets. For this purpose, STRING, Database for Annotation, Visualization and Integrated Discovery (DAVID), Reactome and Ingenuity Pathway Analysis (IPA) databases were used.

Interestingly, double-edged oncogenic properties of both EFV and LPV/r at different concentrations were identified. The proliferative effects of EFV at 4, 13µM and LPV/r at10 µM, were elucidated, while 26, 50µM of EFV, and 32µM of LPV/r had slight inhibitory effects on cell proliferation. LPV/r at concentrations of 50 and 80µM exerted cytotoxic effects on the cells, as demonstrated by the AB and xCELLigence RTCA assays. Cell-cycle analysis using PI staining, particularly showed cell-cycle arrest at 32µM LPV/r, and a shift to G2/M by 13µM EFV, plasma relevant doses, compared to the untreated cells. An increasing apoptosis percentage was observed with increasing LPV/r concentrations, that is, 80µM LPV/r raised the apoptosis percentage almost two-fold compared to 32µM. This was coupled by necrosis, observed in a time-dependant manner. DAPI staining confirmed loss of nuclear integrity post ARV exposure, suggesting that both EFV and LPV/r impose damage to the genomic DNA. To further assess the observed changes in nuclear morphology, the effects of EFV and LPV/r on the expression of an arrayed panel of human cell-cycle genes in cancer and normal lung cells was determined. Significantly differentially expressed targets were identified and further quantified and confirmed by RT-qPCR. Such targets included ATM, p53, cyclin-dependant kinase inhibitors (CDKIs), such as, p21, aurora kinase B (AURKB), Mitotic Arrest Deficient-Like 2 (MAD2L2) and the apoptosis related gene, caspase 3 (CASP3). Bio-Informatics analyses revealed close and direct protein-protein interactions (PPIs) between these targets, notably, with change in interaction between the gene products involved in DNA repair mechanisms, observed between ARV treated and untreated groups, as illustrated by STRING interactions. DAVID, Reactome and IPA analysis showed changes in expression of genes related to stress and toxicity and DNA damage response genes. In particular, ATM, p53 and its downstream targets such as GADD45A (growth arrest and DNA damage inducible alpha) gene were up-regulated by ARV treatment, while cyclin/CDK activity was down-regulated, resulting in reduced cell proliferation. Thus in summary, both EFV and LPV/r altered the expression levels of cell-cycle related genes, influencing overall cellular health, acting to either inhibit or stimulate cell proliferation. This suggests EFV's and LPV/r's proliferative and

inhibitory roles in the proliferation of lung cells. Moreover, future directions can include the transfection of lung cells with HIV provirus followed by treatment of the cells with the same ARVs under study. This could be substantiated by including HIV positive patient samples on and off ARV drug treatment with lung cancer, including HIV negative patients with cancer as one of the controls.

TABLE OF CONTENTS

LIST OF ABBREVIATIONS

%	Percentage
9-1-1	RAD9-HUS1-RAD1
A549	Human lung adenocarcinoma epithelial cell line
aa	Amino acid
ACTB	Actin, beta
ADC	AIDS defining cancer
AIDS	Acquired Immunodeficiency Syndrome
ANOVA	Analysis of Variance
APC	Anaphase Promoting Complex
ARV	Antiretroviral
ATCC	American Type Culture Collection
ATM	Ataxia telangiectasia mutated
ATR	Ataxia telangiectasia mutated and Rad3 related
AURKB	Aurora kinase B
BLAST	Basic Local Alignment Search Tool
bp	base pair
BRCA1	Breast cancer Gene 1
CANSA	The Cancer Association of South Africa
CASP3	Caspase 3
CC	Cell-cycle
CCN	Cyclin
CDC	Cell division cycle
CDK	Cyclin dependent kinase
CDKN	Cyclin dependent kinase inhibitor
cDNA	Complementary deoxyribonucleic acid
CHEK1/CHK1	Checkpoint homologue 1
CHEK2/CHK2	Checkpoint homologue 2
CIP1/KIP1	CDK-interacting protein 1
Cmax	Steady-state plasma peak concentration

CO_2	Carbon dioxide
CPC	Chromosome Passenger Complex
CPT	Camptothecin
CT	Threshold cycle
CYP450	Cytochrome P450
DAPI	4',6-diamidino-2-phenylindole
DAVID	Database for Annotation, Visualization and Integrated Discovery
DDR	DNA damage response
dH_2O	Distilled water
DMEM	Dulbecco's Modified Eagle's Medium
DMSO	Dimethyl sulfoxide
DNA	Deoxyribonucleic Acid
dNTP	Deoxynucleotide triphosphate
DSB	Double strand break
EFV	Efavirenz
FACS	Fluorescence activated cell sorter
FBS	Fetal Bovine Serum
FDA	Food and Drug Administration
FITC	Fluorescein-isothiocyanate
FTC	Emtricitabine
G1	Gap phase 1
G2	Gap phase 2
GADD45A	Growth arrest and DNA damage inducible alpha
GAPDH	Glyceraldehyde 3-phosphate dehydrogenase
gDNA	genomic DNA
h	hour(s)
HAART	Highly Active Anti-retroviral Therapy
HIV	Human Immunodeficiency Virus
HKG	House keeping gene
HPV	Human papilloma virus
IPA	Ingenuity Pathway Analysis

Kb	Kilo base pair
kDA	Kilo Dalton
KEGG	Kyoto Encyclopedia of Genes and Genomes
KS	Kaposi's Sarcoma
LPV	Lopinavir
LPV/r	Lopinavir/ritonavir
M phase	Mitotic phase
MAD2L2	Mitotic Arrest Deficient-Like 2
MAPK	Mitogen-activated protein kinase
MCM	Minichromosome maintenance
mg	Milligram
ml	Millilitre
MRC-5	Medical Research Council 5
MRN	MRE11A-RAD50-NBS1
mRNA	Messenger Ribonucleic acid
NADC	Non-AIDS Defining Cancer
NBS1	Nijmegen breakage syndrome 1
NCBI	National Centre for Biotechnology Information
NHL	**N**on-Hodgkin's Lymphoma
NSCLC	Non-small cell lung cancer
nm	Nanometre
NNRTI	**N**on-Nucleoside/Nucleotide Reverse Transcriptase Inhibitor
NRTI	Nucleoside/Nucleotide Reverse Transcriptase Inhibitor
^{O}**C**	Degrees Celsius
P53/TP53	Protein 53/Tumour protein 53
PBS	Phosphate Buffered Saline
PCD	Programmed cell death
PCR	Polymerase Chain Reaction
Pen/strep	Penicillin/streptomycin
pH	Potential hydrogen
PI	Propidium iodide

PI	Protease inhibitor
PLWHA	People living with HIV/AIDS
PPC	Positive PCR control
QRT-PCR	Quantitative Real time polymerase chain reaction
RB1	Retinoblastoma 1
REV	Reversionless
RNA	Ribonucleic Acid
RNase	Ribonuclease
Rpm	Revolutions per minute
RT	Reverse Transcription
Rt	Room temperature
RTCA	Real-time cell analysis
RTV	Ritonavir
SAC	Spindle assembly checkpoint
S phase	Synthesis phase
SCLC	Small-cell lung cancer
SEM	Standard Error Mean
STRING	Search Tool for the Retrieval of Interacting Genes/Proteins
TDF	Tenofovir Disoproxil Fumarate
TF	Transcription factor
UNAIDS	United Nations Programme on AIDS
V	Volts
Veh	Vehicle
WHO	World Health Organisation
α	Alpha
β	Beta
ΔCT	Change in threshold cycle
µg	Micro gram
µl	Microlitre
µM	Micro molar
ς	Zeta

LIST OF FIGURES

LIST OF TABLES

CHAPTER 1: INTRODUCTION AND LITERATURE REVIEW

1.1 INTRODUCTION

Currently, human immunodeficiency virus/ acquired immunodeficiency syndrome (HIV/AIDS) and lung cancer are arising as colliding epidemics and urgent interventions are necessary to combat these leading causes of morbidity and mortality. In addition, cancer incidence rates are also shown to be increased in people living with HIV/AIDS (PLWA) compared to the general population (reviewed in Corti, 2016). To date, there is no cure for HIV/AIDS and the highly active antiretroviral treatment (HAART) is the most effective regimen. Additionally, there has been a decline in cancers previously associated with HIV/AIDS, also known as the AIDS defining cancers (ADCs): including Kaposi's sarcoma, primary central nervous system lymphoma, non-Hodgkin lymphoma, and cervical cancer. On the contrary, non-ADCs have been documented to be on the rise in the HAART era, with lung cancer emerging as a leading NADC ((reviewed in Corti, 2016), (Rubinstein *et al.*, 2014)). In addition, when compared to the same age group in the general population, the risk of developing non-small cell lung carcinoma (NSCLC), the most predominant form of lung cancer, is higher in HIV positive patients. Furthermore, South Africa has the largest HIV epidemic and HAART programme in the world. The poor understanding between the use of HAART and tumourigenesis especially lung cancer has placed a burden on public health, globally and in South Africa.

HIV infection accompanied by low CD4 count, smoking and aging, have been eliminated as the main risk factors to HAART associated carcinogenesis ((Koegelenberg *et al.*, 2016), (Rubinstein *et al.*, 2014)). This has led to the conclusion that lung carcinogenesis in the HAART era is a multifactorial process. The deregulation of the cell-cycle is a hallmark of all cancers, including lung cancer ((Walter *et al.*, 2015), (Eymin and Gazzeri, 2010)). A few previous reports have demonstrated the potential of efavirenz (EFV), (Hecht *et al.*, 2015) and

lopinavir/ritonavir (LPV/r), (Chow *et al.*, 2009) to either influence or inhibit cell proliferation and alter gene expression (Adefolaju *et al.*, 2014). With no clear evidence as yet, in the present study, such recent studies raised the query as to whether the cell-cycle related genes controlling cell proliferation and cell death can be targeted as either potential bio-markers or HAART associated lung cancer therapeutics. Molecular profiling of lung cancer is a promising diagnostic and therapeutic tool in the fight against lung cancer, which still has a poor survival rate of 14% (Corti, 2016). The synergic effect of both HIV infection and HAART on lung tumourigenesis is not covered in this study. Therefore, in the context of the NADCs epidemic and the rising/increasing prevalence of NSCLC, the present study focused on investigating the effects of EFV and LPV/r on cell-cycle related genes in lung cancer.

1.2 LITERATURE REVIEW

1.2. 1 HIV epidemic and prevalence

It has been more than 55 years since the first proven case of HIV infection and HIV/AIDS continues to be a deadly epidemic. Despite medical and social interventions made, the number of people living with HIV and AIDS (PLWHA) remains on the rise in the general population. To date, there is no cure for HIV/AIDS. However, the highly active antiretroviral treatment (HAART) is the most effective regimen against HIV/AIDS (UNAIDS, 2016).

According to the 2016 Joint United Nations Programme on HIV/AIDS report, 18.2 million people had access to the antiretroviral therapy by June 2016, and 36.7 million people worldwide were living with HIV by the end of 2015, while 1.1 million people died from AIDS-related illnesses in 2015. Since the beginning of the epidemic, 78 million people have become infected with HIV, and, almost 46% of all people living with HIV had access to treatment by the end of 2015. In 2015, some 77% of pregnant women living with HIV had access to antiretroviral (ARV) medicines to prevent mother-to-child transmission of HIV. This has resulted in a 50% decline in new HIV infections since 2010. Every year since 2010, about 1.9 million adults have become newly infected with HIV. Nevertheless, AIDS-related deaths since they peaked in 2005 have fallen by 45%, by end of 2015. In East and Southern Africa, there were 19 million people living with HIV by the end of 2015, with women accounting for

more than half the total number of people living with HIV in this region. Even though in 2015, there were an estimated 960000 new HIV infections in Eastern and Southern Africa, there was a 14% drop in new HIV infections between 2010 and 2015. Furthermore, Eastern and Southern Africa accounts for 46% of the global total of new HIV infections. From 2010 to 2015, the number of AIDS-related deaths in Eastern and Southern Africa fell by 38%, also with 66% decline in HIV infection in children in this region. In sub-Saharan Africa, about 54 % of HIV positive people accessed HAART. South Africa has the highest burden of HIV epidemic in the world, with an estimated 7 million people living with HIV in 2015, Figure 1.1 (sanac.org.za).

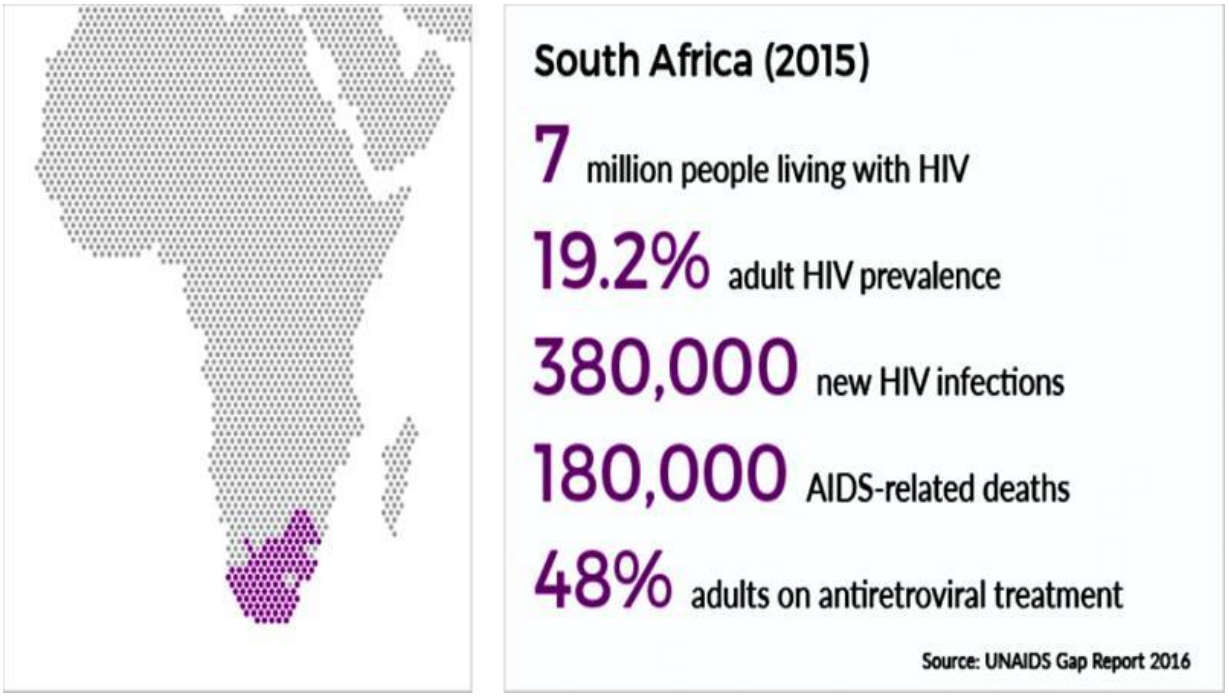

Figure 1.1: The prevalence of HIV/AIDS in South Africa by the year 2015 (adopted from UNAIDS Gap Report 2016).

In the same manner, South Africa has the largest antiretroviral treatment (ART) programme in the world. However, HIV prevalence remains high (19.2%) among the general population, although it varies significantly between regions, with Kwa-Zulu Natal being highest (40%) and Northern Cape being lowest (18 %).

1.2.2 Introduction to Highly Active Anti-Retroviral Treatment (HAART)

Currently, there is no drug capable of curing HIV infections. The Highly Active Antiretroviral Therapy (HAART) also known as the combined antiretroviral therapy (cART) is a treatment against HIV and consists of three ARV drugs, each from a different class of drugs. These classes include; Non-Nucleoside Reverse Transcriptase Inhibitors (NNRTIs), Nucleotide/ Nucleoside Reverse Transcriptase Inhibitors (NRTIs), the Protease Inhibitors (PI's), Integrase or Integrase Strand Transfer Inhibitors (INSTIs), Chemokine Receptor Antagonists (CRAs) and Fusion Inhibitors (FIs) (Karanja *et al.*, 2016). These are summarized diagrammatically (Figure 1.2) and each category is further discussed below.

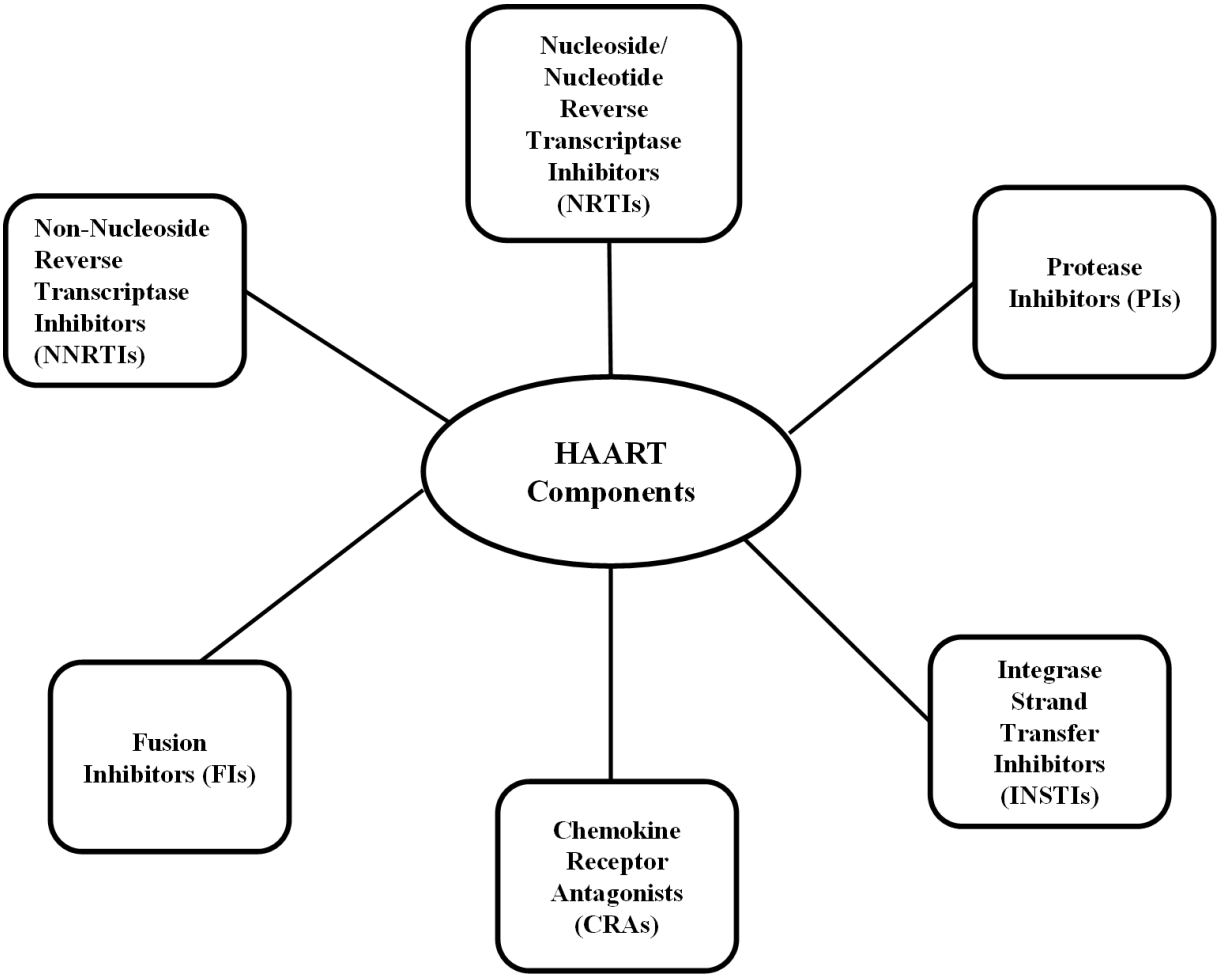

Figure 1.2: Different classes of the ARV drugs, which make up HAART when combined as first-line, second-line or third-line of treatment.

1.2.2.1 Classes of ARV drugs and mode of action

There are a number of categories of antiretroviral drugs and these are described below.

i) Nucleoside/ nucleotide reverse transcriptase inhibitors (NRTIs)

Nucleoside reverse transcriptase inhibitors (NRTIs), also known as nucleoside analogs or "nukes," contain faulty forms of the building blocks (nucleotides) used by reverse transcriptase (RT) enzyme. This enzyme reverse transcribes the viral RNA into complementary DNA. RT incorporates the faulty NRTI building blocks, disrupting the DNA synthesis of the virus (reviewed in (Berretta *et al.*, 2016),(Torres and Mulanovich, 2014)).

ii) Non-nucleoside reverse transcriptase inhibitors (NNRTIs)

Non-nucleoside reverse transcriptase inhibitors (NNRTIs) also called the "non-nukes" bind to the RT enzyme. The binding occurs allosterically in a hydrophobic pocket located around 10 angstroms (Å) from the catalytic site of the p66 subunit of the enzyme all at the equivalent site in the RT, in spite of their chemical diversity. In the NNRTI binding site (NNIBP), every NNRTI interacts with different amino acid residues (Mounier *et al.*, 2009).

iii) Protease inhibitors (PIs)

Protease Inhibitors (PIs) selectively bind to HIV-1 protease and block the proteolytic cleavage of protein precursors necessary for the production of new infectious viral particles. The HIV protease contains a binding pocket into which drugs bind to inhibit its activity. As HIV replicates, mutations occur changing this conformation. This may then prevent or inhibit the binding of one or more PIs to the HIV protease. All of the resistance mutations differ with PIs, but are all located near the substrate-binding gap of the enzyme. These primary mutations cause simultaneous resistance to multiple PIs ((Shafer, 2006), (Kiser *et al.*, 2008)).

iv) Integrase strand transfer inhibitors (INSTIs)

Integrase inhibitors also known as Integrase strand transfer inhibitors (INSTIs) block the activity of the integrase enzyme. Integrase is a viral enzyme that enables the insertion and

integration of the viral genome into the host DNA (Berretta *et al.*, 2016). The INSTIs block the integration of viral DNA with host DNA, thus interrupting with the HIV's spread.

v) Chemokine receptor type 5 (CCR5) receptor antagonists

Chemokine (CCR5) receptor antagonists block the CCR5 receptor. The C-C pattern chemokine receptors CCR5 and Chemokine receptor type 4 (CXCR4) are the most important chemokine receptors implicated in the entry of HIV into host cells (Berretta *et al.*, 2016). The virus uses CCR5 mostly during initial infection, while CXCR4 is used in the later HIV infection stages (Barmania and Pepper, 2013). These receptors form part of the seven transmembrane G-protein-coupled receptor (GPCR) family and are mainly expressed on macrophages, T-cells, dendritic cells, and Langerhans cells. They cooperate as co-receptors that HIV-1 uses to bind cells before viral fusion and entry (Ritchie *et al.*, 2006).

vi) Entry/Fusion inhibitors (FIs)

Fusion inhibitors (FIs) are a class of drugs intended to disrupt the HIV-1 fusion protein equipment at the final stage of fusion with the host cell, to prevent the infection of non-infected cells (Beumer *et al.*, 2014). Fusion inhibitors bind to and block the HIV gp41 fusogenic protein, thereby inhibiting the viral entry into healthy cells. Enfuvirtide (T20) has been used in therapy as FI, and binds to gp41, preventing the fusion of the viral and cellular membranes (Harman *et al.*, 2012).

1.2.2.2 Approved WHO ARV guidelines, 2013-2016

It is recommended by WHO, with South Africa also adhering to these HAART guidelines, that the first-line ART should consist of two nucleoside reverse transcriptase inhibitors (NRTIs) and a non-nucleoside reverse-transcriptase inhibitor (NNRTI) (WHO 2015). Tenofovir and lamivudine or emtricitabine and efavirenz (TDF + 3TC (or FTC) + EFV) as a fixed-dose combination is recommended as the preferred option to initiate ART. While second-line ART for adults should consist of two nucleoside reverse-transcriptase inhibitors (NRTIs) + a ritonavir-boosted protease inhibitor (PI). It is important to note that in 2016, a new ARV based regimen has been launched globally. This treatment includes dolutegravir-an

integrase inhibitor based combination that includes the ARVs abacavir and lamivudine (DTG/ABC/3TC). It is a three-in-one pill that has been proven to outperform South Africa's current EFV three-in-one combination ARV in effectiveness and tolerability. Patients on the dolutegravir-based combination treatment also had been shown to have a lower incidence of side effects, for example, psychiatric, skin and gastrointestinal disorders. This new pill can be taken with or without food, and patients would still retain the drug concentrations high enough in the blood even 72h post their previous dose. This has been proven to be highly effective and helps protect patients against the development of drug resistance ((Taha *et al.*, 2015), (Barnhart and Shelton, 2015), (Gubavu *et al.*, 2016)). Furthermore, DTG has all the potential to be used as a first-line drug in combination with other nucleoside backbones, especially in the form of a single tablet in combination with abacavir (ABC) and lamivudine (3TC) ((Cottrell *et al.*, 2013), (Taha *et al.*, 2015)). Table 1.1 below shows the ARV drugs under different ARV classes.

Table 1.1: The WHO 2016 approved ARV drugs

NRTIs	**NNRTIs**	**PIs**	**INSTIs**
3TC lamivudine	EFV efavirenz	ATV atazanavir	DTG dolutegravir
ABC abacavir	ETV etravirine	DRV darunavir	EVG elvitegravir
AZT zidovudine	NVP nevirapine	FPV fosamprenavir	RAL raltegravir
d4T stavudine	RIL rilpivirine	IDV indinavir	
ddI didanosine		LPV/r lopinavir/ritonavir	
FTC emtricitabine		RTV ritonavir	
TAF tenofovir		SQV saquinavir	
alafenamide fumarate		TPV tipranavir	

1.2.3 The use of ARV drugs as chemotherapeutic agents

The use of anti-HIV drugs as cancer regimes is not new. For instance, Azidothymidine/zidovidine (AZT) was studied as an anti-cancer (AC) drug in the 1990s. However, this drug demonstrated insignificant anti-tumour activity in clinical trials, even

though it was promising with *in vitro* models. On the other hand, PIs have been documented to significantly treat HIV-related Kaposi's sarcoma. The anti-tumorigenic activities of PIs were further shown by their ability to inhibit tumour-cell invasion and angiogenesis, inhibition of inflammatory cytokine production, proteasome activity, cell proliferation and survival, and induction of apoptosis as reviewed in (Chow *et al.*, 2009). The potential anti-cancer properties of ARVs are considered below.

i) Efavirenz and Nevirapine

NNRTIs such as nevirapine (NVP) and efavirenz (EFV) have been shown to reduce cell proliferation, induce morphological differentiation, and reprogram gene expression in transformed melanoma and prostate carcinoma cells without inducing apoptosis. Additionally, efavirenz was shown to inhibit the growth of xenografted melanoma, prostate, colon, and small-cell lung carcinoma tumours in nude mice. Furthermore, NVP and EFV were illustrated to significantly retard growth of thyroid cancer cells. In addition, Hetch *et al*., (2015) demonstrated that EFV has the highest anti-proliferative activity as an NNRTI, against pancreatic cancer cells.

ii) Ritonavir

The anti-tumour activity of ritonavir (like saquinavir and indinavir) was first shown *in vitro* for Kaposi's sarcoma and *in vivo* for a xenograft mouse model (Pati *et al.*, 2002). Ritonavir was shown to inhibit proliferation of primary endothelial cells and induced apoptosis in Kaposi's sarcoma cell-lines by inhibiting the production of cytokines that contribute to neovascularisation (including TNFα, interleukin 6 (IL6), and vascular endothelial growth factor-VEGF) and inhibiting the transcriptional activation of nuclear factor kappa B (NFκB) at clinically relevant concentrations (3–15 μM). Similarly with saquinavir, the anti-tumorigenic effects of ritonavir seem to be concentration dependent. At lower concentrations (~2.5–μM), ritonavir was demonstrated to induce apoptosis and inhibit activation of NFκB in primary adult T-cell leukaemia (ATL) cells (Dewan *et al.*, 2006). In a similar manner, breast carcinoma is sensitive to ritonavir. The increased sensitivity of oestrogen-receptor-positive breast carcinoma cells could be partly explained by ritonavir-mediated downregulation of oestrogen-receptor expression. Furthermore, in cell lines both negative and positive for

oestrogen receptors, ritonavir induced G_1 arrest, reduced expression of cyclin-dependent kinases (CDK) 2, 4, and 6 and cyclin D1, induced apoptosis independent of G_1 arrest, inhibited Akt-phosphorylation, and inhibited the chaperone function of heat shock protein 90 (Hsp90) (Laurent *et al.*, 2004). In addition, at high concentrations of ritonavir (50–100 μM), proliferation of glioma cells was inhibited by blocking G_1 and inducing apoptosis. Finally, ritonavir inhibited growth of HEP2 head and neck carcinoma in nude mice at high concentrations (20–2000 μM). Despite the toxicity of RTV at high concentrations, this drug could still be used as an AC drug at low concentrations (Chow *et al.*, 2009).

iii) Lopinavir

When administered alone, Lopinavir has insufficient anti-HIV viral activity. However, like other HIV protease inhibitors, its blood concentrations are significantly increased by low-dose ritonavir boost. Lopinavir was illustrated to inhibit the growth of cervical carcinoma cell lines infected with human papilloma virus (HPV) 16. This was achieved by inhibiting the viral E6-activation of proteasomal degradation of nuclear p53 and followed by induction of apoptosis (Chow *et al.*, 2009).

1.2.4 The effect of HAART on cancer: ADCs and NADCs.

Like any other treatment components, HAART agents are associated with a number of adverse effects including; hepatotoxicity, hypersensitivity rash, lactic acid, osteoporosis, lipodystrophy, macular disorders, cardiovascular disorders, neurological disorders, liver disorders and metabolic abnormalities (Hima Bindu and Naga Anusha, 2011). A rise in malignancies both related to and unrelated to HIV-infection and HAART has been documented.

1.2.4.1 HAART and ADCs and NADCs

Even though there's a decline in the incidence of AIDS-defining cancers (ADCs), including Kaposi's sarcoma, primary central nervous system lymphoma, non-Hodgkin lymphoma, and cervical cancer following the introduction of (HAART), this incidence rate is still greater in

PLWHA compared to the general population (Rubinstein *et al.*, 2014). The non-AIDS-defining cancers (NADCs) include those associated with viral infections (such as anal cancer caused by the Human Papilloma Virus (HPV), liver cancer caused by the Hepatitis C (HCV) and Hepatitis B Viruses (HBV), head and neck cancer caused by (HPV) and those cancers not associated with viral infections (such as lung and melanoma). NADCs are a leading cause of morbidity and mortality for PLWHA ((Clifford *et al.*, 2005), (Herida *et al.*, 2003), (Powles *et al.*, 2009), (Lewden *et al.*, 2008), (Rodger *et al.*, 2013)). Longevity and immune status may be the associated risk factors. However, these alone are insufficient to fully explain these trends in cancer epidemiology. For PLWHA, even those with normal CD4+ T cell counts, the risk for many NADCs remains greater than for their age-matched HIV-negative counterparts (Powles *et al.*, 2009). Furthermore, compared to the general population, PLWHA present with more aggressive and advanced disease at the time of cancer diagnosis. These changes in cancer epidemiology are poorly understood. Furthermore, the risk of cancer in PLWHA can be defined by the standard incidence ratio (SIR) ((Jones and Swerdlow, 1998), (Rubinstein *et al.*, 2014)). For malignancies in HIV, the SIR compares the rate of cancers in the HIV/AIDS population to the number expected in the general population at any given time (Shiels *et al.*, 2011). In the HAART era, the SIR has decreased for all ADCs, with the exception of invasive cervical carcinoma (Powles *et al.*, 2009). When PLWHA are compared to recipients of solid organ transplants, both populations have similar risks for KS and NHL as well as certain NADCs including HL, anal, liver and lung cancer (Grulich *et al.*, 2007). However, in the case of lung cancer, even when correcting for cigarette smoking, the incidence remains greater in PLWHA than in the general population, although no correlation between low CD4+ T cell count and lung cancer risk has been identified (Kirk *et al.*, 2007). The etiological factors that contribute to both ADCs and NADCs are multifactorial. PLWHA are susceptible to infection by oncogenic viruses. Kaposi sarcoma-associated herpes virus (KSHV) or human herpes virus 8 (HHV-8), Epstein Barr Virus (EBV), HPV, and hepatitis B and C viruses are implicated in various ADCs and NADCs and are more prevalent in PLWHA than the general population ((El-Serag, 2012)), (Guech-Ongey *et al.*, 2010). These viruses can alter apoptosis and cell-cycle regulation, activate oncogenes, and inhibit the activity of tumor suppressor genes. In addition, viruses associated with ADCs and NADCs can also express micro-ribonucleic acids (miRNAs), which are small non-coding RNAs that act as negative regulators of protein

synthesis by covalently binding to single-stranded mRNA ((Bartel, 2009), (Qi *et al.*, 2006)). Interestingly, HIV has also been implicated in inhibiting the p53 tumour suppressor gene, altering cell-cycle regulation, and activating proto-oncogenes that can lead to cellular transformation (Amini *et al.*, 2004).

1.2.5 Cancer

According to the World Health Organization (WHO) 2015, cancer remains one of the leading causes of morbidity and mortality globally, with approximately 14 million new cases and 8.2 million cancer related deaths by the end of 2012. The WHO estimates that the number of new cases is expected to rise by about 70% over the next 2 decades, from 14 million in 2012 to 22 million. In men, the 5 most common sites of cancer diagnosed in 2012 were lung, prostate, colorectum, stomach, and liver cancer (WHO 2015). Among women, breast, colorectum, lung, cervix, and stomach cancers were the most diagnosed types of cancer. Around one third of cancer deaths are due to the 5 leading behavioral and dietary risks, which are high body mass index (BMI), low fruit and vegetable intake, lack of physical activity, tobacco use and alcohol use (WHO 2015), while cancer causing viral infections such as HBV/HCV and HPV are responsible for up to 20% of cancer deaths in low- and middle-income countries. It has also been documented by WHO (2015) that more than 60% of the world's total new annual cases occur in Africa, Asia, Central and South America. In addition, these regions account for 70% of the world's cancer deaths.

1.2.5.1 Causes of cancer

Cancer arises from one single cell. The transformation from a normal cell into a tumour cell is a multistep process, progression from a pre-cancerous lesion to malignant tumours (Hashim *et al.*, 2016). The acquired changes are a result of the interaction between a person's genetic factors and external factors which include physical carcinogens, such as ultraviolet and ionizing radiation; chemical carcinogens, such as asbestos, components of tobacco smoke, aflatoxin (a food contaminant), arsenic (a drinking water contaminant); and biological carcinogens, such as infections from certain viruses, bacteria or parasites.

Cancer remains a leading cause of mortality in South Africa as well. According to the Cancer Association of South Africa (CANSA) 2016, one in four South Africans are affected by cancer through diagnosis of family, friends or self. More than 100 000 South Africans are diagnosed with cancer every year, and the survival rate of South African cancer patients is 6 out of 10. Globally and in South Africa, lung cancer is prevalent in both men and women and remains the leading cause of mortality ((WHO 2016), (CANSA 2016), (Hashim *et al.*, 2016)).

1.2.5.2 The hallmarks of cancer

The hallmarks of cancer, acquired during the multistage tumour developmental process include; sustained proliferative signaling, evasion of growth suppressors, enabling replicative immortality, induction of angiogenesis, and activation of invasion and metastasis, resisting cell-death and deregulating the cell-cycle. ((Hanahan and Weinberg, 2000), (Hanahan and Weinberg, 2011)).

1.2.6 Cell division and the cell-cycle

An adult human is built from about 10^{13} cells which were generated through cell divisions from a single cell, the fertilized egg. The proper regulation of cell division is essential towards producing large number of cells and also generating distinct cell types. Thus the cell division processes can either be symmetric or asymmetric. A diversity of cell types is generated through asymmetric cell division, during which daughter cells inherit different cellular components such as proteins, RNAs and organelles ((Noatynska *et al.*, 2013), (Barnum and O'Connell, 2014)). Cells divide through a series of stages (events) known as the cell-cycle.

1.2.6.1 Introduction to the cell-cycle

The cell-cycle is the series of events in which cellular components are doubled, and then segregated accurately into the daughter cells. The replication of DNA forms part of this fundamental process. In eukaryotes, DNA is replicated during the Synthesis or S-phase, and then chromosome segregation occurs during Mitosis or M phase. Two Gap phases separate S phase and M phase, known as Gap 1(G1) and Gap 2 (G2) (Noatynska *et al.*, 2013). Furthermore, the gap phases are not periods of inactivity, but rather phases where cells obtain

mass, integrate growth signals, organize a replicated genome, and prepare for chromosome segregation, Figure 1.3. The progression of the cell-cycle is tightly regulated by its checkpoints, the G1/S, G2/M and the mitotic spindle assembly checkpoint (SAC).

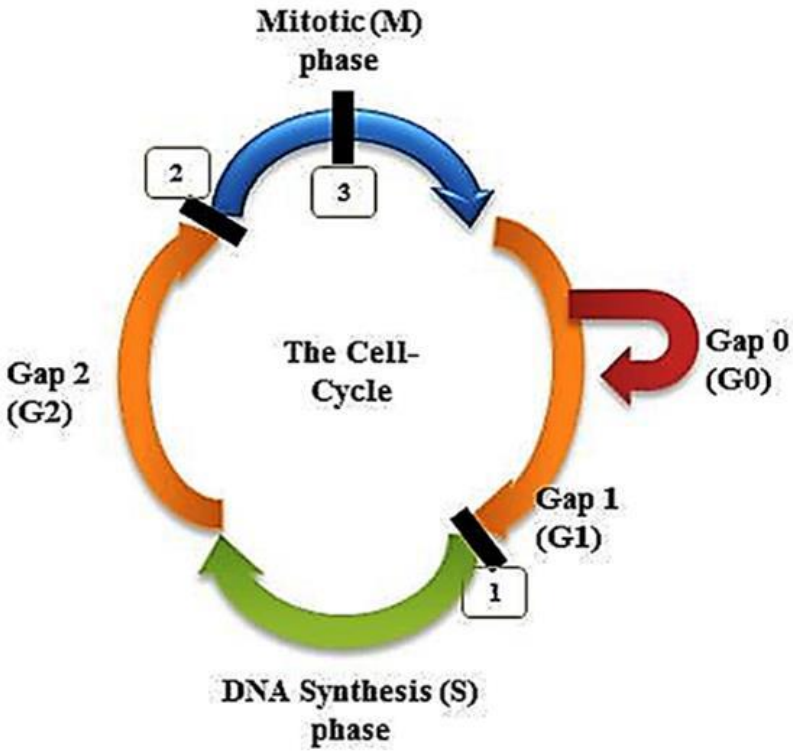

Figure 1.3: Diagrammatic representation of the cell-cycle. The cell-cycle is divided into the G1, G2, S and the M phases. The numbers denote the cell-cycle checkpoints with (1) representing the G1/S checkpoint, (2) indicating the G2/M checkpoint and (3) showing the mitotic spindle assembly checkpoint (SAC) (Own figure).

The progression of the cell-cycle is driven by the cyclin-dependent kinases (CDKs). These are serine/threonine protein kinases that phosphorylate key substrates to promote DNA synthesis and mitotic progression ((Fisher *et al.*, 2012), (Malumbres and Barbacid, 2009)). The CDKs are active when bound to cyclins, to form the cyclin/CDK complexes. Contrarily, the activity of CDKs can also be negatively regulated by the binding of small inhibitory proteins, known as the CDK-inhibitors (CKIs), or by inhibitory tyrosine phosphorylation which blocks phosphate transfer to substrates (Coudreuse and Nurse, 2010).

1.2.6.2 Cyclins and CDK complexes

In higher eukaryotes, multiple CDKs and cyclins exist, but only five types CDKS (CDK1, 2, 3, 4, 6) are generally associated with cell-cycle control (Malumbres and Barbacid, 2009). Usually, CDK1 is activated by A- and B-type cyclins, CDK2 by E- and A-type cyclins, CDK3by C-type cyclins, while CDK4 and CDK6 are activated by D-type cyclins (Homem and Knoblich, 2012). Cyclin E/CDK2 complex is required for S phase (Knoblich *et al.*, 1994), and cyclin A and B/CDK1 complexes regulate M phase (Knoblich and Lehner, 1993). Although CDK4 and cyclin D are not critical for cell proliferation, they are required for cell growth (Emmerich *et al.*, 2004). The cell-cycle regulation and the fidelity of checkpoints are crucial for the maintenance of genome integrity.

1.2.6.3 The cell-cycle and its regulation

The cell-cycle checkpoints are surveillance mechanisms that monitor the order, integrity, and fidelity of the cell-cycle process. These control measures include cell growth to the appropriate size, the replication and integrity of the chromosomes, as well as the timely and accurate segregation at mitosis. These mechanisms are highly conserved and of ancient origin. Cell-cycle checkpoints can be activated by damage to DNA ((Barnum and O'Connell, 2014), (Casimiro *et al.*, 2012)). Depending on the severity of the cell-cycle defect, checkpoint dysfunction can result in outcomes ranging from cell-death to cell-cycle reprogramming, which can lead to cancer (Barnum and O'Connell, 2014).

1.2.6.4 The Mitotic Spindle Checkpoint

Prior to sister-chromatid segregation, it is essential that spindle attachment of sister-chromatids occurs in a bi-oriented fashion such that they are under tension at metaphase, and attached to both poles of the spindle (Wittmann *et al.*, 2001). Once all kinetochores are attached and properly aligned at the metaphase plate, anaphase can proceed. This process is promoted by the activity of Anaphase-Promoting Complex or Cyclosome (APC/C), an E3 ubiquitin ligase. This ligase targets a number of proteins which include the mitotic cyclins.

Furthermore, APC activity is controlled by the cell-division-cycle protein (CDC20), which functions up to the metaphase–anaphase. Once sister chromatid cohesion is released, spindle tension and the associated motor proteins enable sister chromatids to dissociate and move apart to form identical daughter nuclei (McLean *et al.*, 2011).

The spindle checkpoint functions to prevent activation of APC and CDC20, for example, where kinetochores are not occupied by spindle microtubules, or are attached but not under tension. Under these conditions, the spindle checkpoint protein Mad2 (Mitotic Arrest Deficient) inhibits the activity of CDC20 activity both at unattached kinetochores, where it forms a mitotic checkpoint complex, resulting in the inactivation of CDC20 and APC, and hence, cells cannot enter anaphase ((McLean *et al.*, 2011), (Barnum and O'Connell, 2014)).

Additionally, the spindle checkpoint includes a number of other proteins, such as the Polo kinases, Aurora kinases (AURKs), and never in mitosis gene (NIMA)- a related (Nek) kinase ((O'Connell *et al.*, 2003), (Barnum and O'Connell, 2014)). In a similar manner, the spindle checkpoint shares the basic principles as those controlling DNA integrity discussed above, that is, to prevent a cell-cycle progression while other effectors correct a genome altering defect. Contrarily, the mitotic checkpoint functions to maintain CDK activity, while the interphase checkpoints maintain CDK inactivity. Among mitotic kinases, Aurora kinases' (AURKs) dysregulation have been previously associated with loss of p53 activity, and implicated in many cancers. Thus, Aurora kinases (AURKs) are emerging as potential targets in cancer therapeutics (Barnum and O'Connell, 2014).

1.2.6.5 Aurora kinases and tumourigenesis.

Aurora kinases belong to a family of conserved serine/ threonine kinases, with three types of these kinases in mammals, AURKA, AURKB and AURKC (Sasai *et al.*, 2016). Although very close in protein sequence and structure (70% identity in the catalytic domain), Aurora A and B have distinct localizations and functions during mitosis. Aurora B is a component of the chromosomal passenger complex (CPC) interacting with inner centromere protein (INCENP), survivin and borealin, and is essential for chromosome segregation and cytokinesis. Furthermore, Aurora B localizes at centromeres in prophase and metaphase, at the cortex and

spindle midzone in anaphase, and at the mid-body in telophase (Carmena *et al.*, 2012). Aurora C has a similar localization but is specifically expressed in mammalian germ cells and has not been found in other organisms (Carmena *et al.*, 2009). Aurora A localizes at centrosomes and at the spindle poles, and is required for mitotic entry, centrosome maturation and spindle formation. In addition, the mammalian Aurora A promotes mitotic entry by phosphorylating and activating cell-division-cycle 25B (CDC25B). Activation of Aurora kinases occurs by autophosphorylation of the T-loop. This is promoted by the interaction with cofactors such as the microtubule-associated protein TPX2 for Aurora A and INCENP for Aurora B (Bishop and Schumacher, 2002). In addition, AURKs have been shown to interact with p53. In particular, AURKB phosphorylates p53 at serine 269 and threonine 284, thus inhibiting p53 transactivation activity (Wu *et al.*, 2011). Furthermore, phosphorylations at serine 183, threonine 211, and serine 215 drives the degradation of p53 through polyubiquitination-mediated proteasome pathway (Gully *et al.*, 2012). Additionally, the abnormal expression of the Aurora kinases interacting with p53 signaling protein family has been shown to be critical in nullifying p53 protein family mediated tumor suppressor pathways (Sasai *et al.*, 2016). P53 signaling protein family has been shown to play a significant role in the DNA damage response pathways (Zhang *et al.*, 2009).

1.2.6.7 DNA Damage Responses (DDR) and the tumour suppressor P53

Throughout interphase, DNA damage stimulates a cell-cycle arrest that permits sufficient time for repair pathways to be activated and allow for DNA repairs before progression to following phases (Barnum and O'Connell, 2014). DNA can be damaged by intrinsic and/or extrinsic agents. Intrinsic factors may include; intermediates of metabolism, wearing down of telomeric activity, oncogene overexpression, and DNA replication errors. Extrinsic sources such as exposure to; sunlight, ionizing radiation or other anticancer therapeutics. Different lesions in genomic DNA activate common checkpoint pathways. These pathways when activated maintain CDKs in an inactive state until repairs are done. P53 located on chromosome 17p13 encodes a nuclear phosphoprotein of 53 kDa (TP53) that identifies and binds to regions of damaged DNA and acts as a transcription factor controlling the expression of a multitude of different downstream genes. Furthermore, damaged DNA or carcinogenic stress induces *TP53*

leading to cell-cycle arrest by inducing expression of cyclin dependent kinase inhibitors to enable DNA repair, through DNA damage response (DDR) pathways or apoptosis ((Barnum and O'Connell, 2014), (Goodman and Woodgate, 2013)).

P53 is a critical component of DNA damage response and is regulated by various posttranslational modifications, which include N-terminal phosphorylation on serine-15, which is catalyzed by ATR and its relatives ATM (Ataxia Telangiectasia Mutated) and DNA-PKcs (DNA-dependent protein kinase, catalytic subunit). Similar to ATR, these kinases (ATM) are targeted to double-strand DNA breaks by interacting proteins: the MRN (Mre11-Rad50-Nbs1) complex, interacting with ATM. Activated p53 is then stabilized through protection from Mdm2, its E3 ubiquitin ligase. Then p53 trans-activates the expression of a large number of genes, including the cyclin-dependent kinase inhibitor (CKI) p21. By this mechanism, the G1 CDKs activity is inhibited, and DNA damage is repaired prior to DNA replication. Moreover, p53 can also repress the expression of genes, and is also required for G2 arrest in case of persistent DNA damage ((Carvajal *et al.*, 2012), (St Clair *et al.*, 2004)). The deregulation of the p53 pathway has been implicated in tumourigenesis.

Once stabilised, the replisome may stay in position until the blockade is removed or deoxy-nucleotide-triphosphates (dNTPs) restored. Otherwise, the cell can employ post-replication repair pathways to bypass the lesion, either by recruiting mutagenic bypass polymerases, or switching templates by recombination and then replicate using the other nascent strand as a template (Lee and Myung, 2008). In either event, checkpoints must be employed to prevent the onset of mitosis until the completion of replication. Translesion DNA synthesis is one of the mechanisms employed by cells to bypass DNA lesions and continue with DNA replication until the replication process is completed (Lange *et al.*, 2016).

1.2.6.8 DNA repair and tolerance: Translesion DNA synthesis (TLS)

To avoid the damaging effects of a stalled replication fork, cells use specialized polymerases to bypass the damage. This process is known as “translesion DNA synthesis” (TLS), and grants the cell additional time to repair the damage before the replicase returns to complete genome duplication. Generally, this damage-tolerance mechanism is error-prone, and cell

survival often leads to an increased risk of mutations and tumourigenesis (Ohmori *et al.*, 2001). Furthermore, the error-prone TLS polymerases also gain access to undamaged DNA, where their inaccurate synthesis is beneficial towards genetic diversity and evolutionary fitness (Goodman and Woodgate, 2013).

DNA damage interferes with DNA replication and hinders transcription, thereby affecting gene expression and cellular physiology. An estimated 30,000 lesions are generated spontaneously in a mammalian cell per day (Lindahl and Barnes, 2000). Usually DNA lesions cannot be used as a template by the high–fidelity replicative DNA polymerases, which are optimized to replicate the entire genome with high accuracy, efficiency and integrity (Baker and Bell, 1998). However, TLS polymerases can use damaged DNA as templates and insert nucleotides opposite lesions, irrespective of the conformational constraints that many modified bases may impose (Baker and Bell, 1998). Most TLS polymerases are members of the Y family of DNA polymerases. These polymerases have specialized structures to allow replication on damaged DNA substrates. In addition, other classes of DNA polymerases, such as the A and X polymerase families, can demonstrate the TLS activity. Another eukaryotic DNA polymerase, polymerase zeta (Pol ζ), is a member of the B family of DNA polymerases. This family, includes replicative DNA polymerases, and is also capable of TLS (Waters *et al.*, 2009).

The action of the TLS polymerases has been shown to be crucial to limit cancer. This was demonstrated by (Lange *et al.*, 2016) in mice, where the complete deletion of DNA pol zeta (ζ) leads to embryonic lethality and conditional deletion augmented tumorigenesis. In mammalian cells, Reversionless (REV) 3L is a large protein with over 3000 aa and multiple functional domains. The DNA polymerase domain occupies only the last third of the protein. The structural integrity of REV3L may be required in DNA processing complexes and for protein-protein interactions necessary to maintain cell viability and DNA integrity. The central region of REV3L has two adjacent binding domains for REV7 (also known as MAD2L2). REV7 is essential for pol ζ activity *in vitro* and functions as a bridge protein for interaction with the REV1 protein ((Kikuchi *et al.*, 2012), (Hanafusa *et al.*, 2010), (Wojtaszek *et al.*, 2012b)). REV1 in turn interacts with the Y-family DNA polymerases that insert bases opposite the sites of DNA damage and work together with pol ζ ((Guo *et al.*, 2003),

(Wojtaszek *et al.*, 2012a), (Pozhidaeva *et al.*, 2012)). REV7/MAD2L2 also has other cellular functions in the maintenance of chromatin assembly and structure (Lange *et al.*, 2016). The dysregulation of MAD2L2 has been documented in solid tumours such as colon and lung cancers (Rimkus *et al.*, 2007).

1.2.7 Lung cancer

1.2.7.1 Biology of lung cancer

Lung cancer is highly heterogeneous and can arise in many different sites in the bronchial tree. The symptoms and signs may differ, depending on the anatomic location. Lung cancer is a highly invasive and rapidly metastasizing prevalent cancer. Seventy-percent of patients diagnosed with lung cancer are diagnosed at already advanced stages (III or IV). Lung cancer is divided into non-small-cell lung cancer (NSCLC) and small-cell lung cancer (SCLC), which comprise 85% and 15% of all cases, respectively (Wu *et al.*, 2013). Deregulation of the cell-cycle and the cell-cycle related components such as p53 and RB have been implicated in lung cancer (Eymin and Gazzeri, 2010). Furthermore, the deregulation of the pRB pathway through p16 (CDKI) loss and overexpression of cyclin D1 during the G1 phase is a crucial event during lung carcinogenesis, in both NSCLC and SCLC. The deregulation of the p53 pathway particularly during the S-phase also plays a key role in lung carcinogenesis (Zhang *et al.*, 2009). The transformation from a normal to malignant lung cancer phenotype arises in a multistep manner, involving a series of genetic and epigenetic alterations, consequently evolving into invasive cancer by clonal expansion (Nowell, 1976). Following the development of the primary cancer, continued accumulation of genetic and epigenetic abnormalities, acquired during clonal expansion, effects contribute to the processes of invasion, metastasis, and resistance to cancer therapy (Lemjabbar-Alaoui *et al.*, 2015).

1.2.7.2 Molecular pathology of lung cancer

Although tobacco consumption remains the primary risk factor for the development of lung cancer, it has been documented that only 10% of smokers develop lung cancer. Thus, lung cancer is a multi-step and a multi-factorial process. Molecular diagnostics tools may be used to distinguish tumour cells on the basis of the presence or the absence of receptor proteins,

driver mutations, or oncogenic fusion rearrangements. In NSCLC, EGFR, ALK, KRAS, HER2, MET, BRAF, PIK3CA, MEK1, NRAS, AKT1 and ROS1 have been identified as molecular markers. Furthermore, multiple mutations may occur in variable oncogenes leading to transcription of mutated signals. These mutations lead to changes in protein structure and copy number (Pendharkar *et al.*, 2013). Furthermore, kinase genes have been shown to have these driver mutations, and such mutations may be seen in all subtypes of non-small cell lung cancer. For example, females, and non-smokers are more likely to harbor EGFR mutations. In addition, the more common and most studied mutations include EGFR, ALK, HER2, RET and ROS1. Biomarker status is rapidly becoming an important tool based on which treatment is decided (Nana-Sinkam and Powell, 2013). Furthermore, the majority of oncology research today is directed towards molecular profiling of lung cancer. Receptor tyrosine kinases are emerging as major molecular markers and targets (Pendharkar *et al.*, 2013).

1.2.7.3 Lung cancer in HIV positive compared to HIV negative population

It has been documented that the risk of developing lung cancer, especially non-small cell lung carcinoma (NSCLC), seems to be higher in HIV infected patients compared to the same age group in the general population (Suneja *et al.*, 2013). Furthermore, lung cancer in HIV-infected individuals is frequently diagnosed at younger ages than in the general population ((Louie *et al.*, 2002); (Makinson *et al.*, 2011)), with a median age at diagnosis of 47 years compared to 70 years in the general population ((Hessol *et al.*, 2007), (Sigel *et al.*, 2013)). Additionally, it has been documented that the majority of lung cancers in HIV-infected patients are diagnosed at advanced stages, with more than half of the cases being diagnosed at stage III or IV ((Lavole *et al.*, 2009). Adenocarcinoma is the most common histological type, followed by squamous cell carcinoma, large-cell carcinoma and small-cell lung carcinoma (Bearz *et al.*, 2014). Bronchogenic lung cancer in HIV/AIDS patients presents different characteristics in comparison with the general population (Worm *et al.*, 2013). In regard to prognosis and survival, Biggar *et al.* (2005) reported a 2-year survival rate of only 10% in patients with HIV, compared with 31% in the general population. Similarly, the 5-year survival rate for lung cancer was 10% in HIV-infected patients compared to HIV negative counterparts ((Biggar *et al.*, 2005), (Marcus *et al.*, 2015)). Contrarily, Rengan *et al.* (2012)

found that the survival rates were similar for both HIV-positive and HIV-negative patients diagnosed with non-small-cell lung cancer (NSCLC) between 2000 and 2005. Similarly, Hakimian *et al.* (2007) reported comparable survival rates in patients with advanced non-small-cell lung cancer (NSCLC) between HIV-positive patients with CD4 cell counts >200 cells/mm3 and HIV negative patients. Therefore, these data suggest that, although HIV infection could have been a significant contributory factor in the pre-HAART era, this effect alone does not account for lung cancer epidemiology in PLWHA in the HAART era ((Rengan *et al.*, 2012), (Hakimian *et al.*, 2007), (Moltó *et al.*, 2015)).

1.2.8 HAART and Chemotherapy drug-drug interactions (DDIs)

With increasing incidence rates of the NADCs in PLWHA, a better understanding towards an integrated approach in treating both HIV/AIDS and cancer is needed. In most cases, the drug-drug interactions (DDIs) are frequently encountered in the therapy of cancer patients with HIV. For example, all PIs are inhibitors of CYP3A, which is a central route in the metabolism of almost 50% of all anti-cancer (AC) drugs, with, ritonavir being the strongest inhibitor of CYP3A activity. On the other hand, NNRTIs can induce metabolism and potentially reduce the efficacy of AC drugs ((King *et al.*, 2004), (Moltó *et al.*, 2015)). Ritonavir is also an inhibitor of P-glycoprotein, which leads to increased exposure to many AC drugs. Table 1.2 outlines the low, moderate and high risk DDIs between HAART components and AC drugs.

Table 1.2: The outline of potential high, moderate and low DDIs between HAART components and AC drugs

High risk	**Moderate risk**	**Low risk**
-Boosted protease inhibitors (PIs): Atazanavir/ritonavir Atazanavir/cobicistat Darunavir/ritonavir Darunavir/cobicistat	-Nucleoside reverse transcriptase inhibitors (NRTIs): Tenofovir -Non-nucleoside reverse	-Nucleoside reverse transcriptase inhibitors (NRTIs): Abacavir Lamivudine Emtricitabine

Lopinavir/ritonavir -Non-nucleoside reverse transcriptase inhibitors (NNRTIs): Nevirapine Efavirenz Etravirine -Integrase inhibitors (INSTIs): Elvitegravir/cobicistat	transcriptase inhibitors (NNRTIs): Rilpivirine	 -Integrase inhibitors (INSTIs): Raltegravir Dolutegravir -Entry inhibitors Maraviroc Enfuvirtide

Contrarily, integrase inhibitors are considered to be among the most preferred options for HAART in HIV patients with cancer. This is due to their favourable drug interaction profile with antineoplastic drugs (Cottrell *et al.,* 2013) . For instance, raltegravir and dolutegravir are mainly metabolized by glucuronidation through UGT1A1 and they do not have any inducer or inhibitor effect on either P450 enzymes or drug transporters, thus minimizing their potential for drug interactions (Liedtke *et al.*, 2014).

1.2.9 Integrated approach for combating the colliding epidemics-HIV/AIDS and lung cancer

The optimum health care for PLWHA and with cancer, lung cancer in particular may be complex, but is very similar to treating lung cancer patients with other treatment agents, such as those used for cardiovascular or chronic respiratory diseases, avoiding DDIs ((Sparano *et al.*, 2004), (Moltó *et al.*, 2015)). Currently, a multidisciplinary approach in the treatment of lung cancer is a preferred option and it involves thoracic surgeons, pulmonary specialists, radiologists, and medical and radiotherapy oncologists. In the context of treating HIV patients

with lung cancer, the participation of a physician with expertise in treating HIV infection is critical. Importantly, the therapeutic approach for lung cancer in PLWHA should not differ from that of the general population, although with a consideration that DDIs between HAART and chemotherapeutic drugs may occur resulting in overlapping toxicity (Moltó *et al.*, 2015) . Furthermore, PLWHA should still be maintained on HAART when concurrently treated for lung cancer. Thus, multidisciplinary collaboration between oncologists and HIV specialists is crucial for the optimal treatment for PLWHA and lung cancer.

CHAPTER 2: AIMS AND OBJECTIVES

2.1 INTRODUCTION

The molecular basis of lung cancer is heterogeneous and complex. Understanding the genetic and molecular alterations and their functional significance is rapidly influencing the potential impact molecular markers have on lung cancer diagnosis, prognosis and treatment (Cooper *et al.*, 2013). Furthermore, the numbers of HIV-positive patients with lung cancer as a leading NADC will most likely increase over the next 2 decades. This highlights the importance of further research on lung cancer, and HIV epidemic as well as the potential interactions between the two diseases as the number of individuals with both diseases increases (Koegelenberg *et al.*, 2016).

The South African (SA) healthcare system has to deal with the largest HIV burden in the world, has the largest HAART programme globally, one of the highest incidences of TB, and a high prevalence of NADCs in the HAART era. Additionally, lung adenocarcinoma has been shown to be the most common form (Koegelenberg *et al.*, 2016). To date, the relationship between the use of HAART and lung carcinogenesis is poorly understood. While the deregulation of the cell-cycle is one of the hallmarks of lung cancer, this study aimed at elucidating the effects ARV drugs have on lung cancer in *in vitro* cell-line models.

2.2 HYPOTHESIS

Antiretroviral treatment (ART) modulates the expression of cell-cycle related genes, leading to lung tumourigenesis.

2.3 AIM

The broad aim of this study was to investigate the effect of antiretroviral drug treatment (ART) in the regulation of the cell-cycle related genes in lung cancer.

2.3.1 Objectives

a) To determine the cytotoxic effect (s) of antiretroviral drug treatment (ART) on lung cancer. For this purpose, the Alamar Blue (AB) assay was used to measure effects of EFV and LPV/r on cell viability and cell death, pre-and-post ARV treatment.

b) To investigate the ARVs' pro-or-anti-oncogenic properties. To achieve this, effects of EFV and LPV/r on cell proliferation and cell death/apoptosis were monitored in real-time, using the real time cell impedance (xCELLigence) assay.

c) To determine the ARVs' regulatory effects on the cell-cycle in lung cells. Propidium iodide (PI) staining together with FACS analysis was used to quantify the DNA present at each of the cell-cycle stages before and after ARV treatment. Furthermore, the cytotoxic effects of the ARVs were confirmed by the Annexin V FITC/PI apoptosis assay, using FACS analysis.

d) To assess the ARVs' effects on nuclear morphology. Nuclear changes including DNA fragmentation and chromatin condensation in response to ARV treatment were evaluated with DAPI staining.

e) To investigate which cell-cycle related genes are targeted by the ARV drugs. Effects of these drugs at gene expression level were evaluated using focused human gene arrays. In addition, RT-qPCR was performed to validate selected PCR array targets.

f) To map the molecular pathways involved in response to the ARV treatments. *In silico* Bio-informatics analyses were employed.

CHAPTER 3: MATERIALS AND METHODS

3.1 MATERIALS

For the proposed use of MRC-5 and A549 cell-lines, an ethics waiver was applied for and obtained for this study (see Appendix A).

3.1.1 ARV drugs

The ARV drugs for this study were purchased from Toronto Research Chemicals (Toronto, Ontario, Canada), and dissolved as stock solutions in methanol (see Appendix B1). The two ARVs selected for this study were the non-nucleoside reverse transcriptase inhibitor (NNRTI) Efavirenz (EFV) and the conjugate protease inhibitor (PI) Lopinavir/ritonavir (LPV)/r). The chemical structures of EFV, LPV and RTV (r) are shown in Table 3.1.

Table 3.1: Chemical structures of EFV, LPV and RTV

NNRTI-EFV	PI-LPV	PI-RTV
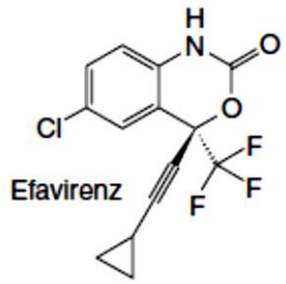	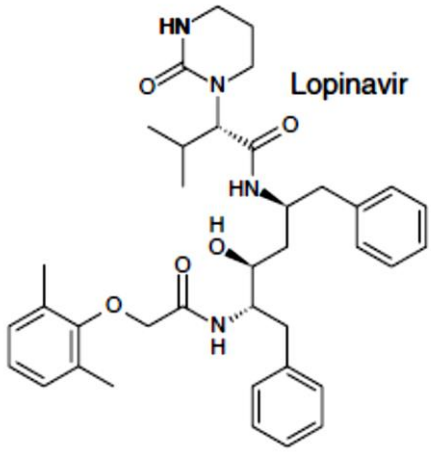	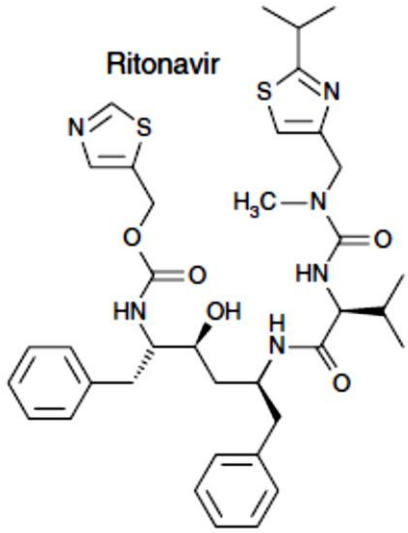

[Adapted from Arts and Hazuda, 2012 (Arts and Hazuda, 2012)].

The choice of ARVs was based on the approved WHO 2013 ART guidelines, the South African 2013 ART guidelines, and potential oncogenic properties from *in vitro* reports ((Sikora *et al.*, 2010) ; (Batman *et al.*, 2011), (Srirangam *et al.*, 2011), (Hecht *et al.*, 2013), (Hecht *et al.*, 2015), (Grossman *et al.*, 2014)).

3.1.2 Cell culture

The lung cell lines MRC-5 ((normal lung fibroblast (ATCC CCL171)) and A549 ((lung adenocarcinoma (ATCC CCL185)) were purchased from the American Type Culture Collection (ATCC). These cell lines are adaptable to a single growth medium and they have been previously demonstrated to show reproducible profiles for growth and drug sensitivity. MRC-5 and A549 cell lines were treated with a range of concentrations including the plasma level ARV concentrations at 24h, 48h and 72h time intervals, for screening purposes. Cells were grown in Dulbecco's Modified Eagle's Medium (DMEM):F12, 10% serum, 1% pen/strep and 5% CO_2 in air and left to grow to 70-80% confluency in a humid chamber at 37°C for 48 to 72h. This was followed by trypsinization, to detach cells from the flask, centrifuging to pellet the cells and to remove the supernatant, washing with PBS and re-suspending the cells in 5ml of fresh DMEM media. The cells were split in a 1:2 ratio and sub-cultured. Cell culture medium containing 10% FBS and 1% pen/strep was replaced every 2-3 days until cells reached 70-80% confluency. Cells were then serum-starved for 24h to synchronise the cell-cycle. The following day, the cells were pharmacologically treated with the ARV drugs, EFV (4, 13, 26, 50µM, respectively) and LPV/r (10, 32, 50, 80µM, respectively) for 24h to 72h. Vehicle control cells were exposed to growth medium and vehicle only (methanol 0.1% v/v).

3.2 Alamar Blue (AB) cell viability assay

Alamar Blue, also known as resazurin, is a water soluble dye stable in a cell culture medium environment, non-toxic to cells and is permeable through cell-membranes. Because of its stability and non-toxicity, continuous monitoring of cell cultures over time is permitted. Alamar Blue has been shown to act as an intermediate electron acceptor in the electron

transport chain without interfering with the normal transfer of electrons ((Page *et al.*, 1993); (Rampersad, 2012)).

Alamar Blue (AB) can be reduced by NADPH, FADH, FMNH, NADH and cytochromes. As it accepts electrons, AB changes from the oxidized, non-fluorescent, blue substrate resazurin to the reduced, fluorescent, pink product, resorufin. This alteration from the oxidized to the reduced state can be quantified fluorometrically or colorimetrically indicating the presence or absence of viable cells, as only viable cells reduce AB (Byth *et al.*, 2001). The latter was used in this study. Spectrophotometric absorbance is measured at two wavelengths 570nm and 600 nm or 540nm and 630 nm. AB can be used in various aspects of monitoring cellular health including cell proliferation, cell death, cell-cycle function and control (Rampersad, 2012). In this study AB (Sigma Aldrich) powder was dissolved in aqueous solution to make up stock solution as described in appendix B2, and was employed to examine the viability of MRC-5 and A549 lung cells pre- and- post ARV drug treatment, with reference to the untreated (vehicle control) group. To achieve this, the following protocol was carried out:

Confluent cells were trypsinised, harvested by centrifuging at 800rpm for 3 minutes; the supernatant was discarded and cell pellets were re-suspended in 1ml of cell culture medium. An aliquot of cells was then counted using an automated cell counter (Bio-Rad) and 2 X 10^3 cells were seeded in triplicate in a 96-well plate. Cells were allowed to grow and attach overnight at 37°C with 5% CO_2 in air. The following morning, cells were serum-starved (to synchronize the cell-cycle) for 24h. Next, the cells were treated with each of methanol (0.1%; v/v), vehicle control), EFV (4, 13, 26, 50 µM) and LPV/r (10, 32, 50, 80 µM), for 24h, 48h and 72h, respectively. The first column on the 96-well plate was always the blank that is, containing cell culture medium and AB without cells. The subsequent columns were seeded with cells and exposed to methanol, EFV and LPV/r at the above mentioned concentrations for 24h, 48h and 72h, with a final volume of 200µl (180µl medium + 20µl AB). The absorbance of control and test wells was measured at 540nm and 630nm using a microplate reader (Biotek), where the number of viable cells is directly proportional to the intensity of the reduced dye and was expressed as AB reduction percentage, using the following formula derived by Willard *et al.*, (1965):

$$\% \text{ Reduction} = \left[\frac{{}^{\varepsilon}\text{oxid 630nm (sample A540nm)} - {}^{\varepsilon}\text{oxid 540nm(sample A630nm)}}{{}^{\varepsilon}\text{red 540nm (oxidised control A630nm)} - {}^{\varepsilon}\text{red 630nm (oxidised control A540nm)}} \right] \times 100$$

The molar extinction coefficients of AB for the oxidised and reduced controls are:

Ɛoxid 630 nm = 34.798, Ɛoxid 540 nm = 47.619, Ɛred 630 nm = 5.494, and Ɛred 540 nm = 104.395 (Willard *et al.*, 1965).

The percentage AB reduction values were corrected for the background values of the blank control wells containing medium only.

The AB assay was however limited by the fact that EFV is primarily metabolized by CYP2B6. To account for a possible drug-drug (EFV-AB) interaction, the AB assay was followed by a label free real-time-cell-analysis (RTCA) xCELLigence assay. Due to the high costs of conducting a RTCA, the AB assay was a useful indicator of cell viability in response to ARV drug treatment over a period of 24h, 48h and 72h, these time periods being similar to the RTCA analysis.

3.3 xCELLigence RTCA cell proliferation and cytotoxicity assay

Measuring cell viability is an essential step in cell biology. There are many ways to quantify cell viability, including the 3-4,5-dimethylthiazol-2-yl-2,5-diphenyl tetrazolium bromide (MTT) reduction and Trypan Blue assays. With modern technology, new alternative viability methods with increased sensitivity and specificity have been developed. The xCELLigence System Real-Time Cell Analyser (RTCA) is one of these newly developed methods. Cellular biological events, such as cell proliferation, cell viability, cell morphology and migration can be analyzed in real time by the xCELLigence system without labeling.

The xCELLigence system uses custom-designed plates, which have a high-density gold electrode array on which the target cells adhere and grow. Cells adhere to the plate surface and influence the electrical impedance across the array. This electrical impedance is monitored and measured by the xCELLigence software. The impedance values are then converted by the xCELLigence software into the Cell Index (CI). The CI is used as a measure of cell adhesion,

that is, in the absence of cells, the CI will be zero. However, as cells adhere to the electrode array, the CI increases. It thus follows, the greater the CI values, the greater the level of cell adhesion. On contrary, the decreasing CI values signify a net decrease in cell adhesion. Primarily, xCELLigence measures the net cell adhesion within the well. As a result, any responses that triggers change in cell morphology, which includes cell size, volume, shape, movement (migration), cell proliferation or cell death can be investigated by the xCELLigence technology (Kho *et al.*, 2015). It is advantageous that data from the xCELLigence assay provides continuous quantitative information about the biological status of cells in real-time. This system was employed in this study to determine the effects of ARV drugs (EFV and LPV/r) in MRC-5 and A549 cells in real-time.

The xCELLigence Real-Time Cell Analyser System was used according to the manufacturer's instructions (ACEA Biosciences). The seeding density of both the MRC-5 and the A549 cells were first optimized using cell titration curves. Briefly, 100µl of cell culture medium was added to each of the sixteen E-plate wells and an automatic scan was performed to verify proper contact between the E-plate and the RTCA analyzer. After this, the background impedance was measured for each well. A 2× dilution series was prepared, that is, 50 000, 25 000, 12500, 6250, 0 cells/ml, and 100µl of each cell suspension was added to duplicate wells. The E-plate was left for 30min to allow the cells to settle in an evenly distributed manner at the bottom of the wells. Following on this, a scanning program was initiated that consisted of measuring the CI every 30min for 200 repetitions. This allowed for the continuous monitoring of cells for up to 100h. During or after the experiment, respective wells were selected in the software analysis page (Plot Page), to determine the Cell Index of a well as a function of time, these being plotted and represented as averages.

3.3.1 Real time evaluation of cytotoxicity

The optimum cell number for each cytotoxicity experiment was determined from the Cell Titration assay as described above. Thirty thousand cells/ml for the MRC-5 cell line and fifty thousand cells/ml for A549 cells were shown to be optimal. The seeding procedure was followed as described above for the cell titration assay. After cells were grown for 24h, cells in appropriate wells were washed with PBS and treated with EFV at concentrations of 4, 13

and 50µM, respectively; or with LPV/r at concentrations of 10, 32 and 80µM, respectively, for up to a time period of 72h. This was relative to the 0.1% (v/v) methanol/ (vehicle) control. The cells were monitored every 15min (instead of 30min as described in the Titration assay).

It is important to note that here the Normalized Cell Index (NCI) instead of the CI was plotted against time. NCI was used following cell treatment with either EFV or LPV/r, being useful to study the change in cell adhesion, selected from a specific time point of 24h. NCI is proportional to cell adhesion and proliferation.

The RTCA data was useful in indicating the optimum and appropriate drug treatments and time-periods for subsequent experiments. Furthermore, changes in cell proliferation patterns in response to ARV treatment were then assessed on the cell-cycle stages using FACS.

3.4 Cell-cycle Analysis by Fluorescence-activated cell sorting (FACS)

Flow cytometry allows for the measurement of physical and chemical characteristics of individual cells rapidly and with high accuracy. For this reason, flow cytometry is widely used in cell-cycle analysis, utilizing a fluorescent compound such as propidium iodide which intercalates within nuclear DNA allowing for its quantification. When PI is bound to nucleic acids, the fluorescence excitation maximum is 535nm and the emission maximum is 617nm, from red to blue. PI has little to no sequence preference and does also bind to double stranded (ds) RNA and thus was used in conjunction with RNAse to remove RNA.

For the purposes of this study, the BD Accuri C6 system (BD Biosciences) was used to quantify the DNA present at each of the stages of the cell-cycle. This was done to examine the effects of ARV drugs on different cell-cycle stages. Single cells with propidium iodide-stained DNA pass in front of a laser beam in the flow cytometer. Each cell absorbs light and emits fluorescence that is proportional to the DNA content of the cell. This measured fluorescence is digitally converted to an electric pulse and the data is visualized as DNA histograms (Dey, 2004). The cells were harvested and stained as follows:

1. Drug treated and control cells were trypsinised at 70-80% confluency, harvested by centrifuging and the cell pellet was re-suspended in 250µl of PBS at room temperature (Rt) for 10min

2. One ml of ice cold absolute ethanol was added drop-wise to the cells while vortexing

3. The fixed cells were stored at -20°C for 1h

4. The cells were centrifuged at 800rpm and the supernatant was discarded

5. The pellets were then re-suspended in 500µl of PBS and allowed to rehydrate at RT for 15min

6. Two µl of 10mg/ml RNAse (Sigma) was added to the resuspended cells and incubated at 37°C to eliminate RNA

7. The cells were centrifuged and resuspended in 500µl of PBS

8. The cells were then stained with 25µl of PI (1mg/ml), (Sigma) and incubated at 4°C overnight in the dark

9. The following morning, stained cells were analysed on the BD Accuri C6 and results were generated and analysed as histogram by the BD C6 Accuri software.

The histograms generated by cell-cycle FACS analysis together with the RTCA data were indicators of ARVs (LPV/r in particular) apoptotic effects and this lead to ARVs (LPV/r) apoptosis evaluation by FACS analysis.

3.5 Dual Staining Annexin V-FITC/ Propidium Iodide (PI) Apoptosis Assay

Apoptosis is a normal physiologic process which is important in the maintenance of tissue homeostasis. Loss of plasma membrane integrity, condensation of the cytoplasm and nucleus, and internucleosomal cleavage of DNA are characteristic features of cells undergoing apoptosis, with loss of plasma membrane being one of the earliest features. An early indicator

of apoptosis is the rapid translocation of the membrane phospholipid phosphatidylserine (PS) from the inner to the outer surface of the plasma membrane (Leventis and Grinstein, 2010). Due to the exposure of the PS membrane to the extracellular surface, Annexin V, a calcium dependent phospholipid binding protein that has a high affinity for PS, and binds to cells with exposed PS can be used to monitor cells undergoing apoptosis. Annexin V may be conjugated to fluorochromes such as Fluorescein isothiocyanate (FITC) and used in conjunction with DNA binding dyes such as Propidium Iodide (PI). This dual staining procedure allows the investigator to distinguish between early apoptotic cells, late apoptotic cells and dead cells. For example, viable cells are Annexin V-FITC and PI negative; early apoptotic cells are Annexin V-FITC positive and PI negative; and cells that are in late apoptosis or already dead are both Annexin V-FITC and PI positive (Sawai and Domae, 2011).

The MRC-5 and A549 cells were cultured and treated with LPV/r at a concentration of 32 and 80µM, respectively for 24h, 48h and 72h. Camptothecin (CPT) (Sigma) treatment (50µM) was used as a positive control. The cells were then rinsed with PBS, trypsinized and centrifuged at 1500g for 5min to collect the cell pellet. The cell pellet was then washed twice in PBS.

The apoptosis kit (Annexin V FITC/PI) from Santa Cruz Biotechnology was used to assess LPV/r apoptotic effects on lung cells. The following protocol was carried out to stain cells for apoptosis as per manufacturer's instructions (Santa Cruz Biotechnology):

Staining

1. Cells were re-suspended in 1× binding buffer at a concentration of 1 x 10^6 cells/ml.

2. One hundred µl of the cell suspension (1 x 10^5 cells) was transferred to a sterile 1.5ml micro-centrifuge tube.

3. Five µl of Annexin V-FITC and 5µl of PI were added to the tube with the cell suspension.

4. The tube containing cells was gently vortexed and incubated for 15min at RT (25°C) in the dark.

5. Four hundred µl of 1× binding buffer was added to each tube, and the cells were then analyzed within one hour by flow cytometry using the BD Accuri C6 Flow Cytometer, and results were generated as cytograms.

This was then followed by the assessment of changes in nuclear morphology following ARV drug treatment using DAPI staining.

3.6 DNA staining using 4, 6-diamidino-2-phenylindole (DAPI)

A variety of fluorescent dyes are available to label DNA and allow for easy visualization of the nucleus in interphase cells and chromosomes in mitotic cells. These stains include Hoechst, 4,6-diamidino- 2-phenylindole (DAPI), ethidium bromide, propidium iodide, and acridine orange. Compared to the Hoechst DNA staining, DAPI has greater photostability (Chazotte, 2011). It is assumed that DAPI associates with the minor groove of double-stranded DNA, with a preference for the adenine-thymine clusters. For DAPI to enter the cell and intercalate into DNA, cells must be first permeabilized with a detergent before or after fixation. Fluorescence increases approximately 20-fold when DAPI is bound to double-stranded DNA. Here, cells (MRC-5 and A549) were treated for 48h with EFV (13 and 50µM) and LPV/r (32 and 80µM). The two concentrations for each drug were selected as plasma relevant and anti-proliferative or cytotoxic, as indicated by preceding experiments. DAPI was used to assess the effects of the ARVs on the cellular DNA using the following protocol:

1. 1×10^4 cells were seeded on the coverslips and allowed to grow overnight in 6-well plates.

2. Cells were rinsed with PBS and serum-starved for 24h.

3. Cells were then treated with 13µM and 50µM of EFV; and with 32µM and 80µM of LPV/r.

4. The DAPI (Sigma) solution was diluted 1:5000 in PBS.

5. The cell culture medium was aspirated from the cells grown on the coverslips, followed by three PBS washes.

6. The cells were fixed for 10min in 3.7% formaldehyde in PBS.

7. The fixative was aspirated and cells were rinsed three times, 5min each, in PBS.

8. The cells were then permeabilized in 0.2% Triton X-100 in PBS for 5min.

9. Triton-X was then aspirated, and the cells were rinsed three times, 5min each, in PBS.

10. The cells were incubated for 10min at room temperature (Rt) with 100µl of DAPI labeling solution (from Step 4).

11. DAPI was aspirated off and cells were rinsed three times in PBS.

12. The coverslips were then mounted with aqueous FluoroMount mounting medium (Sigma) and allowed to dry.

13. The cells were viewed on the Zeiss LSM 780 confocal microscope.

Following assessment of ARVs (EFV and LPV/r) on cellular health, gene expression studies were done to investigate ARVs role on the expression of cell-cycle related genes.

3.7 Human Cell-Cycle Gene (PCR) Arrays

A gene array panel was used to analyze the cell-cycle response pre- and post- antiretroviral treatments of each cell-line. This method provides for a highly reliable and sensitive gene expression profiling of focused panels of genes in signal transduction, biological processes, or disease research pathways using real-time PCR methodology.

In this study, RT² Profiler Human Cell-cycle PCR Arrays were used (Qiagen). This pathway-focused array consists of 84 genes related to the cell-cycle, in a 96-well plate format as illustrated in Appendix C, Figure C5.1. Aside from the pathway-focused genes, the panel contains 5 housekeeping (reference) genes and additionally a panel of proprietary controls that monitor genomic DNA contamination (GDC), first strand synthesis (RTC) and real-time PCR efficiency (PPC).

Use of such a panel requires the isolation of high quality cellular RNA and sufficient cDNA synthesis to provide for the PCR amplification and analysis of gene expression. These steps are described below.

3.7.1 RNA Extraction

RNA was extracted from cells treated for 48h at drug plasma levels (13µM EFV and 32µM LPV/r); and from untreated cells, using the RNeasy Mini Kit (Qiagen) following the manufacturer's instructions. Briefly, cells were washed with PBS twice, and then lysed directly by adding 350µl of Buffer RLT, to T25 cell culture flasks (for A549 cells) and adding 600µl of Buffer RLT to T75 cell culture flasks (for MRC-5 cells). Cell scrapers (Lonza) were used to detach the cells, the lysate was then transferred into sterile 2ml micro-centrifuge tubes. The tubes were then briefly vortexed before equal volumes (350µl or 600µl) of 70% ethanol were added to the lysate. Up to 700µl of the sample was transferred into an RNeasy Mini spin column placed in a 2ml collection tube. These were centrifuged for 15s at 8000g. The flow-through was then discarded and 700µl of Buffer RW1 was added to the RNeasy spin column and centrifuged for 15s at 8000g. Once again the flow through was discarded and 500µl of Buffer RPE was added to the RNeasy spin column, which was centrifuged for 15s at 8000g. The flow through was discarded again, and 500µl of Buffer RPE was added and the tubes were centrifuged for 2min at 8000g. The flow-through was discarded and the RNeasy spin-column was centrifuged at 8000g for 1min. The RNeasy spin column was inserted into a new 1.5ml collection tube and 30µl of RNase-free water was added directly to the spin column membrane. This was incubated at room temperature (Rt) for 1min to allow the RNase free water to cover the spin column membrane. Total RNA was eluted by centrifuging at 8000 x g for 1min. The quality and quantity of RNA was measured using a Nanodrop (Nanodrop ND-1000 spectrophotometer (Nanodrop Technologies)). For highly pure RNA, the 260/280 absorption ratio is ~2, and the 260/230 ratio is 2.0-2.2.

3.7.2 cDNA synthesis

cDNA was synthesized using the RT^2 First Strand cDNA synthesis kit (Qiagen) following the manufacturer's instructions. Briefly, two mixtures were prepared separately, firstly the Genomic DNA (gDNA) elimination mixture (Table 3.2) for each RNA sample and secondly, the reverse transcription (RT) cocktail (Table 3.3).

Table 3.2: gDNA elimination mixture

Reagent	**Volume (µl)**
Total RNA	1µg*
GE (5x gDNA Elimination Buffer)	2
RNase-free water to a final volume	10

*The volume in µl depends on concentration of the RNA in ng/µl

The gDNA mixture was incubated at 42°C for 5min and immediately placed on ice for 1min.

Table 3.3: Reverse transcription (RT) cocktail

Reagent	**Volume (µl)**
BC3	4
P2	1
RE3	2
RNase-free water	3
Final volume	10

The RT cocktail was briefly centrifuged and added to the gDNA mixture to provide a final volume of 20µl. This mixture was then incubated at 42°C for 15min, 95°C for 5min and then at 4°C for 5min. cDNA was diluted to 111µl by adding nuclease-free water, according to the manufacturer's instructions. The cDNA was used immediately for the PCR Arrays or stored at -20°C for future use.

3.7.3 PCR Array plates

The synthesized cDNA was mixed with the Qiagen RT^2 SYBR Green/ROX qPCR master mix, to which nuclease-free water was also added. Thereafter, 25µl per well was loaded in 96-well plates with pre-dispensed primer sets of the RT^2 Profiler PCR Array, as indicated in Table 3.4.

Table 3.4: The RT-qPCR master mix for PCR Arrays

Reagent	**Volume (µl)**
2× SYBR Green/ROX master mix	1350
cDNA	102
Nuclease-free water	1248

The PCR Array plates were centrifuged briefly (Boeco) before they were loaded on the ABI 7500 RT PCR instrument (Applied Biosystems). The following cycling conditions were used: 10min at 95°C, followed by 40 cycles of 15s at 95°C and 1min at 60°C. Data (CT values) was exported as Excel files to (Qiagen, www.qiagen.com) GeneGlobe Database for analysis.

3.7.4 Data Analysis using GeneGlobe

The online GeneGlobe (Qiagen) analysis tool was used to analyse the PCR array data of all treated and untreated samples. A cycle threshold (Ct) of 35 was set as the cut-off value for gene expression. Thus genes with Ct values greater than 35 cycles were considered non-detectable. Five house-keeping genes, including (ACTB-Beta Actin (ACTB); Beta-2-microglobulin (BM2); Glyceraldehyde-3-phosphate dehydrogenase (GAPDH); HPRT1-Hypoxanthine phosphoribosyltransferase (HPRT1); RPLP0-Ribosomal protein, large, P0 (RPLP0)) were used to obtain the change in cycle threshold (ΔCT) value for each gene of interest, where ΔCT is calculated as: CT value of gene of interest less the CT value of reference gene. The difference between the ΔCT of the treatment group and that of the vehicle control group is represented by ΔΔCT value, where the fold-change is calculated by $2^{(-\Delta\Delta CT)}$. (Livak and Schmittgen, 2001). This value represents the level of the expression of each gene in the drug-treated (EFV or LPV/r) sample *versus* that in the vehicle control sample. By convention, the fold difference of ±2 up-or-down regulation was used as a basis of target selection. Due to the costs of running PCR gene arrays, these were confirmed by RT-qPCR.

3.8 Validation of Cell-cycle Array Data

Real-Time quantitative Polymerase Chain Reaction (RT-qPCR) has been proven to be a more sensitive method for gene expression studies, compared to the conventional method (Sanguinetti *et al*., 2003). To validate the PCR Array data, Real-Time quantitative PCR (RT-qPCR) was performed at least three independent times in triplicate. Three representative genes of the array were rationally selected according to their level of expression (above or below two-fold expression).

3.8.1 Primer Design

The Primer 3 tool (http://primer3.wi.mit.edu/) was used to design primers for the selected gene targets, including the house-keeping gene (HKG) GAPDH, based on NCBI accession numbers provided by Qiagen (for all three selected targets), following PCR Array analysis. The target genes selected included MAD2L2 (accession number NM_001127325), CASP3 (accession number NM_004346), AURKB (accession number NM_001256834) and (HKG) GAPDH (accession number NM_002046). The amplicons' sizes were as follows; 157bp for MAD2L2, 149bp for CASP3, 150bp for AURKB and 87bp for GAPDH. Primer sequences of the selected gene targets and GAPDH as a reference gene (one of the internal controls' panel in the PCR Array) are shown in Figure 3.1.

MAD2L2

MAD2L2-Forward: 5'-CGA GTT CCT GGA GGT GGC TGT GCA TC-3'

MAD2L2-Reverse: 5'-CTT GAC GCA GTG CAG CGT GTC CTG GAT A-3'

Caspase 3 (CASP3)

CASP3- Forward: 5'-GCT CAT ACC TGT GGC TGT GTA-3'

CASP3- Reverse: 5'-ATG AGA ATG GGG GAA GAG GCA -3'

AURKB

AURKB- Forward: 5‘-AGC AGC GAA CAG CCA CG-3’

AURKB- -Reverse: 5‘-GCC GAA GTC AGC AAT CTT CA-3’

GAPDH

GAPDH- Forward: 5‘-TGCACCACCAACTGCTTAGC-3’

GAPDH- Reverse: 5’-GGCATGGACTGTGGTCATGAG-3’

Figure 3.1: The forward and reverse primer sequences of the selected gene targets and GAPDH reference gene used to perform Real-Time quantitative PCR (RT-qPCR) in order to validate the PCR Array data.

Total RNA from treated and untreated cells for 24h and 48h was extracted using the RNeasy mini kit (Qiagen), as described in section 3.7.1. The extracted RNA (treated and untreated) samples were used for reverse transcription in RT-qPCR experiments. Briefly, RNA was reverse transcribed to cDNA using the Maxima First Strand cDNA synthesis kit for RT-qPCR with dsDNase (Thermo Scientific), following the manufacturer’s instructions as shown in Table 3.5 and Table 3.6.

Table 3.5: Digestion of gDNA

Reagent	**Volume (µl)**
10× dsDNase Buffer	1
dsDNase	1
Template RNA	1µg*
Nuclease-free water	Up to 10
Total volume	10

*Added volume of RNA template varies, to amount to 1µg.

The contents were gently mixed and centrifuged. This was followed by incubation at 37°C for 2 min, chilling on ice, another brief centrifuge and then placed on ice. Components of Table 3.5 were added to those listed in table 3.6. The two cocktails were gently mixed and briefly centrifuged. The reactions were incubated at 25°C for 10min and 50°C for 15min. The reactions were terminated by heating at 85°C for 5 min. This was followed by 4°C hold for 5min. The cDNA was ready to use, as per table 3.7 or was stored at -20°C for future use.

Table 3.6: Reverse Transcription Components

Reagent	**Volume (µl)**
5X reaction mix	4
Maxima enzyme mix	2
Nuclease-free water	4
Total volume	10

Table 3.7: RT-qPCR master mix cocktail

Reagent	**Volume (µl)**
Fwd Primer*	0.4
Rv Primer*	0.4
2X SYBR Green master mix	5
cDNA	0.8#
Nuclease-free water	3.4
Total volume	10

*10µM of each primer (for all different gene targets) was used.

No template reactions were also included, for negative control(s).

The reactions each consisting of a total volume of 10µl were then loaded into a 96-well PCR plate, which was centrifuged at 1000rpm for 20s, (Boeco) before loading onto the ABI 7500 RT-qPCR Instrument (ABI,) The following thermal profile was used: denaturation at 95°C for 10min; followed by 40 cycles of 95°C for 15s, then 60°C for 1min (data collection point); and finally the dissociation stage, which is pre-set on the ABI 7500 system at 95 °C for 15s, Reps1, 60°C for 1min, 95°C for 15s.

3.8.2 RT-qPCR data analysis

Following the RT-qPCR experimental run on the ABI 7500 light cycler, the CT values were exported as an Excel file to create a table of CT values. This table was then uploaded on to the data analysis web portal at http://www.qiagen.com/geneglobe. Samples were assigned to controls and test groups. CT values were then normalized based on a manual selection of the GAPDH reference gene. The data analysis web portal calculates fold change/regulation using the delta delta CT method ((Livak and Schmittgen, 2001), (Schmittgen and Livak, 2008)) in which delta CT is calculated between genes of interest, (GOI) and HKG, followed by delta-delta CT calculations (delta CT (test/experiment)-delta CT (control/calibrator)). Fold Change is then calculated using 2^ (-delta delta CT) formula, shown below.

$\Delta CT = CT\ (Test_{target} - Test_{HKG})$

$\Delta CT = CT\ (Calibrator_{target} - Calibrator_{HKG})$

$= 2^{-[\Delta CT\ (test) - \Delta CT\ (calibrator)]}$

To map the disease and molecular pathways influenced by the selected up-and-down regulated targets, Bio-informatics tools were employed.

3.9 Bio-informatics for Pathway analysis

In silico analyses using various Bio-informatics tools provide an important means for analyzing genes, their products and the (disease) pathways they are involved in (Bechtel, 2016) . For this purpose, Bio-informatics tools were employed to identify complexes formed by the identified targets and how these interact with other cell-cycle related genes. Next, Bio-Informatics tools were used to identify and map other biological and molecular pathways, except for the cell-cycle, the identified targets are involved in.

Four different Bio-Informatics tools were used: STRING, DAVID, Reactome and IPA databases. The gene-lists represented by the GenBank accession numbers of selected gene targets (from the gene array data) were up-loaded on the databases. Each tool is briefly described below.

1. Search Tool for the Retrieval of Interacting Genes/Proteins (STRING) database (v10.0) was used to establish the protein-protein interactions (PPIs) of the up-or-down regulated genes involved in cell-cycle regulation whose transcription levels were analysed using the RT² Profiler Human Cell-cycle PCR Array panel before and after ARV treatment. The PPIs were constructed before and after ARV treatment.

2. The Database for Annotation, Visualization and Integrated Discovery (DAVID) was used to perform a functional enrichment analysis of the target genes in order to identify those genes of interest involved in cell-cycle regulation and progression pre- and post- EFV and LPV/r drug treatment. The functional annotation tool from DAVID database was used. Gene names of the up-and-downregulated groups were uploaded into the database and Kyoto Encyclopedia of Genes and Genomes (KEGG) pathway was selected for visualization. Figure 3.2 below annotates the KEGG pathway.

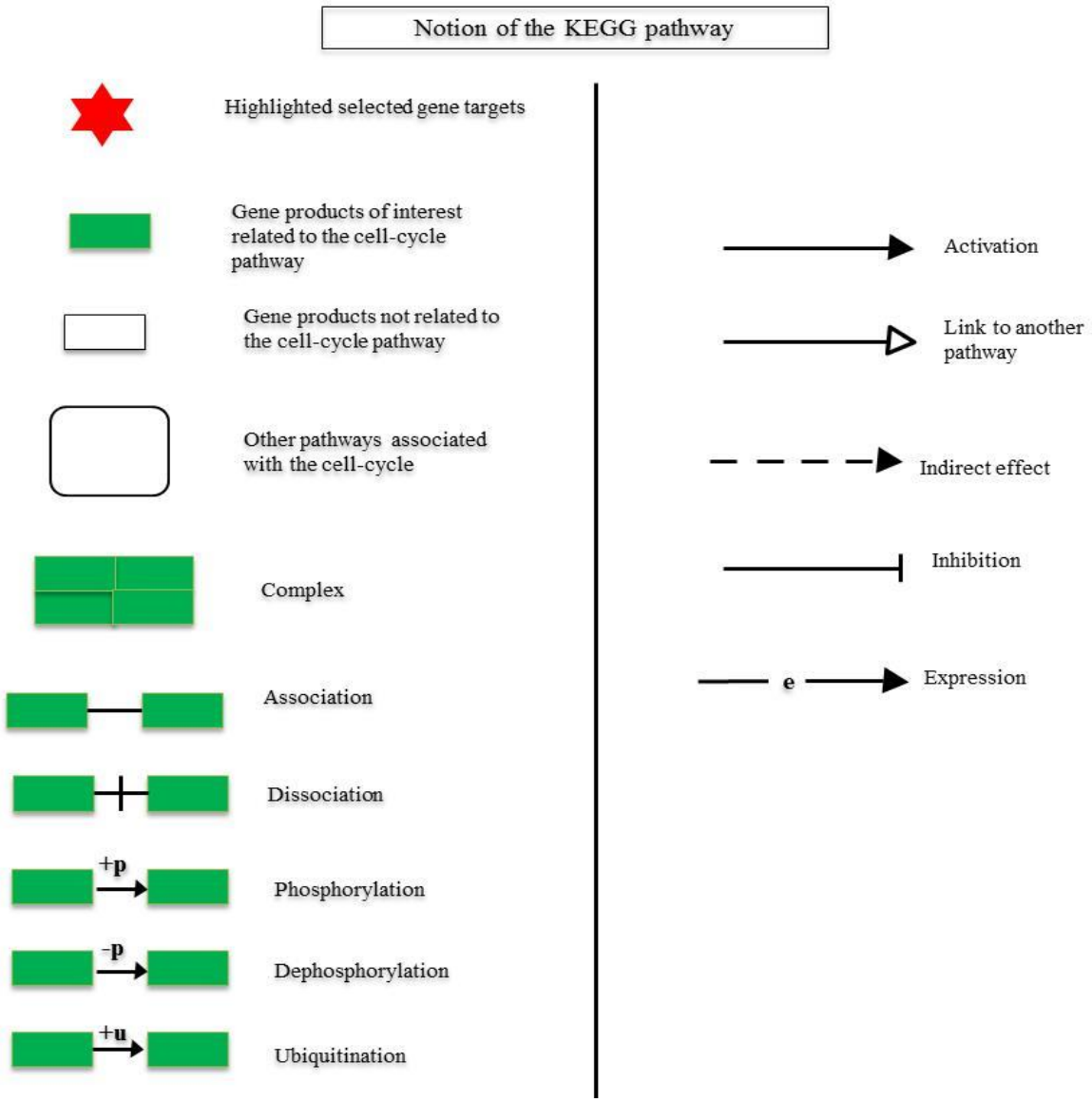

Figure 3.2: The annotation of the KEGG pathway (Own figure)

3. Reactome is an open-source, open access, manually curated and peer-reviewed pathway database. This database is an all-inclusive resource of human pathways for basic research, genome analysis, pathway modelling, systems biology and education. In this study Reactome version (V58) was used to map and analyse biological and molecular pathways other than the focused cell-cycle pathway, which may be influenced by the identified targets

4. Qiagens's Ingenuity Pathway Analysis (IPA) has been widely used to model, analyse and understand the complex biological and chemical systems by the scientific community. In this study, IPA was used to help build a more complete regulatory picture and gain a better understanding of the biology underlying the studied gene expression profiles. To achieve this, the core analysis function of IPA was used. The z core was primarily used to indicate the degree of expression levels, with positive z score denoting upregulation, negative z core representing down-regulation, while zero (0) z core illustrates unchanged gene expression. Figure 3.3 below represent the IPA core-analysis annotation.

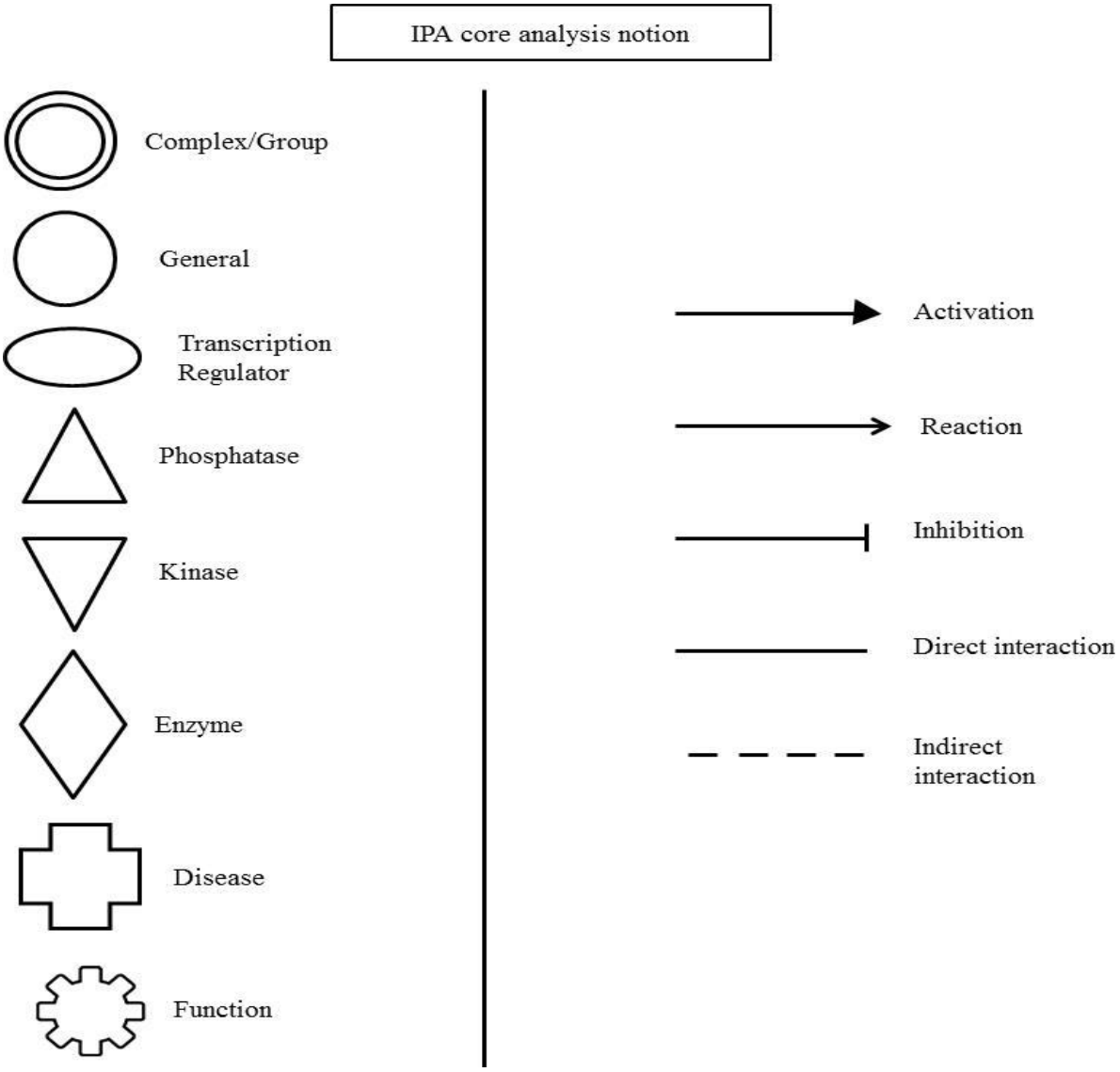

Figure 3.3: The annotation of IPA (Own figure)

3.10 Statistical analysis

Results for this study were analysed using Graph-Pad Prism 5 and expressed as means ± standard error of the mean (SEM) for at least three independent experiments. Significant differences were determined using one-way analysis of variance (ANOVA) followed by Tukey's Post Hoc test. A probability level of $p < 0.05$ was considered significant.

3.11 Diagrammatic summary of the research approach

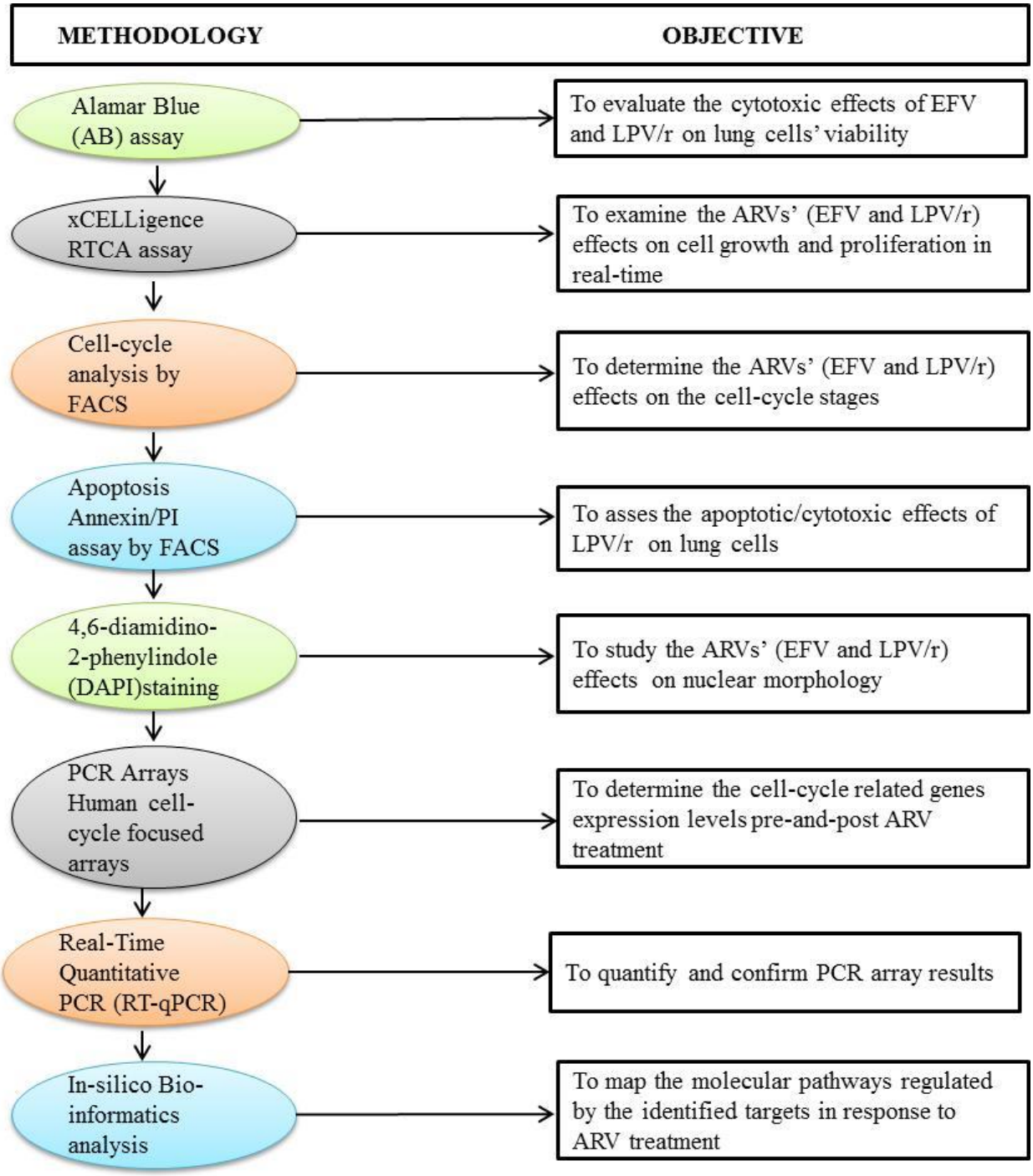

Figure 3.4: The flow-chart summarizing the research approach.

CHAPTER 4: RESULTS

4.1 Introduction

This chapter is presented in two sections, firstly describing the cellular analyses, followed by the molecular and Bio-informatics analyses. The cellular based approach was employed to elucidate the potential cytotoxic effects of ARVs in lung cancer, using *in vitro* cell culture models. To achieve this, Alamar blue (AB) assay, xCELLigence RTCA assay, FACS analysis of the cell-cycle and apoptosis and DAPI staining demonstrated that EFV and LPV/r drug treatment affected cellular health by stimulating either proliferative effects at low doses or anti-proliferative and cytotoxic effects at high doses. These changes in cellular homeostasis post-ARV treatment led to an investigation of the underlying associated molecular and bio-informatics basis of these effects. For this purpose, an evaluation of a focused panel of human cell-cycle related genes pre-and-post ARV treatment showed up-regulation of proliferation inhibitory genes, such as p21 and down-regulation of cyclin/CDK complexes, which drive the cell-cycle progression. The interrogation of gene expression using *in silico* bioinformatics analysis tools, including STRING, DAVID, Reactome and IPA, indicated this to be coupled with the induction of DNA damage response pathways in response to ARV treatment. This proposed DNA damage correlates with the observed changes in nuclear morphology, cell proliferation and death. These results are presented in detail below.

4.2 The Effects of Efavirenz (EFV) and Lopinavir/Ritonavir (LPV/r) on Lung Cancer

4.2.1 Alamar blue (AB) cell viability assay

As previously described, the physiological reduction of the Alamar Blue (AB) dye was used here to quantitatively measure both cell proliferation and viability of MRC-5 and A549 cells pre- and post ARV (EFV and LPV/r) drug treatments.

(i) Efavirenz (EFV) treatment

The reduction of AB was monitored in real-time at 24h intervals (24h, 48h and 72h) and measured spectrophotometrically at 540nm and 630nm. Figure 4.1 and Figure 4.2 illustrate percentage reduction of AB in response to EFV for MRC-5 and A549 cells, respectively. As represented in Figure. 4.1, 4µM EFV did not significantly change cell viability over a 24h to 72h treatment period. However, at 13µM, indicated by the blue box, both cell proliferation and viability increased over 24 to 72h. In contrast, at higher doses, both 26µM and 50µM EFV treatments had anti-proliferative effects on the MRC-5 cells, as indicated by a decline in the percentage reduction of AB over 24 to 72h. Based on this analysis, 13µM EFV would seem to be the most physiologically relevant dose.

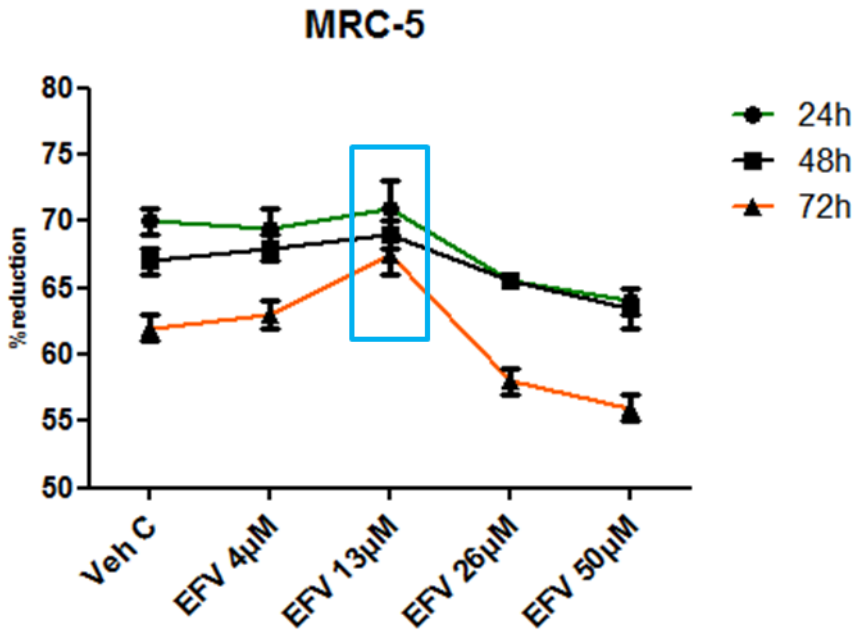

Figure 4.1: The percentage (%) of AB reduction representing the MRC-5 cell viability. The results indicate treated relative to vehicle treated or control cells. Following EFV treatment, 1% (at 24h), 2% (at 48h) and 5% (at 72h) increase in AB % reduction was observed. There is no statistical significance observed, with $p > 0.05$. The blue box indicates the most relevant physiological dose.

With regards to the A549 cells (see Figure. 4.2) a concentration of 4µM EFV had no significant change in AB % reduction at 24h and 72h; but with a slight decrease at 48h. An

increase in cell proliferation was demonstrated by the 13µM EFV treated cells across all three time periods. This was then followed by a slight decline in cell viability at 26 and 50µM EFV at 24h to 72h. A further decrease in cell viability (AB % reduction) was observed irrespective of the time period.

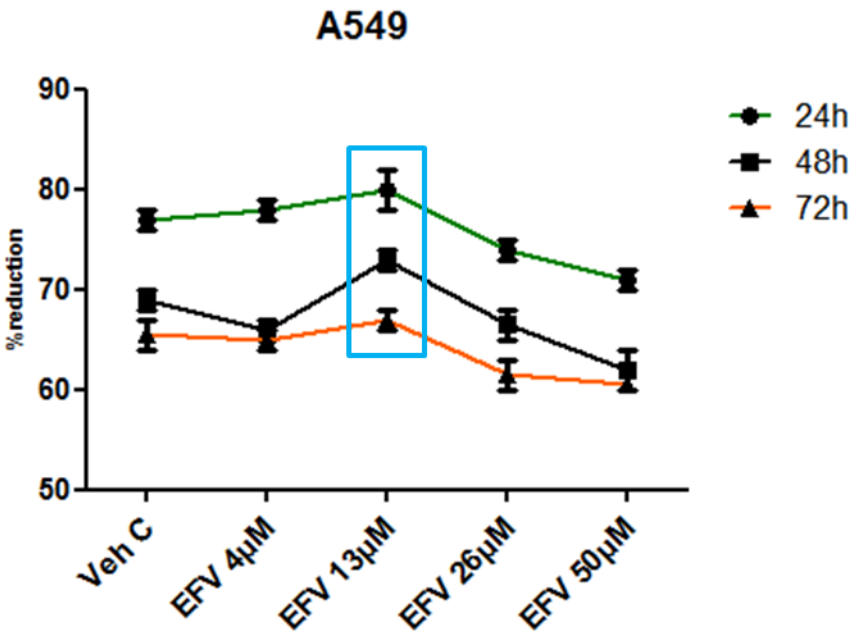

Figure 4.2: The A549 cell viability in response to the EFV drug treatment. The percentage (%) of AB reduction indicates treated relative to vehicle treated or control cells over 24h, 48h and 72h. Three percent (at 24h), 4% (at 48h) and 2% (at 72h) increase in cell proliferation was seen. The increase was not statistically significant with $p > 0.05$. The blue box indicates the most relevant physiological dose.

(ii) Lopinavir/ritonavir (LPV/r) treatment

Cell proliferation and viability following LPV/r treatment is shown in Figure 4.3 and Figure 4.4 for each of the MRC-5 and A549 cell lines, respectively. When compared to the vehicle (veh) control cells, the 10µM LPV/r treatment, was shown to have an increased proliferation, while at 32µM there was a slight but insignificant drop in cell proliferation. At each of 50µM

and 80µM LPV/r, there was an evident decline in cell viability in MRC-5 cells (see Figure 4.3).

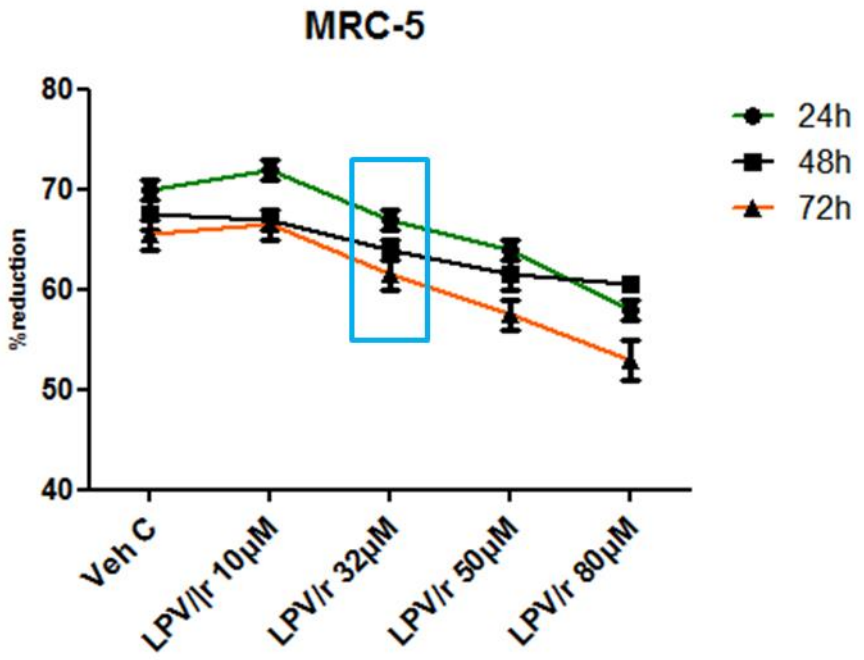

Figure 4.3: The MRC-5 cell viability in response to LPV/r drug treatment relative to vehicle treated cells. This is indicated by AB % reduction over a time period of 24h, 48h and 72h. An overall decrease of ~3% in AB% reduction is observed from 24h to 72h. This decrease is however, statistically insignificant, with $p > 0.05$. The blue box indicates the most relevant physiological dose.

A change in AB % reduction was observed following treatment with a range of LPV/r concentrations (see Figure 4.4). At 10µM, LPV/r treatment was observed to exert an apparent proliferative effect on the cells, compared to the (veh control) cells. A decline in AB % reduction was observed on the 32µM LPV/r treated cells at all three time points. Treatment with both 50µM and 80µM LPV/r had an anti-proliferative effect on the A549 cells, as indicated by the decreased AB % reduction.

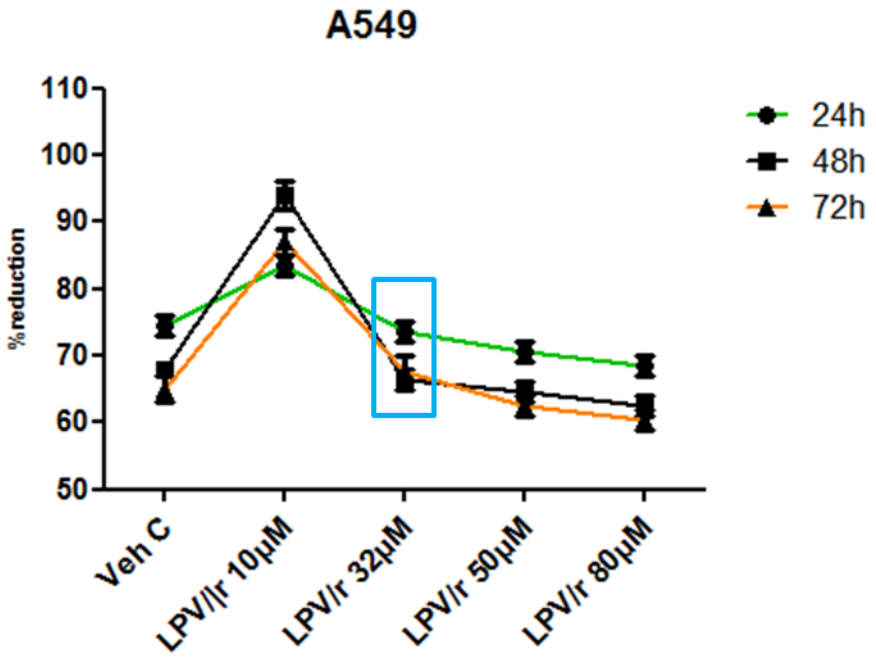

Figure 4.4: The representation of the A549 cell viability in response to the LPV/r cytotoxic effects, at 24h, 48h and 72h. The blue box indicates the most relevant physiological dose, and effects on cell viability are statistically insignificant, with $p > 0.05$.

The mean steady-state peak plasma concentration (Cmax) is the most physiologically relevant concentration for the ARVs because it represents naturally occurring concentrations of the drugs following their intake (Drug Information SUSTIVA® Gilead Sciences 2010); (Drug information, KALETRA® Abbott laboratories, 2010), hence, Cmax was used for subsequent experiments.

4.2.1.1 EFV and LPV/r drug treatment affect cell viability

AB was used to evaluate MRC-5 and A549 cell viability treated with EFV and LPV/r relative to vehicle control cells. The experiment was conducted three independent times in triplicate and the results were spectrophotometrically analysed. The percentage (%) reduction (which is

proportional to cell viability) quantified in treated *versus* vehicle control cells varied with different drug concentrations, but not in a time-dependent manner. In particular, EFV at 13µM was shown to drive cell proliferation in both normal and cancerous cells at all three time points (Figure 4.1 and Figure 4.2). However 4µM EFV did not have significant effects on cell growth and proliferation. On the contrary, at higher concentrations of either 26µM or 50µM, EFV had anti-proliferative effects on the cells at 24h, 48h and 72h, respectively. Thus, the plasma relevant doses (4 and 13µM) of this NNRTI seem to favor cell proliferation, while raised levels (26 and 50µM) EFV exhibited anti-proliferative effects on the cells. Interestingly, similar pro- and anti-proliferative effects were observed with LPV/r treatment. At 10µM, LPV/r favoured cell proliferation, while at higher doses (32, 50 and 80µM) cell proliferation was inhibited, (Figure 4.3 and Figure 4.4). Overall, LPV/r treatment was demonstrated to exert significant anti-proliferative effects, not only on normal lung epithelial cells, but also on the A549 cancerous cells. Both EFV and LPV/r effects on lung cell viability was not statistically significant, with $p > 0.05$.

4.2.2 Real Time Cell Impedance Analysis (RTCA) of EFV and LPV/r Treatment on MRC5 and A549 cells

In the present study, the RTCA xCELLigence (ACEA Biosciences) instrument was used to assay in real time the cytotoxic effects of EFV and LPV/r on MRC-5 and A549 cell proliferation, cell viability and cell death. Prior to assessing drug effects, the optimum seeding cell density was determined for each cell line, (see Figure 4.5 and Figure 4.6). Once this was optimized, ARV drug treatment was administered 24h post seeding.

4.2.2.1 Cell titration assays for optimal seeding densities

This was done to determine the optimum cell density to seed prior to ARV drug treatment. Different titration curves were plotted for MRC-5 cells and for A549 cells, as these are two different cell lines in regard to size, shape and morphology. The cell index (CI) value, which

increases with increasing (attached) cell proliferation, was predetermined using the titration assays for both MRC-5 and A549 cells. For comparison purposes in response to ARV drug cytotoxicity, the CI values for both the cell-lines were plotted in a similar range.

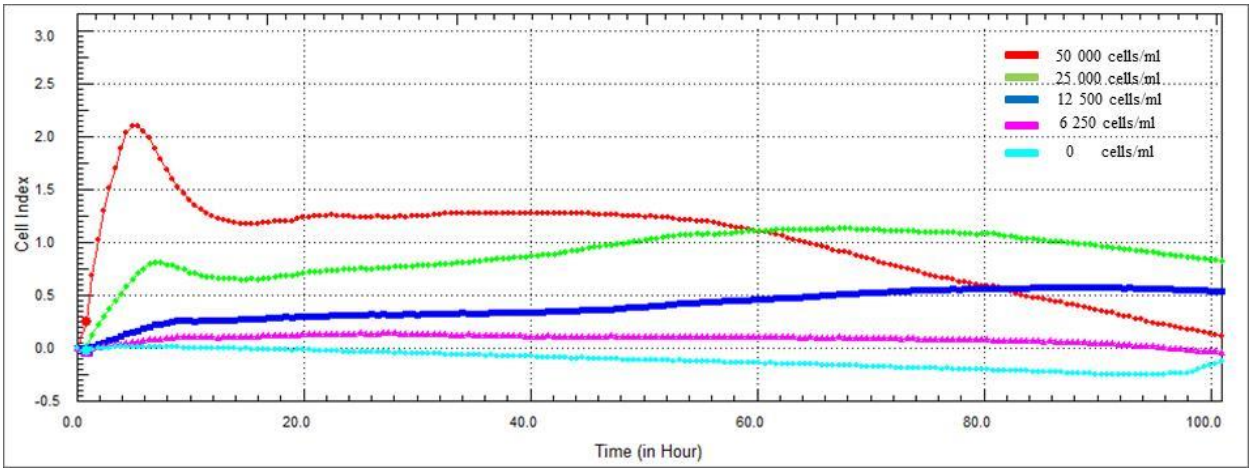

Figure 4. 5: MRC-5 cell titration, represented by Cell Index *versus* Time. A series of 2 fold dilutions was performed, wherein 30 000 cells/ml were selected as optimal for seeding, as recommended by the manufacturer. Cell index (y-axis) should at least be between 0.5 and 1, 24h after seeding, prior to drug treatment.

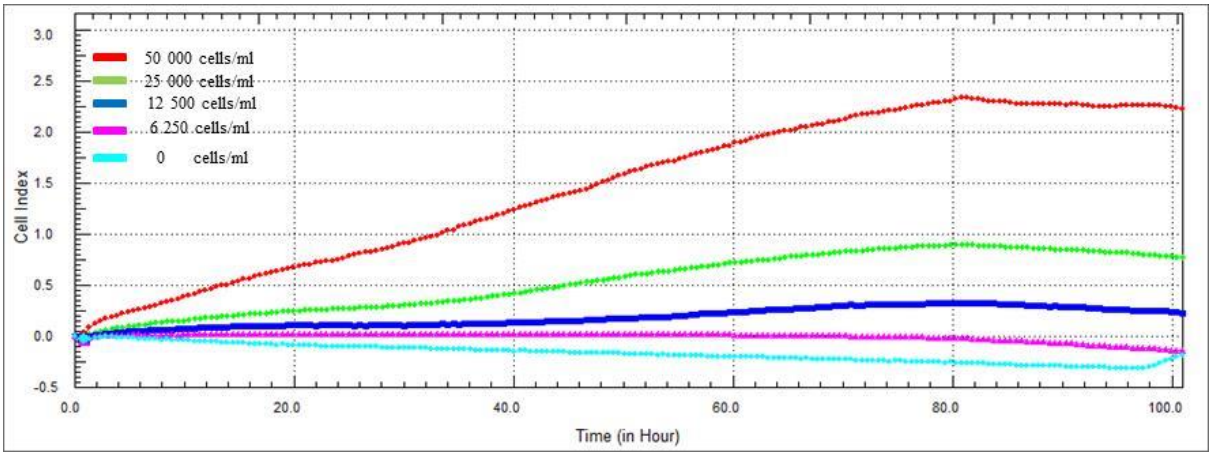

Figure 4.6: A549 cell titration, represented by the Cell Index *versus* Time. A series of 2 fold dilutions was done. Since the cell index should be between 0.5 and 1 post 24h seeding, 50 000 cells/ml were demonstrated to be the optimum seeding density for the A549 cells.

4.2.2.2 RTCA analysis of cytotoxicity

The potential cytotoxic effects of EFV and LPV/r on the MRC-5 and A549 cells were determined using RTCA assays. This was achieved by plotting the growth curves as a function of cell index (normalized to 1) *versus* time (h) over a period of approximately 100h. Since the cell index is proportional to cell viability, the greater the cell index the greater the cell viability. Based on the AB preceding data, three of the four ARV concentrations were further selected for cytotoxic, cell viability and proliferation using RTCA. Both cell lines were treated with EFV (4, 13, 50µM) and LPV/r (10, 32, 80µM).

To further analyse the effects of EFV and LPV/r on cell proliferation and cell death in a time dependent manner, the slope function of the curve was used. This function describes the steepness, incline, gradient or changing rate of a curve within the given time period; and provides a measure for parameters of cell proliferation, cell adhesion, receptor activation, cytotoxicity or other cell based assays. Here, the slope function was used to determine the rate of change of the cell index (CI) or normalized cell index (NCI) for the cells following drug treatment. The slope incline is proportional to the cell index.

4.2.2.3 Dose response profile of MRC-5 and A549 cells to EFV and LPV/r drug treatment

i) EFV treatment response in MRC5 and A549 cells.

a) MRC5 cell response to EFV

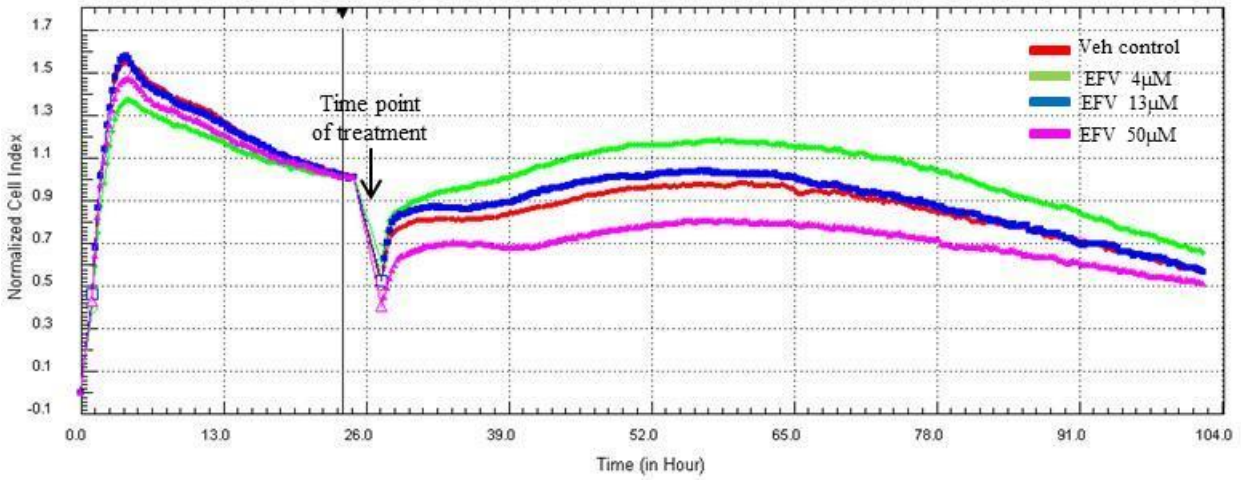

Figure 4. 7: MRC-5 cell growth curves treated with each of 4µM, 13µM and 50µM EFV. The curves were plotted relative to the vehicle control.

With reference to Figure 4.7, following treatment at 24h, all MRC5 cells whether treated or vehicle control with EFV continued to proliferate. In addition, cells treated either with 4µM or 13µM EFV proliferated and grew more than vehicle control cells. In contrast, 50µM treated cells, had a decreased cell proliferation.

In plotting the slope function, an indication of cell detachment/cell death, in MRC-5 cells, an increase in cell proliferation and growth was observed for EFV at 4µM, and particularly for 13µM, after 24h of treatment (see Figure. 4.8). A steady decline in cell proliferation was noted at 48h and was more evident at 72h. On the contrary, for 50µM EFV, a slight increase in cell proliferation and growth was observed at 24h, with further growth at 48h; and a steep decline in cell proliferation at 72h (Figure 4.8).

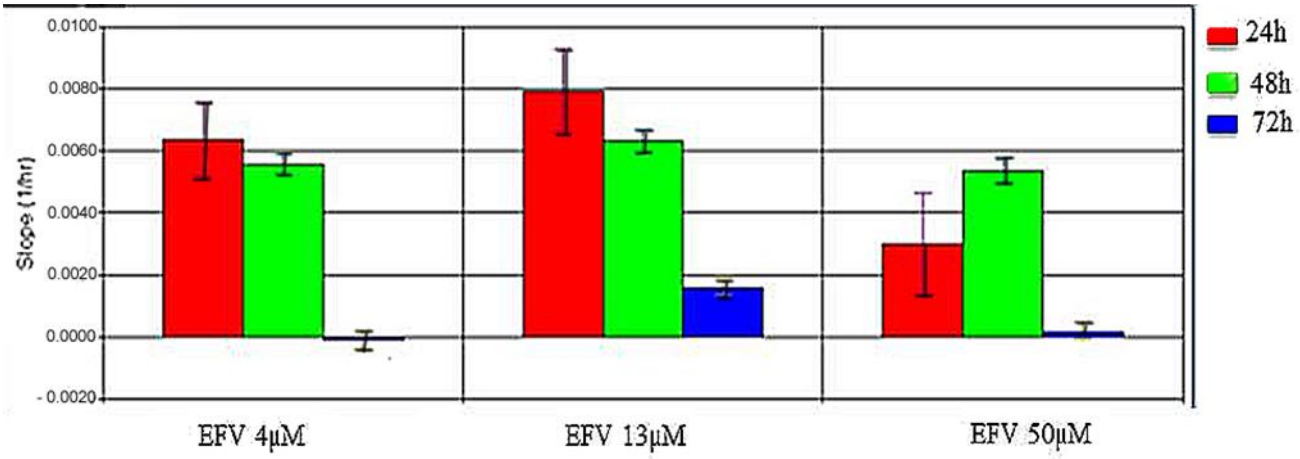

Figure 4.8: The slope function of MRC-5 cells representing the response to EFV treatment, Over 24h time intervals, this plot represents the rate of cell detachment, and thus cell death for each of the three drug concentrations.

(b) A549 cell response to EFV

After 24h of growth, the vehicle control A549 cells grew and proliferated steadily, compared to the treated cells, which continued to proliferate and grew for a further 40h prior to a decrease in cell viability (see Figure. 4.9 below). Conversely, cells treated with 50µM EFV proliferated slowly compared to the vehicle control cells, indicating an anti-proliferative effect of 50µM EFV on the A549 cells (Figure 4.9).

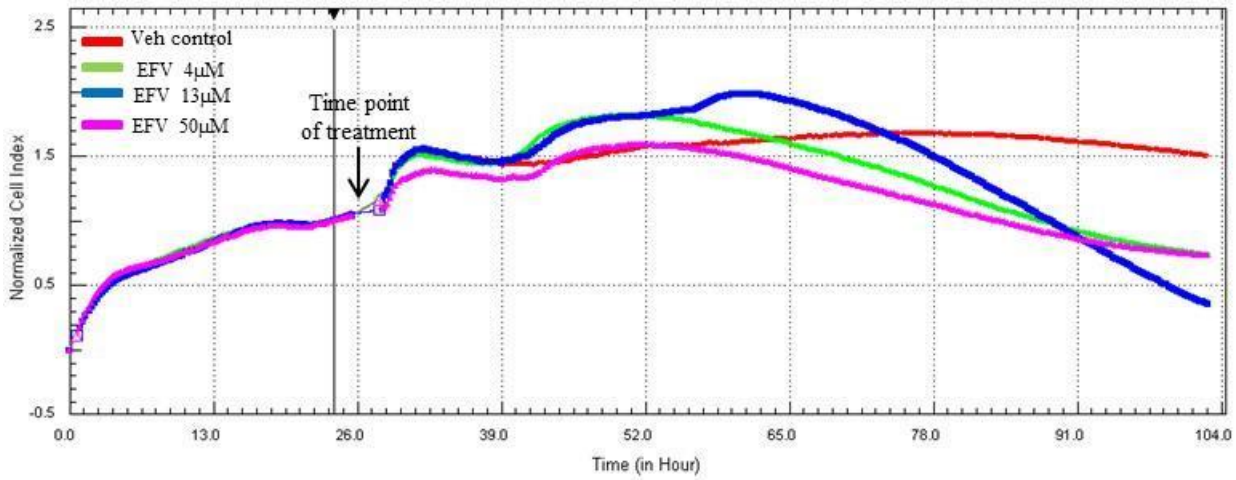

Figure 4.9: Growth curves representative of A549 cells treated with 4µM, 13µM and 50µM EFV, respectively. The curves were monitored and plotted relative to the vehicle control.

The slope function plot for cell response to EFV reflected a slight increase in cell proliferation for 4µM after 24h of treatment (see Figure 4.10). However, a steady increase in cell proliferation and growth was shown for each of the 13µM and 50µM treatments after 24h. At 48h there was decreased cell proliferation, with a sharp decline at 72h in cell viability for the three drug concentrations (Figure 4.10).

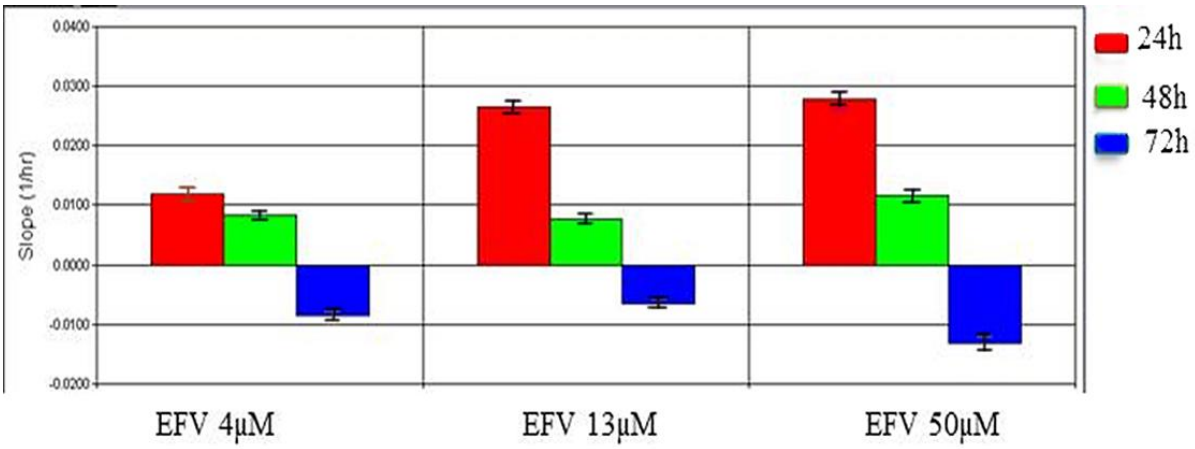

Figure 4.10: The slope function representing the response of A549 cells to EFV drug treatment at 24h time intervals.

ii) LPV/r treatment response

a) MRC-5 cell response to LPV/r

Cell growth and proliferation of LPV/r treated cells relative to vehicle control was monitored over a 72h period. The MRC-5 vehicle control cells continued to grow and proliferate steadily, compared to 10µM treated cells which proliferated at an increased rate (see Figure. 4.11). However, at a concentration of 32µM the cells neither increased nor decreased their proliferation, this being a particular characteristic of cell-cycle arrest. On the other hand, 80µM of LPV/r was clearly cytotoxic to the cells, indicated by an abrupt peak of the normalized CI immediately after drug treatment, followed by a rapid decline in cell viability (see Figure. 4.11 below).

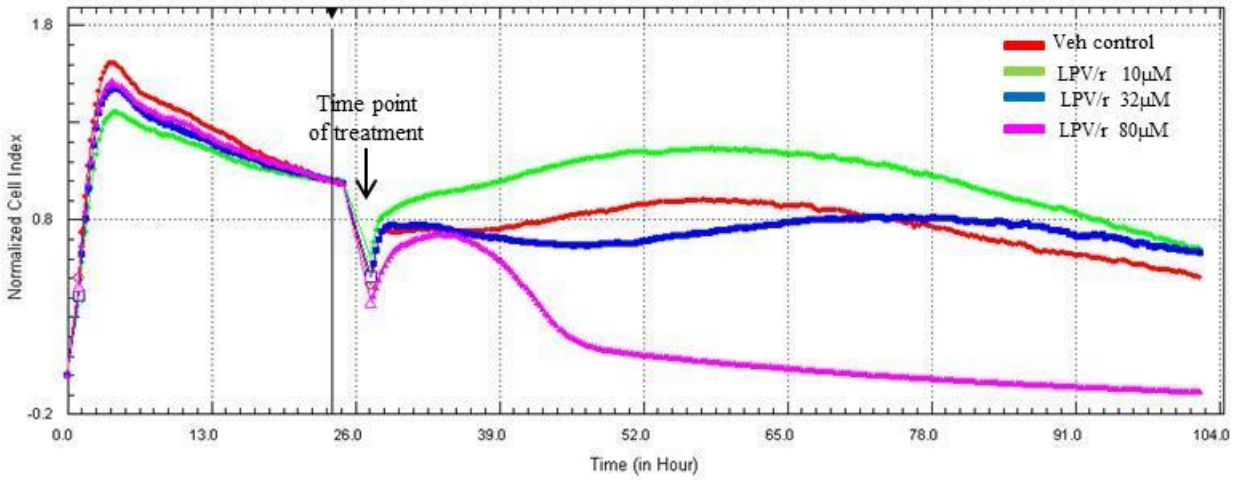

Figure 4.11: MRC-5 growth curves representing cells treated with 10µM, 32µM and 80µM LPV/r. The curves represent the normalized cell index (NCI) which is proportional to cell viability *versus* time (hours).

The slope-function plot reflected the growth trends of the real time growth curves (refer to Figure 4.12 below). With drug treatment, the cells continued to grow steadily after 24h and 48h periods, followed by a decline in cell viability after 72h for 10µM LPV/r. At 32µM, a slight decrease in cell viability subsequent to drug treatment was observed at 24h, followed by a slight incline in cell proliferation at 48h; and this remained steady even after 72h of culture.

At 24h following 80µM LPV/r treatment, a marked decline in cell viability was observed, with decreased cell viability persisting at 48h and 72h.

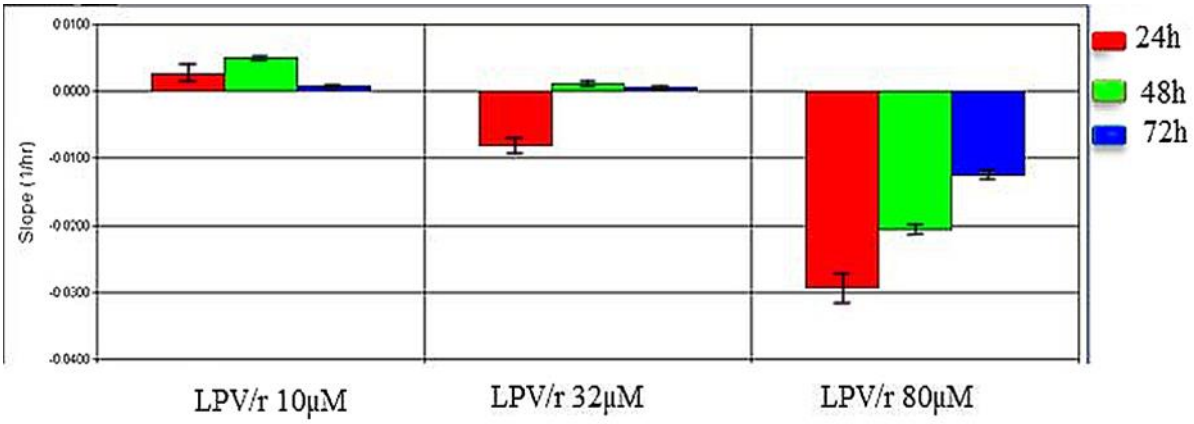

Figure 4.12: The slope function demonstrating MRC-5 cell response to LPV/r drug treatment, monitored at 24h intervals.

b) A549 cell response to LPV/r

The A549 cells were monitored before and after drug treatments at 24h post seeding (refer to Figure 4.13). When compared to the control cells, 10µM and 80µM treated cells showed a proliferative effect, followed by a rapid decline in cell viability. The 32µM treated cells in contrast, displayed a cell-cycle arrest (observed from the time point of treatment), after which there was decreased cell viability (Figure. 4.13).

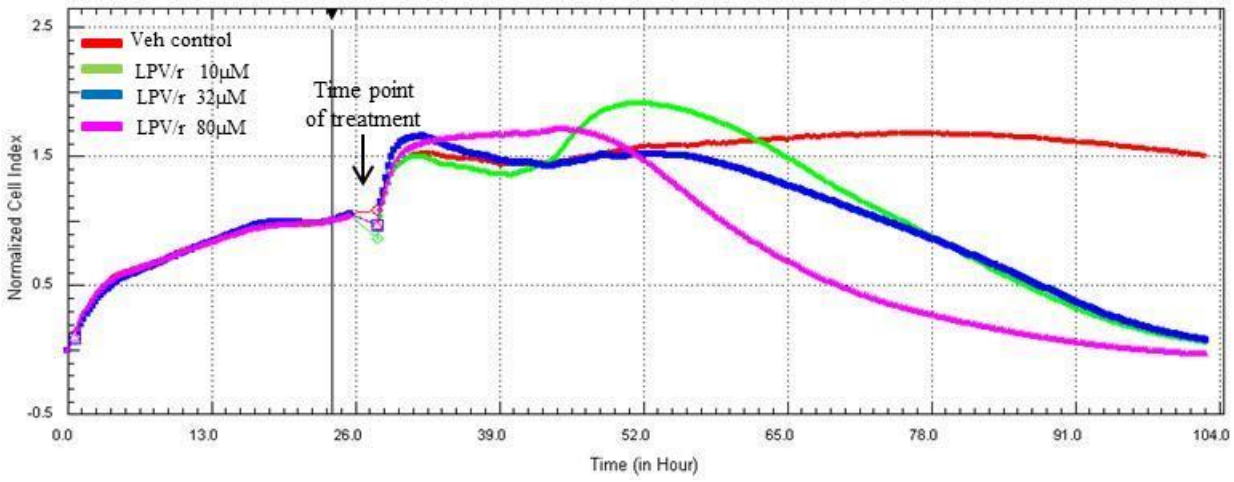

Figure 4.13: Growth curves for A549 cells treated with 10µM, 32µM and 80µM LPV/r in relation to the vehicle control cells. The curves were plotted as a function of normalized CI *versus* time.

The slope function plot for cell response to LPV/r revealed an apparent increase in A549 cell proliferation for 10µM LPV/r at 24h, while there is a decline for 32µM LPV/r and an increase in proliferation for 80µM LPV/r (figure 4.14). There is a consistent decrease in cell viability for 32µM treatment even after 48h and 72h. An abrupt decline in cell viability is observed at 48h and 72h, for 32µM LPV/r treated cells, and particularly observed in 80µM treatment.

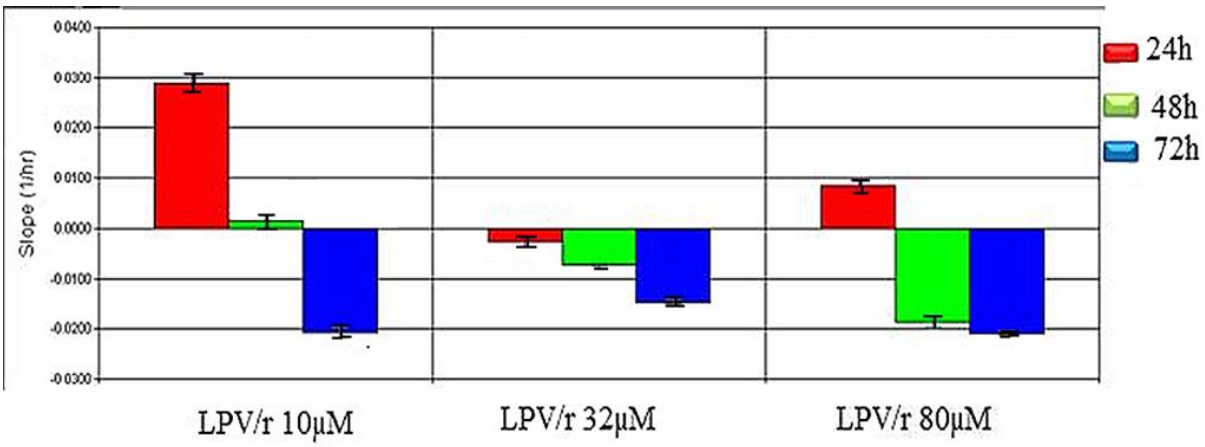

Figure 4.14: A slope function bar graph representing A549 cells treated with LPV/r at 24h intervals.

4.2.2.4 RTCA demonstrates the pro-and-anti-proliferative effects of EFV and LPV/r

The label-free RTCA analysis as measured by the xCELLigence instrument corroborated the results of the Alamar Blue assays. The RTCA very precisely, evaluated the cytotoxic effects of EFV and LPV/r on MRC-5 and A549 cells, assessing cell viability in real-time. This assay was particularly sensitive to and indicative of the window period of the drug efficacy. This was reflected by the growth curves and further analysed by the slope function, showing the associated decline in CI, and therefore in cell viability.

At lower concentrations EFV had the effect of stimulating cell proliferation in both the MRC-5 and A549 cells, this relative to vehicle control cells. Subsequently, proliferation (CI) decreased at higher concentrations with cellular detachment from the culture substrate occurring.

However, notably, while there was no clear distinction here in the growth and proliferation patterns between treated and vehicle control cells, there were nevertheless observed decreases and increases in the proliferation rates between the vehicle control and treated cells. This finding suggests that although EFV treatment does seem to influence cell proliferation it does not necessarily alter cellular health.

Similar to EFV, LPV/r at low concentrations stimulated cell proliferation in both MRC-5 and excessively in A549 cells, followed by cell death. An intermediate dose, caused cell-cycle arrest in both cell types, while high concentrations led to an increase in cell death, preceded by increased cell proliferation.

The following research approach further interrogates the effects of ARVs on the cell-cycle by fluorescence activated cell sorting (FACS).

4.2.3 Cell-cycle Analysis by Fluorescence-Activated Cell Sorting (FACS)

Since RTCA analysis demonstrated some effects of ARVs on the cell-cycle, flow cytometry was next employed to quantify DNA content and thus the particular cell-cycle stage of treated cells, relative to vehicle control cells. Here, the scope of this analysis was to determine the regulatory effects of ARV's on the cell-cycle in lung cells.

4.2.3.1 Cell-cycle analysis of EFV and LPV/r treated cells by flow cytometry

Prior to ARV (EFV and LPV/r) drug treatment and cell-cycle analysis, cells were serum-starved overnight to synchronise the cell-cycle at G0/G1. Results are a representation of at least three (3) independent experiments, represented as histograms and bar graphs. Data is expressed as mean ± SEM. (For supplementary data, see appendix C3).

(a) Cell-cycle analysis of MRC-5 cells treated with EFV

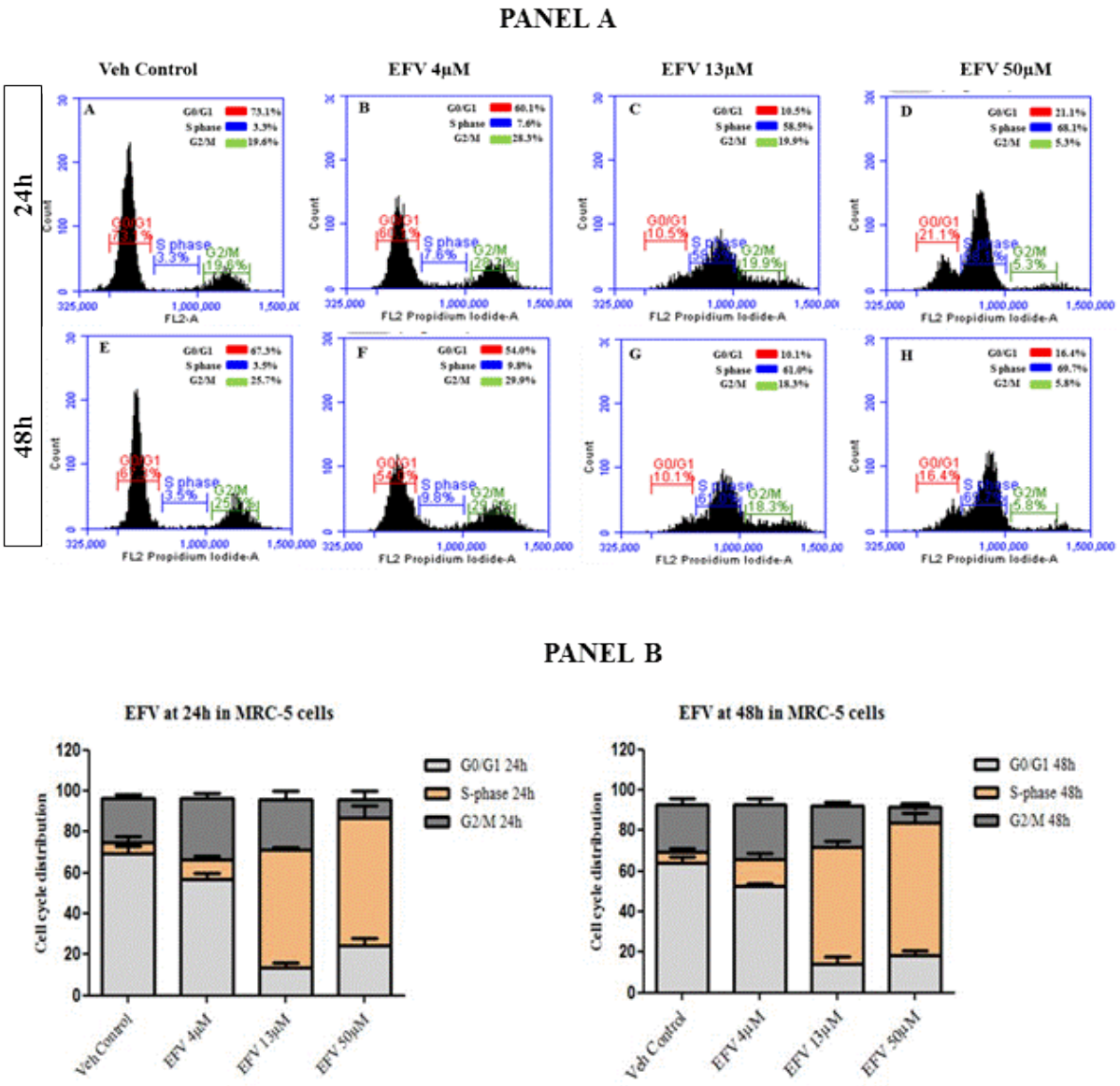

Figure 4.15: **PANEL A**- FACS analysis of the cell-cycle stages in MRC-5 cells treated with (4, 13 and 50 µM) EFV for 24h (A to D) and 48h (E to H), respectively. Vehicle control and drug treated cells (4, 13 and 50µM EFV) were stained with propidium iodide and their DNA content measured using flow cytometry An increase in S-phase is observed with 13µM EFV (C and G) and 50µM EFV (D and H), while there was a slight increase in the percentage of cells in G2/M in 4µM EFV treated cells (B and F), compared to vehicle control cells (A and E).

PANEL B- Bar graphs representing cell-cycle distribution relative to drug concentration at 24h and 48h, respectively. The increase in the proportion of cells in S-phase is evident from these graphs, this increasing with raised EFV concentrations, with $p < 0.01$ at both 24h and 48h compared to vehicle control cells. Error bars denote SEM.

(i) FACS analysis of EFV treated MRC-5 cells

About 73% of the control cells (vehicle control) were located in the G0/G1 phase of the cell-cycle, at both 24h and 48h. Relative to this, the percentage of cells in G0/G1 decreased with increased drug concentration at 24h, reducing to about 60% (4µM), 10.5% (13µM) and 21% at 50µM. At 48h however, 54% cells treated with 4µM were in G0/G1, before decreasing to 10% (13µM) and 16.4% (50µM). In association with this, the percentage of cells undergoing DNA synthesis in S-phase, began to increase, from 3% in (normal) control cells, to 7 to 10% (4µM), 60% (13µM) and peaking at about 70% (50µM), at both the 24h and 48h time points. While about 20% of control cells were in G2/M at 4µM EFV, this percentage increased to approximately 28 to 30% at 4µM EFV; and decreased again to 18-19% of cells at 13µM and further to about 5-6% of cells at 50µM EFV (see Figure 4.15).

(b) Cell-cycle analysis of A549 cells treated with EFV

PANEL A

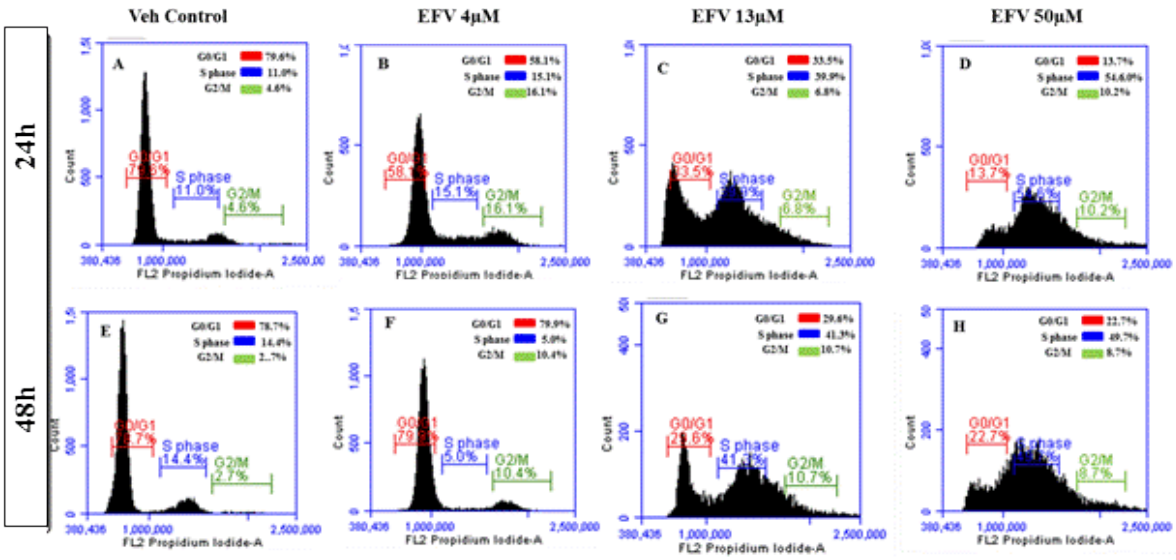

PANEL B

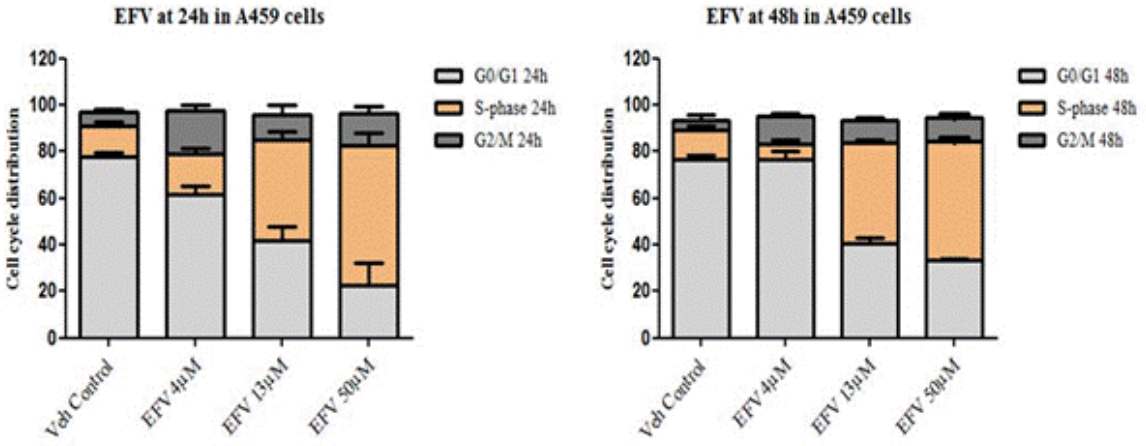

Figure 4.16: **PANEL A-** Histograms representing cell-cycle analysis of A549 cells treated with EFV. A to D represent 24h treatment, while E to H show 48h treatment. A clear induction of the S-phase is observed with 13µM and 50µM EFV treatments (C and G, D and H), while an increase in the G2/M is seen with 4µM EFV (B and F), compared to the vehicle control cells (A and E).

PANEL B- Bar graphs representing cell-cycle distribution in A549 cells relative to drug concentration at 24h and 48h, respectively. Vehicle control and drug treated cells (4, 13 and 50µM EFV) were stained with propidium iodide and their DNA content measured using flow cytometry. The concentration of the drug is proportional to the increase in S-phase, with $p < 0.05$ for 13µM and 50µM EFV treated at both time points. Error bars indicate SEM.

(ii) FACS analysis of EFV-treated A549 cells

Some 80% of the control cells (vehicle control) were located in the G0/G1 phase of the cell-cycle, at both 24h and 48h. Relative to this, the percentage of cells in G0/G1 decreased with increased drug concentration at 24h, reducing to about 58% (4µM), 33% (13µM) and 13% at 50µM. At 48h however, 80% cells treated with 4µM remained in G0/G1, before decreasing to 30% (13µM) and 22% (50µM). In relation to this, an increase in S-phase with increasing EFV dose is observed. This S-phase incline ranges from 11% (vehicle control) to 15% (4µM), to 40% (13µM), to 55 % (50µM) at 24h. This pattern is also seen at 48h, with an exception of 4µM treatment, with 80% of cells remaining at G0/G1. In addition, an increase of G2/M population at 4µM is observed at both time points, from 4.6% to 16.1% at 24h and 2.7% to 10% at 48h (see Figure 4.16).

(c) Cell-cycle analysis of MRC-5 cells treated with LPV/r

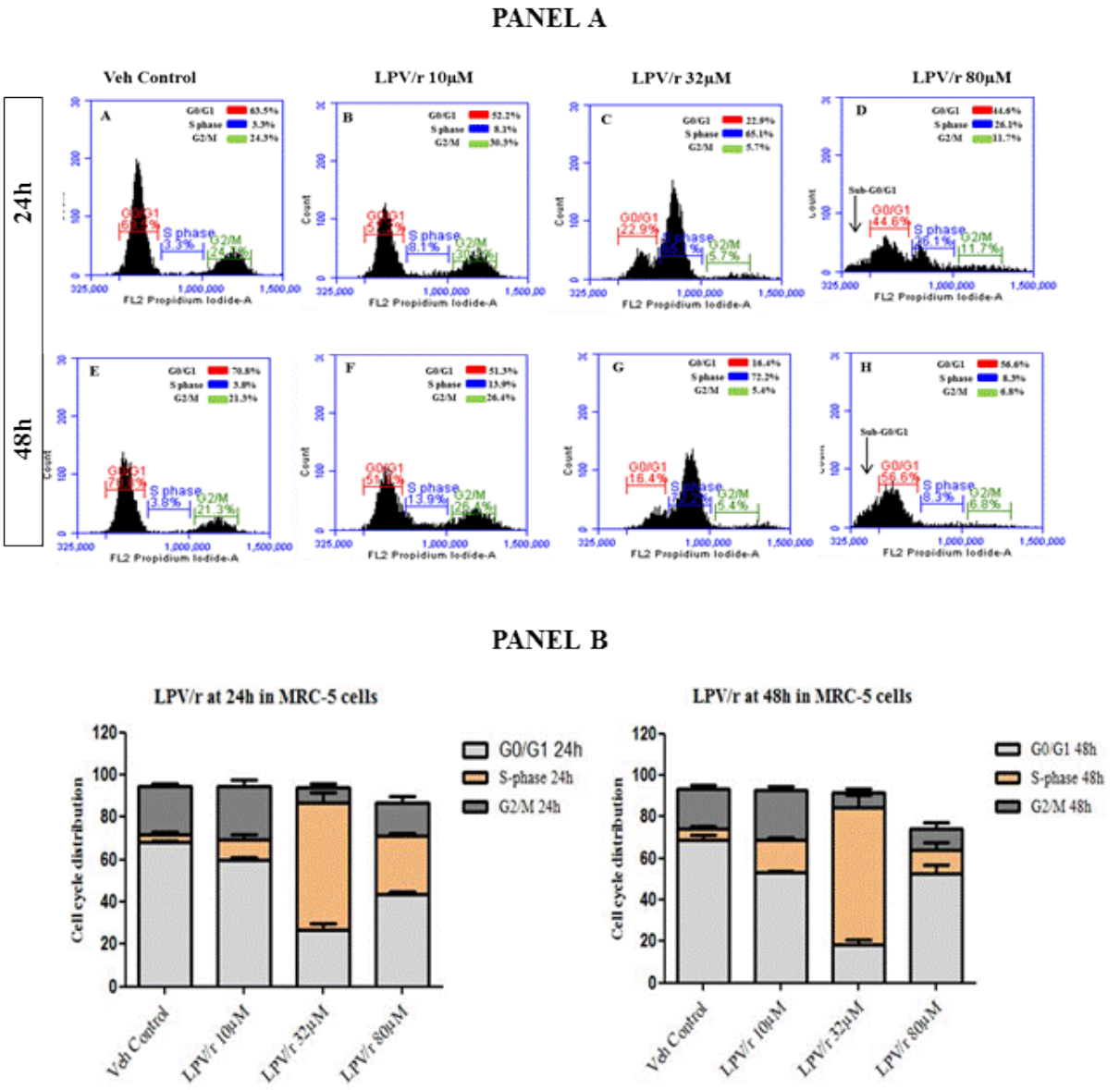

Figure 4.17: **PANEL A-** Histograms representing cell-cycle analysis in MRC-5 cells treated with LPV/r for 24h (A to D) and 48h (E to H). Vehicle control and drug treated cells (10, 32 and 80µM LPV/r) were stained with propidium iodide and their DNA content measured using flow cytometry. An induction of the S-phase arrest is seen at 32µM LPV/r treatment (C and G), with an increase in the percentage of cells in G2/M at 10µM LPV/r treatment (B and F); and a sub-G0/G1 population is observed with 80µM treatment (D and H).

PANEL B- Bar graphs representing cell-cycle distribution in MRC-5 cells relative to LPV/r concentration at 24h and 48h, respectively. Distinct interphases of the cell-cycle in response to LPV/r treatment in MRC-5 cells are represented here. S-phase arrest is observed at 32µM with $p< 0.01$ at 24h and $p< 0.01$ at 48h. LPV/r treatment, while 10µM LPV/r increased G2/M and decreased bars of 80µM LPV/r being attributed to the Sub-G0/G1 population, at 24h and 48h, this observation was not statistically significant. Error bars represent SEM.

(iii) FACS analysis of LPV/r treated MRC-5 cells

At 24h and 48h some 60-70% of the control cells (vehicle control) were located in the G0/G1 phase of the cell-cycle. Relative to this, the percentage of cells in G0/G1 decreased with increased drug concentration at both 24h and 48h, then reducing to about 51 to 52% (10µM) and 16-23% (32µM). However at the highest concentration (80µM), the percentage of cells in G0/G1 increased in the range of 45-57%. The percentage of cells in S-phase increased from approximately 3% at 24h and 48h in control cells to 65 and 72%, respectively at 32µM LPV/r. At 80µM LPV/r, the percentage of cells synthesizing DNA decreased markedly to 26% at 24h and 8% at 48h. For G2/M, the proportion of cells increased marginally from about 30% to about 20% at 24h and 48h at 10µM. After this at the higher concentrations, the cell percentages decreased to below those at the control levels, (see Figure 4.17).

(d) Cell-cycle analysis of A549 cells treated with LPV/r

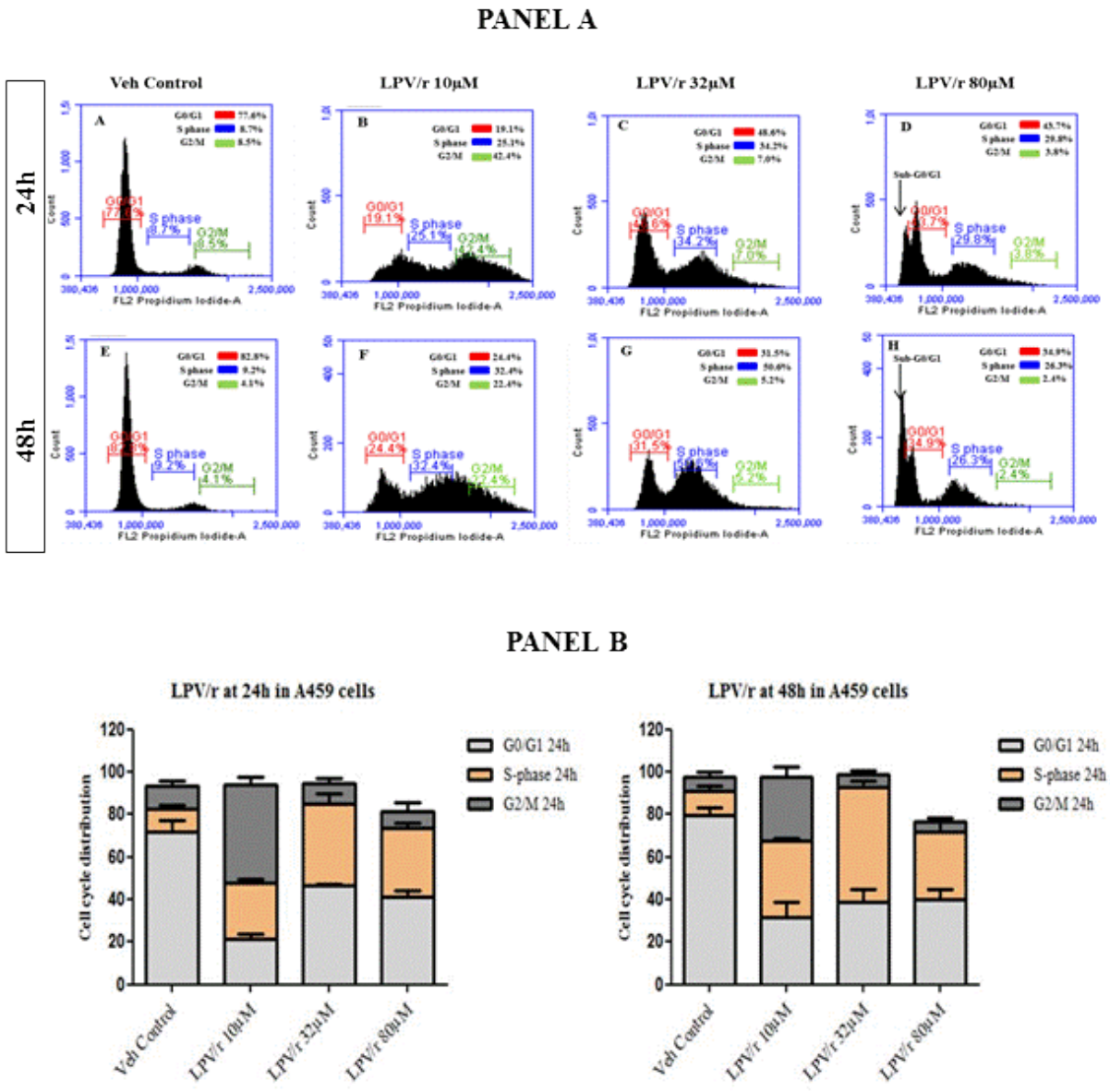

Figure 4.18: **PANEL A-** Histograms representing cell-cycle analysis in A549 cells treated with LPV/r at 24h (A to D) and 48h (E to H). Vehicle control and drug treated cells (10, 32 and 80µM LPV/r) were stained with propidium iodide and their DNA content measured using flow cytometry. An increase in the G2/M phase is seen with 10µM treatment (B and F), while 32µM (C and G) and 80µM LPV/r (D and H) induced S-phase arrest. A sub-G0/G1 population was observed with the 80µM LPV/r treatment.

PANEL B- Bar graphs representing distinct cell-cycle phases in A549 cells treated with LPV/r. The increase in S-phase was observed with increasing LPV/r concentrations, particularly with 32µM with $p < 0.05$. Ten micromolar LPV/r treatment in particular increased the G2/M populations, at both of the 24h ($p < 0.01$) and 48h ($p < 0.05$) time periods. Error bars denote SEM.

(iv) FACS analysis of A549 cells treated with LPV/r

After drug treatment, the percentage of cells in G0/G1 decreased from 78 and 82 %, to 19 and 24%, and increased in G2/M from 8 and 4% to 42 and 22% at 10µM LPV/r for the 24h and 48h time points, respectively; then at 32µM increasing again to about 49 and 32%, respectively; but with these percentages remaining in a similar range at 80µM for both time periods. The relative stability of these proportions at the upper concentrations of LPV/r signifies an S-phase arrest. A sub-G0/G1 population was detected in response to 80µM LPV/r, indicating cell-death (see Figure 4.18).

4.2.3.2 Both EFV and LPV/r alter the cell-cycle stages

FACS analysis more precisely determined the effects of the ARV drugs, EFV and LPV/r on cell-cycle stages. In summary, at low concentrations and at both time points the ARVs effectively stimulated an increased G2/M percentage in normal and cancerous cells. At higher concentrations, an S-phase arrest, which usually follows DNA damage, occurred. This results in cells with damaged DNA being unable to proceed to the G2 phase. Thus it would seem that at higher concentrations LPV/r causes irreparable DNA damage, potentially leading to apoptosis. At the maximum ARV concentrations used here, cell viability was reduced, leading to the detection of a sub-G0/G1 cell population. This ability of ARVs (LPV/r) to induce programmed cell death is further investigated below.

4.2.4 The effect of ARVs on apoptosis

Prior analyses in the present study demonstrated that of the two ARVs tested, LPV/r had cytotoxic effects on both the normal MRC-5 and cancerous A549 cells, whereas EFV in comparison did not seem to predispose cells to apoptosis. Further to this, the demonstration of a sub-G0/G1 population after LPV/r treatment prompted additional investigation of the cytotoxic/ apoptotic effects of LPV/r.

4.2.4.1 Induction of apoptosis by LPV/r

Following 32 and 80µM LPV/r drug treatments, FACS analysis using Annexin FITC and PI staining was used to quantify and analyse apoptosis in the lung cell lines. The experiment was done three times in triplicate (see appendix C for supplementary data); vehicle control and treated cells were labeled with both Annexin FITC and PI. The vehicle control -unstained cells were used as blank, vehicle control and stained cells (negative control), while Annexin-FITC single staining and PI single staining were used for compensation and setting up of quadrants. These results are represented in histograms and bar-graphs depicted below:

(a) Apoptosis in MRC-5 cells

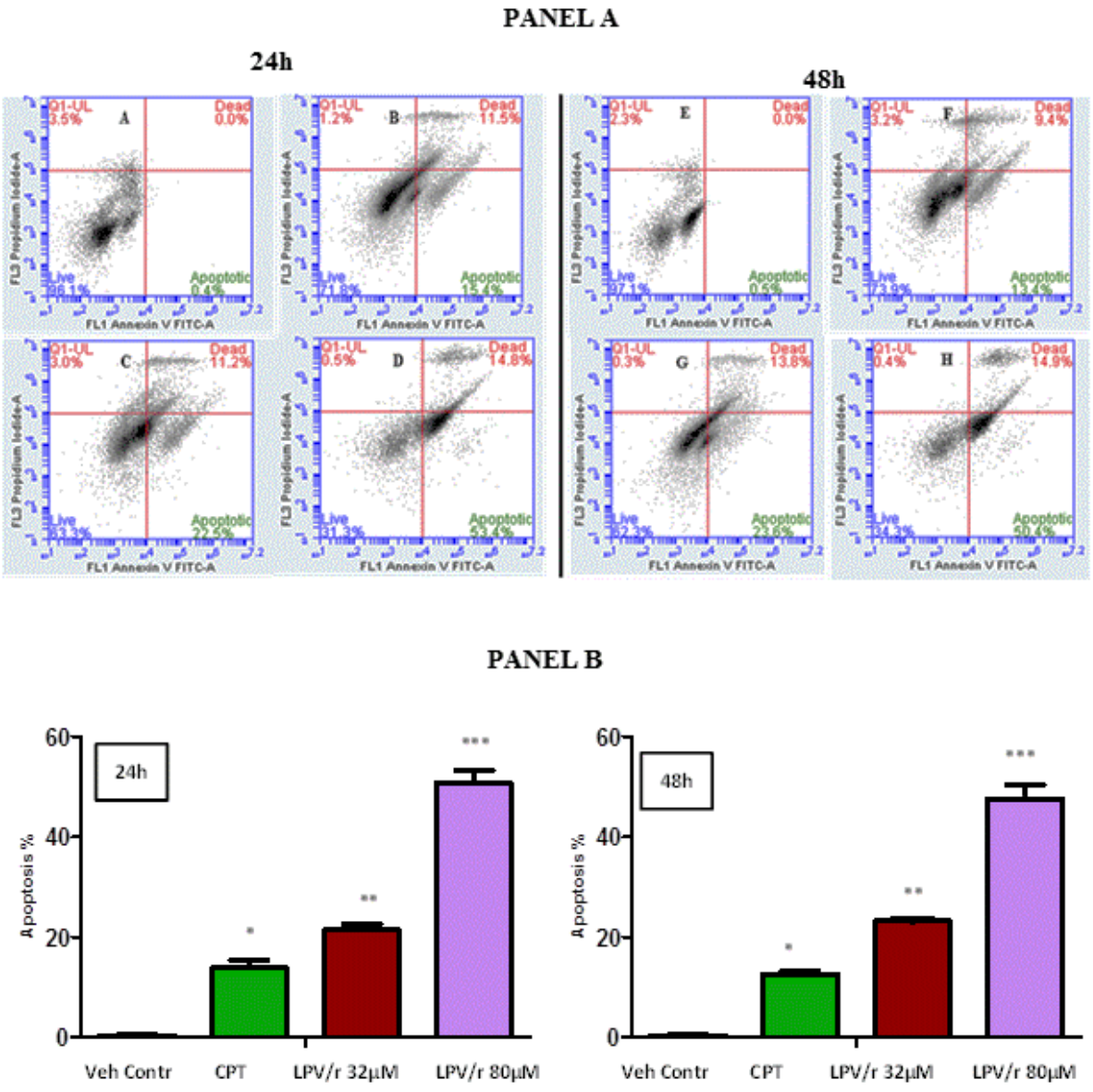

Figure 4.19: **PANEL A-** FACS analysis of MRC-5 cells treated with LPV/r at 24h and 48h. Histograms A to D represent 24h treatment, while E to H denote treatment at 48h. A and E represent vehicle (negative) control stained cells; B and F, camptothecin (CPT) (50µM) treated cells (positive control), C and G, cells treated with 32µM LPV/r; and D and H, cells treated with 80µM LPV/r. The apoptotic quadrant depicted at the lower right of each histogram denotes the percentage of cells undergoing early apoptosis, relative to the viable

population of cells (lower left) and the late apoptotic and/or necrotic cells (upper right quadrant).

PANEL B- Bar graphs representing percentage of apoptosis induction relative to drug dose in MRC-5 cells. The left panel represents apoptosis analysis at 24h; while the right panel represents apoptosis analysis at 48h. ANOVA and Tukey's multiple comparison tests were used to evaluate the significance of apoptosis in treated *versus* vehicle control cells. All three treatments show a significant increase in apoptosis percentage (%) compared to the negative (veh) control. Cells treated with 80µM displayed double and triple fold increases in apoptosis %, respectively [$p<0.001$ (***)], compared to 32µM LPV/r treated [$p<0.01$ (**)]; and CPT treated [$p<0.05$ (*)] cells. Error bar denotes SEM; *$p<0.05$; **$p<0.01$; ***$p<0.001$.

(a) A549 cells (apoptosis)

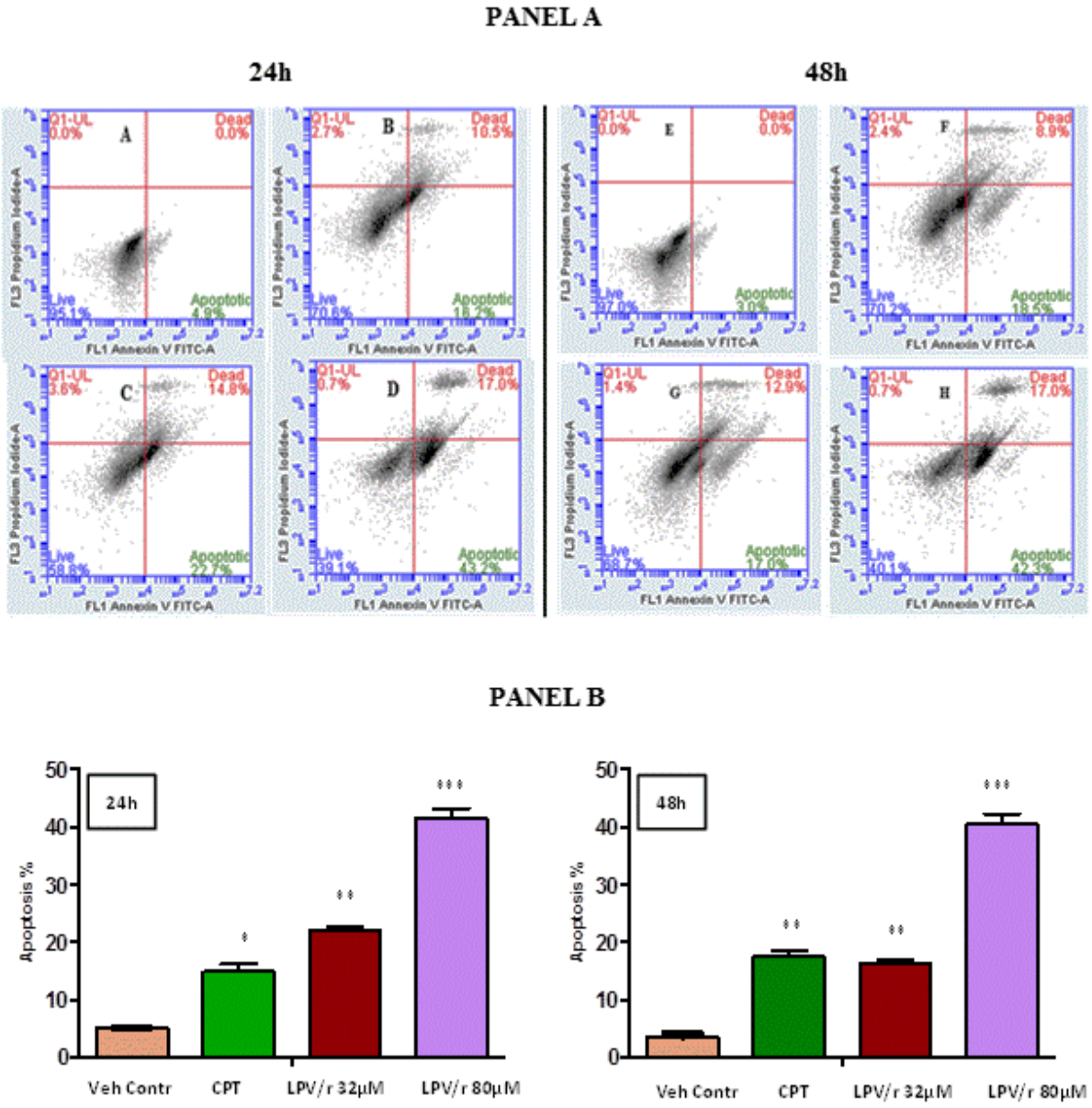

Figure 4. 20: **PANEL A-** FACS analysis of A549 cells treated with LPV/r at 24h and 48h. Histograms A to D represent 24h treatment, while E to H show treatment at 48h. A and E represent vehicle (negative) control stained cells; B and F, CPT (50µM) treated cells (positive control), C and G, cells treated with 32µM LPV/r; and D and H, cells treated with 80µM LPV/r. The apoptotic quadrant depicted at the lower right of each histogram denotes the

percentage of cells undergoing apoptosis, distinguished from a viable population of cells (lower left) and the late apoptotic and/or necrotic cells (upper right quadrant).

PANEL B- Bar graphs representing percentage apoptosis induction relative to drug treatment in A549 cells. The left panel represents apoptosis analysis at 24h; the right panel represents apoptosis analysis at 48h. Camptothecin (CPT) at 50µM was used as a positive control. Using ANOVA and Tukey's multiple comparison test, all three treatments effected a significant increase in apoptosis percentage (%) compared to the negative (veh) control. The 80µM treated cells demonstrated a consistent apoptosis percentage after 24h and 48h, ($p<0.001$). CPT and 32µM LPV/r showed a similar apoptotic effect, especially after 48h ($p<0.01$). Error bar denotes SEM; *$p<0.05$; **$p<0.01$; ***$p<0.001$.

4.2.4.2 LPV/r drug treatment induces cell death (apoptosis and necrosis) in a dose dependent manner

Both LPV/r concentrations, 32 and 80µM, induced apoptotic effects on normal and cancerous lung cells. The raised apoptotic percentage rate increased with LPV/r concentration. However, there was also a significant coupled cellular necrosis observed in both MRC-5 and A549 cells. Thirty-two µM LPV/r effected a slightly higher degree of apoptosis, compared to CPT treated cells (in both MRC-5 and A549 cells). At 80µM LPV/r treated cells had double the apoptosis percentage rate, compared to 32µM treated cells (Figure 4.19 and 4.20). Nevertheless the necrotic cell-death did not seem to increase with increasing LPV/r concentrations.

4.2.5 Evaluation of Nuclear Morphology before and after ARV treatment, using DAPI staining

To determine morphological and nuclear changes such as DNA fragmentation and chromatin condensation in MRC-5 and A549 cells in response to EFV and LPV/r, DAPI staining was used. This analysis is presented below, Figures 4.21 and 4.22.

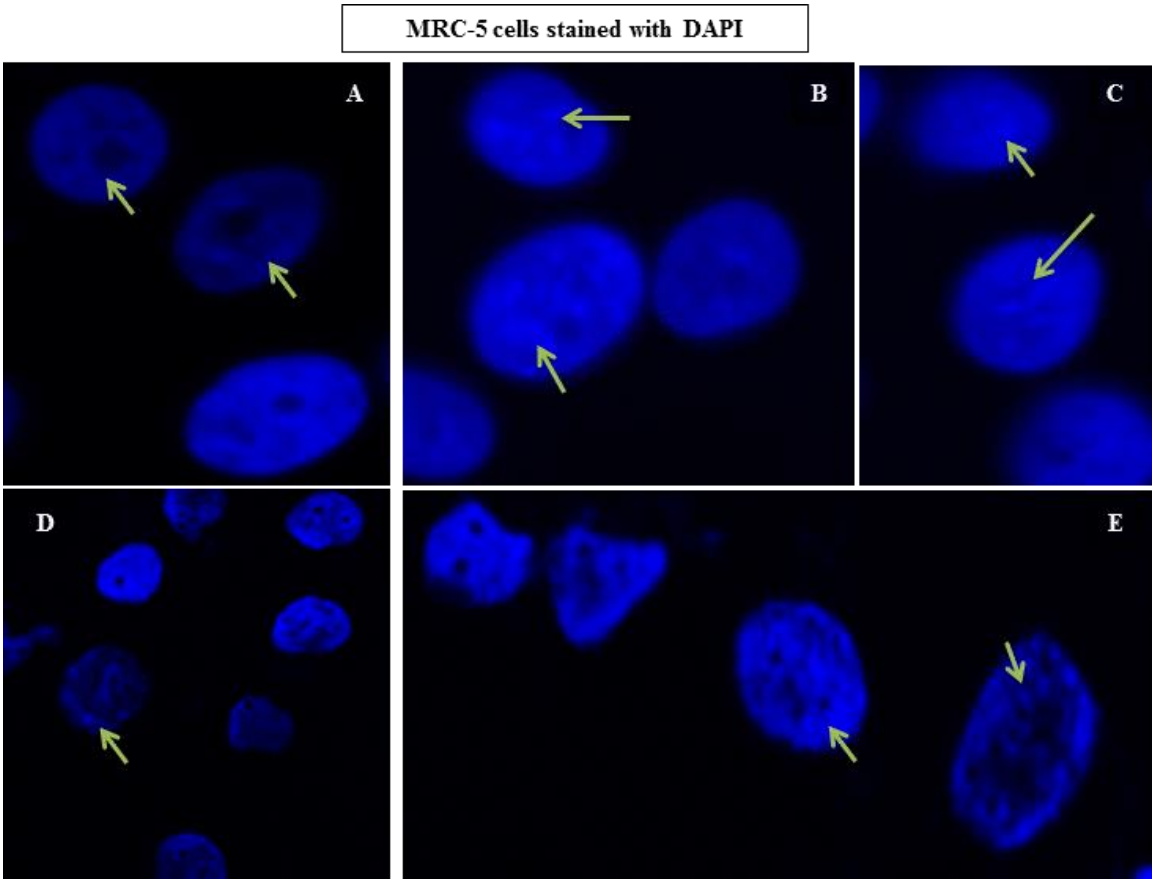

Figure 4.21: DAPI staining of MRC-5 cells. Changes in morphology were assessed in ARV drug treated relative to vehicle control cells. A represents vehicle control cells, B and C show MRC-5 cells treated with 13µM and 50µM EFV. D and E illustrate LPV/r treatment at 32µM and 80µM.

Green arrows point to changes in the nucleus such as DNA fragmentation and chromatin condensation in ARV drug treated (B to E) relative to vehicle control cells (A) (Original Magnification, 63X).

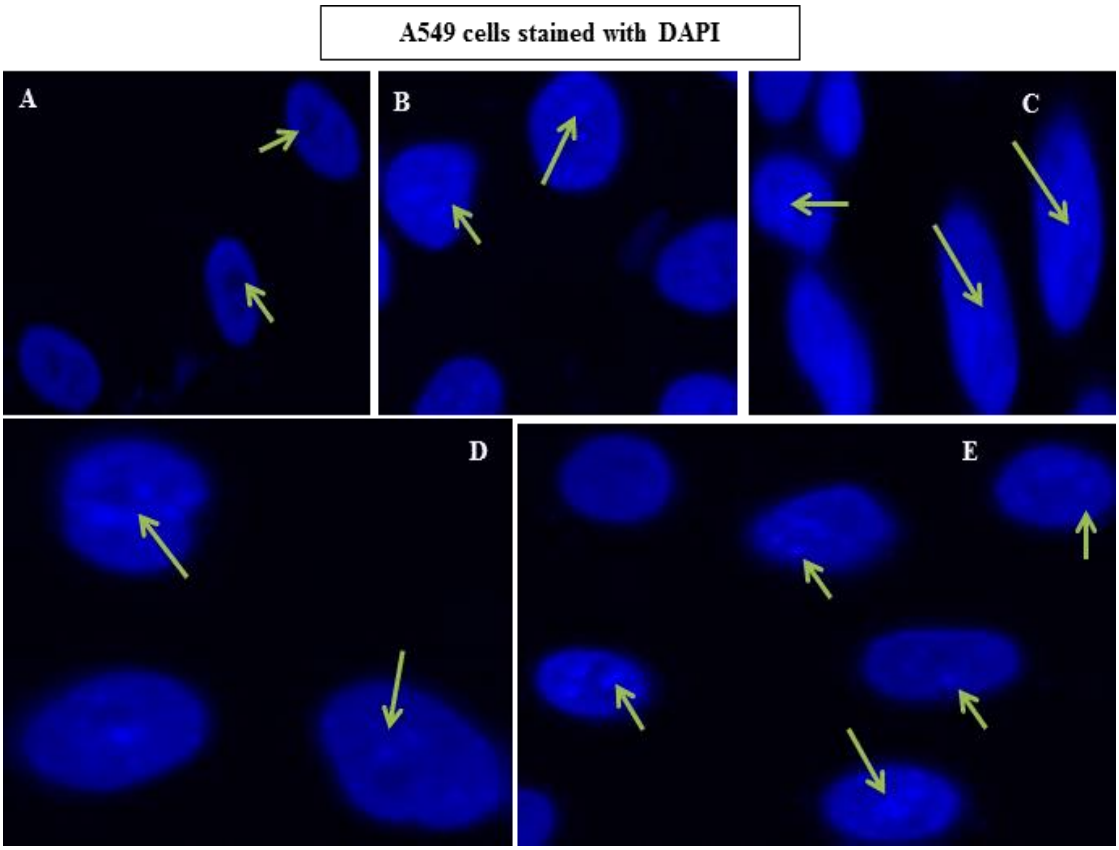

Figure 4.22: DAPI staining of the A549 cells. Nuclear morphology was evaluated before and after EFV and LPV/r treatment. Compared to the vehicle control, (A) 13µM (B) and 50µM (C) EFV treatment, and 32µM (D) and 80µM (E) LPV/r show changes in nuclear morphology as demonstrated by the green arrows (Original Magnification, 63X).

Green arrows point to changes in the nucleus. Such changes may include DNA fragmentation and chromatin condensation in ARV drug treated (B to E) relative to vehicle control cells (A) (Original Magnification, 63X).

4.2.6 Synopsis

In summary, the effects of these ARV drugs on the normal and cancerous lung cells was monitored in real-time, with real time cell impedance assays (xCELLigence system), which particularly served to elucidate the timing and nature of any relevant physiological responses by living cells. In particular, the curves representing cell growth/proliferation over time identified the window period during which these drugs were either pro- or anti-proliferative, where the Cmin of both EFV and LPV/r promoted cell growth and proliferation, while the Cmax and higher concentrations inhibited cell proliferation, leading to cell death. It was interesting to note that the proliferative effects of EFV were effective for at least 40h post-treatment in the A549 cancerous cells, while normal cells continued to proliferate, until a decline in cell viability attributed to possibly nutrient deprivation, was observed.

The Annexin V-FITC/PI apoptosis assay confirmed the cytotoxic effects of LPV/r, as initially observed by the xCELLigence RTCA. While RTCA analysis showed loss of cell viability in LPV/r treated cells, the mode of cell death was confirmed here by the apoptosis assay in both normal lung and cancerous cells. In association with this, the nuclei of ARV treated cells showed changes in morphology. Following on this confirmation of apoptosis and associated nuclear changes, gene expression changes associated with the cell-cycle were evaluated.

4.3 PROFILING OF THE HUMAN CELL-CYCLE GENE RESPONSE AFTER ART TREATMENT IN HUMAN NON-SMALL CELL LUNG CARCINOMA (NSCLC) CELLS

4.3.1 Human cell-cycle PCR Arrays

Following on the aforementioned observations relating to cell proliferation, the involvement of the cell-cycle and potential pathways of apoptosis, a specific gene panel was employed here to more specifically interrogate changes in the expression of cell-cycle related genes in response to ARV treatments. These findings are presented below.

(i) Assessment of Quality Control (QDC)

PCR arrays, incorporating 84 genes related to the cell-cycle were profiled on 6 samples, inclusive of vehicle (methanol) controls on both MRC-5 cells and A549 cells, EFV (13 μM) treated MRC-5 cells and A549 cells; and LPV/r treated (32 μM) MRC-5 cells and A549 cells.

The results of the gene expression arrays were analysed by GeneGlobe program (Qiagen), by comparing the normalised fold changes of the test group against the control group. Potential changes in gene expression were also analysed by the GeneGlobe program (Qiagen), by comparing the normalised fold changes of the test against the control groups.

All six (6) PCR Arrays were subjected to data quality control checks (using the GeneGlobe Program, for monitoring genomic DNA contamination (GDC), the first strand synthesis (RTC) as well as real-time PCR efficiency (PPC). All six arrays passed these checks (see Table 4.1).

Table 4.1: RT Profiler PCR Arrays data quality control checks

Test performed	Test Result
1. PCR Array Reproducibility	All Samples Passed
2. RT Efficiency	All Samples Passed
3. Genomic DNA Contamination	None-All Samples Passed

(*ii*) *Representation of Results*

The data representing changes in gene expression are represented here as fold changes in gene expression, in tables, heat maps and scatter plots. The heat map setting reflects the PCR array layout, where green represents down-regulated genes and red indicates up-regulated genes; and the intensity of the colours correlates with the degree of up- or down-regulation. Thus, the heat map provides a relative visualization of the fold changes in gene expression between the test cells as compared to (vehicle) control samples. Alterations in gene expression were analysed by the GeneGlobe software (Qiagen), by comparing the normalised fold changes of the drug treated cells against the control cells. Group 1 in the Y-axis of scatter plots denotes the test groups. GE represents gene expression. Figure 4.23 illustrates the associated heat map and scatter plot for test (A549) *versus* MRC-5 vehicle control cells. All of the remaining heat maps and scatter plots are included in Appendix C5, for EFV and LPV/r gene array supplementary data. The ±2 fold significantly up-or-down regulated genes for all groups are represented in Tables 4.2 to 4.11.

(iii) Gene expression analysis in fold change

(a) A549 (test) vs MRC-5 (control)-untreated cells

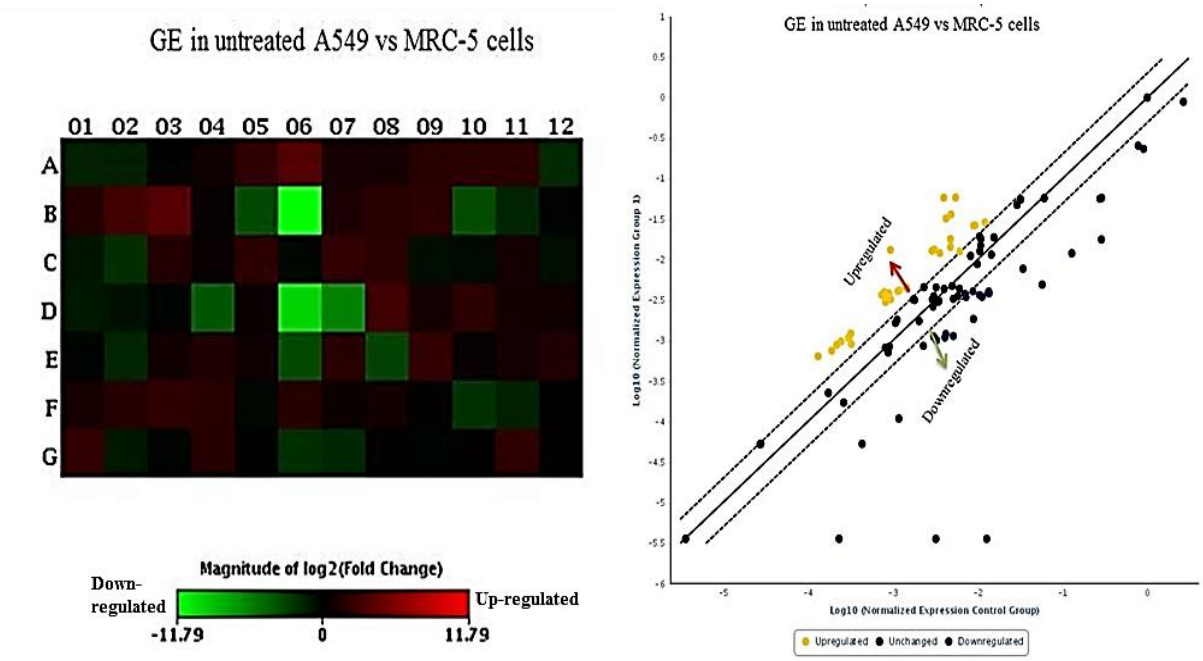

Figure 4. 23: The heat map (left panel) representing gene expression (GE) in untreated A549 (test) *vs* MRC-5 cells (control). Down-regulated genes are represented in green, while overexpressed genes are represented in red and unchanged expression in black. The colour intensity correlates with the degree of up/down regulation. The fold change of ±11.79 represents the lowest and the highest value for down and up-regulation.

The scatter plot shown in the right panel above compares the normalized expression of every gene on the array between the A549 cells and the MRC-5 cells (control), by plotting them relative to one another, to visualize gene expression changes. Each data point on the scatter plot represents a single gene, with normalised expression. The central (unbroken) line indicates unchanged gene expression, while the dotted lines indicate the selected (±2) fold regulation threshold. Up-regulation is indicated by the yellow points/red arrow, while down-regulation is shown by the black points/green arrow.

Table 4.2: The up-regulated genes in untreated (A549 *vs* MRC-5) cells

Gene Symbol	**GenBank Accession no.**	**Fold change/upregulation**
CCNB2	NM_004701	14.62
AURKB	NM_004217	14.12
CCNB1	NM_031966	7.62
CDKN3	NM_005192	7.46
CDC6	NM_001254	5.03
KNTC1	NM_014708	4.96
RAD9A	NM_004584	4.89
AURKA	NM_003600	4.44
TP53	NM_000546	4.32
MCM4	NM_005914	4.29
CHEK2	NM_007194	4.23
CCNF	NM_001761	4.08
BRCA2	NM_000059	4
CDC25C	NM_001790	3.97
BRCA1	NM_007294	3.84
CDK1	NM_001786	3.76
CCNE1	NM_001238	3.68
BIRC5	NM_001168	3.61
GTSE1	NM_016426	3.58
MCM5	NM_006739	3.51
RBL1	NM_002895	3.46
MKI67	NM_002417	3.39
MCM3	NM_002388	3.07
CCNA2	NM_001237	3.01
CDC20	NM_001255	2.95
MAD2L2	NM_006341	2.83
E2F1	NM_005225	2.81
CCND3	NM_001760	2.38
BCCIP	NM_016567	2.06

Table 4.3: The down-regulated genes in untreated (A549 *vs* MRC-5) cells

Gene Symbol	**GenBank Accession no.**	**Fold change/downregulation**
CCND2	NM_001759	-3541.14
CDKN2A	NM_000077	-891.44
CDKN2B	NM_004936	-64.45
CDKN1A	NM_000389	-16.11
CCNG1	NM_004060	-11.63
GADD45A	NM_001924	-10.7
CCND1	NM_053056	-10.7
HUS1	NM_004507	-8.11

Gene Symbol	**GenBank Accession no.**	**Fold change/downregulation**
RAD1	NM_002853	-4.79
SERTAD1	NM_013376	-4.5
CDC16	NM_003903	-4.41
CASP3	NM_004346	-3.73
SKP2	NM_005983	-3.48
CUL2	NM_003591	-3.23
CCNG2	NM_004354	-3.23
ABL1	NM_005157	-2.87
RAD17	NM_002873	-2.71
ANAPC2	NM_013366	-2.64
CDK6	NM_001259	-2.16
RB1	NM_000321	-2.1

(b) EFV treated test vs control gene expression analysis

(i) MRC-5 cells

Table 4.4: The up-regulated genes in EFV-treated *vs* untreated MRC-5 cells

Gene Symbol	**GenBank Accession no.**	**Fold change/upregulation**
CCNG2	NM_004354	8.76
CCNH	NM_001239	7.95
CDKN2B	NM_004936	4.2
CCND2	NM_001759	3.97
MDM2	NM_002392	3.92
CDK7	NM_001799	3.16
RBL1	NM_002895	2.85
CCNB1	NM_031966	2.73
ATM	NM_000051	2.68
ATR	NM_001184	2.57
MCM3	NM_002388	2.51
BRCA1	NM_007294	2.4
BCCIP	NM_016567	2.36
CHEK1	NM_001274	2.28
HUS1	NM_004507	2.13
CDK6	NM_001259	2.13
RAD51	NM_002875	2.11

Table 4.5: The down-regulated genes in EFV-treated *v*s untreated MRC-5 cells

Significantly down-regulated (-2) genes	None

(ii) A549 cells

Table 4.6: The up-regulated genes in EFV-treated *vs* untreated A549 cells

Gene Symbol	GenBank Accession no.	Fold change/upregulation
NBN	NM_002485	3.42
CCNG2	NM_004354	3.32
RAD17	NM_002873	3.3
CDK5RAP1	NM_003885	3.14
SERTAD1	NM_013376	2.76
CASP3	NM_004346	2.74
CCNG1	NM_004060	2.57
CDKN1B	NM_004064	2.57
CDK4	NM_000075	2.43
BRCA1	NM_007294	2.33
CUL2	NM_003591	2.32
RAD1	NM_002853	2.29
HUS1	NM_004507	2.21
SKP2	NM_005983	2.21
CDC20	NM_001255	2.13

Table 4.7: The down-regulated genes in EFV-treated *vs* untreated A549 cells

Gene Symbol	GenBank Accession no.	Fold change/downregulation
MAD2L2	NM_006341	-5.85
AURKB	NM_004217	-4.28
MCM4	NM_005914	-3.65
RBL1	NM_002895	-3.52
ATR	NM_001184	-3.07
CCNB2	NM_004701	-2.71

(c) LPV/r treated test vs control gene expression analysis

Table 4.8: The up-regulated genes in LPV/r-treated *vs* untreated MRC-5 cells

(i) MRC-5 cells

Gene Symbol	GenBank Accession no.	Fold change/upregulation
CDKN2B	NM_004936	5.17

Table 4.9: The down-regulated genes in LPV/r-treated *vs* untreated MRC-5 cells

Gene Symbol	**GenBank Accession no.**	**Fold change/down regulation**
CDC20	NM_001255	-95.67
MCM2	NM_004526	-40.79
GTSE1	NM_016426	-34.3
MKI67	NM_002417	-27.28
CDK1	NM_001786	-27.1
CDK2	NM_001798	-24.25
CCNB1	NM_031966	-21.41
BIRC5	NM_001168	-20.68
STMN1	NM_005563	-18
CCNB2	NM_004701	-17.75
CCNA2	NM_001237	-17.15
CCNF	NM_001761	-14.52
MCM3	NM_002388	-14.32
CDC25C	NM_001790	-14.32
AURKA	NM_003600	-12.82
KPNA2	NM_002266	-12.73
MCM5	NM_006739	-12.3
AURKB	NM_004217	-11.96
RAD51	NM_002875	-11.08
SERTAD1	NM_013376	-10.78
ANAPC2	NM_013366	-10.78
CDKN3	NM_005192	-10.13
MAD2L2	NM_006341	-9.71
MAD2L1	NM_002358	-9.71
SKP2	NM_005983	-9.38
MCM4	NM_005914	-9.06
CCND1	NM_053056	-8.82
CCND3	NM_001760	-8.22
TFDP1	NM_007111	-5.94
CKS1B	NM_001826	-5.66
CKS2	NM_001827	-5.58
CDK5RAP1	NM_016408	-4.41
CASP3	NM_004346	-4.29
E2F1	NM_005225	-4.17
MRE11A	NM_005590	-3.84
KNTC1	NM_014708	-3.73
CDC25A	NM_001789	-3.73
CHEK1	NM_001274	-3.68
CCNG1	NM_004060	-3.61
RBL1	NM_002895	-3.48
CHEK2	NM_007194	-3.46

Gene Symbol	**GenBank Accession no.**	**Fold change/down regulation**
WEE1	NM_003390	-3.36
CDK6	NM_001259	-3.23
E2F4	NM_001950	-3.18
BRCA1	NM_007294	-3.03
CCNE1	NM_001238	-2.83
CCND2	NM_001759	-2.77
TFDP2	NM_006286	-2.75
CDKN1B	NM_004064	-2.71
CDKN2A	NM_000077	-2.66
ABL1	NM_005157	-2.53
RAD1	NM_002853	-2.33
MNAT1	NM_002431	-2.28
HUS1	NM_004507	-2.23
RAD9A	NM_004584	-2.22
CDC34	NM_004359	-2.22
CDC16	NM_003903	-2.19
CDK8	NM_001260	-2.08
CCNG2	NM_004354	-2.04

(ii) A549 cells

Table 4.10: The up-regulated genes in LPV/r-treated *vs* untreated A549 cells

Gene Symbol	**GenBank Accession no.**	**Fold change/upregulation**
GADD45A	NM_001924	40.12
HUS1	NM_004507	23.36
BCL2	NM_000633	10.38
RAD17	NM_002873	5.45
CCNH	NM_001239	4.71
CDK5RAP1	NM_016408	4.52
ATM	NM_000051	4.1
CUL2	NM_003591	4.1
CCNG2	NM_004354	3.55
SERTAD1	NM_013376	3.4
TP53	NM_000546	3.4
RAD1	NM_002853	3.26
CDKN2A	NM_000077	3.24
CDK4	NM_000075	3.17
CDKN1A	NM_000389	3.15
CUL3	NM_003590	3.13
CDKN1B	NM_004064	3.13
RBL2	NM_005611	2.88

Gene Symbol	**GenBank Accession no.**	**Fold change/down regulation**
BCCIP	NM_016567	2.63
CCNT1	NM_001240	2.52
CCNG1	NM_004060	2.42
CASP3	NM_004346	2.34
CCND2	NM_001759	2.18

Table 4.11: The down-regulated genes in LPV/r-treated *vs* untreated A549 cells

Gene	**GenBank Accession no.**	**Fold change/downregulation**
GTSE1	NM_016426	-47.3
CCNB1	NM_031966	-45.69
CCNB2	NM_004701	-44.13
CDC25C	NM_001790	-36.6
CCNA2	NM_001237	-23
CDK1	NM_001786	-20.31
MCM4	NM_005914	-15.93
STMN1	NM_005563	-15.71
E2F1	NM_005225	-14.97
MCM5	NM_006739	-14.66
AURKB	NM_004217	-13.3
MKI67	NM_002417	-13.12
CDC20	NM_001255	-13.03
MAD2L1	NM_002358	-9.34
CDKN3	NM_005192	-9.34
CCND3	NM_001760	-8.02
CCNF	NM_001761	-6.61
RAD51	NM_002875	-6.61
BIRC5	NM_001168	-6.34
MCM2	NM_004526	-5.22
CDC6	NM_001254	-4.94
MAD2L2	NM_006341	-4.84
CHEK2	NM_007194	-4.61
MCM3	NM_002388	-4.61
KNTC1	NM_014708	-4.24
BRCA2	NM_000059	-4.18
CDK2	NM_001798	-3.96
CKS2	NM_001827	-3.85
AURKA	NM_003600	-3.74
CDC25A	NM_001789	-3.47
CCNE1	NM_001238	-3

Gene Symbol	**GenBank Accession no.**	**Fold change/down regulation**
RBL1	NM_002895	-2.8
CHEK1	NM_001274	-2.61

4.3.1.1 EFV and LPV/r treatments modulate the expression of genes related to the cell-cycle in lung cancer cells (A549) and in normal lung cells (MRC-5) groups

Prior to treatment a significant number of genes are shown to be dysregulated, either up-or down, and were represented as shifting from the median-solid line, in the scatter plots as shown in Figure 4.29. The upregulated genes (Table 4.2) included cyclin/CDK complexes, while the down-regulated genes (Table 4.3) included growth-arrest genes, such as p21 and GADD45A. On the other hand, RT-PCR arrays indicated a general up-regulation in the transcription of cell-cycle genes in MRC-5 cells treated with EFV (Table 4.4), while most genes remained in a normal (unchanged) state (Table 4.5). EFV treatment of A549 cells led to the increase (Table 4.6) in the transcription of other cell-cycle genes and a decrease (Table 4.7) in the transcription of others. However, most genes were observed to be normalised across the solid line, as compared to the untreated (vehicle control) cancerous cells.

LPV/r treatment of MRC-5 cells resulted in the upregulation of the CDKN2B gene (Table 4.8) a decreased transcription of cell-cycle genes assayed (Table 4.9). In contrast, LPV/r treatment of A549 cells led to a significant dysregulation of the cell-cycle genes arrayed, moving away from the normal level of expression. Most of the upregulated genes here (Table 4.10) include the DNA damage response genes such as ATM, p53 and GADD45A, while the downregulated genes are shown in Table 4.11 (please refer to appendix C5 for all heat maps and scatter plots).

4.3.2 Validation of selected cell-cycle associated gene targets using Real-Time quantitative Polymerase Chain Reaction (RT-qPCR)

4.3.2.1 Introduction

The Real-Time quantitative Polymerase Chain Reaction (RT-qPCR), a highly sensitive method for gene expression studies was used here to assess and confirm the relative gene expression levels of selected target genes from the cell-cycle expression study.

Three differentially expressed genes were selected, shown to be either up-or-down-regulated, from the gene array studies. The rationale for the selection of the target genes was based on the following: the differential expression (significantly up-or-down-regulation) across most/all template samples and their role in the cell-cycle in relation to the observed phenotypic changes in the upstream experiments such as the xCELLigence-RTCA, the cell-cycle and the apoptosis assays. The three genes selected were Mitotic Arrest Deficient-Like 2 (MAD2L2) which functions at the cell-cycle checkpoint, Caspase 3 (CASP3) which is apoptosis related and Aurora Kinase B (AURKB), a mitotic gene.

Primers' description details for these gene targets, including GAPDH as a housekeeping (HKG) gene are shown in section 3.8.1 and Appendix C6, Table C6.1. These were designed using the online program, Primer 3 (http://primer3.wi.mit.edu/), then optimized by conventional PCR by running a gradient PCR (53°C to 65°C). The specificity of primer sets at 60°C was demonstrated by single bands on 1% agarose gel electrophoresis, and single peaks on the melt-curves, as shown in Appendix C6, Figure C6.1 to Figure C6.5.

Following fold change calculations, (see section 3.8.2), the calculated fold changes were then exported to GraphPad Prism 5, for further statistical analysis, plotting test against control, for all three selected target genes. Results are represented as fold changes in tables and bar graphs.

4.3.2.2 Analysis of MAD2L2, CASP3 and AURKB gene expression levels before and after ARV treatment

(i) Expression of target genes in untreated A549 vs MRC-5 cells

Prior to assessing the effects of ARVs on target gene expression, the expression levels of MAD2L2, CASP3 and AURKB were first assessed in untreated (vehicle control) A549 *vs* MRC-5 cells, respectively. The relative gene expression levels are represented in Table 4.12 and Figure 4.24 below. Both MAD2L2 (~3 fold) and AURKB (3-4 fold) at 24h and 48h were significantly upregulated in A549 cells relative to the normal MRC-5 fibroblasts. Caspase 3 in contrast was significantly down-regulated (~ -5 fold) at both 24h and 48h in A549 lung cancer cells.

Table 4.12: Target gene expression levels in untreated A549 *vs* MRC-5 cells

Gene	Fold change 24h	Fold change 48h
MAD2L2	3.06	3.0
CASP3	-4.48	-5.30
AURKB	3.33	4.02

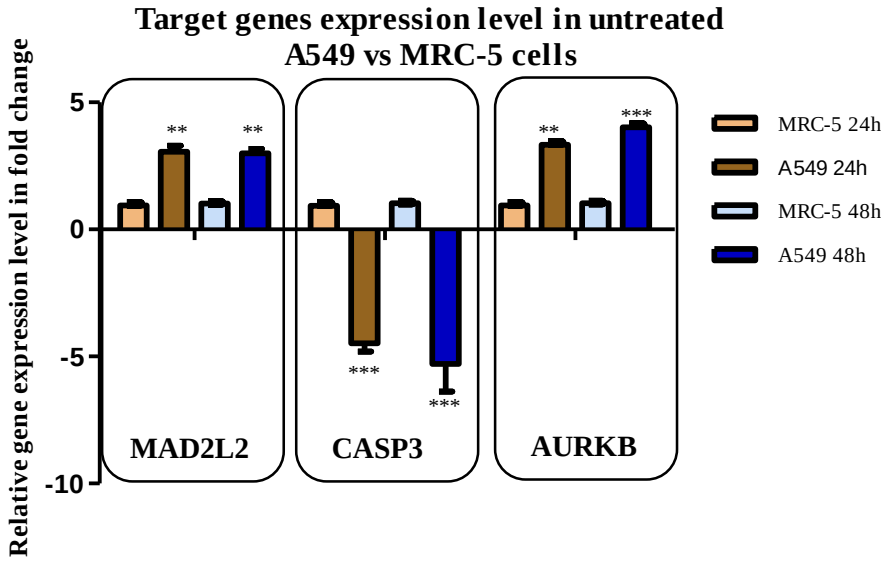

Figure 4.24: Bar graph representing MAD2L2, CASP3 and AURKB relative gene expression levels in the untreated cancerous A549 cells compared to the normal MRC-5 lung fibroblasts. The relative gene expression levels are represented as a fold change as compared to MRC-5 cells. An upregulation of MAD2L2 and AURKB is observed, as opposed to the downregulated CASP3 in A549 cells relative to the non-cancerous counterpart, observed at 24h and 48h. * $p< 0.05$, ** $p<0.01$, *** $p<0.001$.

(ii) Expression of target genes in cells treated with EFV

After assessing target gene expression in untreated cells, gene expression was assessed following treatment with 13µM EFV (physiologically relevant dose) at 24h and 48h, respectively.

(a) Target gene expression analysis in EFV-treated MRC-5 cells

In MRC-5 cells, MAD2L2 was significantly upregulated (~2 fold) at 24h, followed by a -1.34 down-regulation at 48h (see Table 4.13 and Figure 4.31). In contrast, CASP3 (~ -1.8 fold) and AURKB (~ -1.5 fold) were significantly down-regulated at 24h and 48h, as shown in Table 4.13 and Figure 4.25.

Table 4.13: Target gene expression levels in 13µM EFV treated MRC-5 *vs* untreated cells

Gene	**Fold change 24h**	**Fold change 48h**
MAD2L2	1.97	-1.34
CASP3	-1.77	-1.88
AURKB	-1.76	-1.32

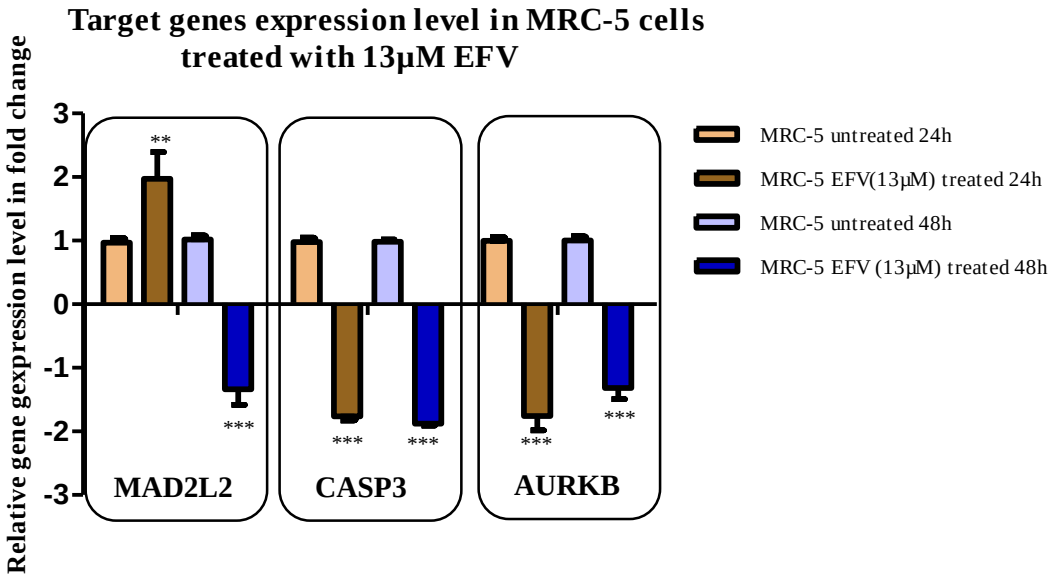

Figure 4.25: Representation of the expression levels of MAD2L2, CASP3 and AURKB in MRC-5 cells treated with 13µM EFV at 24h and 48h, relative to untreated cells. The relative gene expression levels are represented as a fold change as compared to untreated MRC-5 cells. MAD2L2 was upregulated at 24h post 13µM EFV treatment, followed by a significant downregulation at 48h. Both CASP3 and AURKB were significantly down-regulated at 24h and 48h. * $p < 0.05$, ** $p<0.01$, *** $p<0.001$ levels of significance.

(b) Target gene expression analysis in EFV-treated A549 cells

In EFV treated A549 lung cancer cells, EFV significantly decreased expression levels of both MAD2L2 (fold changes, $p < 0.001$ and $p < 0.01$) and AURKB (fold changes, $p < 0.001$) genes at 24h and 48h. The expression of CASP3, though upregulated (~ 2 fold) at 24h and 48h post treatment, was not statistically significant (see Table 4.14 and Figure 4.26).

Table 4.14: Target gene expression levels in 13µM EFV treated A549 *vs* untreated cells

Gene	**Fold change 24h**	**Fold change 48h**
MAD2L2	-4.43	-2.94
CASP3	2.01	1.88
AURKB	-38.91	-8.0

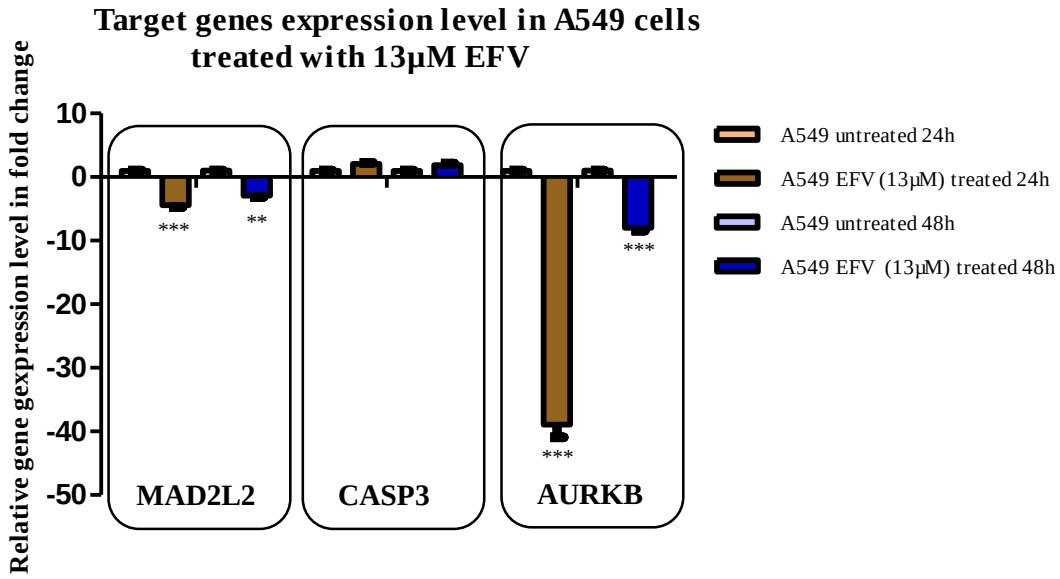

Figure 4.26: Expression levels of MAD2L2, CASP3 and AURKB genes in A549 cells treated with 13µM EFV at 24h and 48h, respectively. The relative gene expression levels are represented as a fold change as compared to untreated cells. * $p < 0.05$, **$p<0.01$, ***$p<0.001$ levels of significance.

(iii) Expression of target genes in cells treated with LPV/r

Gene expression of MAD2L2, CASP3 and AURKB were evaluated in both MRC-5 and A549 cells after treatment with 32µM LPV/r (physiologically relevant dose) at 24h and 48h, respectively.

(c) Target gene expression analysis in LPV/r-treated MRC-5 cells

All three target genes were down-regulated following 32µM LPV/r drug treatment at 24h and 48h in MRC-5 cells ($p < 0.001$), as shown in Table 4.15. CASP3 gene expression although marginally up-regulated at 24h, was not statistically significant, as represented in Table 4.15 and Figure 4.27.

Table 4.15: Target gene expression levels in 32µM LPV/r treated MRC-5 *vs* untreated cells

Gene	Fold change 24h	Fold change 48h
MAD2L2	-1.64	-1.57
CASP3	1.47	-2.02
AURKB	-6.69	-15.28

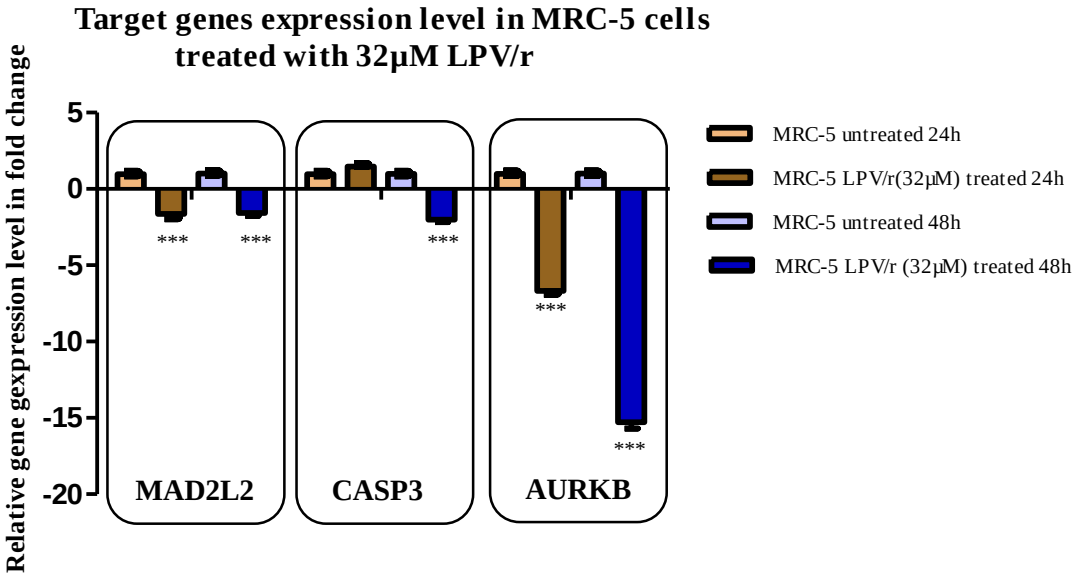

Figure 4.27: Representation of MAD2L2, CASP3 and AURKB gene expression in MRC-5 cells treated with LPV/r. The relative gene expression levels are represented as a fold change as compared to control MRC-5 cells. * p< 0.05, **p< 0.01, ***p< 0.001 levels of significance.

(d) Target gene expression analysis in LPV/r-treated A549 cells

In A549 cells, both MAD2L2 (-5.57 and -2.57 fold) and AURKB (-11.42 and -19.33) genes were significantly down-regulated at 24h and 48h post 32µM LPV/r treatment. In comparison, however, CASP3 gene expression (2.2 fold) though up-regulated, was not statistically significant (see Table 4.16 and Figure 4.28).

Table 4.16: Target gene expression levels in 32µM LPV/r treated A549 *vs* untreated cells

Gene	Fold change 24h	Fold change 48h
MAD2L2	-5.57	-2.57
CASP3	1.79	2.72
AURKB	-11.42	-19.33

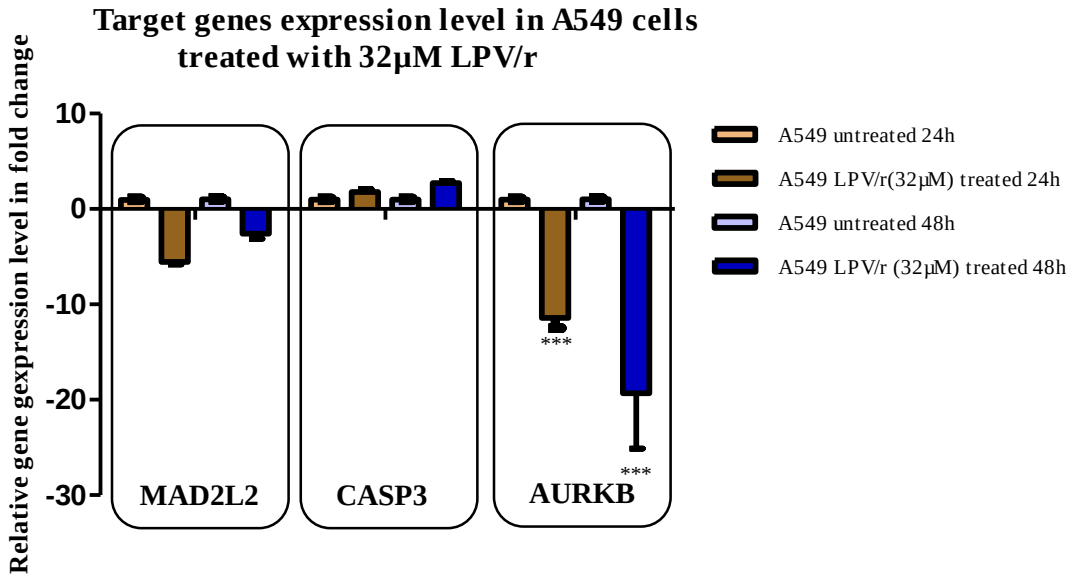

Figure 4.28: Representation of the gene expression levels MAD2L2, CASP3 and AURKB in A549 cells treated with LPV/r. The relative gene expression levels are represented as a fold change as compared to untreated cells. * p< 0.05, **p< 0.01, ***p< 0.001 levels of significance.

(iv) MAD2L2, AURKB and CASP3 expression are altered by EFV and LPV/r drug treatments at 24h and 48h

The drug naïve lung cancer cells had raised expression levels of both MAD2L2 and AURKB and decreased CASP3 levels, relative to the normal MRC-5 cells. Following ARV treatment, the overall effects of both drugs were essentially to down-regulate target gene expression in the normal lung fibroblasts and the lung cancer cells. Whilst there was a minor up-regulation of CASP3 in lung cancer cells, this was not statistically relevant.

Abnormal cell proliferation associated with the deregulation of CASP3 and overexpression of AURKB and MAD2L2 has been previously reported ((Hochegger *et al.*, 2013); (Boersma *et al.*, 2015)). While both AURKB and MAD2L2 function at the mitotic spindle assembly checkpoint, the down-regulation of these genes after ARV treatment here, particularly in the A549 cells portrays an anti-cancer characteristic. This is also associated with the CASP3 (an apoptosis related gene) up-regulation, post ARV treatment. Notably, the GAPDH levels were not affected by any of the treatments.

The relationship between these selected target genes and their potential interactions with relevant signalling pathways are further evaluated using a number of *in silico* analyses. These are elaborated on below.

4.4 IN SILICO BIO-INFORMATICS ANALYSIS OF CELL-CYCLE RELATED GENES TREATED WITH EFAVIRENZ (EFV) AND LOPINAVIR/RITONAVIR (LPV/r) IN HUMAN LUNG CANCER CELLS

The next approach in this study was to engage a series of bioinformatics tools to determine potential interactions between differentially expressed gene products elucidated in the cell-cycle array analysis and to then map the molecular pathways that are regulated by these targets. The programmes used here included, STRING to determine protein-protein interactions; Database for Annotation, Visualisation and Integrated Discovery (DAVID) that provides a functional interpretations of genes; the Reactome Pathway Database, a database of biological pathways; and Ingenuity Pathway Analysis (IPA), which analyses pathway relationships. The findings ensuing from these analyses are presented below.

4.4.1 A STRING analysis of gene products whose transcription levels change following EFV or LPV/r treatment indicate a change in the expression of proteins involved in genotoxic damage response pathways.

The STRING database (v10.0) was used to establish the protein-protein interactions of the 84 cell-cycle genes profiled in response to ARV treatments (see section 3.9 above). The resulting interaction is depicted in Figure 4.29. STRING was then used to construct protein-protein interaction pathways for genes which expression was significantly up-or down-regulated in untreated A549 cells as compared to MRC-5 cells.

In the network generated by STRING V10, each node represents a protein and each edge represents an interaction. Furthermore, network nodes represent proteins, where either splice isoforms or post-translational modifications are collapsed, that is, each node represents all the proteins produced by a single, protein-coding gene locus. The STRING interaction threshold was set at 0.40 (medium). Protein nodes lacking or with weak interaction (< 0.40) are not shown. The PPIs were determined for untreated A549 cells vs MRC-5 cells, EFV and LPV/r

treated MRC-5 and A549 cells. The significance of node sizes and their colour in relation to their protein association is summarized below.

Node Size:

Small nodes represent: 	protein of unknown 3D structure
Large nodes depict: 	some 3D structure is known or predicted

Node Color:

Colored nodes: 	query proteins and first shell of interactors
White nodes: 	second shell of interactors

The resulting protein-protein interaction network of up-regulated gene transcription in untreated cells is depicted in Figure 4.30, while the network of down-regulated genes in untreated cells is depicted in Figure 4.31. The transcriptionally up-regulated gene targets in the cancer cells included the AURKB and TP53 interaction, known to be dysregulated in cancer cells, while RAD1 and HUS 1, which form part of the RAD9-RAD1-HUS1 (9-1-1) DNA damage response, were displaced from the interaction network.

Treatment of MRC-5 cells and A549 cells with 13µM EFV led to an increase or decrease in the transcription levels of various gene targets. STRING was then used to construct protein-protein interaction networks for both those gene targets whose transcription level increased or decreased. Pathways whose members show an increase in transcription include the ATR-

BRCA1 DNA damage response pathways, Figure 4.32 for MRC-5 cells. In the A549 cells, the protein-protein interaction network of those gene targets whose expression is upregulated is depicted in Figure 4.33. As shown here, there is an increase in the transcription of members of the genotoxic cell-cycle checkpoint pathway (RAD1 and HUS1). Pathways whose members demonstrate a decrease in transcription include members of the DNA replication pathway (MCM4), stress response pathway (ATR); and also noting the presence of AURKB in this network, (see Figure 4.34).

Treatment of MRC-5 and A549 cells with 32μM LPV/r led to an upregulation or down-regulation in the transcription level of multiple genes. STRING was then used to construct protein-protein interaction networks based on these gene targets. A representation of the resulting protein-protein interaction pathway for down-regulated gene expression in MRC-5 cells is depicted in Figure 4.35 and Figure 4.37 for the A549 cells. What is evident here is a decreased expression of the E2F (TFs), survivin (BIRC5), the MCM DNA synthesising genes and AURKB, in both groups of cells. An illustration of the resulting protein-protein interaction pathway for up-regulated gene expression in A549 cells is shown in Figure 4.36, where an increase in the expression of members of the genotoxic cell-cycle checkpoint (RAD1 and HUS1), as well as GADD45 was observed.

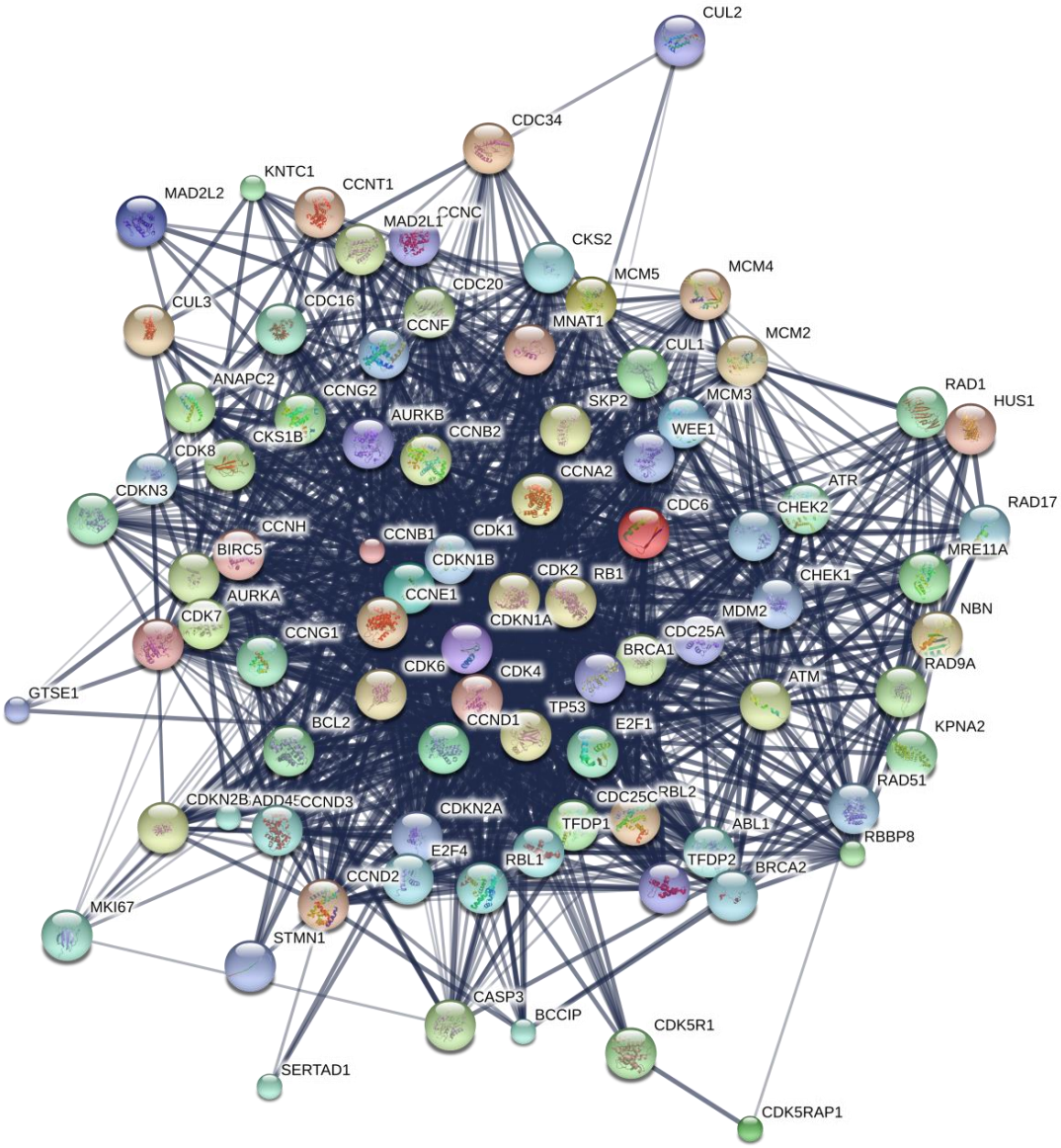

Figure 4.29: STRING protein-protein interaction (PPI) analysis of cell-cycle related proteins in untreated A549 compared to MRC-5 cells. The medium threshold (0.4) was set, and therefore weaker interactions (<0.4) are not shown. The intensity of the blue colour in this network denotes a strong interaction and relation between these proteins.

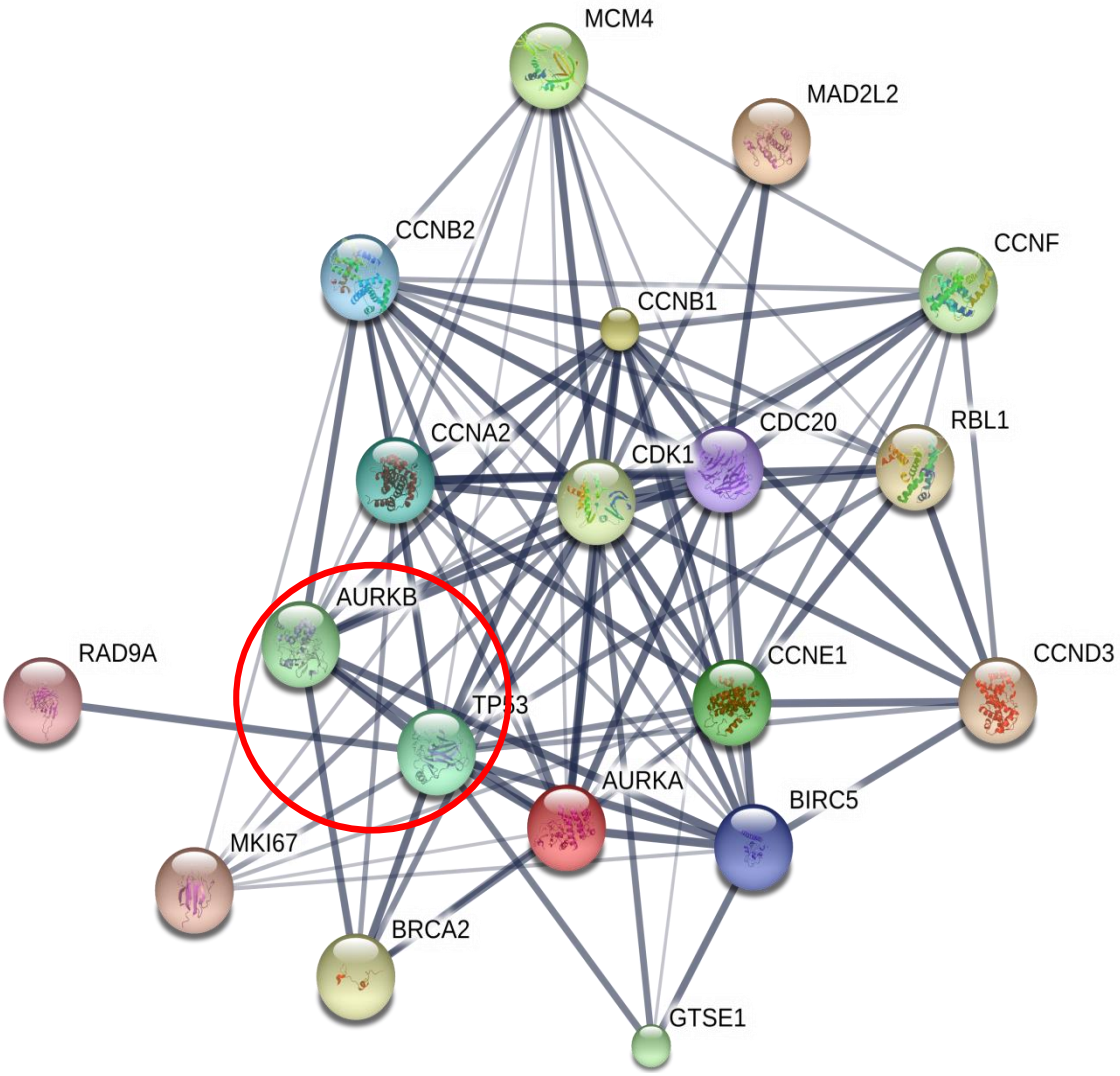

Figure 4.30: STRING protein-protein interaction (PPI) analysis of proteins significantly increased in vehicle control A549 cells. The interaction threshold was set at 0.40. Protein nodes with no or weak (< 0.40) interactions are not shown. Thick lines depict stronger interactions. The stronger interaction observed between TP53 and AURKB is indicated by the red circle.

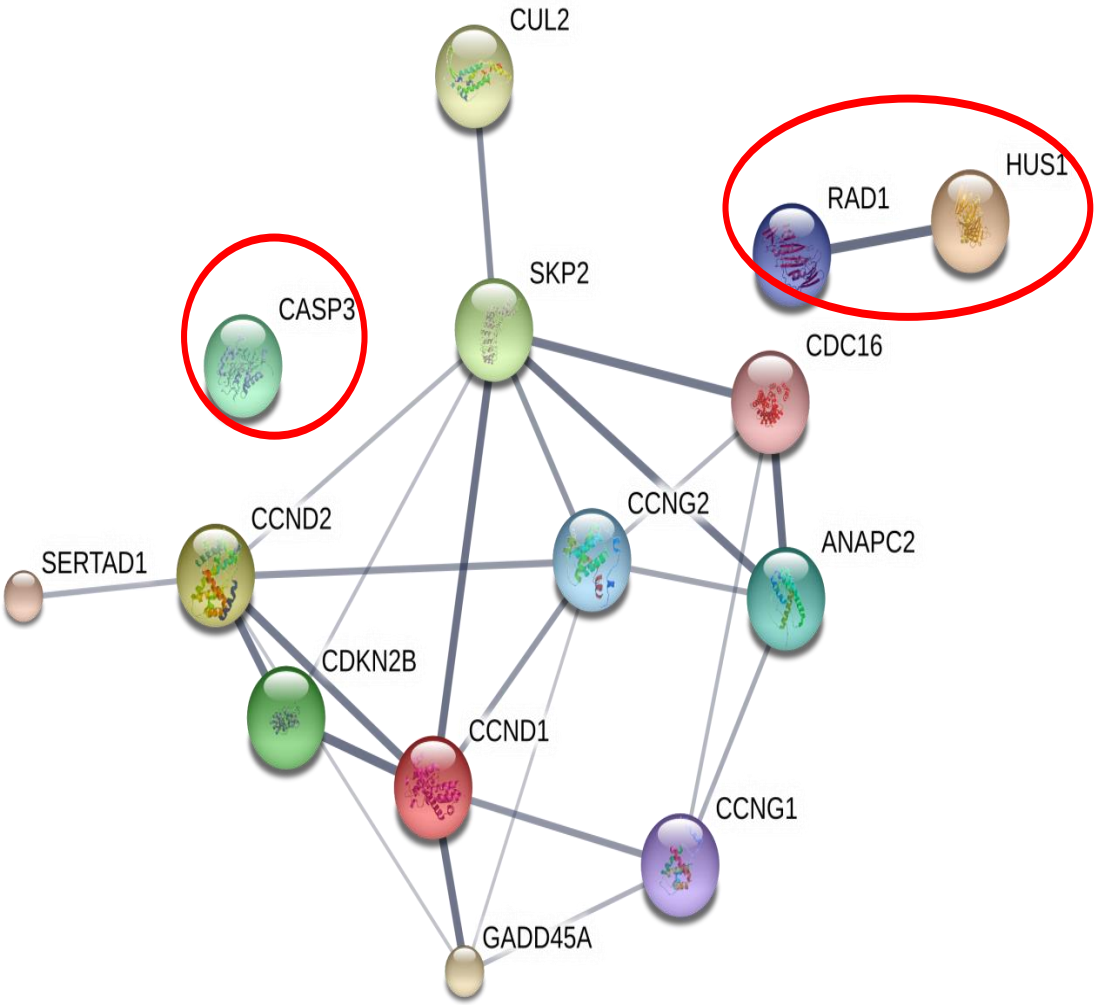

Figure 4.31: STRING protein-protein interaction (PPI) analysis of proteins significantly decreased in untreated A549 cells. The threshold of the interaction was set at 0.40. Weak or no interactions (<0.4) are not shown here. CASP3 is isolated as it does not directly interact with any of the other down-regulated targets in the network. Similarly, RAD1 and HUS1 (which are shown to directly interact, highlighted in red) are observed to be dissociated from the network.

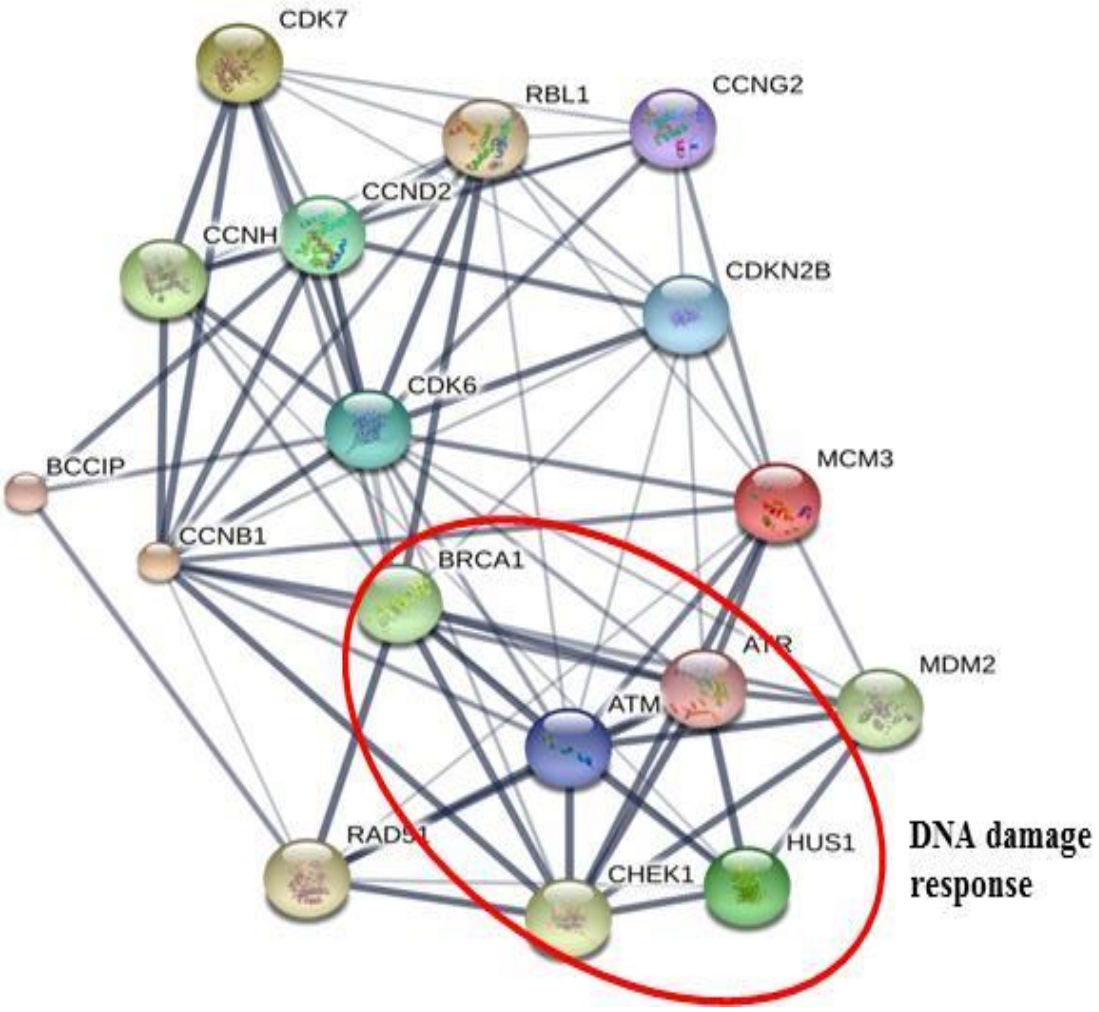

Figure 4.32: STRING protein interaction analysis of proteins significantly upregulated in MRC-5 cells treated with 13µM EFV. The interaction threshold was set at 0.40, only depicting stronger interactions. Therefore weak or no interactions (<0.4) are not shown in this network. The thickness of the lines illustrates a stronger interaction. The DNA damage response ATR/ATM, CHEK, HUS1 and BRCA1 proteins are shown to strongly interact.

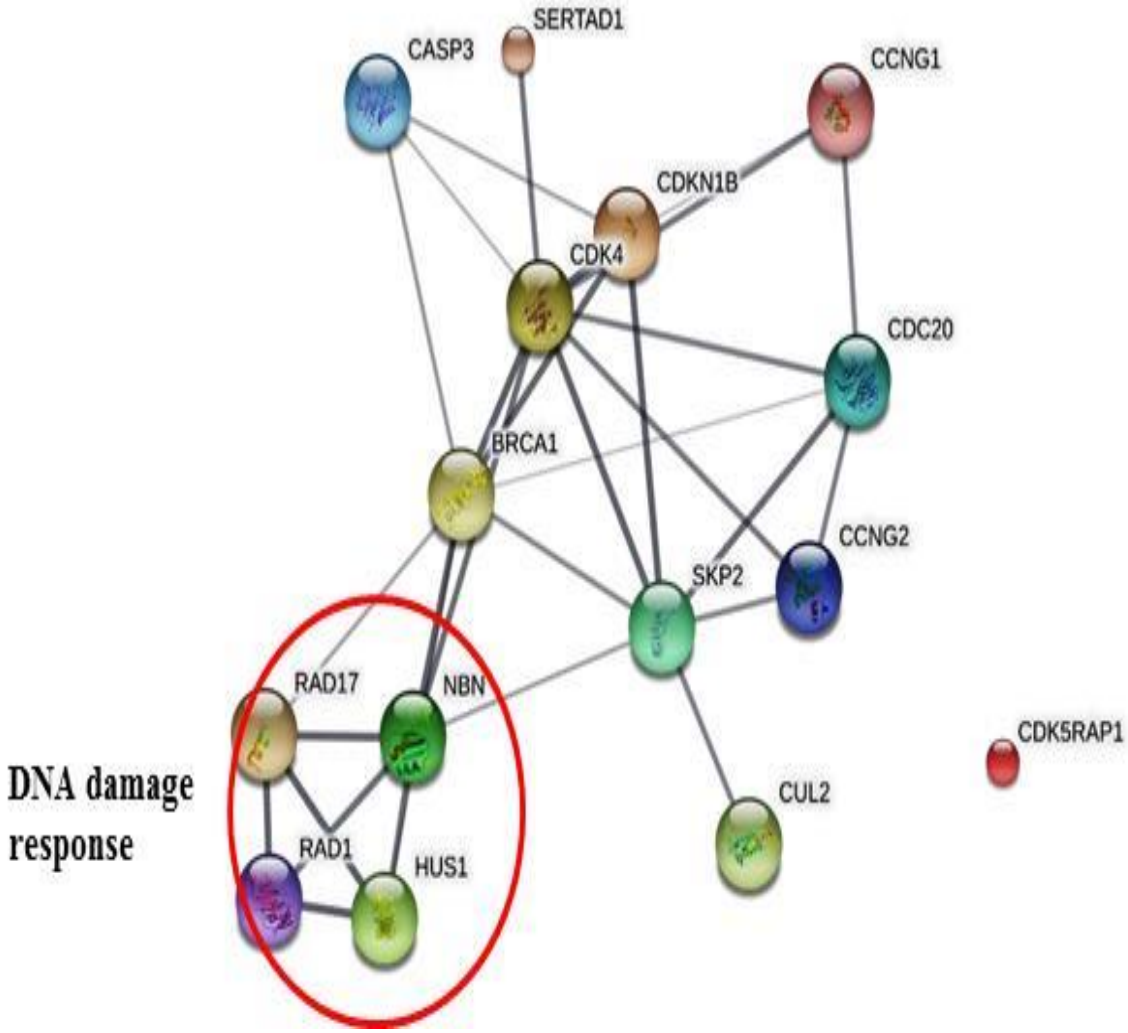

Figure 4.33: STRING protein-protein interaction (PPI) analysis of proteins significantly increased in A549 cells treated with 13µM EFV. The threshold of the interaction was set at 0.40. Weak or no interactions (<0.4) are not shown in this network. Stronger interactions are shown by dark blue lines. CDK5RAP1 is distanced from the network, as its direct interactor (CDK5R) that associates it to the main network was not co-upregulated. DNA damage response genes such as RAD 1 and RAD 17, NBN and HUS1 form a close association, depicted in a red circle.

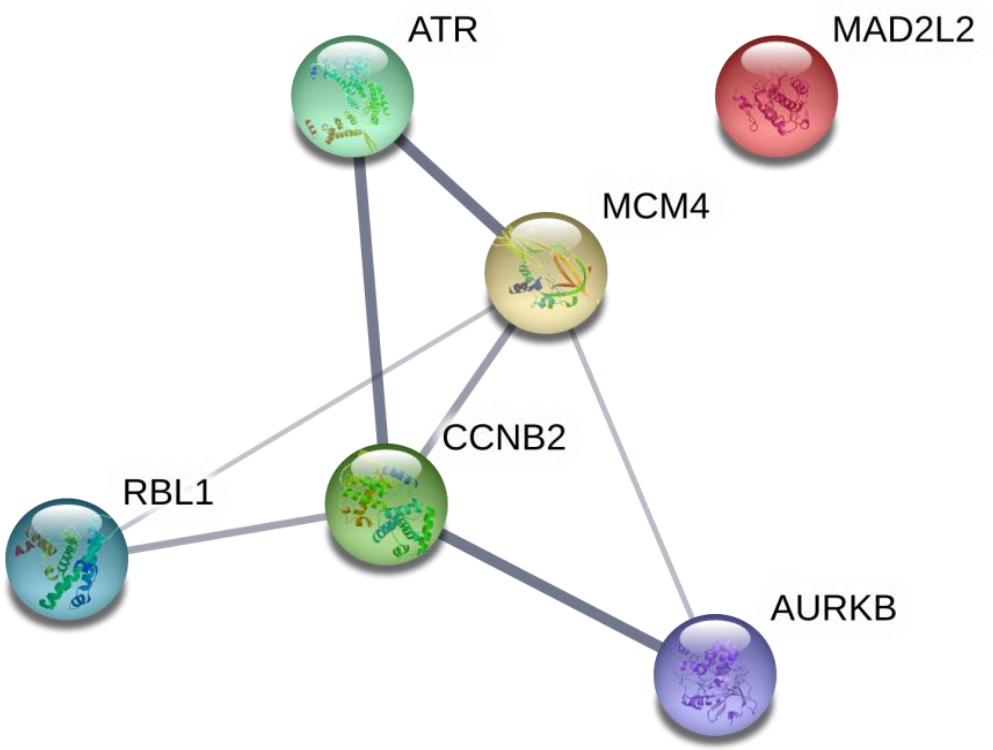

Figure 4.34: STRING protein-protein interaction (PPI) analysis of proteins significantly down-regulated in A549 cells treated with 13µM EFV. The interaction threshold was set at 0.40, with weak or no interactions (<0.4) not depicted. No direct interaction is observed between MAD2L2 and the other five down-regulated targets in this network. A strong interaction is observed between AURKB and cyclin B2 (CCNB2), which directly interacts with ATR.

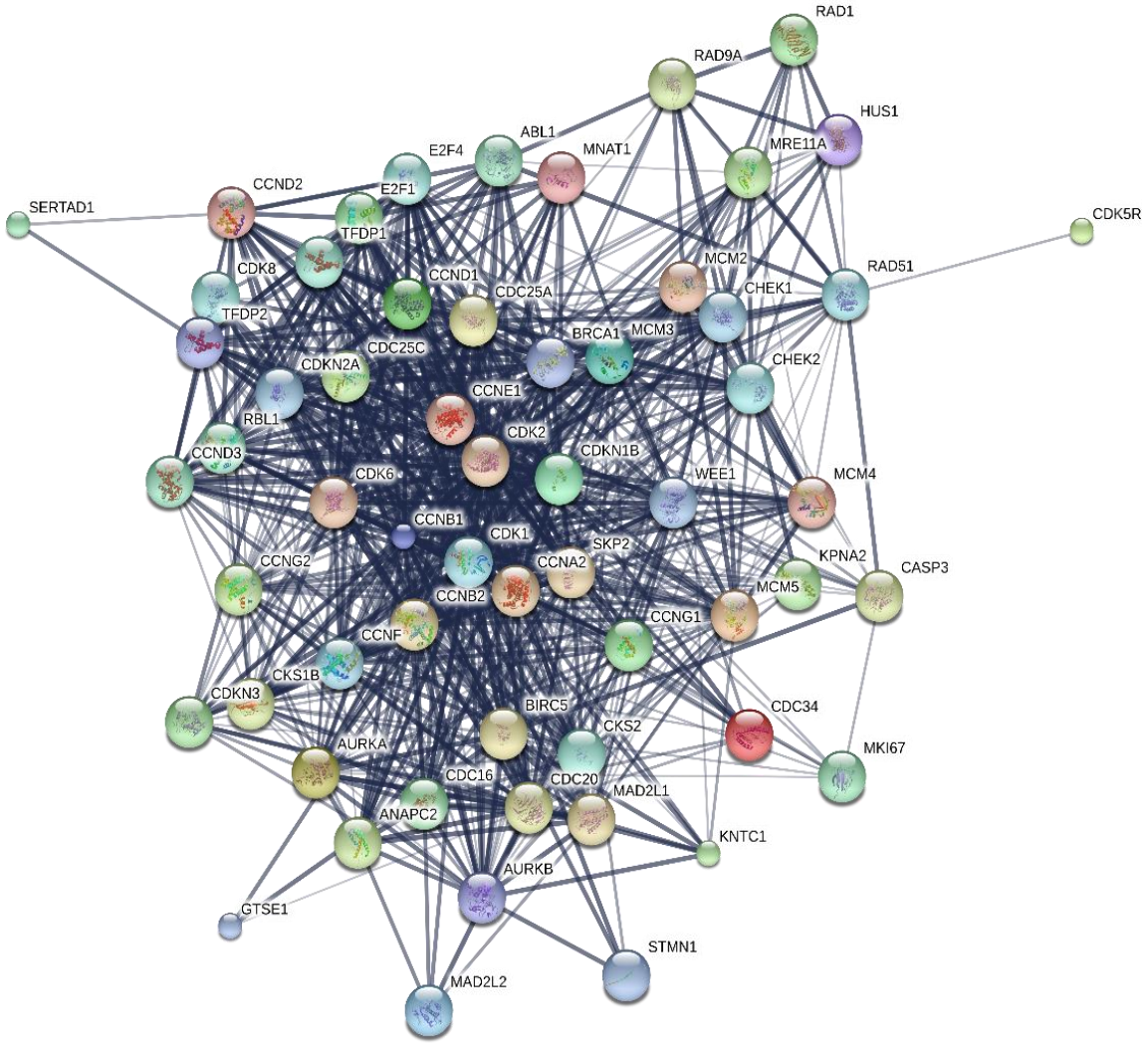

Figure 4.35: STRING protein interaction analysis of proteins significantly decreased in MRC-5 cells treated with 32µM LPV/r. The interaction threshold was set at 0.40, thus only permitting stronger interactions. In this network, there is no stand-alone target, and the intensity of the blue colour indicates a strong and direct interaction between the down-regulated targets.

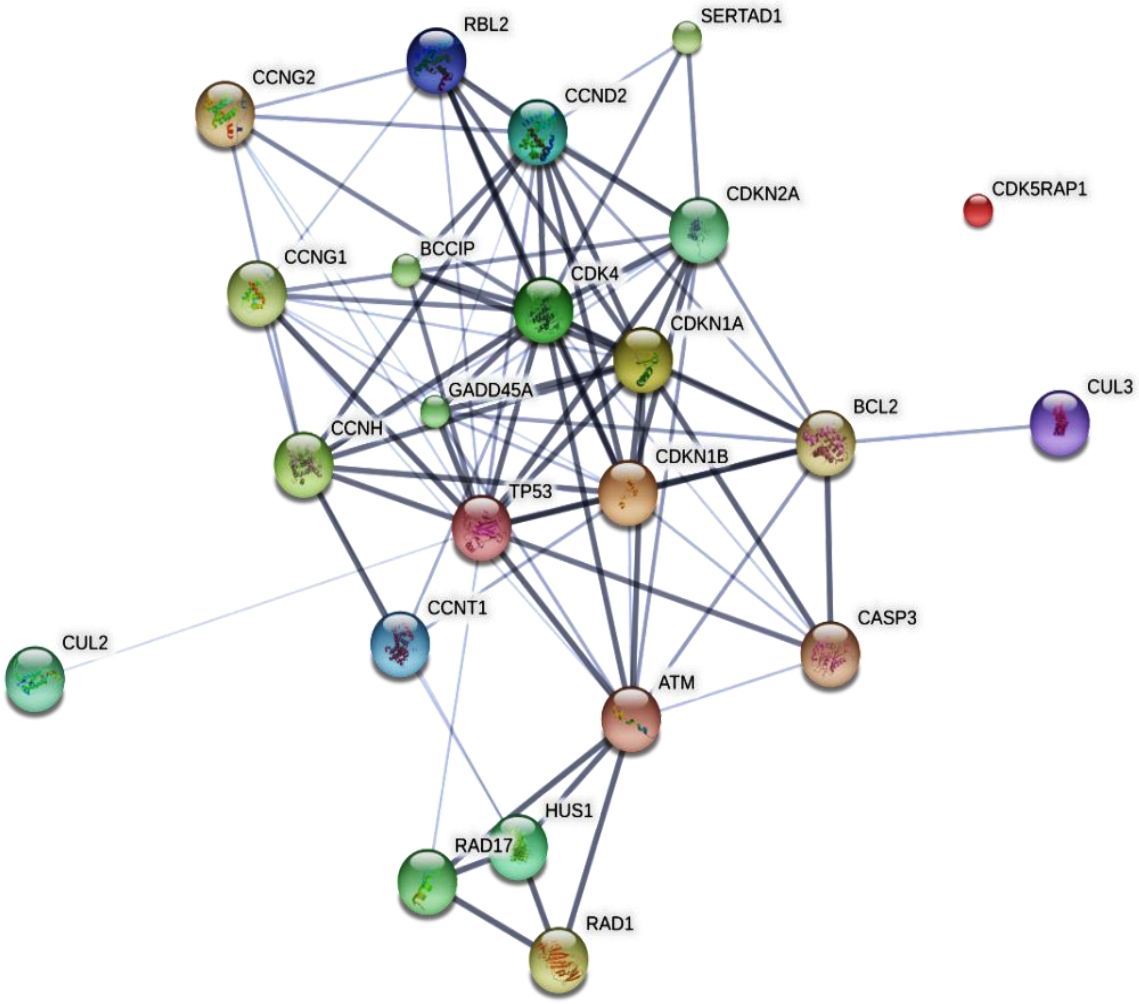

Figure 4.36: STRING protein-protein interaction (PPI) analysis of proteins significantly increased in A549 cells treated with 32µM LPV/r. The interaction threshold was set at 0.40 and therefore weak or no interactions (<0.4) are not shown in this network. The line intensities are indicative of the strength of the interactions. The stand-alone CDK5RAP1 is not directly linked to this network, due to the absence of its direct interactor CDK5R1 in this network.

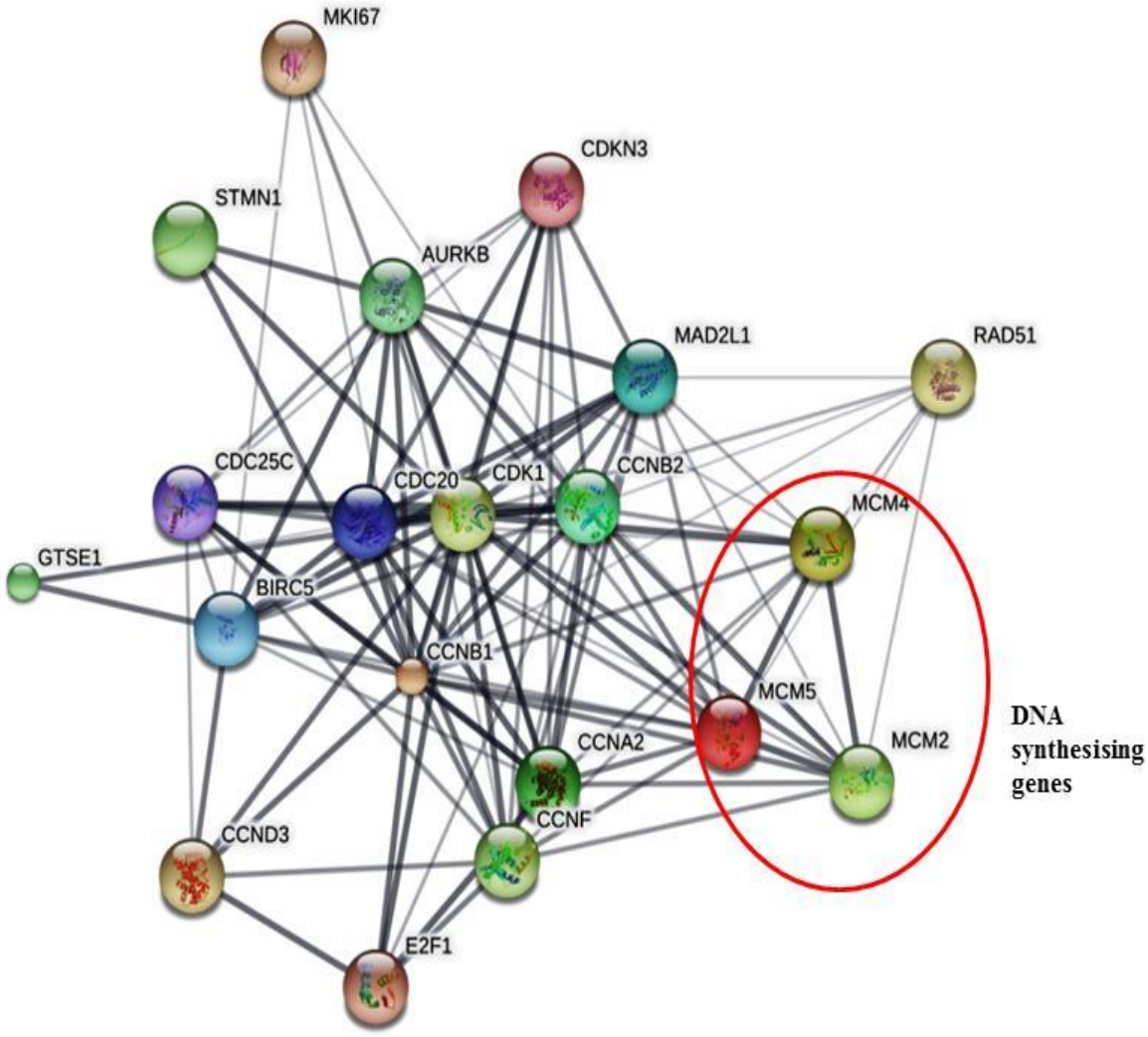

Figure 4.37: STRING protein-protein interaction (PPI) analysis of proteins significantly decreased in A549 cells treated with 32µM LPV/r. The interaction threshold was set at 0.40, with interactions below this threshold (<0.4) not being shown in this network. The thickness of the lines indicates stronger direct interactions between targets, while a co-down-regulation of the MCM DNA synthesising family of genes is observed here, in a red circle.

4.4.2 DAVID was used to perform a functional enrichment analysis of the target genes in order to identify those genes of interest involved in cell-cycle regulation and progression pre- and post-EFV and LPV/r drug treatment.

The Database for Annotation, Visualisation and Integrated Discovery (DAVID) v6.7 was used for functional enrichment analysis in a set of genes, to visualise differentially expressed genes within a particular KEGG pathway. Within the KEGG representations, the red stars represent the input target genes/products; the green boxes represent (all) genes related to the cell-cycle pathway (Figure 4.38), while white boxes denote other pathways associated with the cell-cycle (see section 3.9, Figure 3.2 for annotation).

A functional enrichment analysis of differences in the gene expression between vehicle control A549 *vs* MRC-5 cells indicated that most of the up-regulated gene targets are also related to cell-cycle progression in the form of cyclin/ CDK complexes (Figure 4.39). Those cell-cycle related genes whose expression was down-regulated include Anaphase-Promoting Complex or Cyclosome (APC/C) and Rb (Figure 4.40), which lead to uncontrolled cell division. Treatment of MRC-5 and A549 cells with 13µM EFV resulted in the up-regulation of cell-cycle regulators in MRC-5 cells. The ATM/ATR DNA repair pathway was also activated in MRC-5 cells. This pathway is known to negatively regulate the cell-cycle (Figure 4.41). In A549 cells the APC complex which regulates cell-cycle protein expression (CDC 20) was up-regulated (Figure 4.42), while EFV treatment of A549 cells resulted in the down-regulation of MAD2L2, an important cell-cycle checkpoint and arrest protein (see Figure 4.43).

Treatment of MRC-5 cells with 32µM LPV/r resulted in the up-regulation of a single target CDKN2B (p15/INK4b) (Figure 4.44), and the down regulation of cyclin/CDK complexes, known to inhibit cell-cycle progression (Figure 4.46). Treatment of A549 cells with 32µM LPV/r activated DNA damage response gene targets such as ATM/ATR, p53 and GADD45 and suppressed cell-cycle progression (Figure 4.45) by down-regulating cyclin/CDK complexes (Figure 4.47).

KEGG visualisation pathway for untreated cells

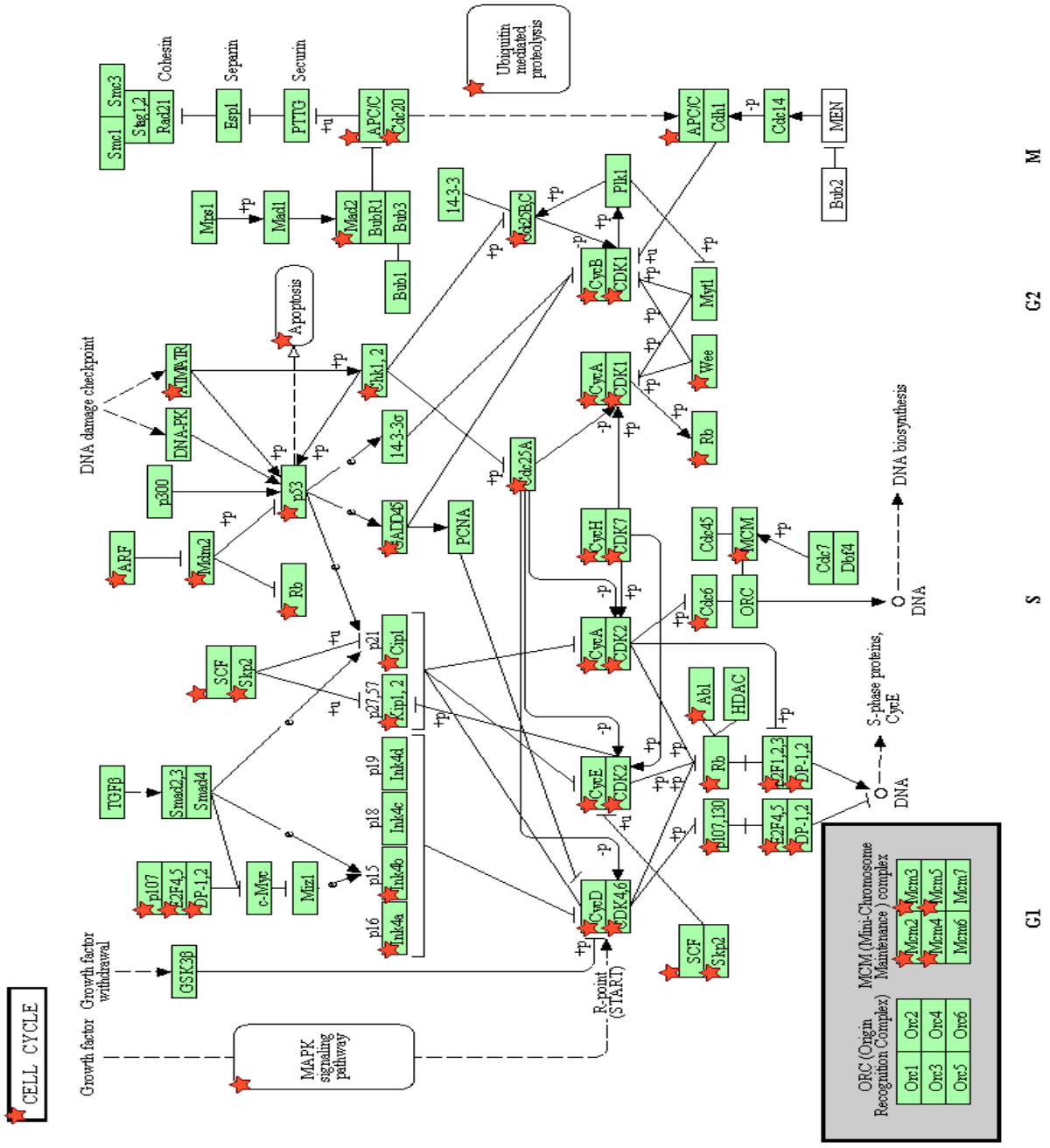

Figure 4. 38: The KEGG pathway visualisation of cell-cycle related genes of the RT^2 Profiler human cell-cycle gene array. The input genes of interest are shown by the red stars across the pathway.

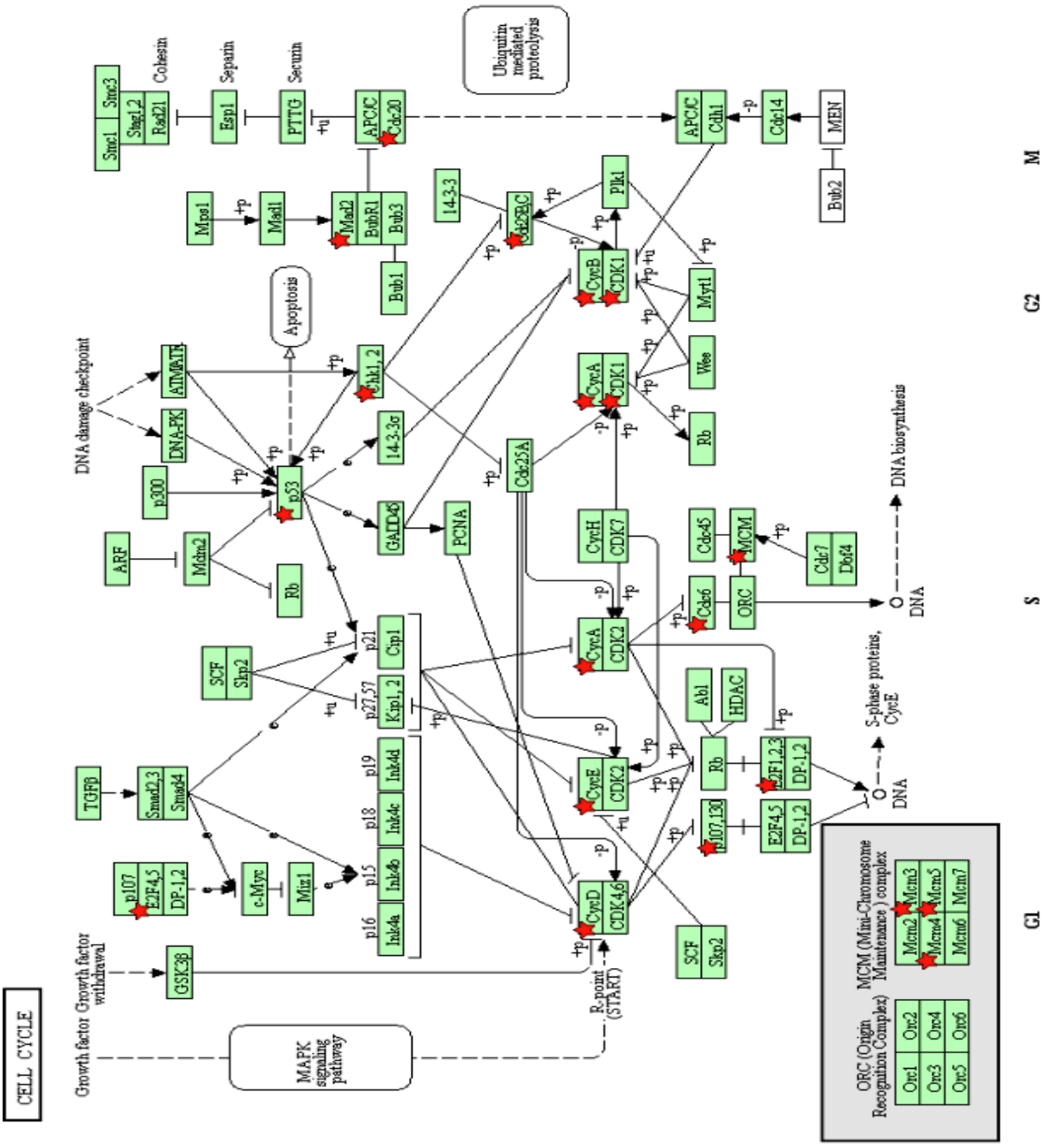

Figure 4.39: The KEGG pathway depiction of the up-regulated target genes in untreated A549 *vs* MRC-5 cells. A representation of the upregulated gene targets in untreated cells is shown by the red stars. Most of these up-regulated targets are cyclin/CDK complexes, as shown in the diagram.

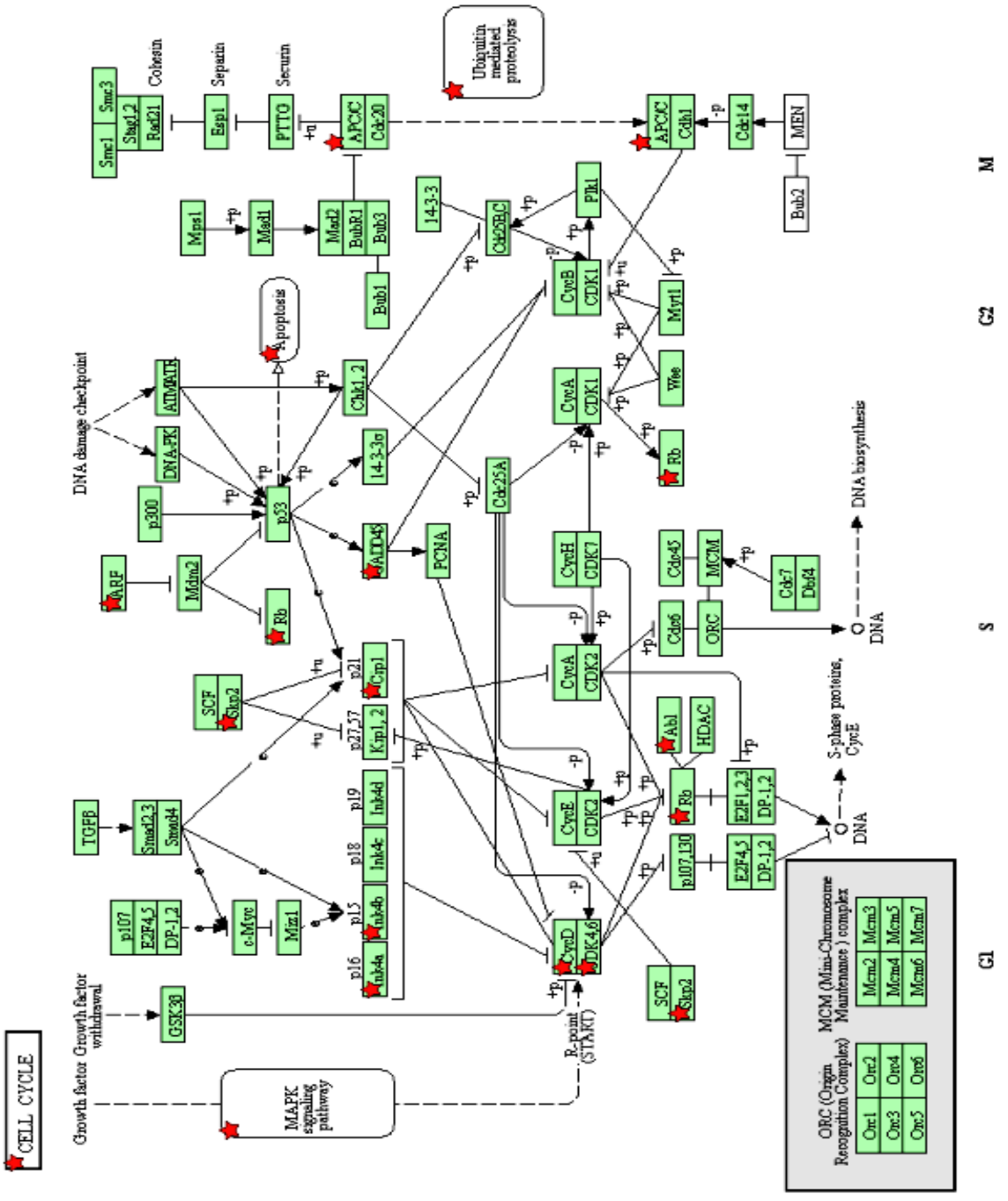

Figure 4.40: The KEGG pathway demonstration of the down-regulated gene targets in untreated A549 *vs* MRC-5 cells. A representation of the down-regulated gene targets in untreated cells is shown by the red stars. The deregulation of important cell-cycle regulatory elements such as the APC/C, the tumour suppressor Rb is observed here.

KEGG visualization pathway for EFV treated (MRC-5 and A549) lung cells

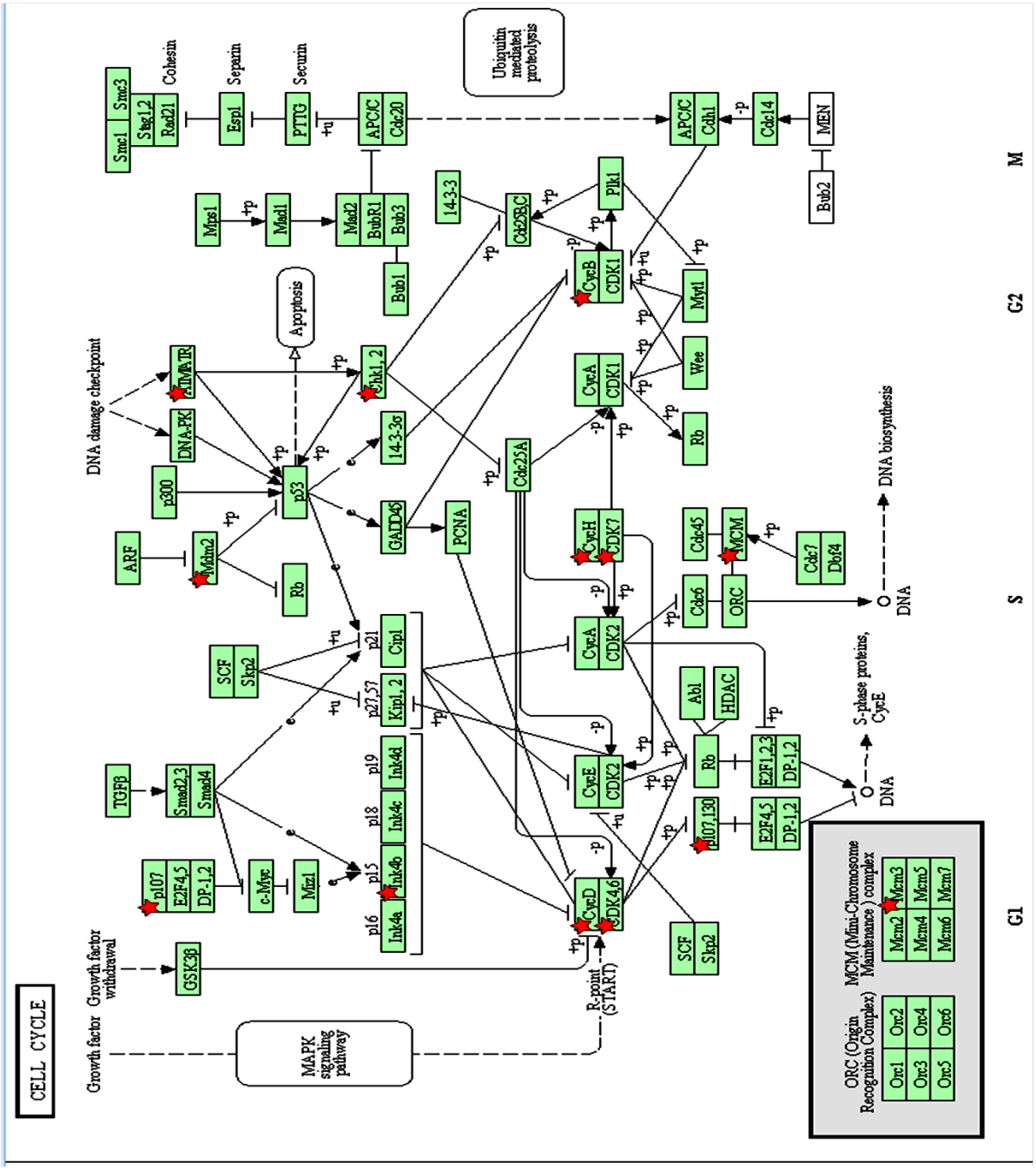

Figure 4.41: The KEGG pathway illustration of the up-regulated target genes in response to 13µM EFV treatment in MRC-5. The up-regulation of cell-cycle regulators such as cyclin D, B and H is seen. Interestingly, an activation of the ATM/ATR, which negatively regulates the cell-cycle is observed upstream of the cyclins.

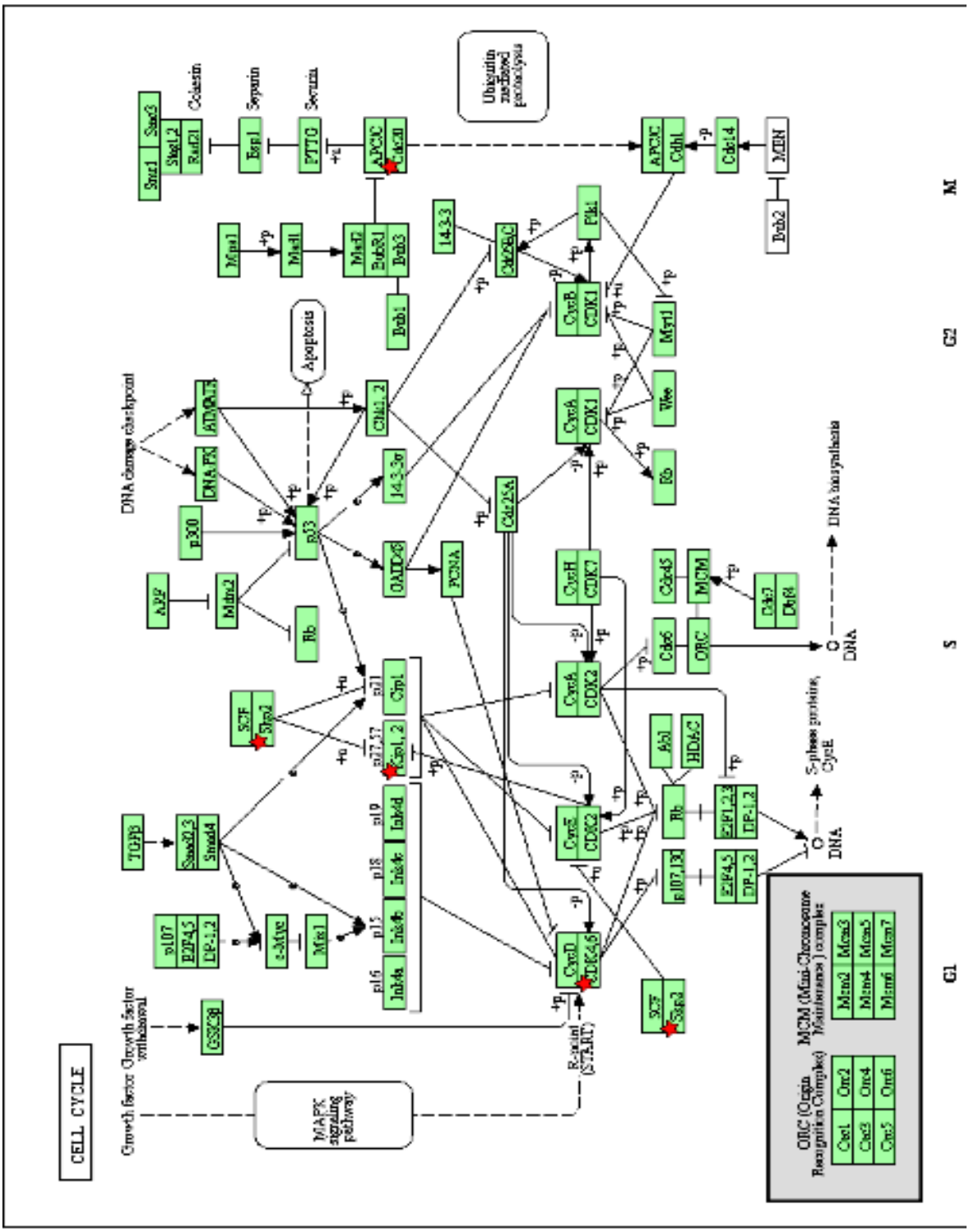

Figure 4.42: The KEGG pathway representation of up-regulated gene products in A549 cells treated with 13µM EFV. Few targets which include the APC complex are shown to be upregulated in response to EFV drug treatment.

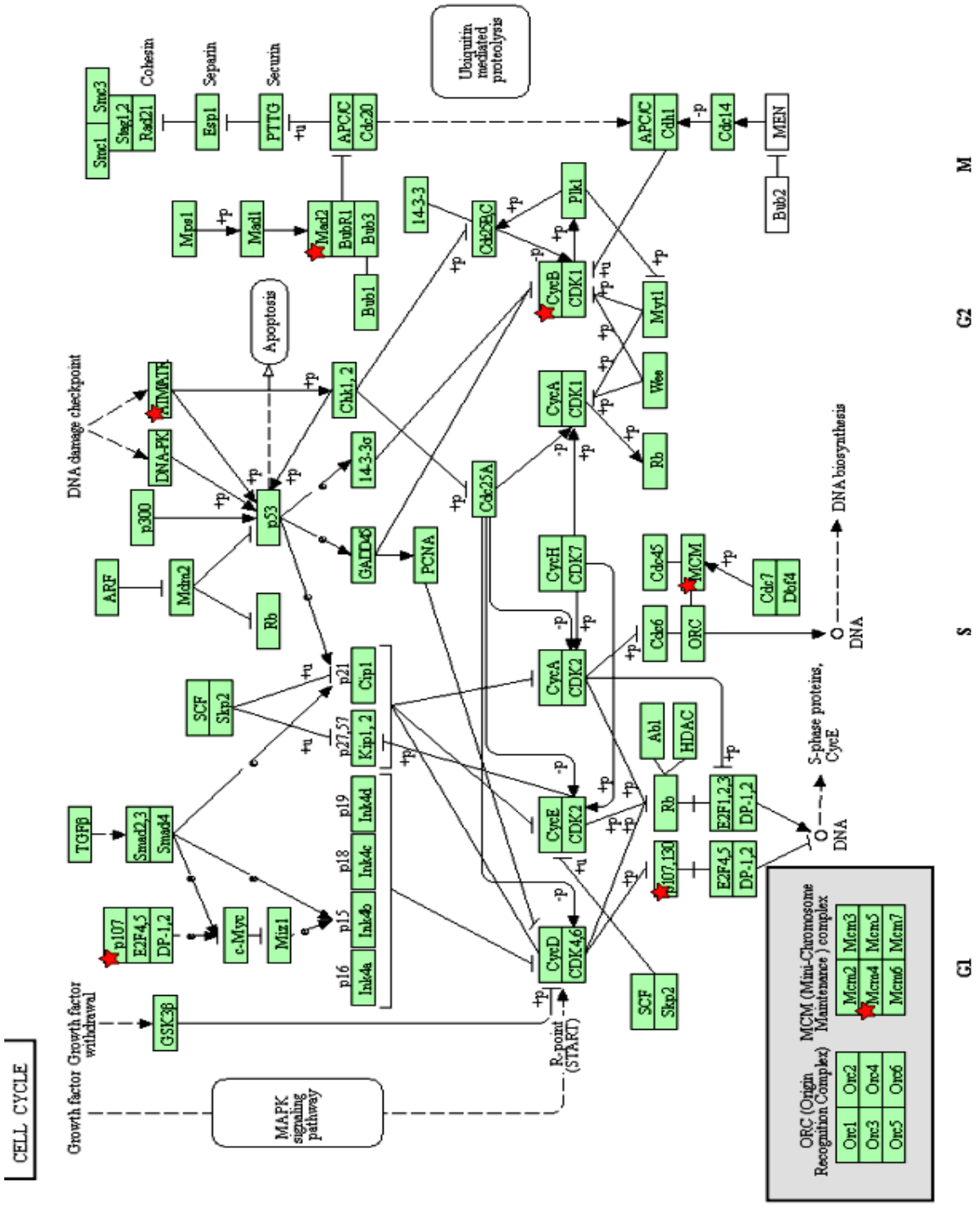

Figure 4.43: The KEGG pathway visualization of down-regulated gene targets in A549 cells treated with 13µM EFV. The deregulation of MAD2L2, an important cell-cycle checkpoint and arrest protein is observed here.

KEGG visualisation pathway for the LPV/r treated (MRC-5 and A549) lung cells

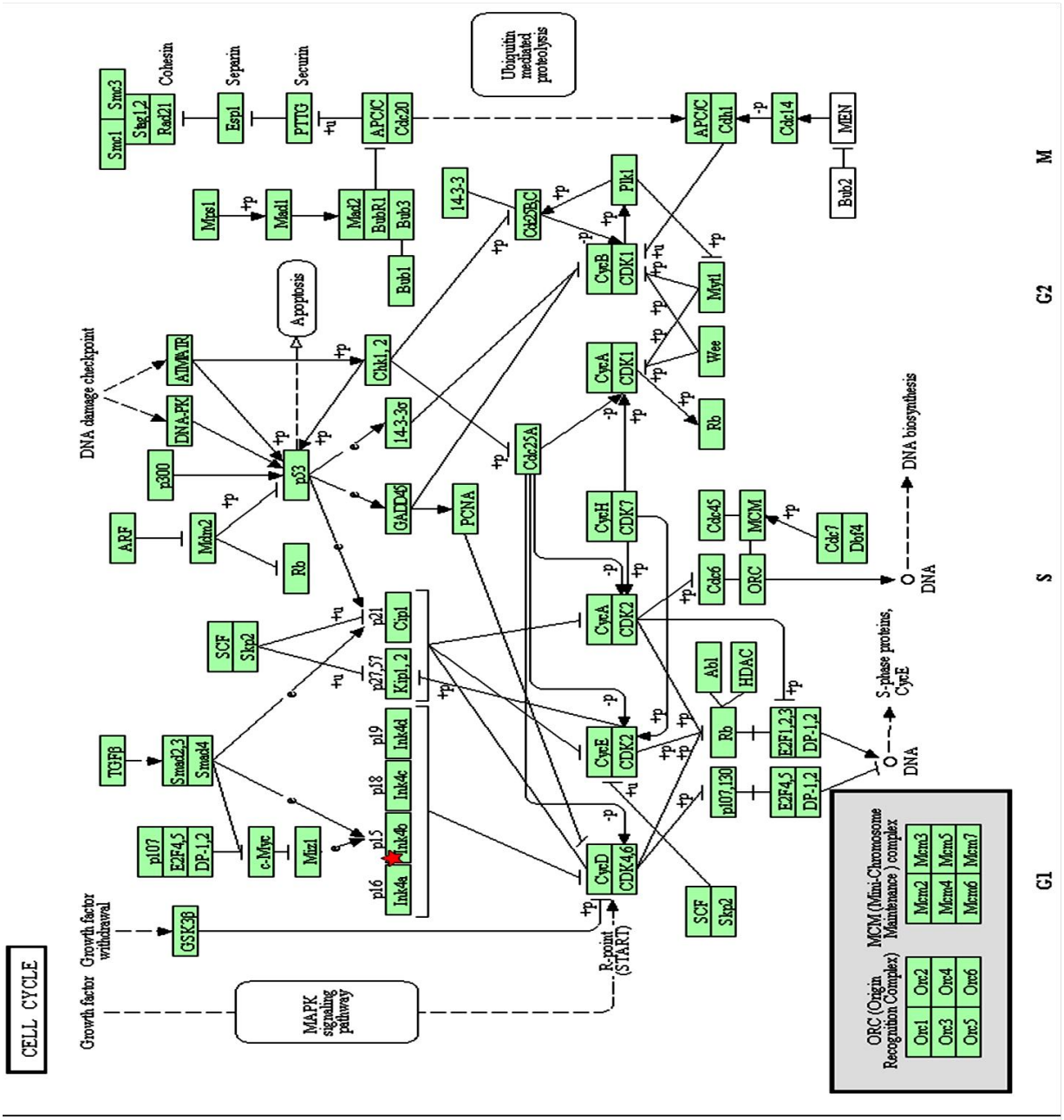

Figure 4.44: The KEGG pathway illustration of the up-regulated target(s) in MRC-5 cells in response to 32µM LPV/r treatment. Only one target (CDKN2B (p15/INK4b)) is shown to be activated by the LPV/r treatment in the normal cells. This target forms part of the cell-cycle checkpoint and arrest.

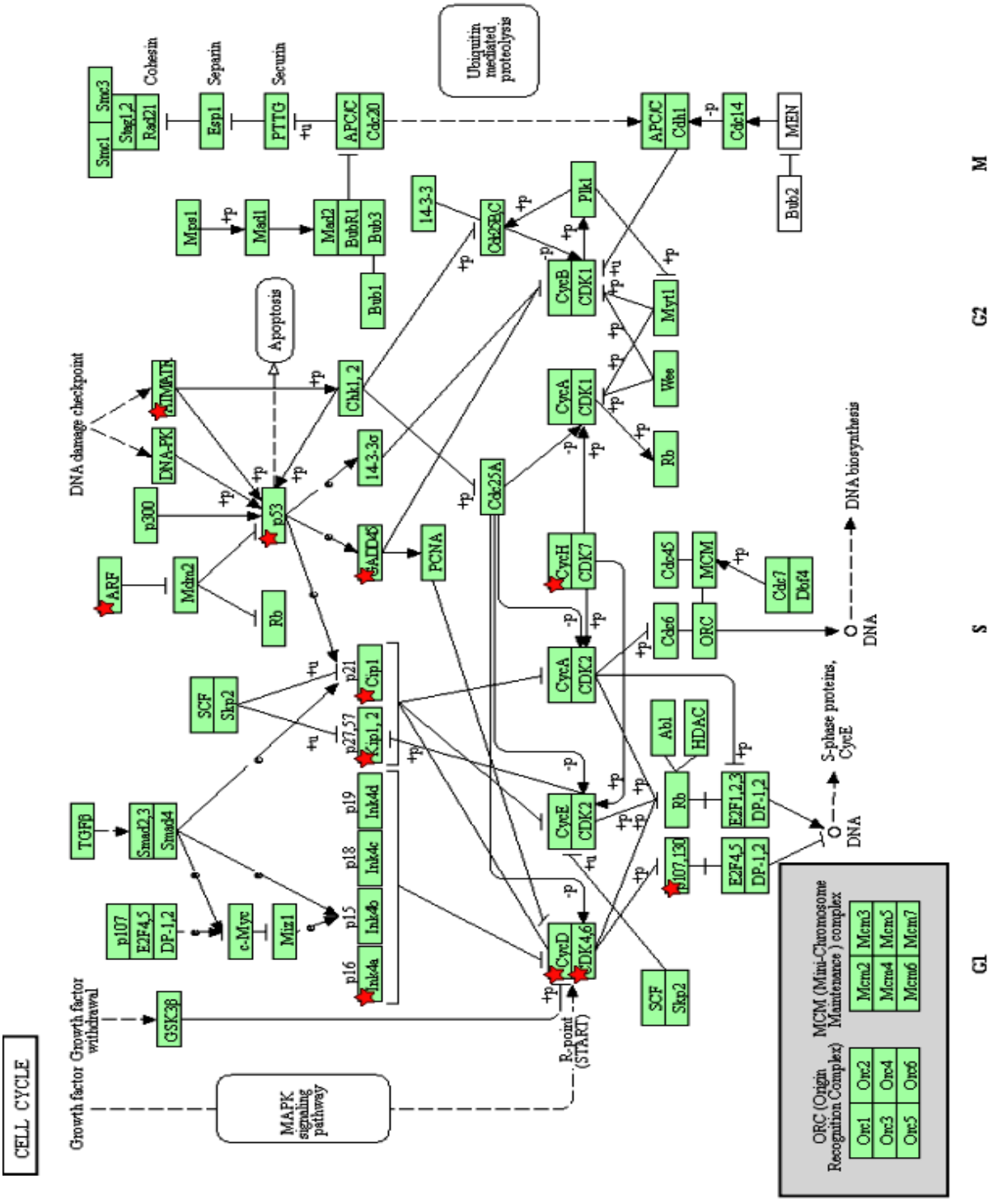

Figure 4.45: The KEGG pathway demonstration of up-regulated target genes in A549 cells treated with 32μM LPV/r. Here, an activation of DNA damage response gene targets such as ATM/ATR, p53 and GADD45 is observed.

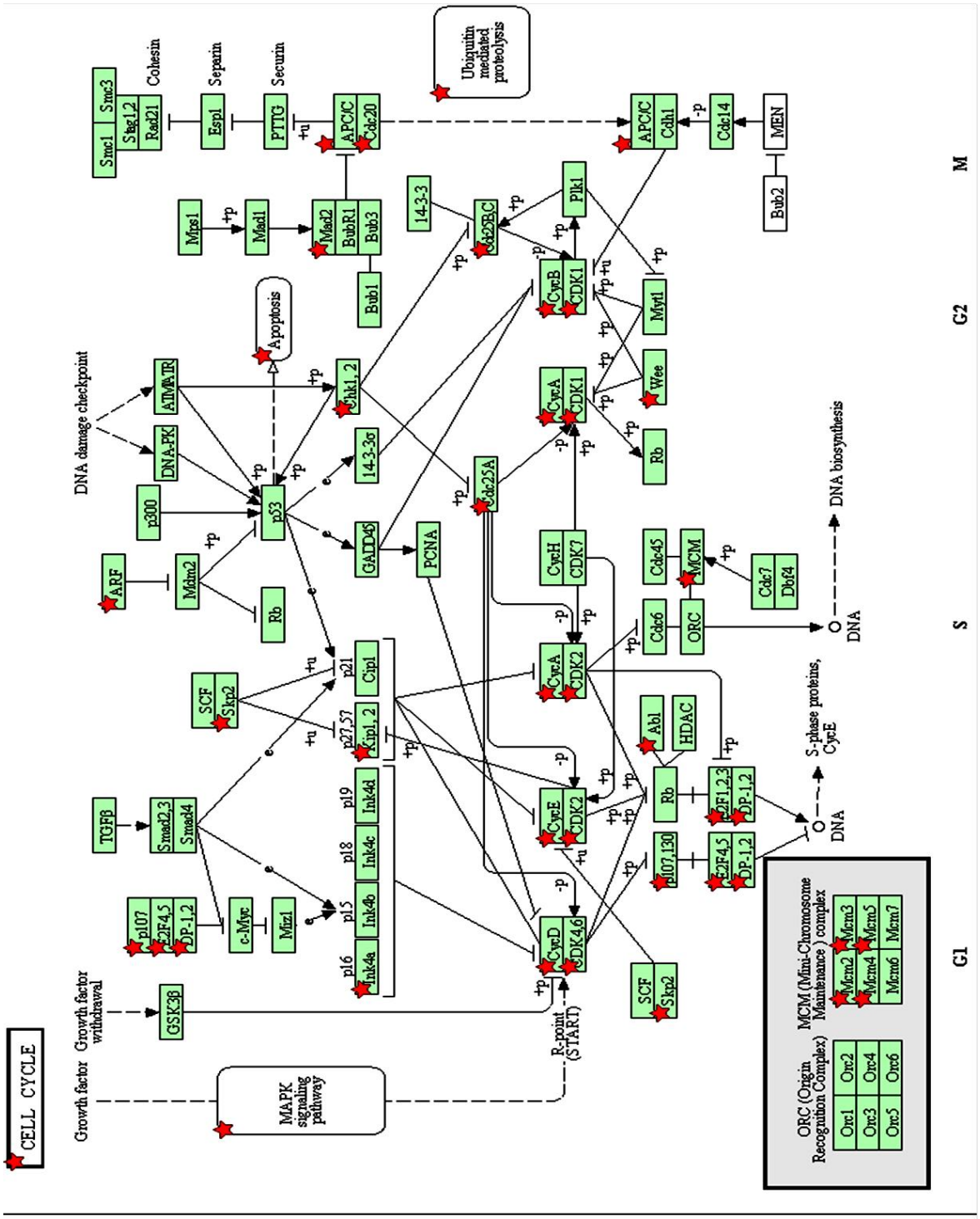

Figure 4.46: The KEGG pathway representation of down-regulated gene targets in MRC-5 cells treated with 32µM LPV/r. Most of the cyclin/CDK complexes are shown to be repressed here, restricting cell-cycle progression and cell proliferation in normal cells.

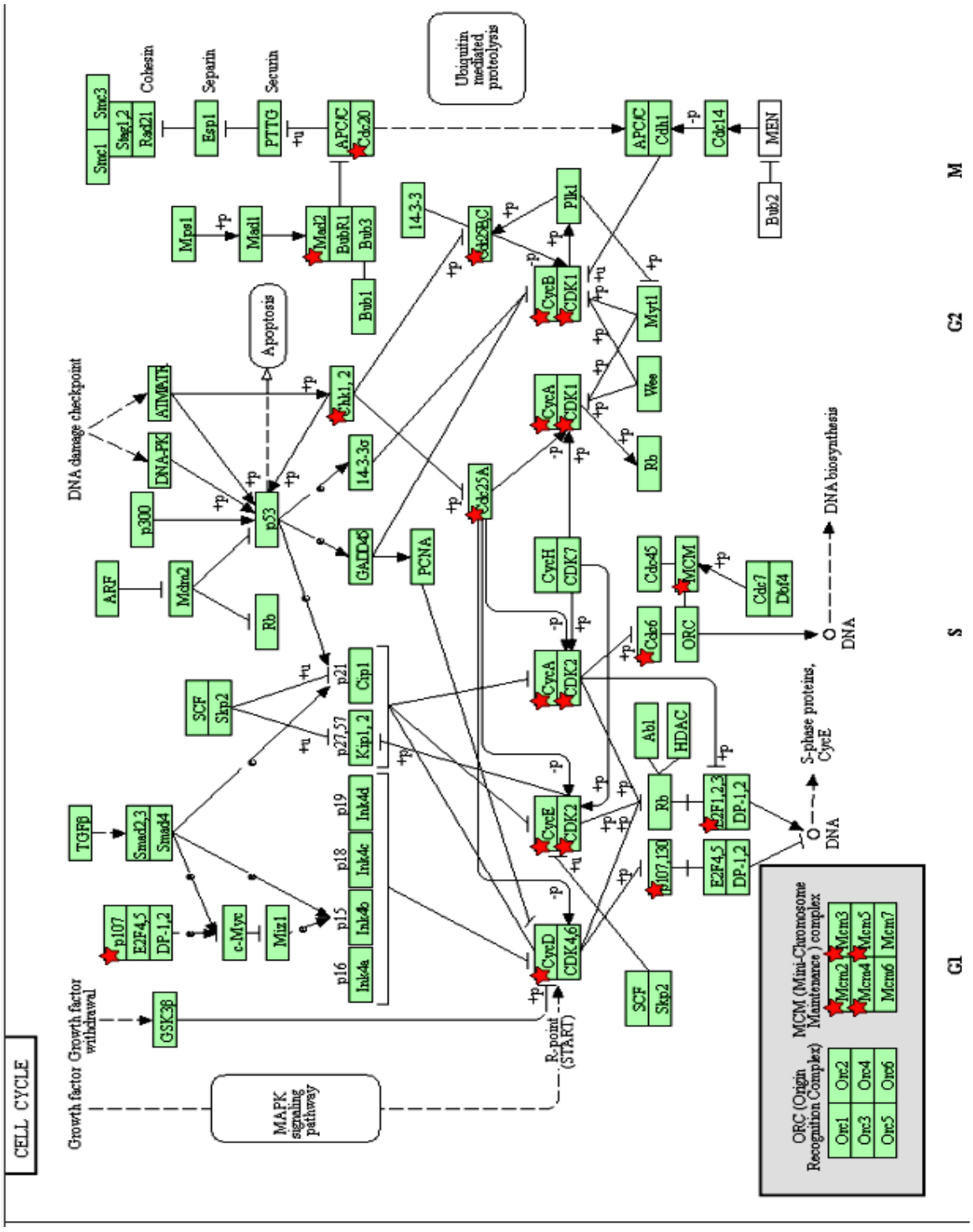

Figure 4.47: The KEGG pathway illustration of down-regulated genes in A549 cells in response to 32μM LPV/r drug treatment. The deregulation of cyclin/CDK complexes is observed here, as these positively regulate the cell-cycle. This inactivation of the cyclin/CDK complexes suppresses the progression of the cell-cycle.

4.4.3 Reactome analysis indicates that EFV alters cellular response to stress, DNA repair and programmed cell death (PCD)/apoptosis, while LPV/r treatment leads to an increase in PCD genes in A459 cells

Reactome is an open-source, open access, manually curated and peer-reviewed pathway database. This database is an all-inclusive resource of human pathways for basic research, genome analysis, pathway modelling, systems biology and education. In this study Reactome version V58 was used to map and analyse biological and molecular pathways other than the focused cell-cycle pathway, which may be influenced by the identified targets. Within the generated maps, gene expression level corresponds to the yellow colour, and the degree of expression correlates with the colour intensity.

A comparison between untreated cancer and untreated normal cells showed an increase in the expression of genes involved in DNA replication and cell-cycle regulation in the cancer cells (Figures 4.48 and 4.49). The exposure of A549 and MRC-5 cells with 13µM EFV, led to changes in the expression of genes involved in the cellular response to stress, DNA repair and programmed cell death (PCD)/apoptosis (Figure 4.48).

There was an up-regulation of the cellular response to stress genes, in both normal and cancerous cells at 32µM LPV/r. Genes associated with DNA repair were not up-regulated in MRC-5 cells, while the up-regulation of PCD genes is evident in A549 LPV/r treated cells (Figure 4.49).

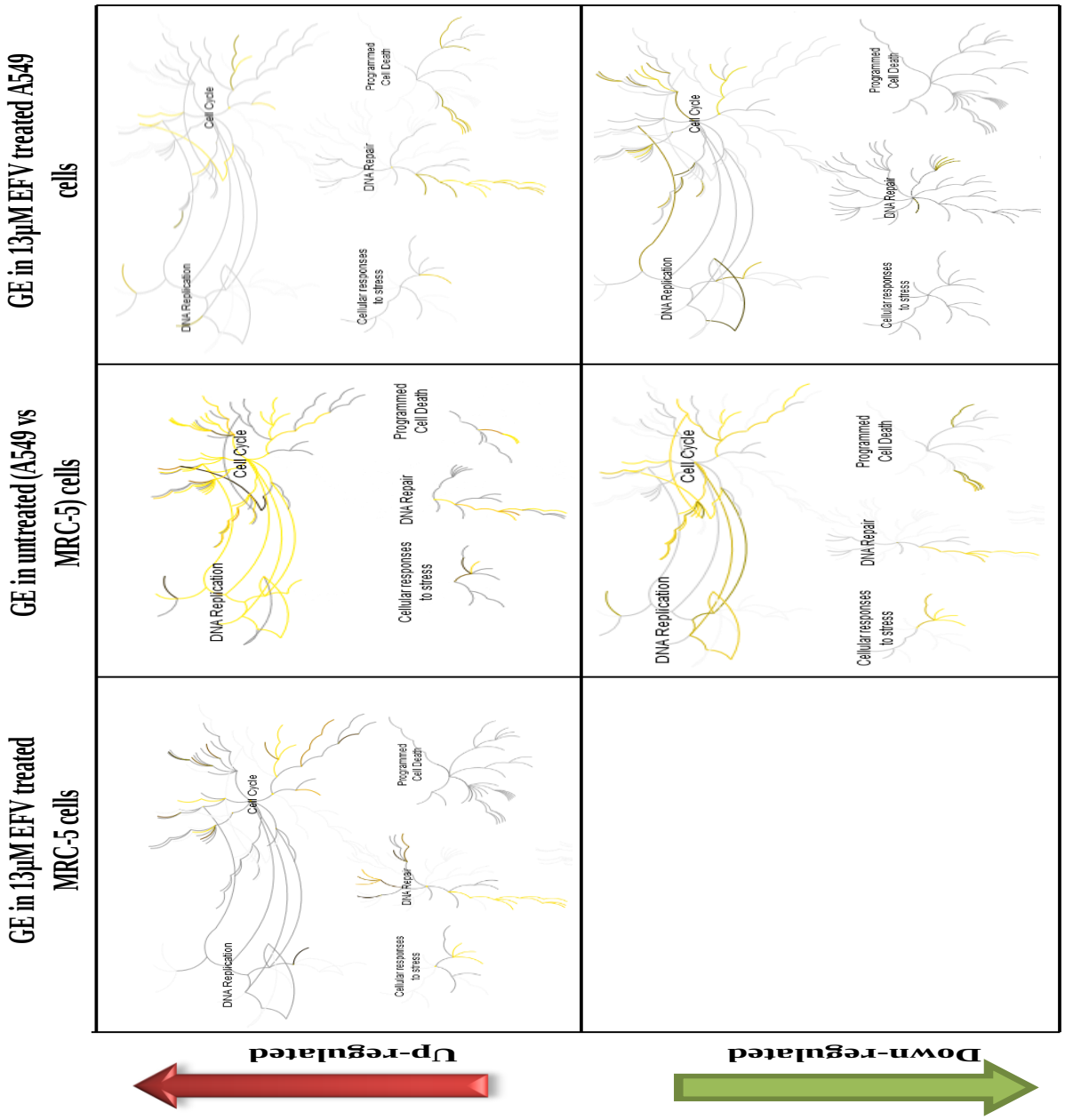

Figure 4.48 The Reactome map illustration of biological/molecular pathways influenced by the identified targets in response to 13μM EFV drug treatment. Change in gene expression (GE) patterns of the targets was compared between untreated cells and EFV treated A549 and MRC-5 cells. Change in GE patterns is represented between three pathways: Cellular response to stress, DNA repair and programmed cell death (PCD)/apoptosis. In response to EFV drug treatment, the DNA repair genes are up-regulated in both normal and cancerous cells, extending to the activation of apoptosis genes in the A549 cells.

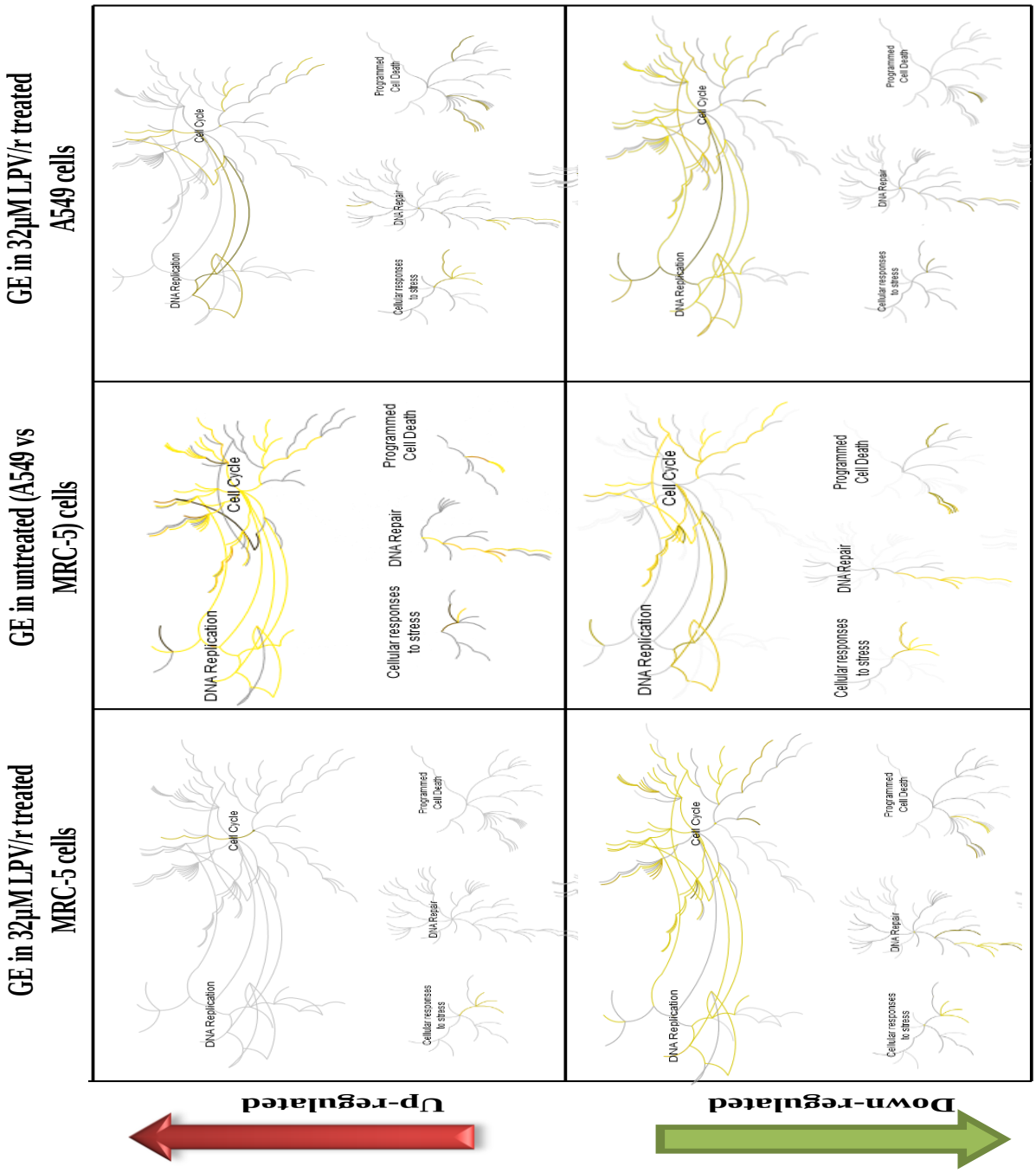

Figure 4.49: The Reactome map representation of biological/molecular pathways influenced by the selected targets in response to 32µM LPV/r drug treatment. Compared to the untreated cells, cellular response to stress genes are activated in response to LPV/r drug treatment, observed in both MRC-5 and A549 cells. Interestingly, DNA repair genes are not up-regulated in MRC-5 cells, while the up-regulation of PCD genes is evident in A549 LPV/r treated cells.

4.4.4 IPA analysis demonstrates ATM-pathway activation in EFV treated MRC-5 cells, while LPV/r treatment particularly triggers the p53-pathway in A549 cells.

Qiagens's Ingenuity Pathway Analysis (IPA) has been widely used to model, analyse and understand complex biological systems. In this study, the core analysis function of IPA was used to help build a more complete regulatory picture to better elucidate the biology underlying the studied gene expression profiles. The analyses are represented as bar graphs, with the z-score referring to the activation state, either up- (orange bars) or down (blue bars) regulation of the pathway.

IPA allows for the identification of well-characterized metabolic and cell signalling pathways (canonical pathways) that the genes whose expression is altered by drug treatment are involved in. The untreated cancer cells showed higher transcription levels of genes involved in DNA damage response and cell checkpoint pathways (Figures 4.50 and 4.51). EFV treatment of MRC-5 and A549 cells led to the activation of the cell-cycle regulation pathway in MRC-5 cells. Based on the observed change in expression of genes involved in cellular response to stress, DNA repair and PCD pathways, the p53 pathway was selected as the pathway of interest as it plays a significant role in the identified pathways by Reactome. In EFV treated cells the ATM signalling pathway activates its down-stream effector pathway, p53, Figure 4.50. Both the ATM and the p53 pathways are activated in response to DNA damage.

LPV/r treatment does not activate the ATM and the p53 signalling pathways in MRC-5 cells, while treatment of the A549 cells resulted in the activation of the p53 pathway despite the repressed upstream ATM pathway, which is vice versa to the untreated cells (Figure 4.51). These results led to the selection of the ATM and the p53 signalling pathways as the pathways of interest (POI) for the core analysis. The pink/red and green colours represent upregulation and down-regulation, respectively with the colour intensity corresponding to the degree of expression level (please refer to section 3.9 above, Figure 3.3 for further annotation details).

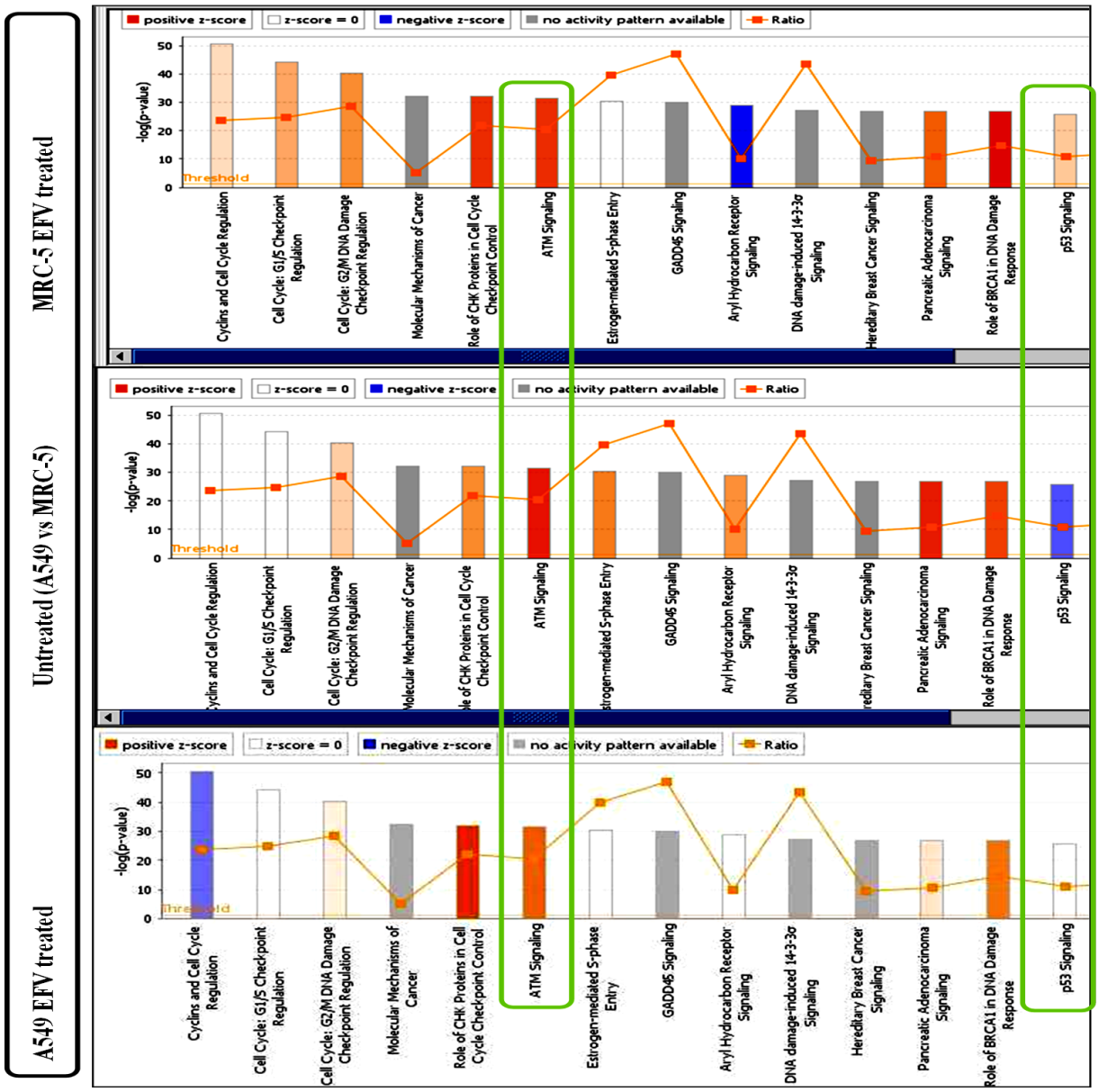

Figure 4.50: IPA Canonical Pathway analysis of differentially expressed genes in EFV treated vs untreated cells. The orange bars indicate activated pathways, while blue bars indicate repressed pathways. The colour intensity is proportional to the degree of in/activation. The green boxes highlight pathways of interest, the ATM signalling pathway and the p53 signalling pathway. Being upstream of the p53 pathway, the ATM signalling pathway does not activate its down-stream effector p53 pathway in untreated cells, compared to EFV-treated cells.

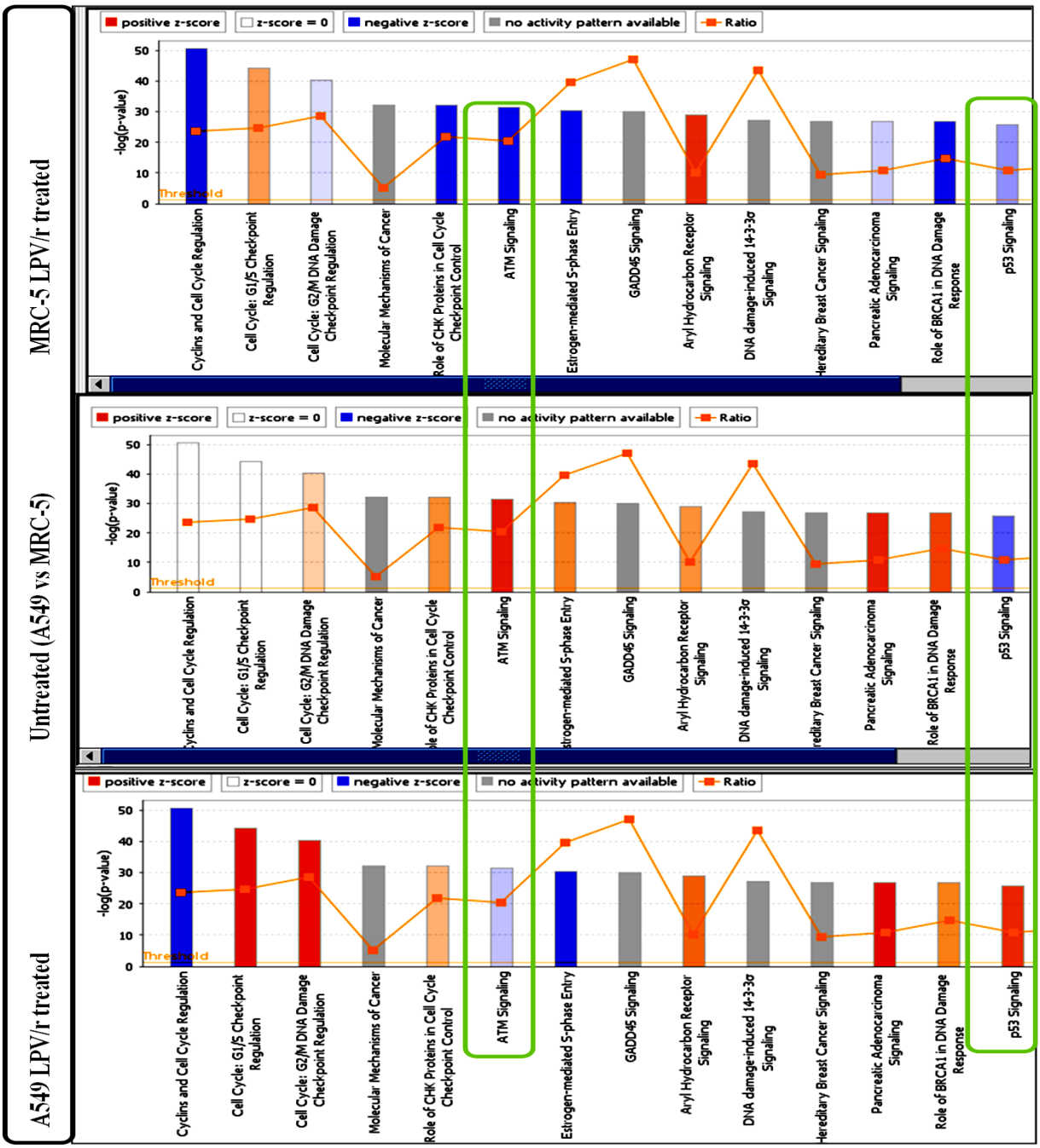

Figure 4.51: IPA Canonical pathway analysis of gene targets in cells treated with 32µM LPV/r *vs* untreated cells. The ATM and the p53 signalling pathways (highlighted in green boxes) are shown not to be activated by the LPV/r drug treatment in normal MRC-5 cells. Contrarily, the p53 pathway is activated in the A549 cells irrespective of the repressed upstream ATM pathway, which is opposite to what is observed in the untreated cells.

4.4.4.1 The downstream effectors of the ATM signalling pathway are activated in both cancer and normal cells following EFV treatment

The transcription of the ATM gene was increased in MRC-5 cells following EFV treatment. This leads to the downstream activation of the targets of ATM such as p53, BRCA-1 and CHK1 leading to DNA repair, cell-cycle arrest, DNA damage checkpoint regulation or apoptosis (Figure 4.52). EFV treatment of the A459 cells does not lead to an increase in the transcription of ATM. However, the downstream effectors of ATM are still activated due to DNA damage induced by the drug treatment. These include the p53 targets such as p21 and GADD45 and the DNA damage response molecules BRCA1 and NBS (Figure 4.53).

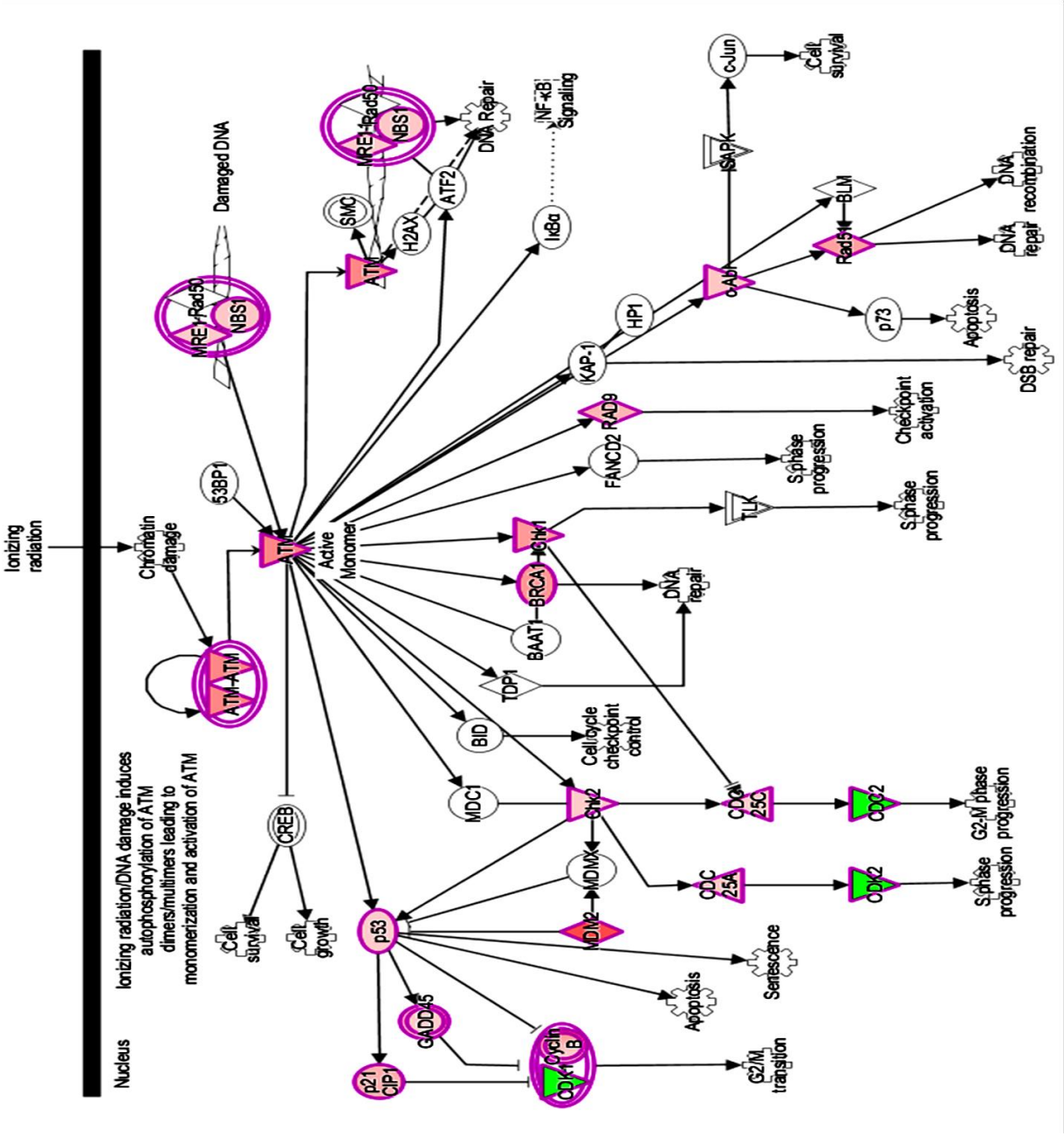

Figure 4.52: IPA ATM-signalling pathway in EFV treated MRC-5 cells. The green and the red colours indicate down and up-regulation. The activated ATM activates its downstream targets such as p53, BRCA-1 and CHK1, which in turn further activate their downstream targets to initiate DNA repair and growth arrest mechanisms.

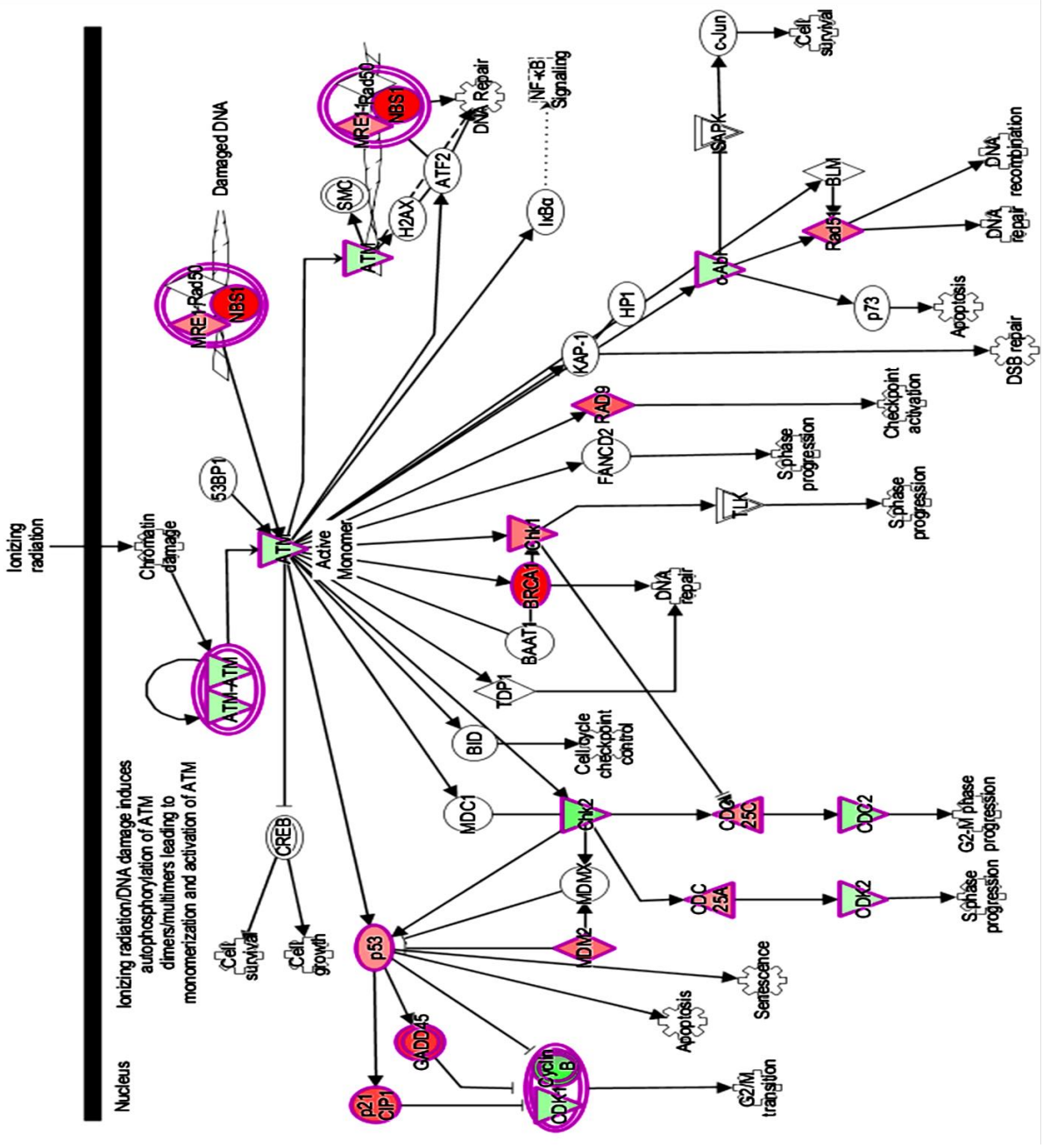

Figure 4.53: IPA ATM-signalling pathway in EFV-treated A549 cells. The green and red colours denote down and up-regulation. Here the downstream effectors of ATM in response to DNA damage are activated regardless of the ATM being inactive. The overexpression of the up-regulated p53 targets such as p21 and GADD45 (inhibiting the cyclin/CDK activation and thus the cell-cycle progression) is denoted by the intensified red colour. The increased expression of BRCA1 and NBS are also observed in response to damaged DNA.

4.4.4.2 LPV/r drug treatment activates the p53 signaling pathway in cancer cells

The downstream effectors of the p53 pathway are repressed in untreated cancer cells compared to normal cells. This would allow for the cancer cells to continue to proliferate and survive (Figure 4.54 and Figure 4.55). Following treatment of A549 cells with 32µM LPV/r, the p53 pathway and its downstream effectors were activated, leading to growth arrest and a decrease in cell survival (Figure 4.56 and Figure 4.57). A further demonstration of MAD2L2, CASP3 and AURKB interacting with p53 and p53 signalling proteins is shown in Figures 4.58 and 4.59.

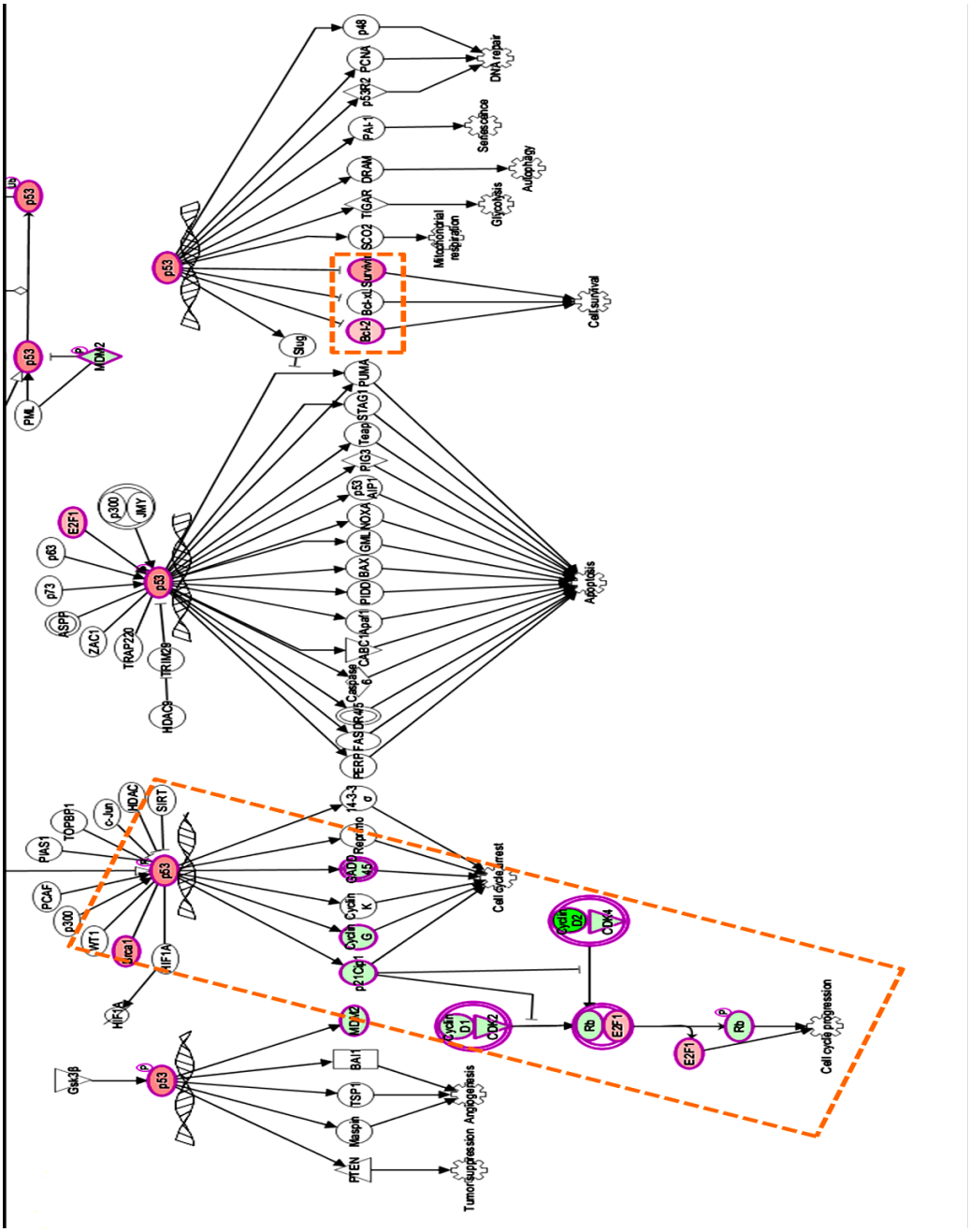

Figure 4.54: IPA p53 signalling pathway in untreated A549 *vs* MRC-5 cells. The green and red colours represent down and up-regulation. The orange boxes encompass most of the activity in this pathway. Although p53 is active here, its downstream effectors (p21, Cyclin G and GADD45) are repressed. The down-regulation of Rb is also observed, leading to cell-cycle progression. The overexpression of pro-survival targets such as Bcl-2 and survivin (BIRC5) leading to cell survival is also seen.

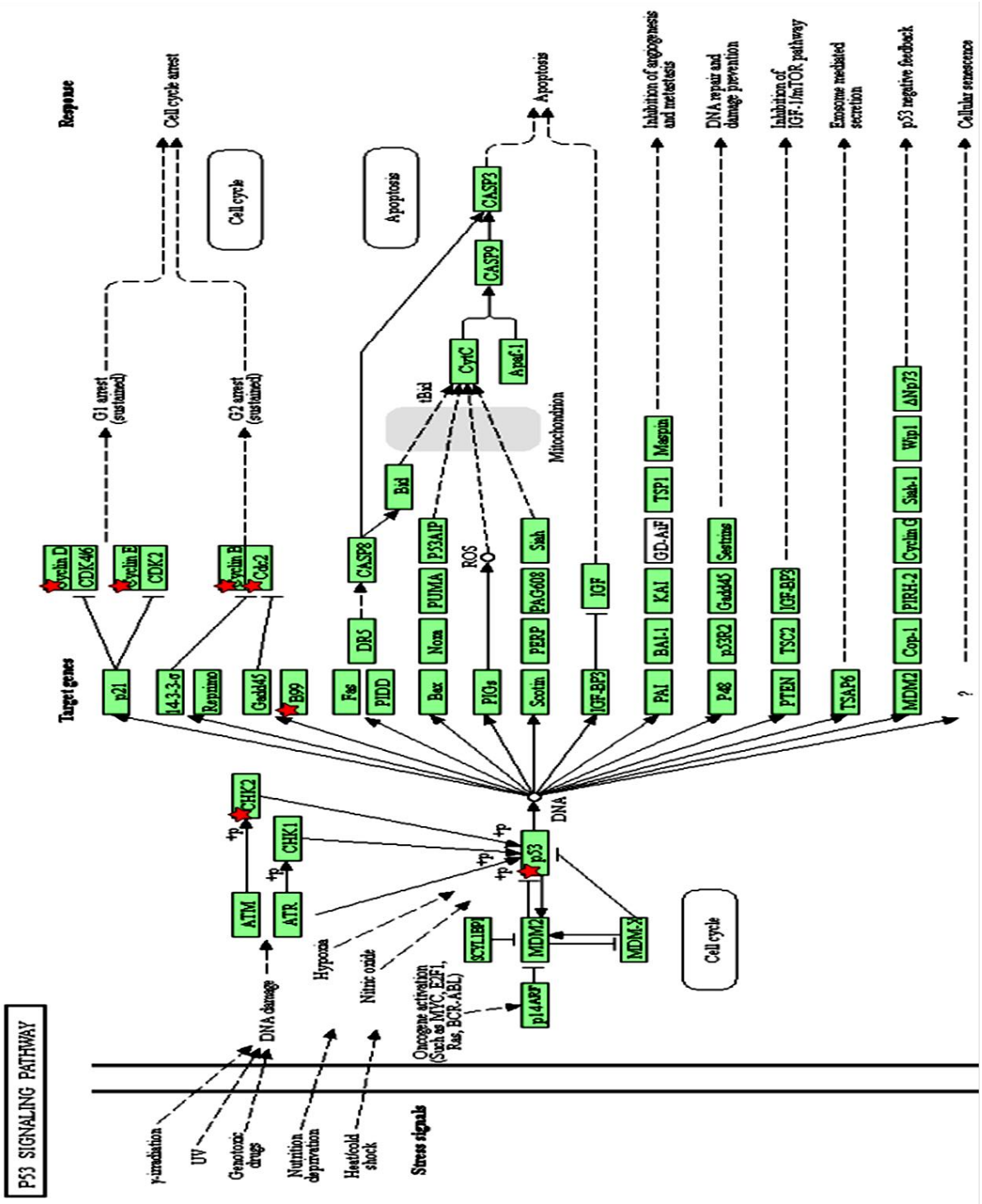

Figure 4.55: The KEGG pathway illustration of p53-signalling pathway in untreated A549 *vs* MRC-5 cells. Although p53 is active here, its downstream targets such as p21 and GADD45 are not activated in response to p53 up-regulation. This leads to a bypass of cell-cycle checkpoints and arrest, thus promoting cell survival.

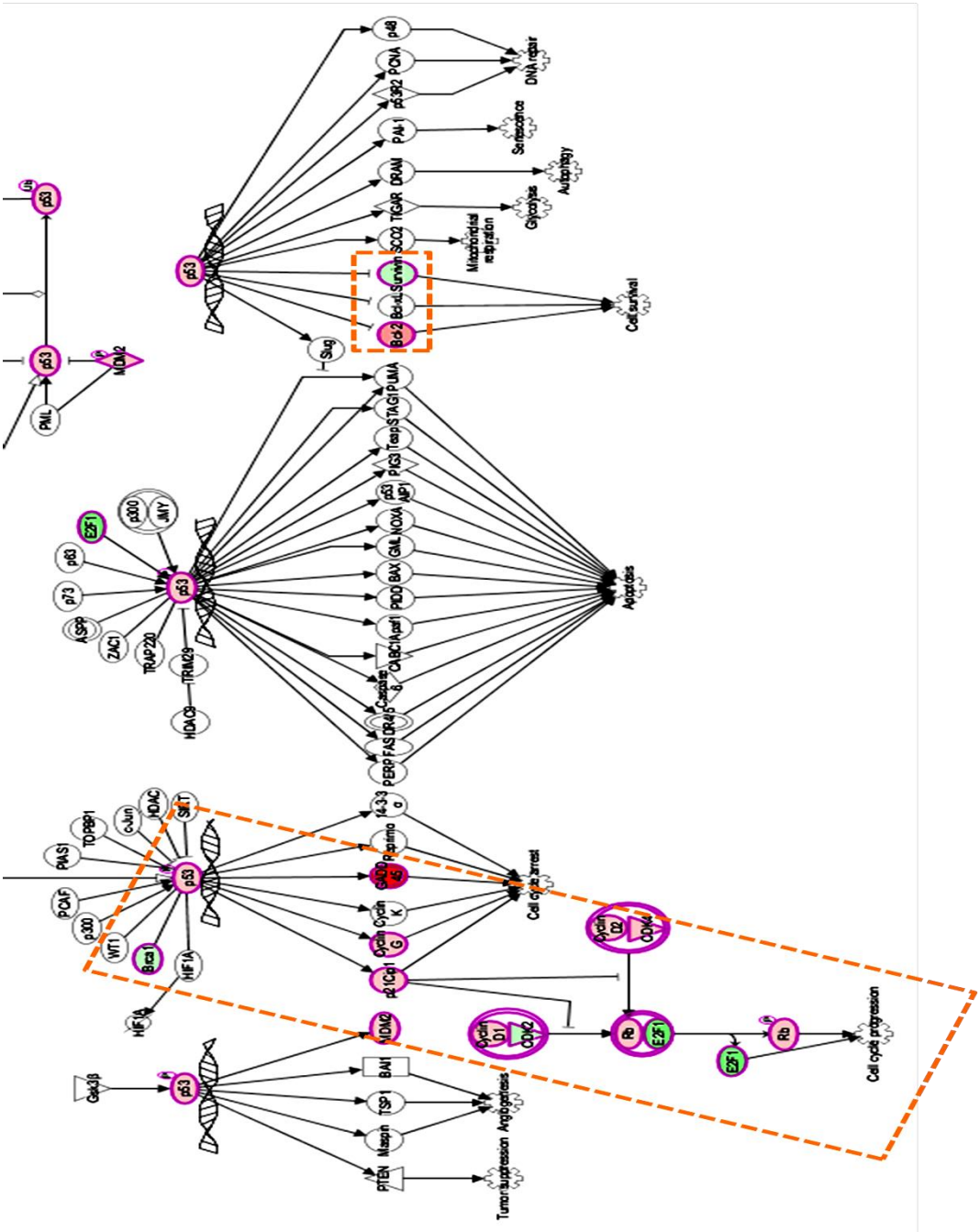

Figure 4.56: IPA p53-signalling pathway in A549 cells treated with 32µM LPV/r. The green and the red colours signify down and up-regulation. The over expression of growth arrest molecules such as p21, Cyclin G and GADD45 in response to the activated p53 is represented here. The active (unphosphorylated) Rb is bound to and represses E2F1, with the deregulated CDK2, and thus arresting the progression of the cell-cycle. The activation of Bcl-2 is obscure here, while the expected down-regulation of survivin is observed.

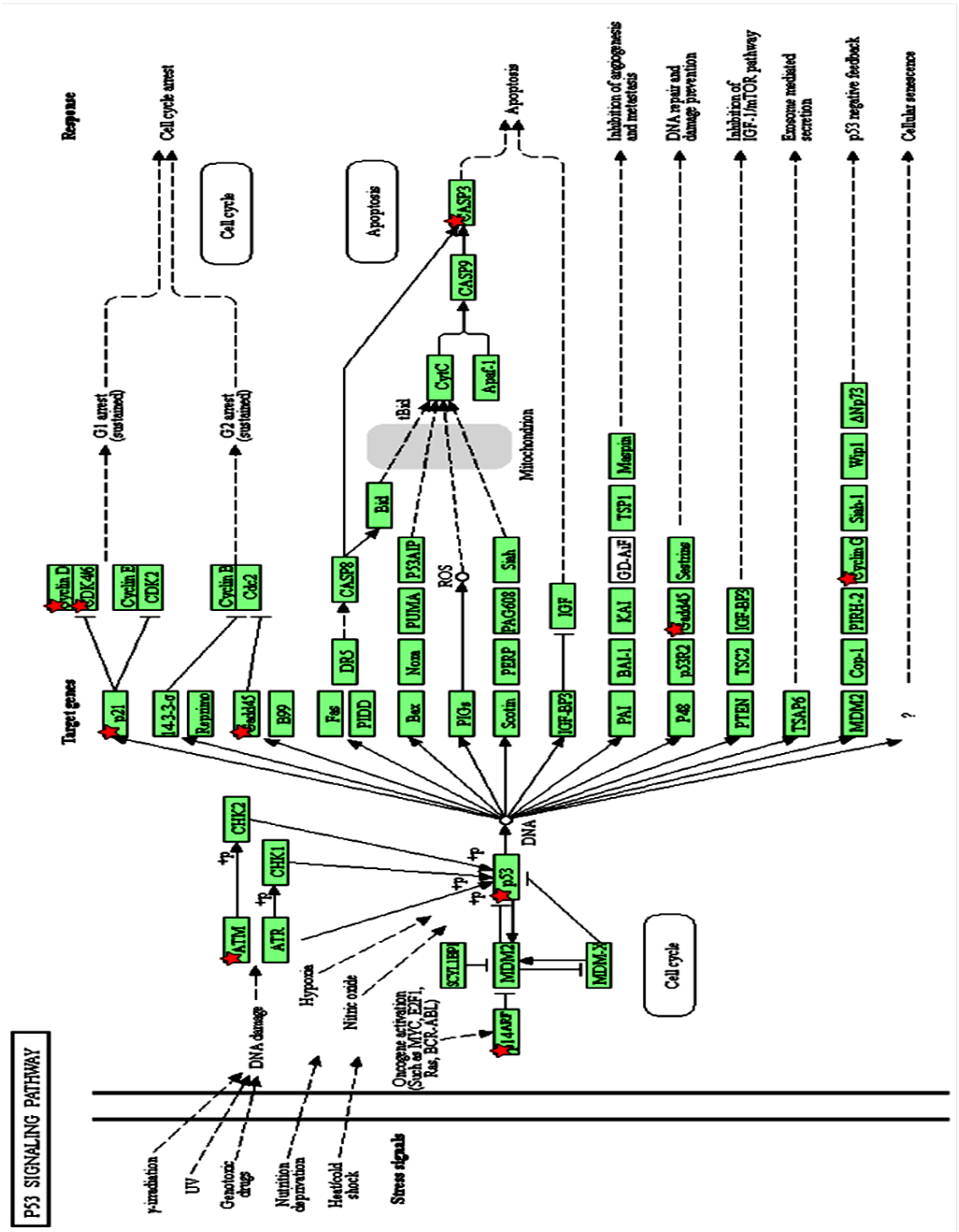

Figure 4.57: The KEGG pathway demonstration of the p53-signalling pathway in A549 cell treated with 32μM LPV/r. ATM signaling is up-regulated in response to genotoxic stress, which in turn activates the p53 signaling pathway. P21, Cyclin G and GADD45 are activated downstream of p53, effecting cell-cycle checkpoint and arrest.

4.4.5 The integration of MAD2L2, CASP3 and AURKB to the p53 signaling pathway.

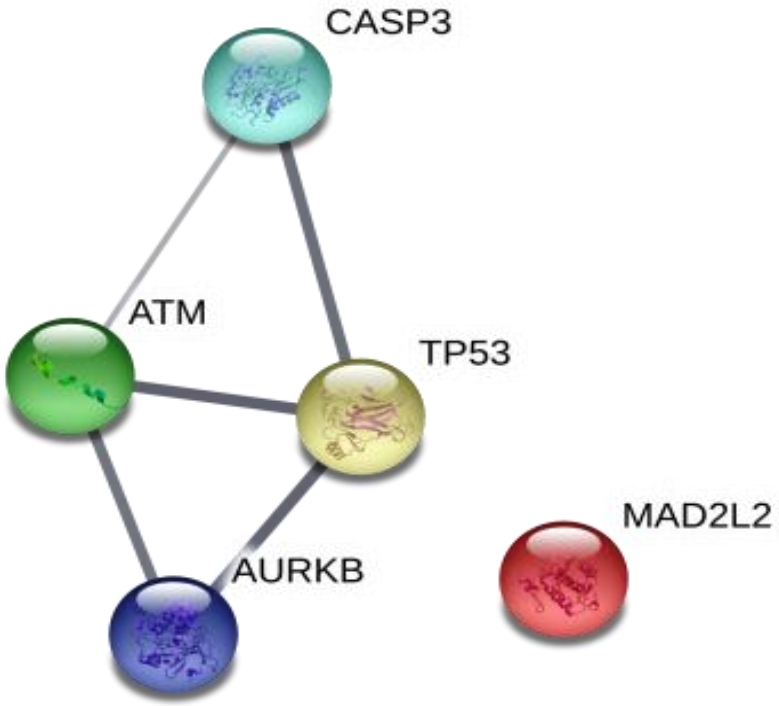

Figure 4.58: STRING protein-protein interaction (PPI) analysis between ATM, p53 and selected targets. The interaction threshold was set at 0.4. In this interaction, MAD2L2 is a stand-alone due to lack of evidence of either direct or indirect interaction with all four of the proteins. Both CASP3 and AURKB show a strong and direct interaction to p53, while AURKB strongly interacts with both ATM and p53, as illustrated by bold lines.

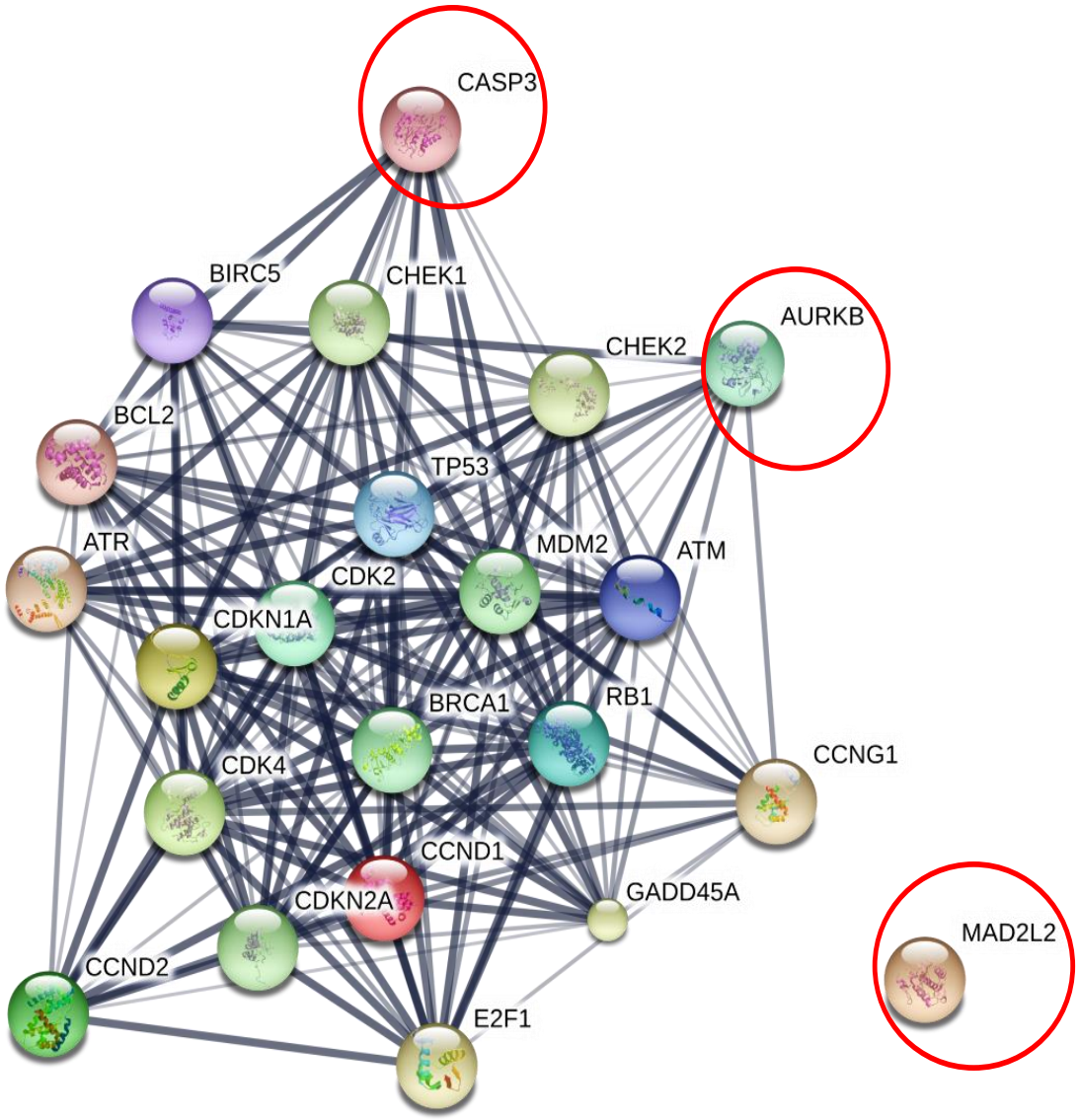

Figure 4.59: STRING protein-protein interaction (PPI) analysis between p53 signalling pathway and selected targets MAD2L2, CASP3 and AURKB. The interaction threshold was set at 0.4. CASP3 and AURKB show a strong and direct interaction to p53 and other proteins within the pathway such as BIRC5 (Survivin), while MAD2L2 is secluded from the interaction network.

CHAPTER 5: DISCUSSION

5.1 Cell Biological Response to ARV Treatment

5.1.1 ARVs affect cell proliferation by modulating cell-cycle progression

The cell responses to antiretroviral treatment were assessed in real time to quantitate cell proliferation and to effectively determine cellular response to the pharmacological treatments. The ARTs acted to decrease cell viability in a dose-dependent manner in both cell lines. Notably, however, the two plasma level EFV concentrations increased cell proliferation, while only the lowest LPV/r treatment caused a proliferative increase. Moreover, the most physiologically relevant LPV/r dose resulted in growth arrest, in lung cancer cells. Thus dependent on concentration and at specific window periods of treatment, both EFV and LPV/r can exert either pro- or anti-tumorigenic effects on cells.

As previously described, the cell-cycle is normally a tightly regulated process with multiple control points at different phases of cell growth, with the failure or improper functioning of these check points potentially leading to abnormal cell proliferation or apoptosis. In association with increased cell proliferation, subsequent cell-cycle analyses showed a significant increase in S-phase in response to ARV treatments; with an apoptotic induction for one of the ARVs (LPV/r). However, it was noted that besides apoptosis, LPV/r treatment additionally triggered necrotic cell death in a time-dependent manner. A model summarizing the pro- and anti-proliferative effects of EFV and LPV/r is represented below (Figure 5.1).

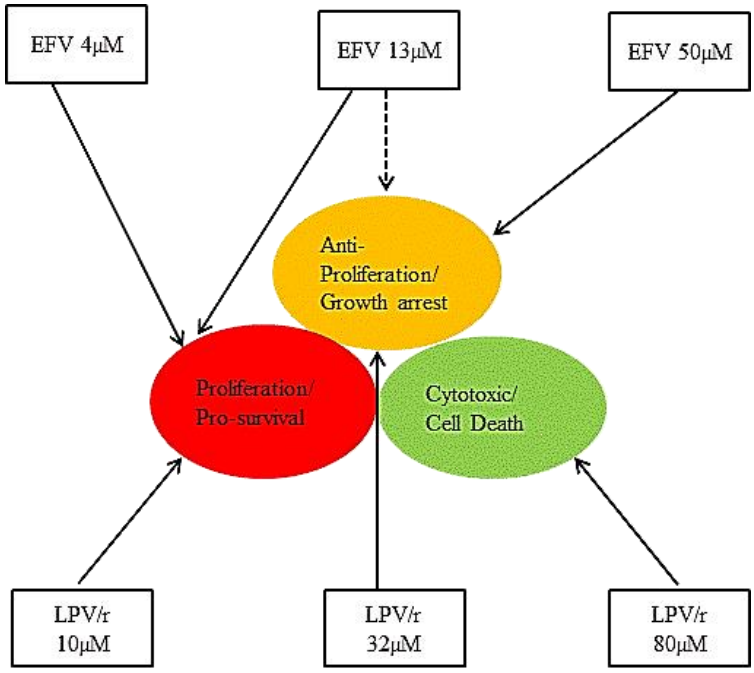

Figure 5.1: Diagrammatic representation of the effects of EFV and LPV/r at low and high doses. Both EFV and LPV/r exhibit pro-survival effects at low doses, while anti-proliferative and cytotoxic effects are observed at high doses. The solid arrows represent the effects of the drugs on cellular health, while the dashed line shows partial/dual effect. At a high dose, EFV is anti-proliferative, arresting cellular growth, while low doses favour survival modes, as also observed with low LPV/r dose. In contrast, moderate (plasma-level) and high LPV/r doses have anti-proliferative and cytotoxic properties on the cells.

Based on these observations, it is proposed here that both EFV and LPV/r alter the cell-cycle progression of both normal and cancerous cells, especially arresting cells at S-phase to inhibit further progression through the cycle, with extended LPV/r apoptosis inducing properties.

The apoptotic inducing properties of LPV/r merit further investigations not only as an ARV drug, but also as an anti-cancer treatment. However, a current limitation of LPV/r is its ability to not only kill tumour cells, but also to eliminate normal healthy cells, On the other hand, while an S-phase arrest is evident from both EFV and LPV/r treated cells, DNA damage usually precedes S-phase arrest. It follows then that both EFV and LPV/r could potentially be causing damage to the genomic DNA, with an arrest at S-phase, during which time there may

be an attempt to either repair the damaged DNA or an induction of premature senescence or cell death. While the S-phase arrest is induced in the A549 lung cancer cells, it is also evident in the normal MRC-5 cells. This observation particularly implicates EFV and LPV/r as inducing stress on the DNA, with cells attempting to establish defense mechanisms by blocking the transmission to G2/M phase.

5.2 *In silico* analyses of cell-cycle associated pathways

5.2.1 The DNA damage response pathway

DNA damage can be caused by genotoxic agents and if not repaired, could result in chromosomal changes, gene mutations, excessive cell death or ultimately cancer. When encountering genotoxic stress, cells respond by activating DNA repair mechanisms. Depending on the degree of DNA damage, the induced repair mechanisms either eliminate the DNA lesions or bypass them. Most of the DNA repair mechanisms involve nucleases, which in themselves pose a threat to the genome if not carefully regulated (Christmann and Kaina, 2013).

In response to DNA damage imposed by genotoxic stress, DNA damage sensors must first detect the DNA lesions, in order to initiate the DNA damage response (DDR). DNA damage is detected by the Mre11–Rad50–Nbs1 (MRN) complex which acts as the sensor of damaged DNA and maintains genomic stability by processing DNA ends and recruiting other members of the DNA damage response pathway ((Li *et al.*, 1999), (Christmann *et al.*, 2005), (Islaih *et al.*, 2004)). In particular, Rad50 recognizes the damaged DNA, Nbs1 recruits other DNA repair proteins to DSB lesions, and Mre11 processes the DNA ends with its DNA nuclease activity (Christmann *et al.*, 2005). This then leads to activation of Ataxia Telangiectasia Mutated (ATM) or Ataxia Telangiectasia and Rad3 Related (ATR), depending on where the damage is. ATM is activated in response to DSDs on DNA and chromatin remodeling while ATR is activated in response to stalled replication forks ((Myung *et al.*, 1998), (Montecucco *et al.*, 1995)). This is followed by a signalling cascade that activates repair checkpoints and recruits the remaining members of the DNA repair complex.

In mammalian cells the DNA damage response includes ATM, ATR and PARP1 as well as key transcription factors, which in turn target their downstream effectors such as BRCA1, NF-Κβ, AP-1 and p53. Following the induction of DNA damage response (DDR), transcription factors are activated. In addition, the induction of DNA repair genes in mammalian cells is lower, for example, for Methylguanine-DNA Methyltransferase (MGMT) up to 15-fold in rat liver, which is a comparatively high level;and in rat hepatoma cells *in vitro*, 2–4-fold ((Chan *et al.*, 1992), (Christmann and Kaina, 2013)), compared with bacteria, in which the induction of DNA repair genes such as *ADA* is 1000-fold, following Methylnitronitrosoguanidine (MNNG) exposure. However, this does not essentially mean that the induction of DNA repair genes is biologically insignificant noting the fact that mammalian cells express DNA repair genes at a detectable basal level and that even a slight upregulation may significantly improve repair ability.

The activation of ATM requires the activation of the MRN complex comprising of MRE11, NBS1 and RAD50 that triggers ATM auto-phosphorylation. This leads to dissociation of inactive ATM dimers to active monomers. The ATM monomers then interact with the MRN complex and single-stranded DNA (ssDNA) (Lee and Paull, 2005). The MRN complex itself recognizes and moves to DSBs induced by ionizing radiation (Mirzoeva and Petrini, 2001) and to ssDNA on replication blockages (Mirzoeva and Petrini, 2003) and remains at the site of DNA damage. In the deregulation of the MRN complex, the autophosphorylation of ATM is inhibited, and thus cannot be recruited to the DSB site (Lee and Paull, 2005). On the other hand, ATR is activated following blockage of DNA polymerases and the formation of lengthy ssDNA, which are formed by uncoupling of the mini-chromosome maintenance (MCM) helicase from the replication fork and then binding of replication protein A (RPA) to ssDNA ((Byun *et al.*, 2005). RPA labelled ssDNA activates the recruitment of ATR complexed with ATR-interacting protein (ATRIP) and the Rad9, Hus1 and Rad1 (9–1–1) complex to the site of damage (Parrilla-Castellar *et al.*, 2004).

p53 is a sequence-specific transcription factor that plays a major role in DNA repair, apoptosis and cell-cycle regulation ((Haupt *et al.*, 2003), (Wu *et al.*, 2013)). P53 is activated by DNA replication arrest following the formation of DSBs caused by genotoxins and irradiation *via* the ATM/ATR pathway. In turn, ATM phosphorylates the checkpoint kinase-2

(CHK2), following replication blockage while, ATR phosphorylates CHK1. Then, CHK2 and CHK1 activate p53 by phosphorylation. ATM and ATR can also directly phosphorylate p53. Furthermore, ATM/ATR also phosphorylates MDM2, resulting in MDM2 degradation by ubiquitination and thus stabilizing p53 (Khosravi *et al.*, 1999).

During cell division, proper genomic DNA replication is critical towards maintaining genomic instability. This replication process is facilitated by high-fidelity error-free DNA polymerases that cannot synthesize across damaged DNA. Error-prone specialized DNA polymerases, known as DNA translesion synthesis polymerases (TLS polymerases), can replicate damaged DNA thereby avoiding replication fork breakdown and thus chromosomal instability. Among DNA polymerases, the family B DNA polymerases include the highly accurate DNA polymerases δ (delta), ε (epsilon), α (alpha), and the error-prone TLS Pol (zeta) ζ ((Uziel *et al.*, 2003), (Byun *et al.*, 2005), (Zietlow *et al.*, 2009), (Braithwaite and Ito, 1993)). TLS Pol ζ lacks the 3' to 5' exonuclease proofreading activity, unlike the replicative DNA polymerases δ and ε. The human TLS Pol ζ and its yeast homologue are heterodimeric proteins consisting of the catalytic subunit REV3 and the structural subunit REV7 ((Lavon *et al.*, 2007), (Nelson *et al.*, 1996), (Murakumo *et al.*, 2000)).

The DDR pathways includes non-homologous end joining (NHEJ) and homologous recombination (HR) pathways to repair double strand breaks (DSBs), base excision repair (BER) to counteract modification of the nitrogenous bases, nucleotide excision repair (NER) to excise bulky nucleotide alterations, mismatch repair (MMR) to exchange mispaired nucleotides and direct damage repair and the translesion DNA synthesis (TLS), which tolerate and bypass DNA lesions.

DNA damage response (DDR) genes have been shown to play a role not only in tumour initiation, at least in part when they fail to properly repair the damaged DNA, but in tumour progression and metastasis ((Knobel and Marti, 2011), (Broustas and Lieberman, 2014)).

Due to the use of the homologous sister chromatid as template, it has been reported that HR is an error free repair pathway and the major mechanism used by cells for repairing DSBs and restarting stalled replication forks ((Nowsheen and Yang, 2012), (Falck *et al.*, 2012)). If DNA repair is unsuccessful, then p53 initiates apoptosis by activating pro-apoptotic proteins such as

BAX, BID, PUMA and NOXA which permeabilizes the mitochondrial membrane leading to the release of pro-apoptotic factors ((Pauklin *et al.*, 2005), (Levine, 1997)).

5.2.2 *In Silico* Bio-Informatics analysis of cell-cycle related genes treated with Efavirenz (EFV) and Lopinavir/ritonavir (LPV/r) in lung cells

(a) STRING Analysis

STRING PPI analysis of the cell-cycle genes evaluated here in response to ART treatment elucidated a series of tight interactions. Pivotal factors were identified in relation to the DNA damage response including GADD45, HUS and RAD gene products and are discussed further below.

The emerging evidence of the regulatory role of AURKB on p53 activity is observed by the strong and direct interaction between these two molecules, while MAD2L2 is indicated to strongly interact with CDC20, which forms part of the APC complex (see Figure 4.30). The deregulation of CASP3 and RAD9-HUS1 suggests the malfunctioning of the DNA damage sensors, and the non-functioning of the effector CASP3 in the lung adenocarcinoma cells, thereby preventing them from undergoing CASP3 mediated apoptosis (Figure 4.31). The 13µM EFV drug treatment up-regulates the DNA damage response genes in both normal and cancerous cells, Figure 4.32 and Figure 4.33, while repressing the expression of AURKB and MAD2L2 in the A549 cells, Figure 4.34. In a similar manner, 32µM LPV/r drug exposure stimulates the expression of p53 and its downstream targets such as GADD45A (DNA damage response gene) in the A549 cells, Figure 4.36, while suppressing DNA replication genes (MCM), the cell division cycle genes CDC20 and CDC25, Figure 4.37. In normal cells, most of the genes maintain a suppressed state, even post LPV/r exposure (Figure 4.35). ARV drugs stimulated DNA damage response pathways and repressed cell proliferation in both normal and cancer cells. Figure 5.2 below summarises the findings of the STRING analyses.

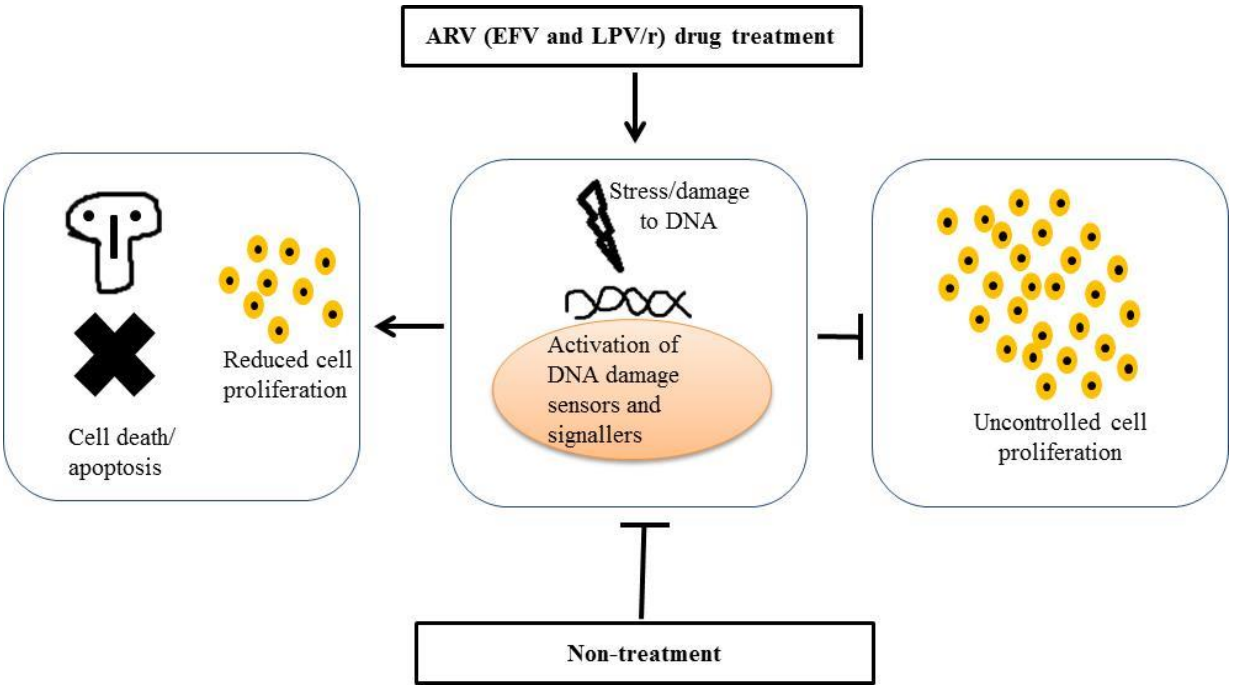

Figure 5.2: Summarized schematic representation of the activated DDR pathway as analysed by STRING database in lung cancer cells. Activated DNA damage sensors and signalers interact subsequent to ARV treatment, while these mechanisms remain inactivated in untreated conditions. This is followed by reduced cell proliferation and or cell death in ARV treated cells, and uncontrolled cell proliferation in vehicle treated lung cancer cells. The observations are based on plasma level doses.

(b) DAVID Analysis

DAVID analysis identified the change in expression of cell-cycle regulatory factors such as the cyclin/CDK activity, and the p53 downstream targets. Even though the p53 tumour suppressor is activated in the cancer cells, its down-stream effector targets such as p21, GADD45A (to arrest growth and possibly repair the damaged DNA) are suppressed (Figure 4.39 and Figure 4.40). In response to 13μM EFV exposure, ATM/ATR DNA damage checkpoints are activated, which in turn activates CHK1 and 2 in the normal cells; and also noteworthy is the up-regulation of the CDK-inhibitor p15 (Figure 4.41). On the other hand, p27/57 is up-regulated by the EFV treatment in the A549 cells (Figure 4.42) and MAD2L2 is repressed in cancer cells following EFV treatment (Figure 4.43) where it is normally up-

regulated in untreated cancer cells (Figure 4.39). Unlike in the untreated cells with repressed CDK-inhibitors' activity (Figure 4.39), the EFV treatment up-regulates the CDK-inhibitors in both cancerous and normal cells, even though the cyclin (D and H)/CDK are active in normal cells. The activation of the CDKIs could be attributed to the drugs repressing progression of the cell-cycle driven by the cyclin/CDK interactions. Similar to EFV, LPV/r treatment up-regulates the CDKI-p15 which inhibits the activity of cyclin/CDK complexes, thereby inhibiting the progression of the cell-cycle in normal cells (Figure 4.44). Similarly, the activation of p16, p21 and p27/57 (dependent on p53 up-stream activation) is observed in A549 EFV treated cells, leading to the reduced activity of the cyclin/CDK complexes in both normal and cancerous cells (Figure 4.46 and Figure 4.47). Both EFV and LPV/r target the activation of growth-arrest genes, leading to the reduction in cell-cycle progression.

(c) Reactome Analysis

This revealed that EFV and LPV/r drug treatment altered the expression of the profiled cell-cycle related genes, affecting other pathways besides the cell-cycle. In particular, EFV was shown to activate the cellular response to stress genes in MRC-5 cells, DNA repair genes in both normal and cancerous cells, while up-regulated programmed cell-death genes and an obvious decline in expression of genes involved in DNA replication in A549 cells was observed compared to the untreated cells (Figure 4.48). LPV/r treatment results in the reduced expression of DNA replication in normal cells, while an increase in genes involved in programmed cell death in the cancerous cells was observed (Figure 4.49).

(d) IPA analysis

To understand the mechanisms underlying the observed change in gene expression in the pathways identified using Reactome, IPA core analysis particularly showed that the ATM and p53-signalling pathways were affected. These are DNA damage response pathways, and the deregulation of these pathways plays an essential role in genomic instability, leading to cancer.

EFV treatment triggered the ATM pathway in A549 cells, and particularly in the MRC-5 cells, with an insignificant increase in the activation of the down-stream p53 pathway, which is not in a repressed state in the untreated cells. Both ATM and p53-signalling pathways remained inactivated in MRC-5 LPV/r treated cells. In contrast, an opposite effect was observed in LPV/r treated compared to the untreated A549 cells. This was indicated by the activation of the p53-pathway in A549 LPV/r treated cells, despite the repressed up-stream ATM-signalling pathway. This suggests that there could be other as yet un-elucidated upstream molecules triggering the p53-signalling pathway in response to DNA damage in A549 LPV/r treated cells.

5.2.3 Details of the ATM and p53 pathways

In EFV-treated MRC-5 cells (Figure 4.52), DNA damage causes the activation of MRN complex (MRE11, NBS1 and RAD50). This leads to ATM-autophosphorylation and then to the dissociation of inactive dimers to active monomers. The ATM monomers then interact with the MRN complex and single-stranded DNA (ssDNA). The MRN complex itself recognizes and moves to DSBs induced by ionizing radiation and to ssDNA on replication blockage and remains at the site of DNA damage. In the deregulation of the MRN complex, the autophosphorylation of ATM is inhibited, and thus cannot be recruited to the DSB site (Christmann and Kaina, 2013).

The active ATM then phosphorylates CHK2 which in turn phosphorylates p53. Active ATM can also directly phosphorylate p53. Furthermore, the MDM2 phosphorylation by ATM results in MDM2 degradation by ubiquitination and thus stabilizes p53. The activated p53 then acts to up-regulate the transcription of down-stream targets, such as p21 and GADD45A, which in turn suppress the expression of cyclin/CDK complexes and thus the progression of the cell-cycle (Nowsheen and Yang, 2012).

In EFV-treated A549 cells (Figure 4.53), the MRN complex is activated upon DNA damage. However, for reasons unknown here, ATM remains inactivated. Even though CHEK2 is inactivated, other ATM down-stream effectors such as CHEK1, BRCA1 and p53 are

activated. P53 then in turn activates p21 and GADD45A, while repressing cyclinB/CDK1 activity.

Previous reports (Zhang *et al.*, 2009) show that the A549 cells have a wild-type p53. Similarly in this study, in untreated cancerous cells, p53 is activated, however, its downstream effectors such as p21, GADD45A and cyclin G are down-regulated, while pro-survival molecules such as survivin and Bcl2 are up-regulated (Figure 4.54 and Figure 4.55). Following exposure to 32µM LPV/r, p53 and its downstream targets are activated (p21, GADD45A and cyclin G) and pro-survival molecules are repressed (survivin) (Figure 4.56 and Figure 4.57). Lack of activity from p53 anti-proliferative downstream effectors in untreated A549 cells allows cells to grow uncontrollably, proliferate and survive. On the other hand, 32µM LPV/r treatment not only activated p53, but ensured the up- and -down-regulation of p53 targets to control and inhibit excessive proliferation. Furthermore, Figure 4.58 and 4.59 illustrate STRING analysis of the selected targets with p53 and p53 signalling pathway members.

Malfunctioning within cell-cycle DNA damage response pathways results in genome instability and often leads to carcinogenesis. The cyclins/CDKs are important regulators of cell-cycle progression, controlling the transition between different cell-cycle interphases. Their activity is regulated by CDKIs, and inversely activated by phosphatases, such as CDC25 that dephosphorylate the inhibitory effects of the CDKIs. p53 also plays a role in DNA repair and it is the main factor determining the choice between DNA damage repair or the induction of senescence or apoptosis (Nowsheen and Yang, 2012). Figure 5.3 below summarises this study's p53 pathway in relation to ARV treated as compared to untreated cells.

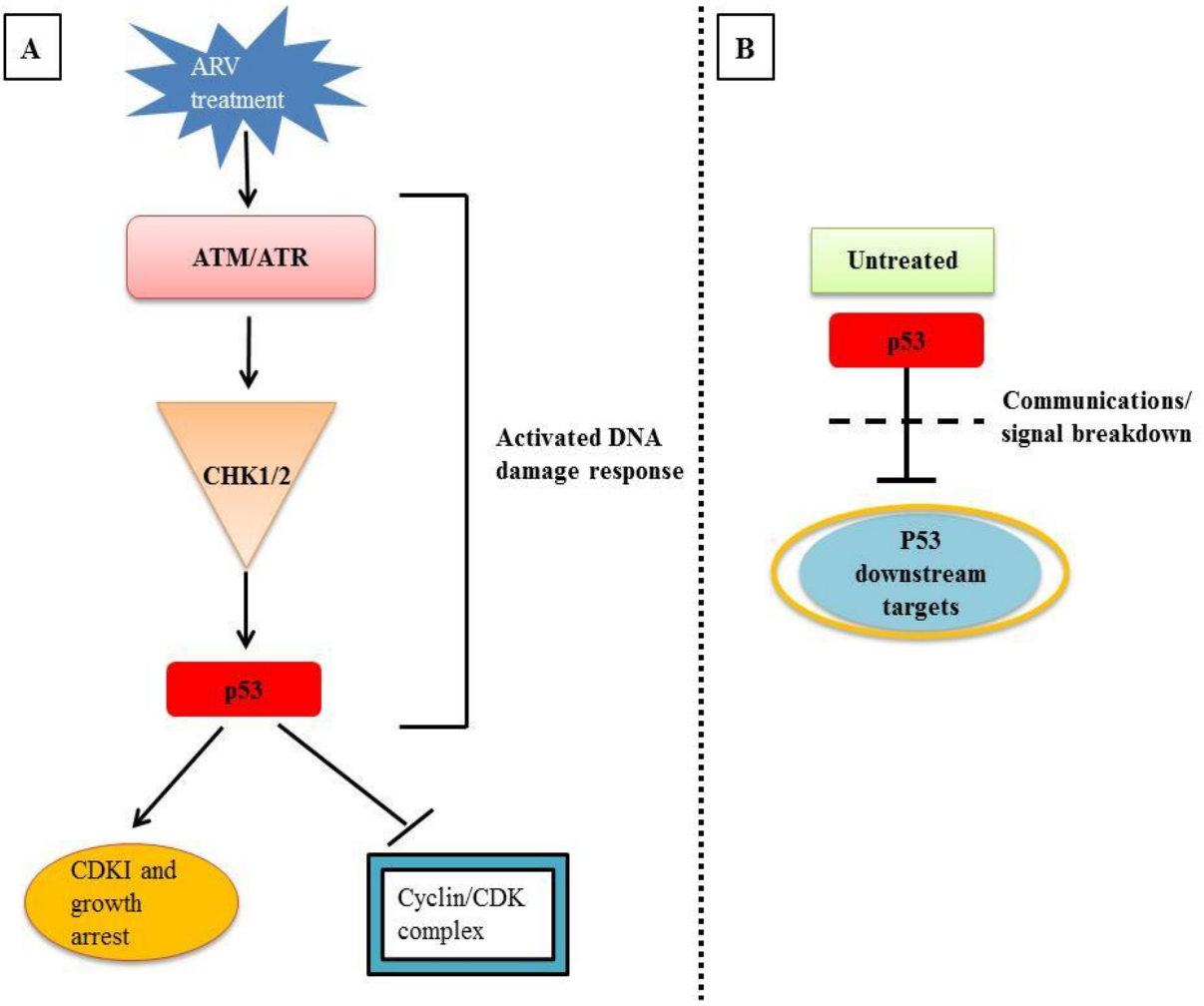

Figure 5.3: Summarised diagrammatic illustration of the p53 pathway as analysed by DAVID, Reactome and IPA. A represents ARV treatment, and B denotes untreated cells. ARV drug treatment activates the p53 anti-proliferative mechanisms by the repression of cyclin/CDK activity and induction of CDKIs such as p21. In the absence of ARV treatment, the p53 downstream targets are not activated.

5.2.4 EFV and LPV/r alter cycle associated gene expression

The emergence of regulatory roles of cell-cycle related genes in ARV associated carcinogenesis is likely to contribute to the development of novel diagnostic, prognostic and therapeutic markers, for NADCs in the HAART era. The present study provides the first evidence regarding the double-edged anti- or- pro oncogenic properties of two anti-retroviral drugs (EFV and LPV/r) in lung cancer.

5.2.5 Effects of EFV and LPV/r on cell-cycle related gene expression

Progression through the cell-cycle is a finely regulated process, wherein cyclins and CDKs promote the cell-cycle whilst the CDKIs inhibit progression. The balance between cyclins/CDKs and CDKIs is essential in maintaining cellular homeostasis, and determines cell fate, that is, proliferation, senescence or cell death (apoptosis). To ensure integrity of DNA replication and cell division, cell-cycle checkpoints exist at the key transition points of G1/S and G2/M, respectively. As the CDKIs act at multiple phases of the cycle, they are particularly important at these checkpoints. Prior to the synthesis of DNA (during the S-phase), the G1/S checkpoint allows for the monitoring of DNA integrity before the cell's DNA is replicated. The G2/M checkpoint allows the cell-cycle to pause prior to mitotic cell division. P53 is an important regulator of these checkpoints (Lim and Kaldis, 2013).

In the present study, gene expression in the untreated tumour *versus* the normal lung cells' array, p53 was 4.32 fold up-regulated. However, most of the CDKIs (which also act as p53 down-stream effectors), were significantly down-regulated and these included CDKN3, p21, p15 and most significantly p16 at -891 fold. CASP3, an effector caspase in apoptosis was also significantly down-regulated. In addition, GADD45A, which is also triggered by p53 in response to DNA damage and growth-arrest was significantly down-regulated (-10.7 fold). Cyclin G1 and G2, which are both induced following DNA damage and maintain the p53-dependent cell-cycle arrest and RAD DNA repair genes were also down-regulated. On the other hand, the cyclins such as cyclin A, B, D3, E and F and CDK1 were found to be significantly upregulated. Also, survivin (BIRC5), a pro- survival gene was up-regulated here. Further, the E2F1 transcription factor, important for the transcription of S-phase genes was up-regulated. Additionally, genes required for S-phase and DNA replication, the MCM gene family was significantly up-regulated. Furthermore, the AURK family (A and B), as well as MAD2L2 (involved in the mitotic spindle-checkpoint), were significantly up-regulated.

The treatment of MRC-5 and A549 cells with EFV alters the gene expression of important factors that are essential in the maintenance of genomic stability in relation to the cell-cycle. This is particularly observed in the cancerous cells, with the significant down-regulation of AURKB and MAD2L2. Even though the normal p53 (1.02 fold) expression was shown here,

p27, CASP3, Cyclin G1 and G2, NBN, RAD1 and RAD17 were significantly up-regulated. The E2F4 transcription factor, important for the transcription of S-phase genes, was also 1.93 (~2) fold up-regulated. Interestingly, the S-phase and DNA replication genes were down-regulated; MCM4 in particular was -3.65 significantly down-regulated. These EFV-treated genotypic alterations observed here are characteristic of anti-tumour properties.

The LPV/r treatment resulted in very similar effects to those observed following EFV treatment. Post LPV/r exposure p53 expression was triggered, by inhibiting AURKB in A549 cells, and this in-turn repressed MAD2L2 expression. This was then followed by the activation of p53 downstream targets including p21, p27 and p16. A significant down-regulation of cyclins A, B, D3, E and F was observed. CDK1 and 2 (except for CDK4) were also down-regulated. E2F1 transcription factor, important for the transcription of S-phase genes was additionally down-regulated. Further, the MCM family of DNA synthesis genes was significantly down-regulated. Survivin (BIRC5) was down-regulated, while CASP3 was up-regulated. Moreover, GADD45A was 40 fold significantly up-regulated. Similarly in MRC-5 cells, insignificant (1.26 fold) p53 activation led to p15 activation, resulting in inactivation of cyclins/CDKs, deregulation of AURKB and subsequent MAD2L2 down-regulation, and a repression in the expression of the MCM gene family. LPV/r exhibited characteristics of anti-tumour agents. From this dataset, it is evident that both EFV and LPV/r induce DNA damage response pathways. With respect to the DDR pathway, members such as Aurora kinases (AURKB) and MAD2L2, have previously been shown to be frequently overexpressed in human tumours, causing aberrations in the spindle assembly checkpoint, resulting in chromosomal mis-segregation and centrosome amplification, leading to chromosomal instability and tumorigenesis (Hochegger *et al.*, 2013). Failure to arrest the cell-cycle and repair the DNA damage, may lead to apoptosis. CASP3, an effector caspase important in apoptotic-mediated cell death, was also shown here to be differentially expressed in response to EFV and LPV/r drug treatment. All three gene targets (MAD2L2, AURKB and CASP3) were selected on the basis of their regulatory involvement in DNA damage response (DDR) pathways for further analysis.

5.2.6 MAD2L2, AURKB and CASP3 as mediators in EFV and LPV/r in lung carcinogenesis via DDR.

The protein encoded by the MAD2L2 gene**,** also known as REV7, is a protein of 211 amino acids and is a component of the mitotic spindle assembly checkpoint (SAC) that prevents the onset of anaphase to permit the correct alignment of all chromosomes at the metaphase plate (Sale, 2015). MAD2L2 also plays important roles in translesion DNA synthesis, mitotic control, and in repair pathway choice during DNA double-strand breaks. REV7 is a subunit of the enzyme DNA polymerase ζ, which is a key enzyme involved in replicating damaged DNA by translesion synthesis. REV7 acts as a connector protein between REV1 and REV3. REV7 is the catalytic subunit of Pol ζ, and helps direct the sequential insertion and extension steps of lesion replication (Sale, 2015). Upon DNA damage, MAD2L2 is recruited to DSB sites but is not needed to initiate damage signalling. While 53BP1 (p53 binding protein) is recruited to DSB and plays an important role in promoting non-homologous end joining (NHEJ). 53BP1 recruits RIF1, (telomere associated protein) and thus inhibits the resection of the DNA ends (Zimmermann and de Lange, 2014). MAD2L2 is proposed to act downstream of RIF1 and is needed for the inhibition of DNA 5' end resection. Furthermore, proper DNA lesion repair and the inhibition of DNA repair activities at telomeres are essential in preventing genomic instability. To date, mechanisms underlying telomere-driven genomic instabilities are poorly understood. However, the findings by Boersma *et al*., (2015) have placed MAD2L2 as a potential contributor to genomic instability, if aberrantly expressed during DNA repair at uncapped telomeres and DSBs.

Furthermore, it has been shown that MAD2L2 is essential for telomere fusion when there are defects in capping. In addition, emerging evidence suggests DNA Pol ζ is important for effective HR (Boersma *et al.*, 2015). As a componential sub-unit of Pol ζ, MAD2L2 may somehow also be involved not just in NHEJ as previously implicated, but also in the coordination of HR.

Aurora kinases (AURKs) have been shown to play a central role in organizing bipolar spindle establishment, chromosome alignment and segregation. Three paralogues have been identified, AURKA, AURKB and AURKC. AURKs activity is required both at the spindle

pole and the kinetochore. Aurora B coordinates kinetochore attachment and cytokinesis (Hochegger *et al.*, 2013).

Aurora B forms part of the Chromosome Passenger Complex (CPC) and is partnered with Incenp, Survivin and Borealin. Chromosomal bio-orientation prior to segregation is ensured by AURKB and the CPC. AURKB destabilizes incorrectly attached microtubule (MT)–kinetochore connections via mitotic centromere associated kinesin (MCAK) ((Lan *et al.*, 2004), (Andrews *et al.*, 2004)). The phosphorylations (by AURKB) are removed by protein-protein interactions (PPIs), once tension is established and the outer kinetochore is separated from the centromeric Aurora B ((Emanuele *et al.*, 2008), (Liu *et al.*, 2010), (Liu *et al.*, 2009)). By generating unattached kinetochores during error correction, Aurora B then effects the spindle assembly checkpoint (SAC) by recruiting SAC components such as BubR1 and MAD2L2 to the kinetochore. Furthermore, CASP3 is an effector CASP3, playing a critical role in apoptotic cell death. De-regulation of CASP3 underlies human diseases including cancer.

5.2.7 Target gene validation using qRT-PCR

QRT-PCR was done to validate the target genes' expression level, originally obtained from the PCR array data. Prior to EFV and LPV/r drug treatment (in untreated A549 *vs* MRC-5 cells), CASP3 was down-regulated at both 24h and 48h. AURKB and MAD2L2 were also validated to be up-regulated at both time periods. Following treatment with EFV and LPV/r, all three gene targets relatively remained in the insignificantly repressed state in the normal cells. This however, was not the case in the adenocarcinoma cells. Both EFV and LPV/r drug treatment altered the expression of all targets, with a down-regulation of CASP3, and up-regulation of AURKB and MAD2L2 at 24h and 48h, as indicated in the gene array data. Figure 5.4 below illustrates the summarised p53 pathway targeted by AURKB.

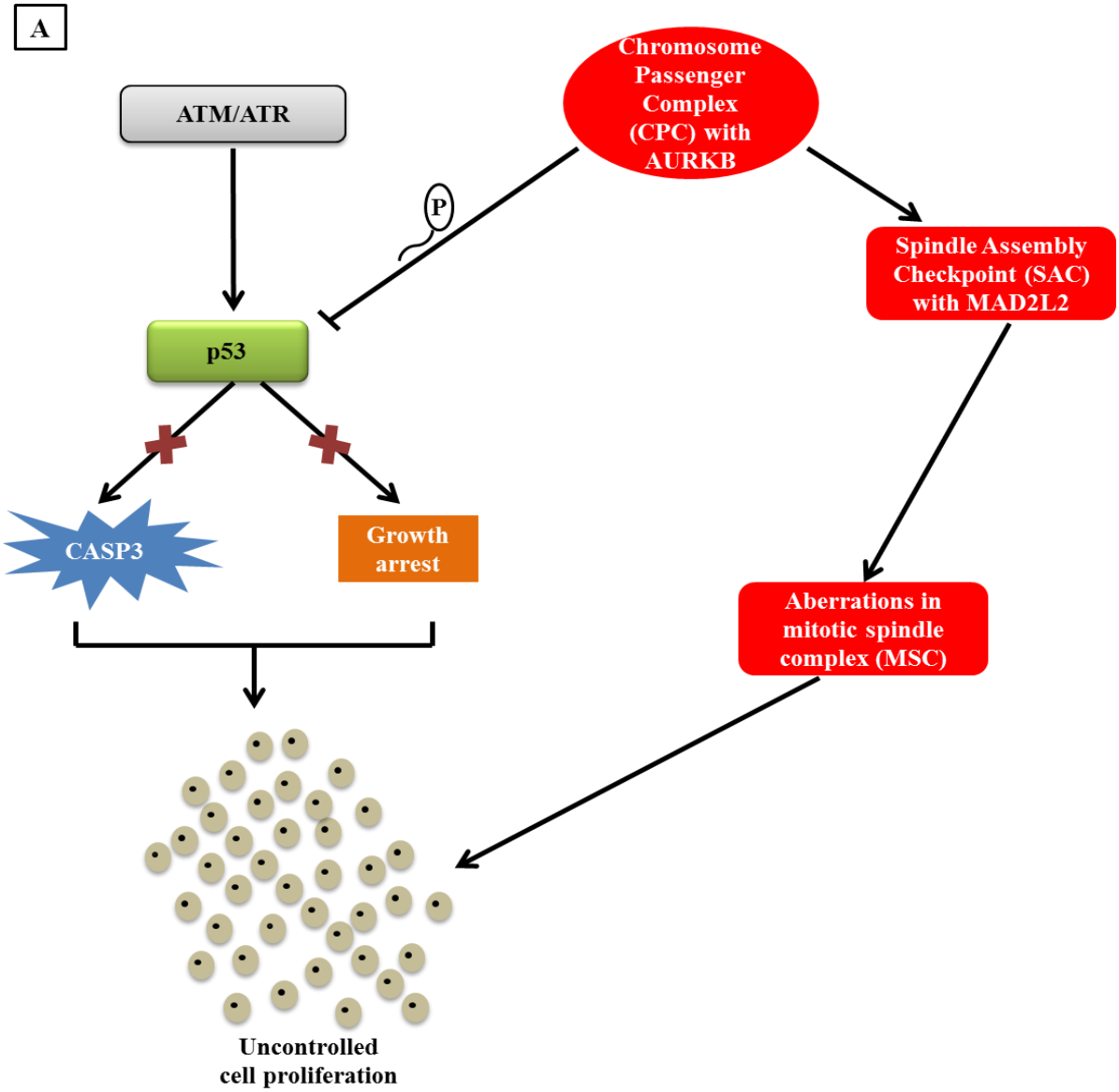
A
ATM/ATR
Chromosome Passenger Complex (CPC) with AURKB
P
Spindle Assembly Checkpoint (SAC) with MAD2L2
p53
CASP3
Growth arrest
Aberrations in mitotic spindle complex (MSC)
Uncontrolled cell proliferation

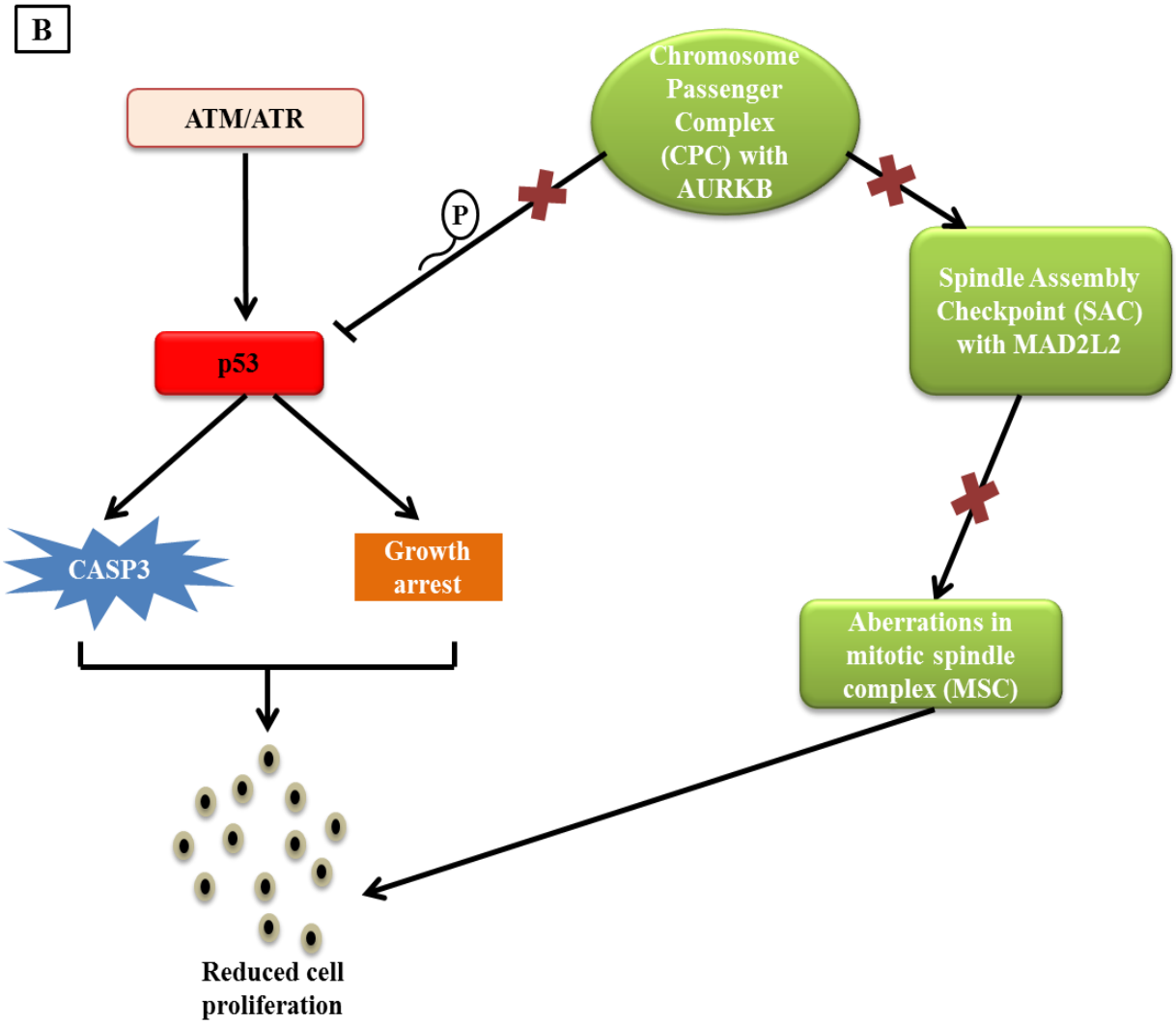

Figure 5.4: Summarised diagram of p53 pathway targeted by AURKB. As part of the chromosome passenger complex (CPC), AURKB overexpression affects the spindle assembly checkpoint (SAC) by recruiting its (SAC) components such MAD2L2, leading to aberrations in the mitotic spindle complex (MSC). The overexpression of AURKB also augments the expression of MAD2L2. In turn or perhaps simultaneously, p53 activity is inhibited by AURKB phosphorylation resulting in excessive cell proliferation, as demonstrated in panel A. However, ARV treatment down-regulates AURKB expression, thus also leading to reduced MAD2L2 activity, while p53 activity is induced, with subsequent p53 downstream targets activated, thus inhibiting cell proliferation in panel B.

5.3 Study limitations

As this study evaluated a single non-small lung adenocarcinoma cell-line, this analysis will be expanded to include a number of other NSCLC cell lines, for example, NCI –H228, Calu-3, NCI-HI563, NCI-H522, NCI-H2122, NCI-HI993 and SK-LU-1.

Another consideration in the present analysis is that it focussed on an *in vitro* cell culture model and not on patients undergoing ARV treatment. While the cells were subjected to an intense exposure of ARVs, the time period of cell treatment for 24h, 48h and 72h may not reflect the extended years of ARV treatment in HIV-infected people. In this regard, it would be useful to validate selected findings of this study in samples from patients who have been treated with ART for many years, with and/or without lung cancer. The identification of cell-cycle related genes treated with ARVs in lung cancer cells transfected with the HIV pro-virus could also be beneficial to this study's findings.

The possible contribution of HIV proteins and inflammation on the NADC's tumourigenesis was not explored in the present study and the knowledge generated from these collaborative findings could aid in revealing the mechanisms underlying NADCs. The oncogenic potential of the HIV virus was not covered here.

5.3.1 NADCs in the context of HIV infection

A better understanding of HIV induced oncogenesis, viral mechanisms of immune suppression and HAART cytotoxicity will provide for the basis for better diagnosis and treatment of cancer in PLWHA. NADCs can be classified as either virus or non-virus related, depending on whether some of these cancers are directly linked to HIV infection, or not. Lung cancer in particular, is one of the NADCs that is non-virus related (Chiao, 2010). A number of factors have been identified to contribute to the increased risk of NADCs, including CD4+ T-cell counts, chronic inflammation, tobacco usage, alcohol exposure, long-term ART exposure, advanced age and co-infection with oncogenic viruses (Loarca *et al.*, 2017).

5.3.2 Multifactorial agents contributing to the NADCs

HIV proteins, such as HIV-1 Tat has been shown to be involved in altering the DNA repair mechanism in host cells, possibly leading to genomic instability which may give rise to mutations and contribute to oncogenesis (Nunnari *et al*., 2008). In addition, Tat induces expression of the DNA polymerase beta gene, which codes for a central mediator in the DNA base-excision repair pathway (Srivastava *et al*., 2001). HIV-1 Tat has also been implicated in playing a direct role in double-strand break DNA repair (Chipitsyna *et al*., 2004). Additionally, HIV-1 Tat expression was reported to regulate gene expression levels of important cell-cycle regulators, and further decreased the mRNA levels of cyclin-dependent kinase inhibitors p21 and p17 (Nyagol *et al*., 2006).

On the other hand, the tumour micro-environment includes a number of immune cellular components, which include activated T cells, B cells and macrophages. HIV infection results in a major perturbation of cytokine/chemokine levels, which facilitates the development of antiviral immunity (reviewed in Reuter *et al*., 2012). For example, elevated levels of interleukin (IL) IL-6, IL-10, CXCL13 and tumour necrosis factorα (TNFα) are associated with increased risk for the development of NHL in HIV-infected individuals (Breen *et al*., 2011). The induction of pro-inflammatory mediators by HIV infection is likely to influence other immunomodulatory factors, affecting cellular proliferation, apoptosis sensitivity and other physiological functions associated with the microenvironment (De Paoli and Carbone, 2015).

With regard to HAART cytotoxicity, HAART components such raltegravir, an integrase inhibitor, was found to induce host DNA rearrangements, which may lead to an increased risk of cancer (Varadarajan *et al*., 2013). To gain a better understanding of ARV impact on NADCs, continuous epidemiological surveillance is necessary to monitor the trends in NADCs.

While this study aimed at the identification of cell-cycle related genes treated with ARVs in lung cancer, research groups and pharmaceutical companies are now trying to design and use modulators of the cell-cycle and cell-death programs as therapeutic tools. Understanding the

regulation of cell-cycle and cell-death may aid in knowledge application for the generation of improved treatment of human diseases such as HIV/AIDS and ARV mediated tumourigenesis. The cell-cycle and cell-death pathways are being targeted to better treat human diseases such as cancer in this era (Wiman and Zhivotovsky, 2017). Therefore, the cell-cycle related genes and their products can be targeted as promising therapeutic targets in the ART-mediated tumourigenesis.

5.4 Future directions

This study focused on identifying cell-cycle related genes targeted by EFV and LPV/r and demonstrated how these ARVs may cause damage to the genome. Future work may include *in vitro* functional studies, that is, it would be instructive to perform knockdown experiments using specific siRNA targeting the identified gene targets in lung cells. These findings demonstrate the double-edged oncogenic properties of both EFV and LPV/r, also implicating their role in genotoxicity. As a result, patients exposed to these ARVs seem to be vulnerable to continuous DNA damage, leading to NSCLC tumorigenesis.

While the scope of this study sought to identify the cell-cycle related genes treated with EFV and LPV/r in lung cancer, expanded future directions of this study may include the exploration of other modes of cell-death (such as autophagy) other than apoptosis, as LPV/r in particular was shown to induce cell-death. This could aid in better understanding of the ARVs effects on cell-proliferation and cell-death.

The transfection of lung cells (both control and cancer) with the HIV provirus and testing of patient samples that have been on HAART for years, could better establish the findings and determine if HIV oncogenic potential , HIV proteins and inflammation, immunosuppression and HAART cytotoxicity act individually or in synergy to promote NADCs. It is also not clear whether HIV proteins and human disease pathway (such as cancer) proteins interact together to promote tumourigenesis. Therefore functional enrichment of genes and proteins to gain a deeper understanding of the association between HIV and human genes, proteins and pathways could be further explored.

CHAPTER 6: CONCLUSIONS

A series of *in silico* analyses including STRING, DAVID, REACTOME and IPA were performed on the gene expression data obtained from the focused cell-cycle gene arrays. Protein-protein-interaction (PPI) network PI analysis of the cell-cycle genes in response to ART treatment elucidated a series of tight interactions, identifying pivotal factors associated with the DNA damage response, including amongst others GADD45, HUS and RAD. Changes in expression of cell-cycle regulatory factors, including cyclin/CDK activity, and the downstream targets of p53 were elucidated using DAVID analysis. In particular, the p53 effector targets p21 and GADD45A, to arrest growth and possibly repair the damaged DNA, were suppressed. The analysis of biological pathways using Reactome showed that ARV treatments, dependent on the ARV and cell type, affected other pathways besides the cell-cycle; EFV activated DNA repair genes in both normal and cancerous cells and the cellular response to stress genes was activated in normal cells. In lung cancer cells, genes associated with programmed cell-death were up-regulated, with an allied decline in the expression of genes involved in DNA replication. A further understanding of the mechanisms underlying the observed changes in gene expression in the pathways identified by Reactome was gained by employing the Ingenuity Pathway Analysis (IPA) tool. This particularly showed that the DNA damage response pathway, the ATM pathway was activated in both lung cancer and in normal cells by EFV. Lopinavir/ritonavir, even though it reduced DNA synthesis in normal MRC-5 cells, it however failed to activate ATM. Regardless of the up-stream ATM pathway repression, the p53-signalling pathway was activated in lung cancer cells. Notably, the de-regulation of these two pathways play essential roles in genomic instability, leading to cancer.

The anti-proliferative and cytotoxic properties of EFV and LPV/r are evident from this study. However, these properties should be tested on different types of cancer and the associated response profiles evaluated. Although there may be further steps to be considered, EFV and LPV/r demonstrate unique but also at the same time similar mechanisms, whereby they both dose dependently retard and inhibit cell proliferation. The recruitment of DNA damage response pathways following EFV and LPV/r treatment in both normal and cancer cells

indicates that these drugs possess anti-tumour activity, similar to those demonstrated by chemotherapeutic drugs. However, proper consideration is necessary as LPV/r in particular also poses the danger of excessive cell-death, as was particularly observed here in the normal lung cells. In the same manner, PLWHA previously not pre-disposed to cancer, particularly lung cancer, may be undergoing similar processes, where the administration of EFV and LPV/r impose damage to the genome, resulting in the activation of cellular response to stress and DNA damage response genes/pathways. Being actively induced by consistent and continuous HAART administration, these pathways may be dysregulated (possibly due to constant activation), ultimately leading to tumorigenesis. This however, does not exclude ARVs from being explored as anti-cancer drugs, due to their anti-cancer properties.

Aberrant expression of AURKB seems to inhibit p53 activity, thereby suppressing CASP3, and impacting on the constitutive expression of SAC components such as MAD2L2, resulting in loss of maintenance of the SAC leading to chromosomal mis-segregation, genome instability and tumorigenesis.

REFERENCES

Adefolaju, G. A., Theron, K. E.andHosie, M. J. 2014. Effects of HIV protease, nucleoside/non-nucleoside reverse transcriptase inhibitors on Bax, Bcl-2 and apoptosis in two cervical cell lines. *Biomed Pharmacotherapy,* 68**,** 241-51.

Amini, S., Khalili, K.andSawaya, B. E. 2004. Effect of HIV-1 Vpr on cell cycle regulators. *DNA Cell Biology,* 23**,** 249-60.

Andrews, P. D., Ovechkina, Y., Morrice, N. *et al.,* 2004. Aurora B regulates MCAK at the mitotic centromere. *Developmental Cell,* 6**,** 253-68.

Arts, E. J. and Hazuda, D. J. 2012. HIV-1 antiretroviral drug therapy. *Cold Spring Harbor Perspectives in Medicine,* 2**,** a007161.

Baker, T. A.andBell, S. P. 1998. Polymerases and the replisome: machines within machines. *Cell,* 92**,** 295-305.

Barmania, F. and Pepper, M. S. 2013. CC chemokine receptor type five (CCR5): An emerging target for the control of HIV infection. *Applied & Translational Genomics,* 2**,** 3-16.

Barnhart, M. and Shelton, J. D. 2015. ARVs: the next generation. Going boldly together to new frontiers of HIV treatment. *Global Health Science Practice,* 3**,** 1-11.

Barnum, K. J.and O'connell, M. J. 2014. Cell cycle regulation by checkpoints. *Methods Molecular Biology,* 1170**,** 29-40.

Bartel, D. P. 2009. MicroRNAs: target recognition and regulatory functions. *Cell,* 136**,** 215-33.

Batman, G., Oliver, A. W., Zehbe, I. *et al.,* 2011. Lopinavir up-regulates expression of the antiviral protein ribonuclease L in human papillomavirus-positive cervical carcinoma cells. *Antiviral Therapy,* 16**,** 515.

Bearz, A., Vaccher, E., Martellotta, F. *et al.,* 2014. Lung cancer in HIV positive patients: the GICAT experience. *European Review for Medical and Pharmacological Sciences,* 18**,** 500-8.

Bechtel, W. 2016. Using computational models to discover and understand mechanisms. *Studies in History and Philosohpy of Science,* 56**,** 113-21.

Berretta, M., Caraglia, M., Martellotta, F. *et al.,* 2016. Drug–Drug Interactions Based on Pharmacogenetic Profile between Highly Active Antiretroviral Therapy and Antiblastic Chemotherapy in Cancer Patients with HIV Infection. *Frontiers in Pharmacology,* 7**,** 71.

Beumer, J. H., Venkataramanan, R. and Rudek, M. A. 2014. Pharmacotherapy in cancer patients with HIV/AIDS. *Clinical Pharmacology & Therapeutics,* 95**,** 370-372.

Biggar, R. J., Engels, E. A., Ly, S. *et al.,* 2005. Survival after cancer diagnosis in persons with AIDS. *Journal of Acquired Immune Deficiency Syndrome,* 39**,** 293-9.

Bishop, J. D. and Schumacher, J. M. 2002. Phosphorylation of the carboxyl terminus of inner centromere protein (INCENP) by the Aurora B Kinase stimulates Aurora B kinase activity. *Journal of Biological Chemistry,* 277**,** 27577-80.

Boersma, V., Moatti, N., Segura-Bayona, S. *et al.,* 2015. MAD2L2 controls DNA repair at telomeres and DNA breaks by inhibiting 5' end resection. *Nature,* 521**,** 537-40.

Braithwaite, D. K. and Ito, J. 1993. Compilation, alignment, and phylogenetic relationships of DNA polymerases. *Nucleic Acids Research,* 21**,** 787-802.

Breen, E. C., Hussain, S. K., Magpantay, L. *et al*., 2011. B-cell stimulatory cytokines and markers of immune activation are elevated several years prior to the diagnosis of systemic AIDS-associated non-Hodgkin B-cell lymphoma. Cancer Epidemiology, Biomarkers & Prevention: a publication of the American Association for Cancer Research, cosponsored by the American Society of Preventive Oncology. 20(7):1303–1314.

Broustas, C. G. and Lieberman, H. B. 2014. DNA Damage Response Genes and the Development of Cancer Metastasis. *Radiation Research,* 181**,** 111-130.

Byth, H. A., Mchunu, B. I., Dubery, I. A. *et al.,* 2001. Assessment of a simple, non-toxic Alamar blue cell survival assay to monitor tomato cell viability. *Phytochem Analysis,* 12**,** 340-6.

Byun, T. S., Pacek, M., Yee, M.-C. *et al.,* 2005. Functional uncoupling of MCM helicase and DNA polymerase activities activates the ATR-dependent checkpoint. *Genes and Development,* 19**,** 1040-1052.

Carmena, M., Ruchaud, S.and Earnshaw, W. C. 2009. Making the Auroras glow: regulation of Aurora A and B kinase function by interacting proteins. *Current Opinion in Cell Biology,* 21**,** 796-805.

Carmena, M., Wheelock, M., Funabiki, H. *et al.,* 2012. The chromosomal passenger complex (CPC): from easy rider to the godfather of mitosis. *Nature Reviews Molecualr Cell Biology,* 13**,** 789-803.

Carvajal, L. A., Hamard, P. J., Tonnessen, C. *et al.,* 2012. E2F7, a novel target, is up-regulated by p53 and mediates DNA damage-dependent transcriptional repression. *Genes and Development,* 26**,** 1533-45.

Casimiro, M. C., Crosariol, M., Loro, E. *et al.,* 2012. Cyclins and cell cycle control in cancer and disease. *Genes and Cancer,* 3**,** 649-657.

Chan, C., Wu, Z., Eastman, A. *et al.,* 1992. Irradiation-induced expression of O6-methylguanine-DNA methyltransferase in mammalian cells. *Cancer Research,* 52**,** 1804-1809.

Chazotte, B. 2011. Labeling nuclear DNA using DAPI. *Cold Spring Harbor Protocols,* 2011**,** pdb. prot5556.

Chiao EY. Epidemiology and Clinical Characteristics of Non-AIDS-Defining Malignancies. In: Dittmer DP, Krown SE, editors. Molecular Basis for Therapy of AIDS-Defining Cancers. Springer: New York; 2010. p. 17–40.

Chipitsyna G, Slonina D, Siddiqui K, *et al*.,. HIV-1 Tat increases cell survival in response to cisplatin by stimulating Rad51 gene expression. Oncogene. 2004;23(15):2664–2671. DOI: 10.1038/sj.onc.1207417

Chow, W. A., Jiang, C.andGuan, M. 2009. Anti-HIV drugs for cancer therapeutics: back to the future? *The Lancet Oncology,* 10**,** 61-71.

Christmann, M.andKaina, B. 2013. Transcriptional regulation of human DNA repair genes following genotoxic stress: trigger mechanisms, inducible responses and genotoxic adaptation. *Nucleic Acids Research,* 41**,** 8403-20.

Christmann, M., Tomicic, M. T., Origer, J. *et al.,* 2005. Fen1 is induced p53 dependently and involved in the recovery from UV-light-induced replication inhibition. *Oncogene,* 24**,** 8304-8313.

Clifford, G. M., Polesel, J., Rickenbach, M. *et al.*, 2005. Cancer risk in the Swiss HIV Cohort Study: associations with immunodeficiency, smoking, and highly active antiretroviral therapy. *Journal of National Cancer Institute,* 97**,** 425-32.

Cooper, W. A., Lam, D. C., O'toole, S. A. *et al.*, 2013. Molecular biology of lung cancer. *Journal of Thoracic Disease,* 5**,** S479-S490.

Corti, M. 2016. Lung Cancer in HIV-Seropositive Patients. MJ HIV. 1 (1): 007. Citation: Corti M.(2016). *Lung Cancer in HIV-Seropositive Patients. MJ HIV,* 1**,** 007.

Cottrell, M. L., Hadzic, T.andKashuba, A. D. 2013. Clinical pharmacokinetic, pharmacodynamic and drug-interaction profile of the integrase inhibitor dolutegravir. *Clinical Pharmacokinetics,* 52**,** 981-994.

Coudreuse, D.andNurse, P. 2010. Driving the cell cycle with a minimal CDK control network. *Nature,* 468**,** 1074-9.

De Paoli, P., Carbone, A., 2015. Microenvironmental abnormalities induced by viral cooperation: Impact on lymphomagenesis. Seminars in Cancer Biology. 2015;34:70–80.

Dewan, M. Z., Uchihara, J.-N., Terashima, K. *et al.*, 2006. Efficient intervention of growth and infiltration of primary adult T-cell leukemia cells by an HIV protease inhibitor, ritonavir. *Blood,* 107**,** 716-724.

Dey, P. 2004. Aneuploidy and malignancy: an unsolved equation. *Journal of Clinical Pathology,* 57**,** 1245-1249.

El-Serag, H.B. 2012. Epidemiology of viral hepatitis and hepatocellular carcinoma. *Gastroenterology,* 142**,** 1264-1273 e1.

Emanuele, M. J., Lan, W., Jwa, M. *et al.*, 2008. Aurora B kinase and protein phosphatase 1 have opposing roles in modulating kinetochore assembly. *Journal of Cell Bioliogy,* 181**,** 241-54.

Emmerich, J., Meyer, C. A., De La Cruz, A. F. *et al.*, 2004. Cyclin D does not provide essential Cdk4-independent functions in Drosophila. *Genetics,* 168**,** 867-75.

Eymin, B. and Gazzeri, S. 2010. Role of cell cycle regulators in lung carcinogenesis. *Cell Adhesion and Migration,* 4**,** 114-23.

Falck, J., Forment, J. V., Coates, J. *et al.*, 2012. CDK targeting of NBS1 promotes DNA-end resection, replication restart and homologous recombination. *EMBO Reports,* 13**,** 561-8.

Fisher, D., Krasinska, L., Coudreuse, D. *et al.*, 2012. Phosphorylation network dynamics in the control of cell cycle transitions. *Journal of Cell Science,* 125**,** 4703-11.

Goodman, M. F. and Woodgate, R. 2013. Translesion DNA polymerases. *Cold Spring Harbor Perspectives in Biology,* 5**,** a010363.

Grossman, Z., Schapiro, J. M., Levy, I. *et al.*, 2014. Comparable long-term efficacy of lopinavir/ritonavir and similar drug-resistance profiles in different HIV-1 subtypes. *PloS One,* 9**,** e86239.

Grulich, A. E., Van Leeuwen, M. T., Falster, M. O. *et al.*, 2007. Incidence of cancers in people with HIV/AIDS compared with immunosuppressed transplant recipients: a meta-analysis. *Lancet,* 370**,** 59-67.

Gubavu, C., Prazuck, T., Niang, M. *et al.*, 2016. Dolutegravir-based monotherapy or dual therapy maintains a high proportion of viral suppression even in highly experienced HIV-1-infected patients. *Journal of Antimicrobial Chemotherapy,* 71**,** 1046-50.

Guech-Ongey, M., Simard, E. P., Anderson, W. F. *et al.,* 2010. AIDS-related Burkitt lymphoma in the United States: what do age and CD4 lymphocyte patterns tell us about etiology and/or biology? *Blood,* 116**,** 5600-4.

Gully, C. P., Velazquez-Torres, G., Shin, J.-H. *et al.,* 2012. Aurora B kinase phosphorylates and instigates degradation of p53. *Proceedings of the National Academy of Sciences,* 109**,** E1513-E1522.

Guo, C., Fischhaber, P. L., Luk-Paszyc, M. J. *et al.,* 2003. Mouse Rev1 protein interacts with multiple DNA polymerases involved in translesion DNA synthesis. *EMBO J,* 22**,** 6621-30.

Hakimian, R., Fang, H., Thomas, L. *et al.,* 2007. Lung cancer in HIV-infected patients in the era of highly active antiretroviral therapy. *Journal of Thoracic Oncology,* 2**,** 268-72.

Hanafusa, T., Habu, T., Tomida, J. *et al.,* 2010. Overlapping in short motif sequences for binding to human REV7 and MAD2 proteins. *Genes Cells,* 15**,** 281-96.

Hanahan, D.andWeinberg, R. A. 2000. The hallmarks of cancer. *Cell,* 100**,** 57-70.

Hanahan, D.andWeinberg, R. A. 2011. Hallmarks of cancer: the next generation. *Cell,* 144**,** 646-74.

Harman, S., Herrera, C., Armanasco, N. *et al.,* 2012. Preclinical evaluation of the HIV-1 fusion inhibitor L'644 as a potential candidate microbicide. *Antimicrobial Agents and Chemotherapy,* 56**,** 2347-2356.

Hashim, D., Boffetta, P., La Vecchia, C. *et al.,* 2016. The global decrease in cancer mortality: trends and disparities. *Annals of Oncology,* 27**,** 926-933.

Haupt, S., Berger, M., Goldberg, Z. *et al.,* 2003. Apoptosis-the p53 network. *Journal of Cell Science,* 116**,** 4077-4085.

Hecht, M., Erber, S., Harrer, T. *et al.,* 2015. Efavirenz Has the Highest Anti-Proliferative Effect of Non-Nucleoside Reverse Transcriptase Inhibitors against Pancreatic Cancer Cells. *PLoS One,* 10**,** e0130277.

Hecht, M., Harrer, T., Büttner, M. *et al.,* 2013. Cytotoxic effect of efavirenz is selective against cancer cells and associated with the cannabinoid system. *Aids,* 27**,** 2031-2040.

Herida, M., Mary-Krause, M., Kaphan, R. *et al.,* 2003. Incidence of non-AIDS-defining cancers before and during the highly active antiretroviral therapy era in a cohort of human immunodeficiency virus-infected patients. *Journal of Clinical Oncology,* 21**,** 3447-53.

Hessol, N. A., Pipkin, S., Schwarcz, S. *et al.,* 2007. The impact of highly active antiretroviral therapy on non-AIDS-defining cancers among adults with AIDS. *American Journal of Epidemiology,* 165**,** 1143-53.

Hima Bindu, A.andNaga Anusha, P. 2011. Adverse effects of highly active anti-retroviral therapy (HAART). *Journal of Antivirals and Antiretrovirals,* 3**,** 060-064.

Hochegger, H., Hegarat, N. and Pereira-Leal, J. B. 2013. Aurora at the pole and equator: overlapping functions of Aurora kinases in the mitotic spindle. *Open Bioliogy,* 3**,** 120185.

Homem, C. C. and Knoblich, J. A. 2012. Drosophila neuroblasts: a model for stem cell biology. *Development,* 139**,** 4297-310.

Islaih, M., Li, B., Kadura, I. A. *et al.,* 2004. Comparison of gene expression changes induced in mouse and human cells treated with direct-acting mutagens. *Environmental and Molecular Mutagenesis,* 44**,** 401-419.

Jones, M. E. and Swerdlow, A. J. 1998. Bias in the standardized mortality ratio when using general population rates to estimate expected number of deaths. *American Journal of Epidemiology,* 148**,** 1012-7.

Karanja, J., Kiboi, N., Nebere, S. *et al.,* 2016. Highly Active Antiretroviral Therapy and Anti-tuberculosis Drug Interactions with Associated Clinical Implications: A Review. *Journal of Drug Metabolism and Toxicology,* 7**,** 2.

Kho, D., Macdonald, C., Johnson, R. *et al.,* 2015. Application of xCELLigence RTCA Biosensor Technology for Revealing the Profile and Window of Drug Responsiveness in Real Time. *Biosensors (Basel),* 5**,** 199-222.

Khosravi, R., Maya, R., Gottlieb, T. *et al.,* 1999. Rapid ATM-dependent phosphorylation of MDM2 precedes p53 accumulation in response to DNA damage. *Proceedings of the National Academy of Sciences,* 96**,** 14973-14977.

Kikuchi, S., Hara, K., Shimizu, T. *et al.,* 2012. Structural basis of recruitment of DNA polymerase zeta by interaction between REV1 and REV7 proteins. *Journal of Bioligical Chemistry,* 287**,** 33847-52.

King, J. R., Wynn, H., Brundage, R. *et al.,* 2004. Pharmacokinetic enhancement of protease inhibitor therapy. *Clinical Pharmacokinetics,* 43**,** 291-310.

Kirk, G. D., Merlo, C., P, O. D. *et al.,* 2007. HIV infection is associated with an increased risk for lung cancer, independent of smoking. *Clinical Infectious Disease,* 45**,** 103-10.

Kiser, J. J., Carten, M. L., Aquilante, C. L. *et al.,* 2008. The effect of lopinavir/ritonavir on the renal clearance of tenofovir in HIV-infected patients. *Clinical Pharmacology and Therapeutics,* 83**,** 265-72.

Knobel, P. A.andMarti, T. M. 2011. Translesion DNA synthesis in the context of cancer research. *Cancer Cell International,* 11**,** 39-39.

Knoblich, J. A.andLehner, C. F. 1993. Synergistic action of Drosophila cyclins A and B during the G2-M transition. *EMBO Journal,* 12**,** 65-74.

Knoblich, J. A., Sauer, K., Jones, L. *et al.,* 1994. Cyclin E controls S phase progression and its down-regulation during Drosophila embryogenesis is required for the arrest of cell proliferation. *Cell,* 77**,** 107-20.

Koegelenberg, C. F., Van Der Made, T., Taljaard, J. J. *et al.,* 2016. The impact of HIV infection on the presentation of lung cancer in South Africa. *South African Medical Journal,* 106**,** 666-8.

Lan, W., Zhang, X., Kline-Smith, S. L. *et al.,* 2004. Aurora B phosphorylates centromeric MCAK and regulates its localization and microtubule depolymerization activity. *Current Biology,* 14**,** 273-86.

Lange, S. S., Tomida, J., Boulware, K. S. *et al.,* 2016. The Polymerase Activity of Mammalian DNA Pol zeta Is Specifically Required for Cell and Embryonic Viability. *PLoS Genetics,* 12**,** e1005759.

Laurent, N., De Boüard, S., Guillamo, J.-S. *et al.,* 2004. Effects of the proteasome inhibitor ritonavir on glioma growth in vitro and in vivo. *Molecular Cancer Therapeutics,* 3**,** 129-136.

Lavole, A., Chouaid, C., Baudrin, L. *et al.,* 2009. Effect of highly active antiretroviral therapy on survival of HIV infected patients with non-small-cell lung cancer. *Lung Cancer,* 65**,** 345-50.

Lavon, I., Fuchs, D., Zrihan, D. *et al.,* 2007. Novel mechanism whereby nuclear factor κB mediates DNA damage repair through regulation of O6-methylguanine-DNA-methyltransferase. *Cancer Research,* 67**,** 8952-8959.

Lee, J.-H.andPaull, T. T. 2005. ATM activation by DNA double-strand breaks through the Mre11-Rad50-Nbs1 complex. *Science,* 308**,** 551-554.

Lee, K. Y.andMyung, K. 2008. PCNA modifications for regulation of post-replication repair pathways. *Mol Cells,* 26**,** 5-11.

Lemjabbar-Alaoui, H., Hassan, O. U., Yang, Y.-W. *et al.,* 2015. Lung cancer: Biology and treatment options. *Biochimica et Biophysica Acta (BBA)-Reviews on Cancer,* 1856**,** 189-210.

Leventis, P. A.andGrinstein, S. 2010. The distribution and function of phosphatidylserine in cellular membranes. *Annual Review of Biophysics,* 39**,** 407-427.

Levine, A. J. 1997. p53, the cellular gatekeeper for growth and division. *Cell,* 88**,** 323-31.

Lewden, C., May, T., Rosenthal, E. *et al.,* 2008. Changes in causes of death among adults infected by HIV between 2000 and 2005: The "Mortalite 2000 and 2005" surveys (ANRS EN19 and Mortavic). *Journal of Acquired Immune Deficiency Syndrome,* 48**,** 590-8.

Li, Q., Zhang, L., Tsang, B. *et al.,* 1999. Phorbol ester exposure activates an AP-1-mediated increase in ERCC-1 messenger RNA expression in human ovarian tumor cells. *Cellular and Molecular Llife Sciences,* 55**,** 456.

Liedtke, M. D., Tomlin, C. R., Lockhart, S. M. *et al.,* 2014. Long-term efficacy and safety of raltegravir in the management of HIV infection. *Infection and Drug Resistance,* 7**,** 73.

Lim, S. and Kaldis, P. 2013. Cdks, cyclins and CKIs: roles beyond cell cycle regulation. *Development,* 140**,** 3079-3093.

Lindahl, T.andBarnes, D. E. 2000. Repair of endogenous DNA damage. *Cold Spring Harb Symposia on Quantitative Biology,* 65**,** 127-33.

Liu, D., Vader, G., Vromans, M. J. *et al.,* 2009. Sensing chromosome bi-orientation by spatial separation of aurora B kinase from kinetochore substrates. *Science,* 323**,** 1350-3.

Liu, D., Vleugel, M., Backer, C. B. *et al.,* 2010. Regulated targeting of protein phosphatase 1 to the outer kinetochore by KNL1 opposes Aurora B kinase. *Journal of Cell Biology,* 188**,** 809-20.

Livak, K. J. and Schmittgen, T. D. 2001. Analysis of relative gene expression data using real-time quantitative PCR and the 2(-Delta Delta C(T)) method. *Methods,* 25**,** 402-8.

Loarca, L., Fraietta J. A., Pirrone, Vannessa., *et al*., 2017. Human mmunodeficiency and Virus (HIV) Infection and Cancer.

Louie, J. K., Hsu, L. C., Osmond, D. H. *et al.,* 2002. Trends in causes of death among persons with acquired immunodeficiency syndrome in the era of highly active antiretroviral therapy, San Francisco, 1994-1998. *Journal of Infectious Disease,* 186**,** 1023-7.

Makinson, A., Tenon, J. C., Eymard-Duvernay, S. *et al.,* 2011. Human immunodeficiency virus infection and non-small cell lung cancer: survival and toxicity of antineoplastic chemotherapy in a cohort study. *Journal Thoracic Oncology,* 6**,** 1022-9.

Malumbres, M. and Barbacid, M. 2009. Cell cycle, CDKs and cancer: a changing paradigm. *Nature Reviews Cancer,* 9**,** 153-66.

Marcus, J. L., Chao, C., Leyden, W. A. *et al.,* 2015. Survival among HIV-infected and HIV-uninfected individuals with common non-AIDS-defining cancers. *Cancer Epidemiology Biomarkers Prev,* 24**,** 1167-73.

Mclean, J. R., Chaix, D., Ohi, M. D. *et al.,* 2011. State of the APC/C: organization, function, and structure. *Critical Reviews in Biochemistry and Molecualr Biology,* 46**,** 118-36.

Mirzoeva, O. K.andPetrini, J. H. 2001. DNA damage-dependent nuclear dynamics of the Mre11 complex. *Molecular and Cellular Biology,* 21**,** 281-288.

Mirzoeva, O. K.andPetrini, J. H. 2003. DNA Replication-Dependent Nuclear Dynamics of the Mre11 Complex1 1 NIH GM56888 and the DOE ER62859. *Molecular Cancer Research,* 1**,** 207-218.

Moltó, J., Moran, T., Sirera, G. *et al.,* 2015. Lung cancer in HIV-infected patients in the combination antiretroviral treatment era. *Translational Lung Cancer Research,* 4**,** 678.

Montecucco, A., Savini, E., Biamonti, G. *et al.,* 1995. Late induction of human DNA ligase I after UV-C irradiation. *Nucleic Acids Rresearch,* 23**,** 962-966.

Mounier, N., Katlama, C., Costagliola, D. *et al.,* 2009. Drug interactions between antineoplastic and antiretroviral therapies: Implications and management for clinical practice. *Critical Reviews in Oncology/Hematology,* 72**,** 10-20.

Murakumo, Y., Roth, T., Ishii, H. *et al.,* 2000. A human REV7 homolog that interacts with the polymerase zeta catalytic subunit hREV3 and the spindle assembly checkpoint protein hMAD2. *Journal of Biological Chemistry,* 275**,** 4391-7.

Myung, K., Braastad, C., He, D. M. *et al.,* 1998. KARP-1 is induced by DNA damage in a p53-and ataxia telangiectasia mutated-dependent fashion. *Proceedings of the National Academy of Sciences,* 95**,** 7664-7669.

Nana-Sinkam, S. P. and Powell, C. A. 2013. Molecular biology of lung cancer: diagnosis and management of lung cancer: American College of Chest Physicians Evidence-Based Clinical Practice Guidelines. *CHEST Journal,* 143**,** e30S-e39S.

Nelson, J. R., Lawrence, C. W.andHinkle, D. C. 1996. Thymine-thymine dimer bypass by yeast DNA polymerase zeta. *Science,* 272**,** 1646-9.

Noatynska, A., Tavernier, N., Gotta, M. *et al.,* 2013. Coordinating cell polarity and cell cycle progression: what can we learn from flies and worms? *Open Biology,* 3**,** 130083.

Nowell, P. C. 1976. The clonal evolution of tumor cell populations. *Science,* 194**,** 23-8.

Nowsheen, S.and Yang, E. S. 2012. The Intersection Between DNA Damage Response and Cell Death Pathways. *Experimental Oncology,* 34**,** 243-254.

Nunnari G, Smith JA, Daniel R. HIV-1 Tat and AIDS-associated cancer: targeting the cellular anti-cancer barrier? Journal of Experimental & Clinical Cancer Research: CR. 2008;27:3. DOI: 10.1186/1756-9966-27-3.

Nyagol, J., Leucci, E., Onnis, A., et al., 2006. The effects of HIV-1 Tat protein on cell cycle during cervical carcinogenesis. Cancer Biology & Therapy. 2006;5(6):684–690.

O'connell, M. J., Krien, M. J. and Hunter, T. 2003. Never say never. The NIMA-related protein kinases in mitotic control. *Trends Cell Biology,* 13**,** 221-8.

Ohmori, H., Friedberg, E. C., Fuchs, R. P. *et al.,* 2001. The Y-family of DNA polymerases. *Molecular Cell,* 8**,** 7-8.

Page, B., Page, M.andNoel, C. 1993. A new fluorometric assay for cytotoxicity measurements in-vitro. *International Journal of Oncology,* 3**,** 473-6.

Parrilla-Castellar, E. R., Arlander, S. J. and Karnitz, L. 2004. Dial 9–1–1 for DNA damage: the Rad9–Hus1–Rad1 (9–1–1) clamp complex. *DNA Repair,* 3**,** 1009-1014.

Pati, S., Pelser, C. B., Dufraine, J. *et al.,* 2002. Antitumorigenic effects of HIV protease inhibitor ritonavir: inhibition of Kaposi sarcoma. *Blood,* 99**,** 3771-3779.

Pauklin, S., Kristjuhan, A., Maimets, T. *et al.,* 2005. ARF and ATM/ATR cooperate in p53-mediated apoptosis upon oncogenic stress. *Biochem Biophys Res Commun,* 334**,** 386-94.

Pendharkar, D., Ausekar, B.andGupta, S. 2013. Molecular Biology of Lung Cancer—A Review. *Indian Journal of Surgical Oncology,* 4**,** 120-124.

Powles, T., Robinson, D., Stebbing, J. *et al.,* 2009. Highly active antiretroviral therapy and the incidence of non-AIDS-defining cancers in people with HIV infection. *Journal of Clinical Oncology,* 27**,** 884-90.

Pozhidaeva, A., Pustovalova, Y., D'souza, S. *et al.,* 2012. NMR structure and dynamics of the C-terminal domain from human Rev1 and its complex with Rev1 interacting region of DNA polymerase *et al*. *Biochemistry,* 51**,** 5506-20.

Qi, P., Han, J. X., Lu, Y. Q. *et al.,* 2006. Virus-encoded microRNAs: future therapeutic targets? *Cell and Molecular Immunology,* 3**,** 411-9.

Rampersad, S. N. 2012. Multiple applications of Alamar Blue as an indicator of metabolic function and cellular health in cell viability bioassays. *Sensors (Basel),* 12**,** 12347-60.

Rengan, R., Mitra, N., Liao, K. *et al.,* 2012. Effect of HIV on survival in patients with non-small-cell lung cancer in the era of highly active antiretroviral therapy: a population-based study. *The Lancet Oncology,* 13**,** 1203-1209.

Reuter, M. A., Pombo, C., Betts, M.R., *et al*., 2012. Cytokine production and dysregulation in HIV pathogenesis: lessons for development of therapeutics and vaccines. Cytokine & Growth Factor Reviews. 2012;23(4–5):181–191.

Rimkus, C., Friederichs, J., Rosenberg, R. *et al.,* 2007. Expression of the mitotic checkpoint gene MAD2L2 has prognostic significance in colon cancer. *International Journal of Cancer,* 120**,** 207-211.

Ritchie, M. D., Haas, D. W., Motsinger, A. A. *et al.,* 2006. Drug transporter and metabolizing enzyme gene variants and nonnucleoside reverse-transcriptase inhibitor hepatotoxicity. *Clinical Infectious Disease,* 43**,** 779-82.

Rodger, A. J., Lodwick, R., Schechter, M. *et al.,* 2013. Mortality in well controlled HIV in the continuous antiretroviral therapy arms of the SMART and ESPRIT trials compared with the general population. *AIDS,* 27**,** 973-9.

Rubinstein, P. G., Aboulafia, D. M. and Zloza, A. 2014. Malignancies in HIV/AIDS: from epidemiology to therapeutic challenges. *AIDS,* 28**,** 453-65.

Sale, J. E. 2015. REV7/MAD2L2: the multitasking maestro emerges as a barrier to recombination. *The EMBO Journal,* 34**,** 1609-1611.

Sasai, K., Treekitkarnmongkol, W., Kai, K. *et al.,* 2016. Functional Significance of Aurora Kinases–p53 Protein Family Interactions in Cancer. *Frontiers in Oncology,* 6.

Sawai, H. and Domae, N. 2011. Discrimination between primary necrosis and apoptosis by necrostatin-1 in Annexin V-positive/propidium iodide-negative cells. *Biochemical and Biophysical Research Communications,* 411**,** 569-573.

Schmittgen, T. D. and Livak, K. J. 2008. Analyzing real-time PCR data by the comparative C(T) method. *Nature Protocols,* 3**,** 1101-8.

Shafer, R. W. 2006. Rationale and uses of a public HIV drug-resistance database. *Journal of Infectious Disease,* 194 Suppl 1**,** S51-8.

Shiels, M. S., Pfeiffer, R. M., Hall, H. I. *et al.,* 2011. Proportions of Kaposi sarcoma, selected non-Hodgkin lymphomas, and cervical cancer in the United States occurring in

persons with AIDS, 1980-2007. *Journal of the American Medical Association,* 305**,** 1450-9.

Sigel, K., Crothers, K., Dubrow, R. *et al.,* 2013. Prognosis in HIV-infected patients with non-small cell lung cancer. *British Journal of Cancer,* 109**,** 1974-80.

Sikora, M. J., Rae, J. M., Johnson, M. D. *et al.,* 2010. Efavirenz directly modulates the oestrogen receptor and induces breast cancer cell growth. *HIV Medicine,* 11**,** 603-7.

Sparano, J. A., Lee, S., Chen, M. G. *et al.,* 2004. Phase II trial of infusional cyclophosphamide, doxorubicin, and etoposide in patients with HIV-associated non-Hodgkin's lymphoma: an Eastern Cooperative Oncology Group Trial (E1494). *Journal of Clinical Oncology,* 22**,** 1491-1500.

Srirangam, A., Milani, M., Mitra, R. *et al.,* 2011. The human immunodeficiency virus protease inhibitor ritonavir inhibits lung cancer cells, in part, by inhibition of survivin. *Journal of Thoracic Oncology,* 6**,** 661-670.

Srivastava DK, Tendler CL, Milani D, English MA, Licht JD, Wilson SH. The HIV-1 transactivator protein Tat is a potent inducer of the human DNA repair enzyme betapolymerase.

AIDS. 2001;15(4):433–440.

St Clair, S., Giono, L., Varmeh-Ziaie, S. *et al.,* 2004. DNA damage-induced downregulation of Cdc25C is mediated by p53 via two independent mechanisms: one involves direct binding to the cdc25C promoter. *Molecular Cell,* 16**,** 725-36.

Suneja, G., Shiels, M. S., Melville, S. K. *et al.,* 2013. Disparities in the treatment and outcomes of lung cancer among HIV-infected individuals. *AIDS,* 27**,** 459-68.

Taha, H., Das, A.andDas, S. 2015. Clinical effectiveness of dolutegravir in the treatment of HIV/AIDS. *Infection and Drug Resistance,* 8**,** 339-52.

Torres, H. A. and Mulanovich, V. 2014. Management of HIV infection in patients with cancer receiving chemotherapy. *Clinical Infectious Disease,* 59**,** 106-14.

Uziel, T., Lerenthal, Y., Moyal, L. *et al.,* 2003. Requirement of the MRN complex for ATM activation by DNA damage. *The EMBO Journal,* 22**,** 5612-5621.

Varadarajan, J., McWilliams, M. J., Hughes, S. H., Treatment with suboptimal doses of raltegravir leads to aberrant HIV-1 integrations. Proc Natl Acad Sci U S A. 2013; 110:14747–14752.

Walter, R. F., Werner, R., Ting, S. *et al.,* 2015. Identification of deregulation of apoptosis and cell cycle in neuroendocrine tumors of the lung via NanoString nCounter expression analysis. *Oncotarget,* 6**,** 24690-8.

Waters, L. S., Minesinger, B. K., Wiltrout, M. E. *et al.,* 2009. Eukaryotic translesion polymerases and their roles and regulation in DNA damage tolerance. *Microbiology and Molecular Biology Reviews,* 73**,** 134-154.

Willard, H., Merritt, L.andDean, J. 1965. Ultraviolet and visible absorption methods. *Instrumental Methods of Analysis. Van Nostrand: New York***,** 94-95.

Wiman, K. G., Zhivotovsky, B. 2017. Introduction to Nobel Conference: 'The Cell Cycle and Cell Death in Disease'. Journal of Internal Medicine. 281; 418–421.

Wittmann, T., Hyman, A.andDesai, A. 2001. The spindle: a dynamic assembly of microtubules and motors. *Nature Cell Biology,* 3**,** E28-34.

Wojtaszek, J., Lee, C. J., D'souza, S. *et al.*, 2012a. Structural basis of Rev1-mediated assembly of a quaternary vertebrate translesion polymerase complex consisting of Rev1, heterodimeric polymerase (Pol) zeta, and Pol kappa. *Journal of Biological Chemistry,* 287**,** 33836-46.

Wojtaszek, J., Liu, J., D'souza, S. *et al.*, 2012b. Multifaceted recognition of vertebrate Rev1 by translesion polymerases zeta and kappa. *Journal of Biological Chemistry,* 287**,** 26400-8.

Worm, S. W., Bower, M., Reiss, P. *et al.*, 2013. Non-AIDS defining cancers in the D:A:D Study-time trends and predictors of survival: a cohort study. *BMC Infectious Disease,* 13**,** 471.

Wu, L., Ma, C. A., Zhao, Y. *et al.*, 2011. Aurora B interacts with NIR-p53, leading to p53 phosphorylation in its DNA-binding domain and subsequent functional suppression. *Journal of Biological Chemistry,* 286**,** 2236-2244.

Wu, L. C., Wen, Z. S., Qiu, Y. T. *et al.*, 2013. Largazole Arrests Cell Cycle at G1 Phase and Triggers Proteasomal Degradation of E2F1 in Lung Cancer Cells. *ACS Medicinal Chemistry Letters,* 4**,** 921-6.

Zhang, L., Zhang, J., Hu, C. *et al.*, 2009. Efficient activation of p53 pathway in A549 cells exposed to L2, a novel compound targeting p53-MDM2 interaction. *Anticancer Drugs,* 20**,** 416-24.

Zietlow, L., Smith, L. A., Bessho, M. *et al.*, 2009. Evidence for the involvement of human DNA polymerase N in the repair of DNA interstrand cross-links. *Biochemistry,* 48**,** 11817-24.

Zimmermann, M. and De Lange, T. 2014. 53BP1: Pro Choice in DNA Repair. *Trends in Cell Biology,* 24**,** 108-117.

Internet Resources accessed

www.unaids.org/sites/default/files/media_asset/global-AIDS-update-2016_en.pdf
sanac.org.za/
https://www.health-e.org.za/
www.who.int/cancer/en/
http://primer3.wi.mit.edu
www.qiagen.com
https://string-db.org/
https://david.ncifcrf.gov/
https://reactome.org
https://www.qiagenbioinformatics.com
Drug Information SUSTIVA™ GILEAD SCIENCES 2010
Drug Information KALETRA™ ABBOTT LABORATORIES 2010

APPENDICES

Appendix A-Ethics Waiver

Human Research Ethics Committee (Medical)

Research Office Secretariat: Senate House Room SH10005, 10th floor. Tel +27 (0)11-717-1252
Medical School Secretariat: P V Tobias Health Sciences Building, 2nd floor Tel +27 (0)11-717-2700
Private Bag 3, Wits 2050, www.wits.ac.za. Fax +27 (0)11-717-1265

Ref: W-CJ-141013-3 13/10/2014

TO WHOM IT MAY CONCERN:

Waiver: This certifies that the following research does not require clearance from the Human Research Ethics Committee (Medical).

Investigator: **Rahaba Mojakgomo. (Student no. 0216592H).**

Project title: **The identification of cell cycle related genes in response to antiretroviral treatment (ART) in lung cancer.**

Reason: This is an *in vitro* laboratory study with commercial cell lines including MRC-5, A549 and SW 900. There are no human participants.

UNIVERSITY OF THE WITWATERSRAND
PROF PE CLEATON-JONES
HREC (MEDICAL)
2014 -10- 13
JOHANNESBURG

Professor Peter Cleaton-Jones

Chair: Human Research Ethics Committee (Medical)

Appendix B- Drugs and Alamar Blue

B1) Drugs

a) ARV drugs

(i) Efavirenz (EFV) (Toronto Research Chemicals)

0.0158g EFV dissolved in 5ml methanol, to give 10mM.

(ii) Lopinavir/ritonavir (Toronto Research Chemicals)

4:1 ratio (32:8 µM) was used

For (10:2.5) mM LPV/r stock solution,

0.0314g (LPV) plus 0.009g (RTV) dissolved in 5ml methanol

b) Camptothecin (Sigma)

50µM Camptothecin (CPT)

0.0348mg dissolved in 2ml methanol

B2) Alamar Blue (Sigma)
0.0005g in 5ml of sterile distilled water

Appendix C-Supplementary data

C1) Alamar Blue (AB) assay

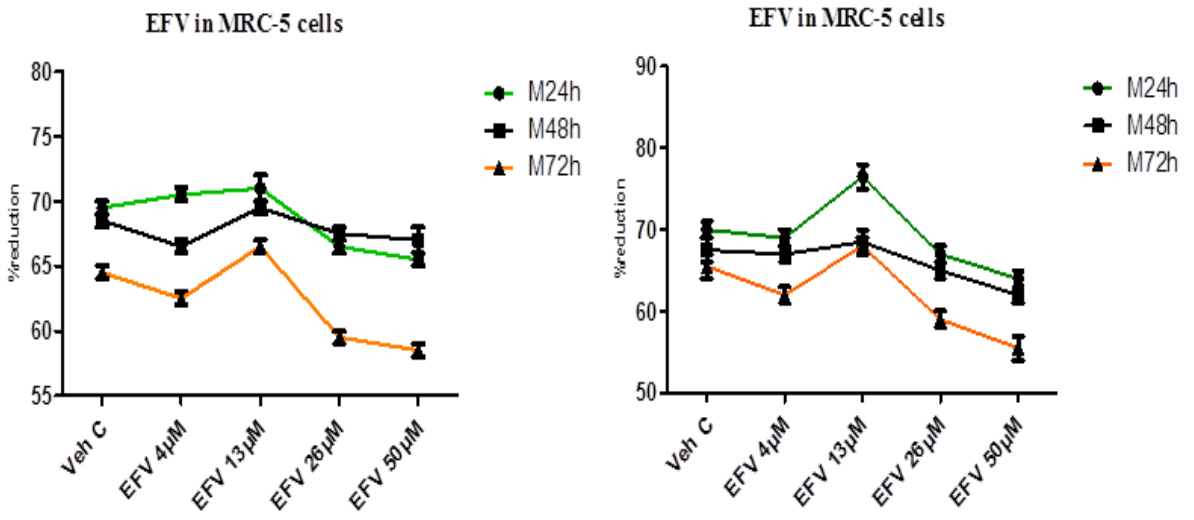

Figure C1.1: Cell viability in response to EFV in MRC-5 cells. Cells were treated for 24h to 72h (M24h to M72h) with 4, 13, 26 and 50µM EFV. Percentage (%) reduction of AB is directly proportional to the number of viable cells.

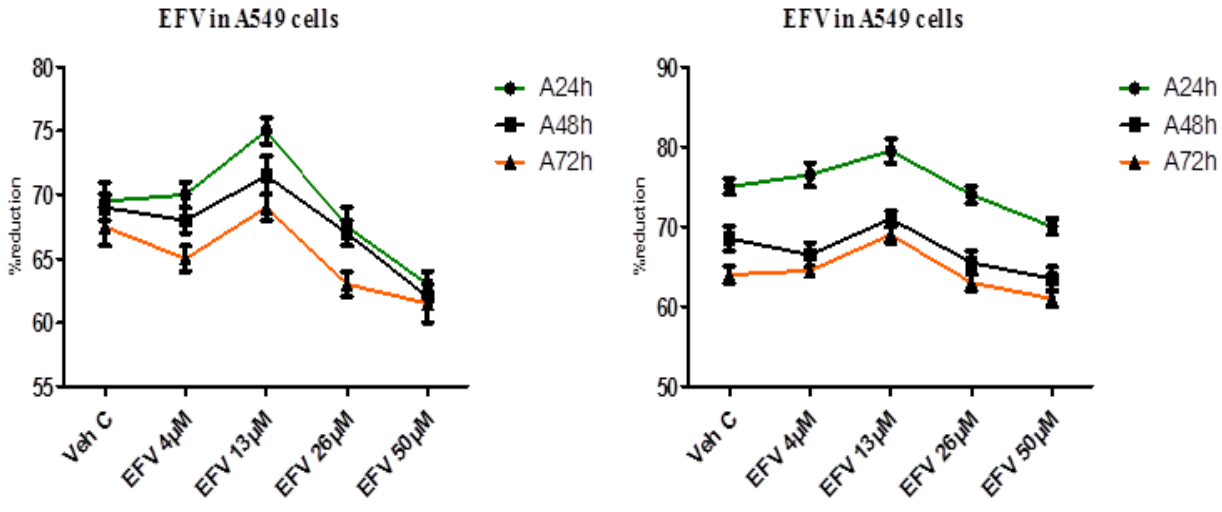

Figure C1.2: Cell viability in response to EFV in A549 cells. Cells were treated for 24h to 72h (A24h to A72h) with 4, 13, 26 and 50µM EFV. Percentage (%) reduction of AB is directly proportional to the number of viable cells.

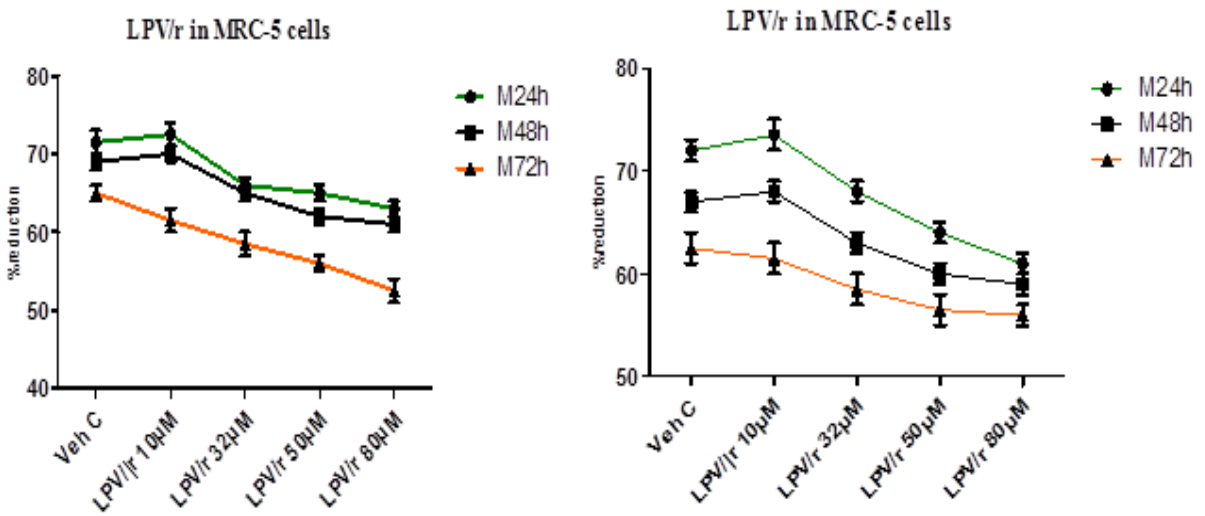

Figure C1.3: Cell viability in response to LPV/r in MRC-5 cells. Cells were treated for 24h to 72h (M24h to M72h) with 10, 32, 50 and 80µM EFV. Percentage (%) reduction of AB is directly proportional to the number of viable cells.

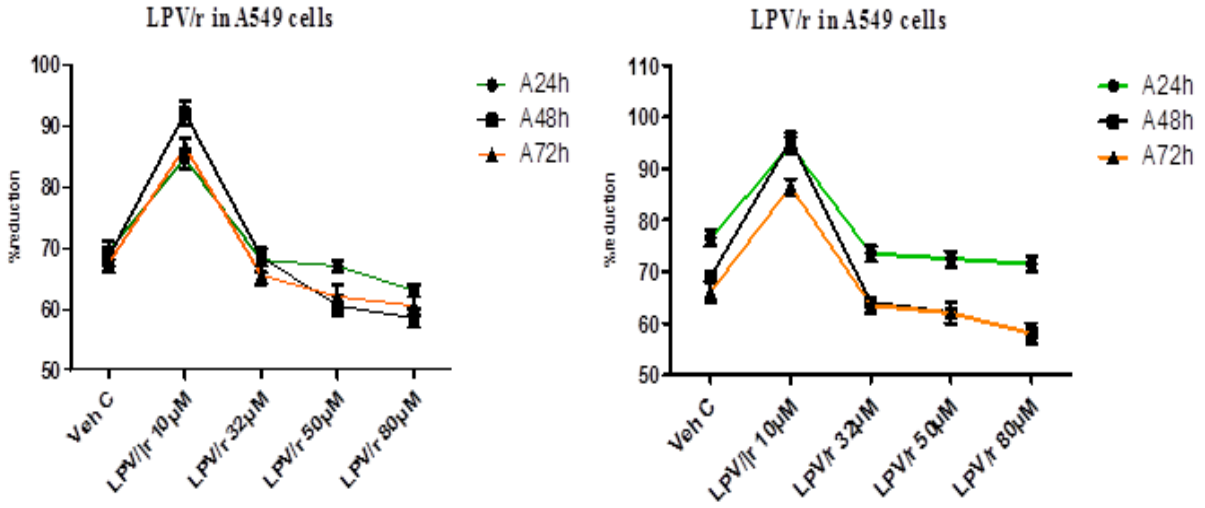

Figure C1.4: Cell viability in response to LPV/r in A549 cells. Cells were treated for 24h to 72h (A24h to A72h) with 10, 32, 50 and 80µM EFV. Percentage (%) reduction of AB is directly proportional to the number of viable cells.

C2) xCELLigence RTCA assay

EFV treatment in MRC-5

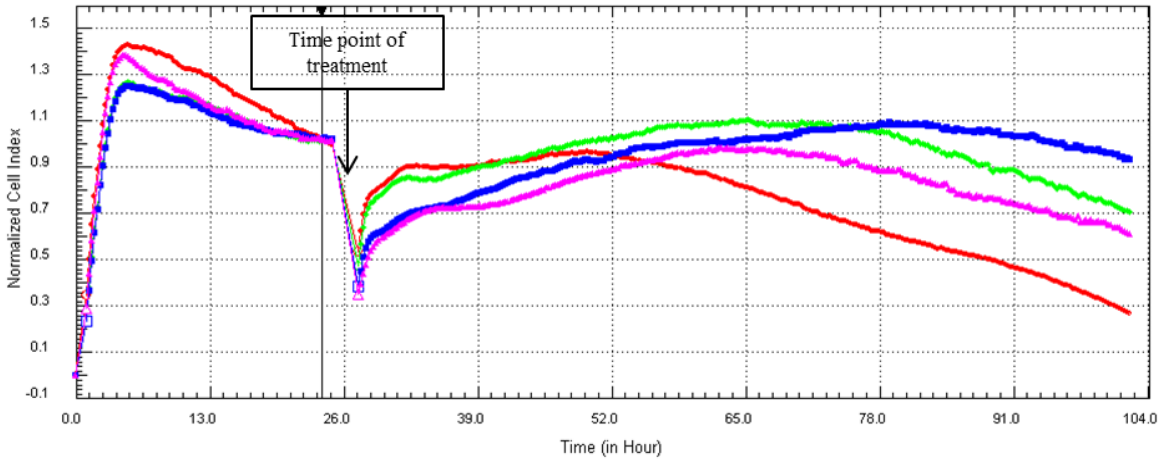

Figure C2.1: MRC-5 cells growth curves treated with EFV. The cells were exposed to 4, 13 and 50µM EFV for 24h to 72h. The curves were plotted in relative to the untreated (veh control).

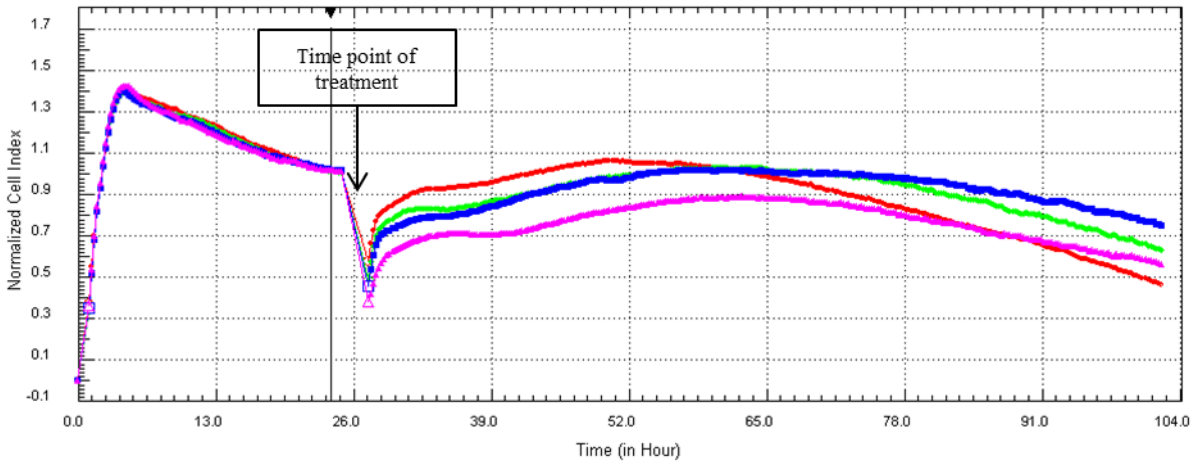

Figure C2.2: MRC-5 cells growth curves treated with EFV. The cells were exposed to 4, 13 and 50µM EFV for 24h to 72h. The curves were plotted in relative to the untreated (veh control).

EFV treatment in A549

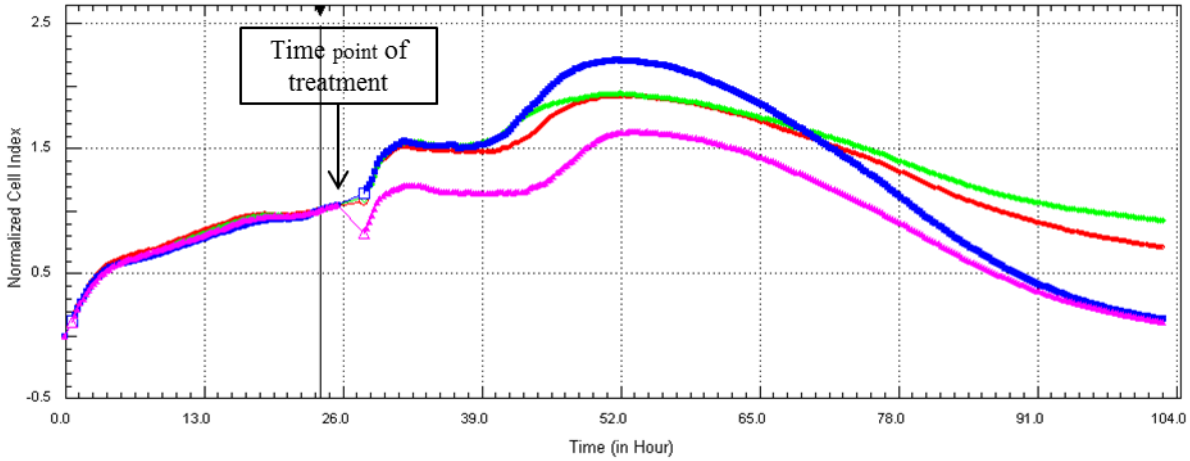

Figure C2.3: A549 cells growth curves treated with EFV. The cells were exposed to 4, 13 and 50µM EFV for 24h to 72h. The curves were plotted in relative to the untreated (veh control).

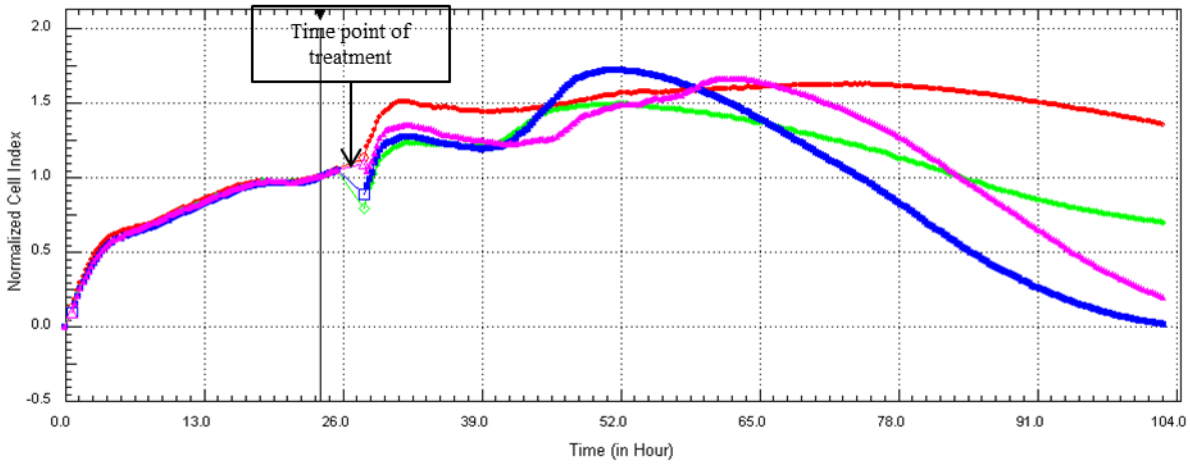

Figure C2.4: A549 cells growth curves treated with EFV. The cells were exposed to 4, 13 and 50µM EFV for 24h to 72h. The curves were plotted in relative to the untreated (veh control).

LPV/r in MRC-5 cells

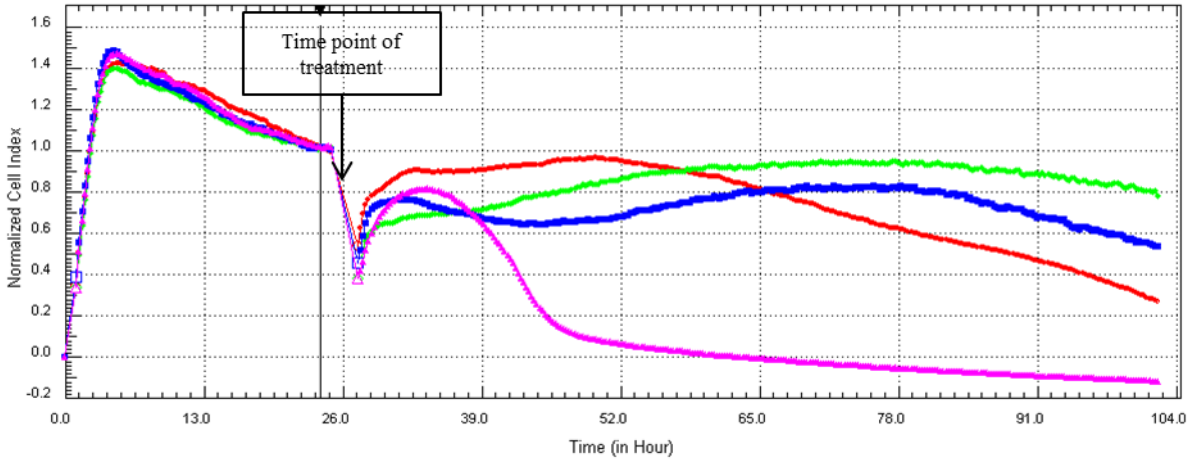

Figure C2.5: MRC-5 cells growth curves treated with LPV/r. The cells were exposed to 10, 32 and 80µM for 24h to 72h. The curves were plotted in relative to the untreated (veh control).

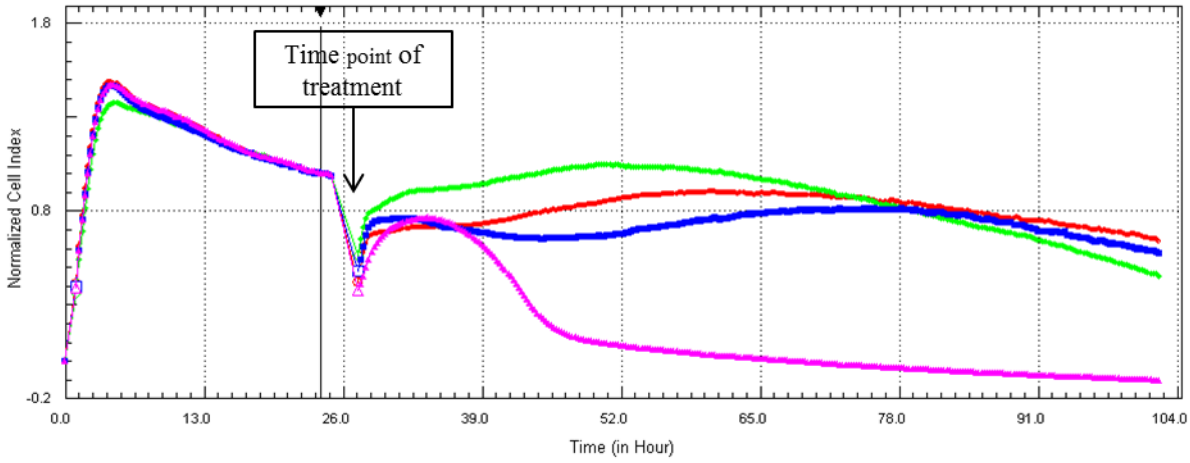

Figure C2.6: MRC-5 cells growth curves treated with LPV/r. The cells were exposed to 10, 32 and 80µM for 24h to 72h. The curves were plotted in relative to the untreated (veh control).

LPV/r in A549 cells

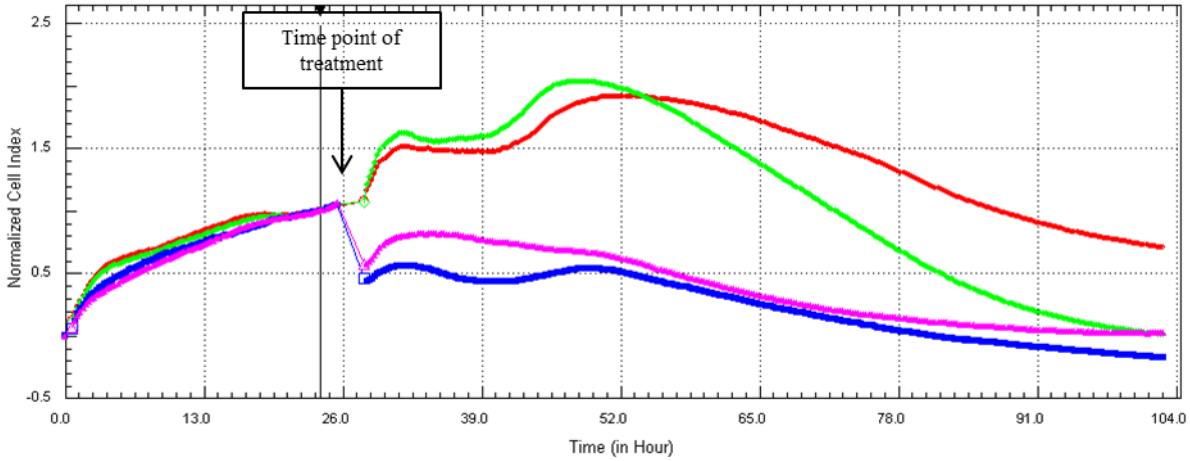

Figure C2.7: A549 cells growth curves treated with LPV/r. The cells were exposed to 10, 32 and 80µM for 24h to 72h. The curves were plotted in relative to the untreated (veh control).

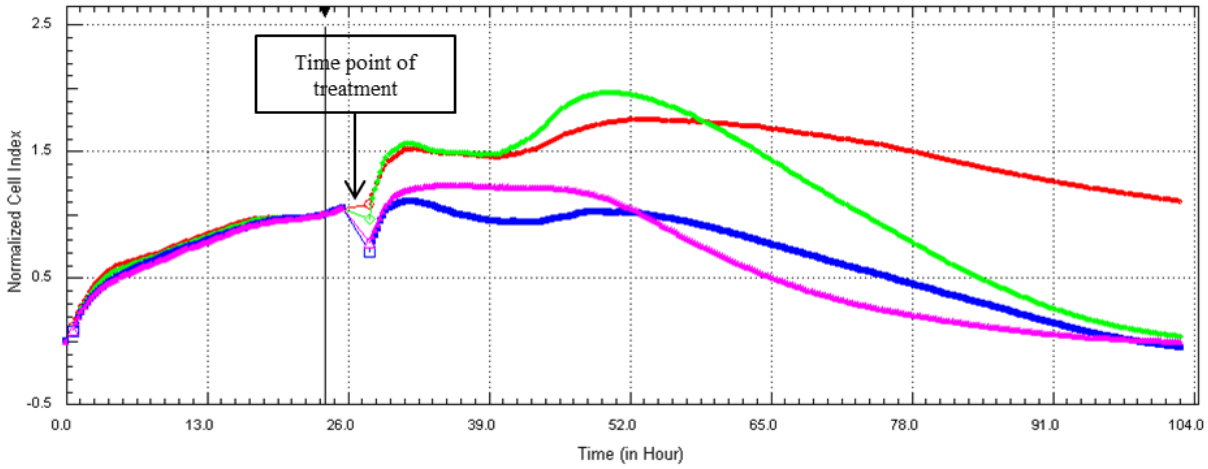

Figure C2.8: A549 cells growth curves treated with LPV/r. The cells were exposed to 10, 32 and 80µM for 24h to 72h. The curves were plotted in relative to the untreated (veh control).

C3) Cell-cycle analysis by FACS

EFV treated cells, first MRC-5 cells then A549 cells.

MRC-5 EFV treated

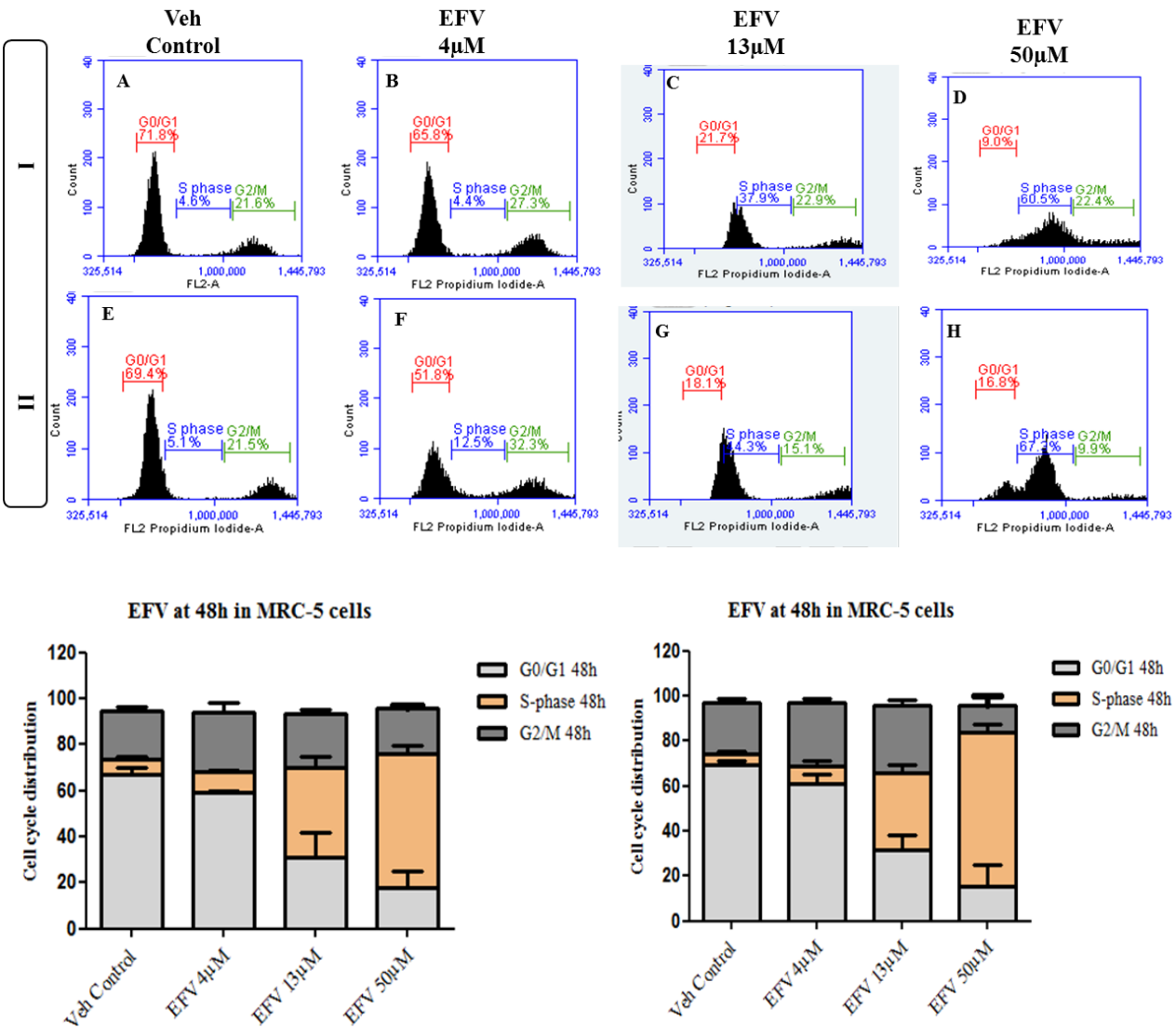

Figure C3.1: Analysis of the cell-cycle stages in MRC-5 cells treated with (4, 13 and 50)µM EFV at 24h and 48h. The histograms and the bar-graphs illustrate an increase in S-phase with increasing EFV concentration.

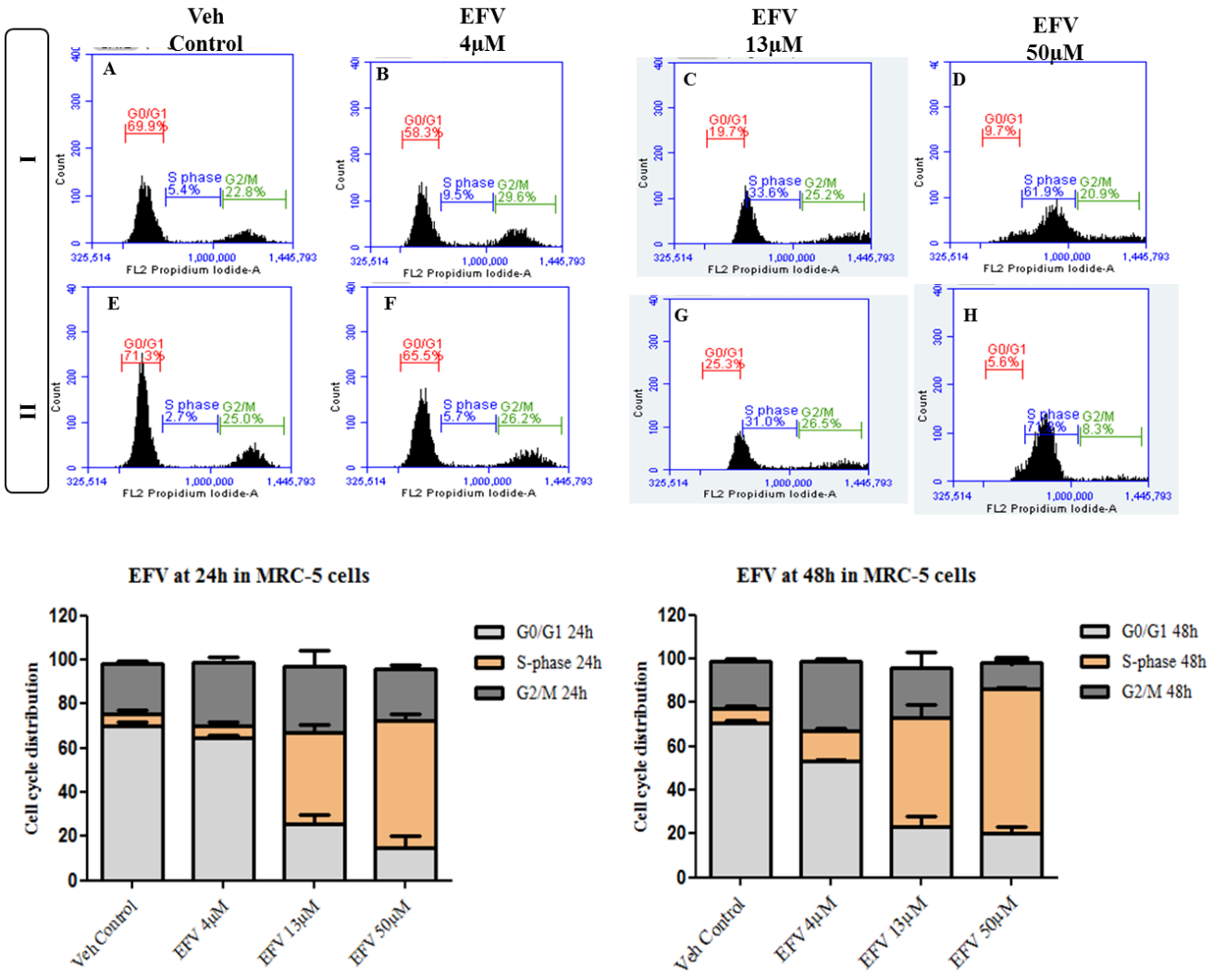

Figure C3.2: Analysis of the cell-cycle stages in MRC-5 cells treated with (4, 13 and 50)µM EFV at 24h and 48h. The histograms and the bar-graphs illustrate an increase in S-phase with increasing EFV concentration.

A549 cells EFV treated

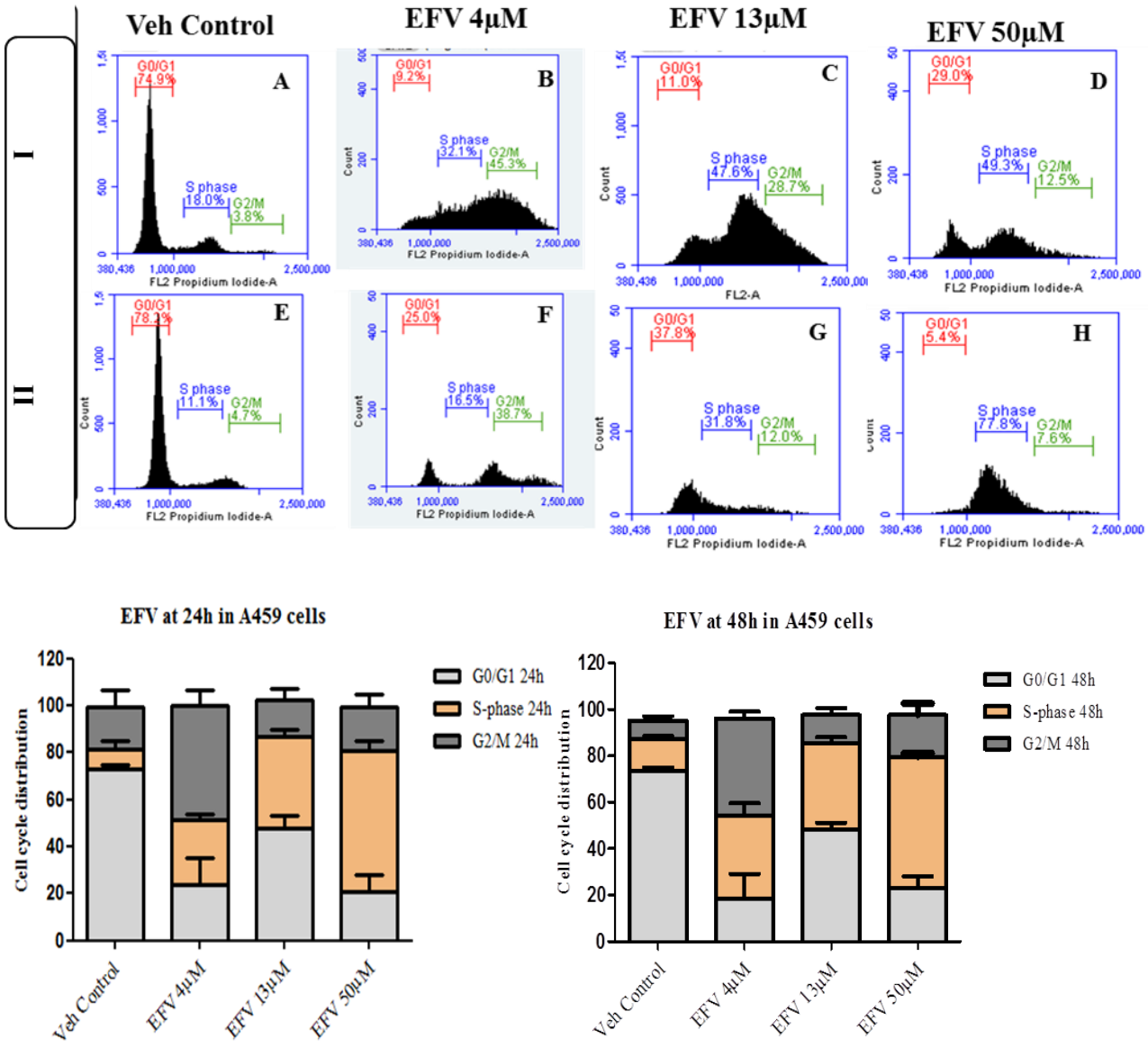

Figure C3.3: Analysis of the cell-cycle stages in A549 cells treated with (4, 13 and 50)µM EFV at 24h and 48h. The histograms and the bar-graphs illustrate an increase in S-phase with increasing EFV concentration.

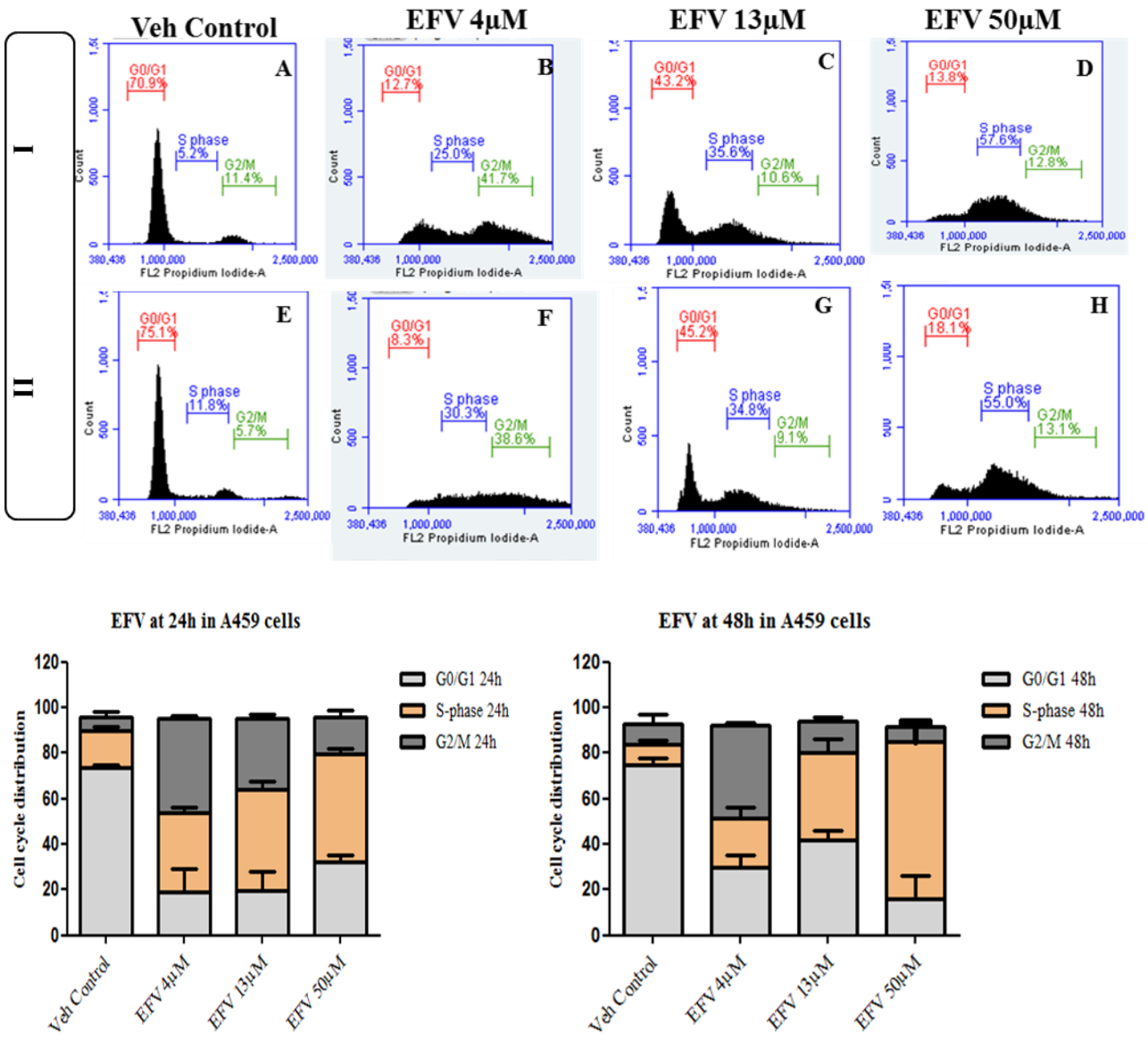

Figure C3.4: Analysis of the cell-cycle stages in A549 cells treated with (4, 13 and 50)µM EFV at 24h and 48h. The histograms and the bar-graphs illustrate an increase in S-phase with increasing EFV concentration.

LPV/r treated cells, first MRC-5 cells, then A549 cells.

MRC-5 LPV/r treated

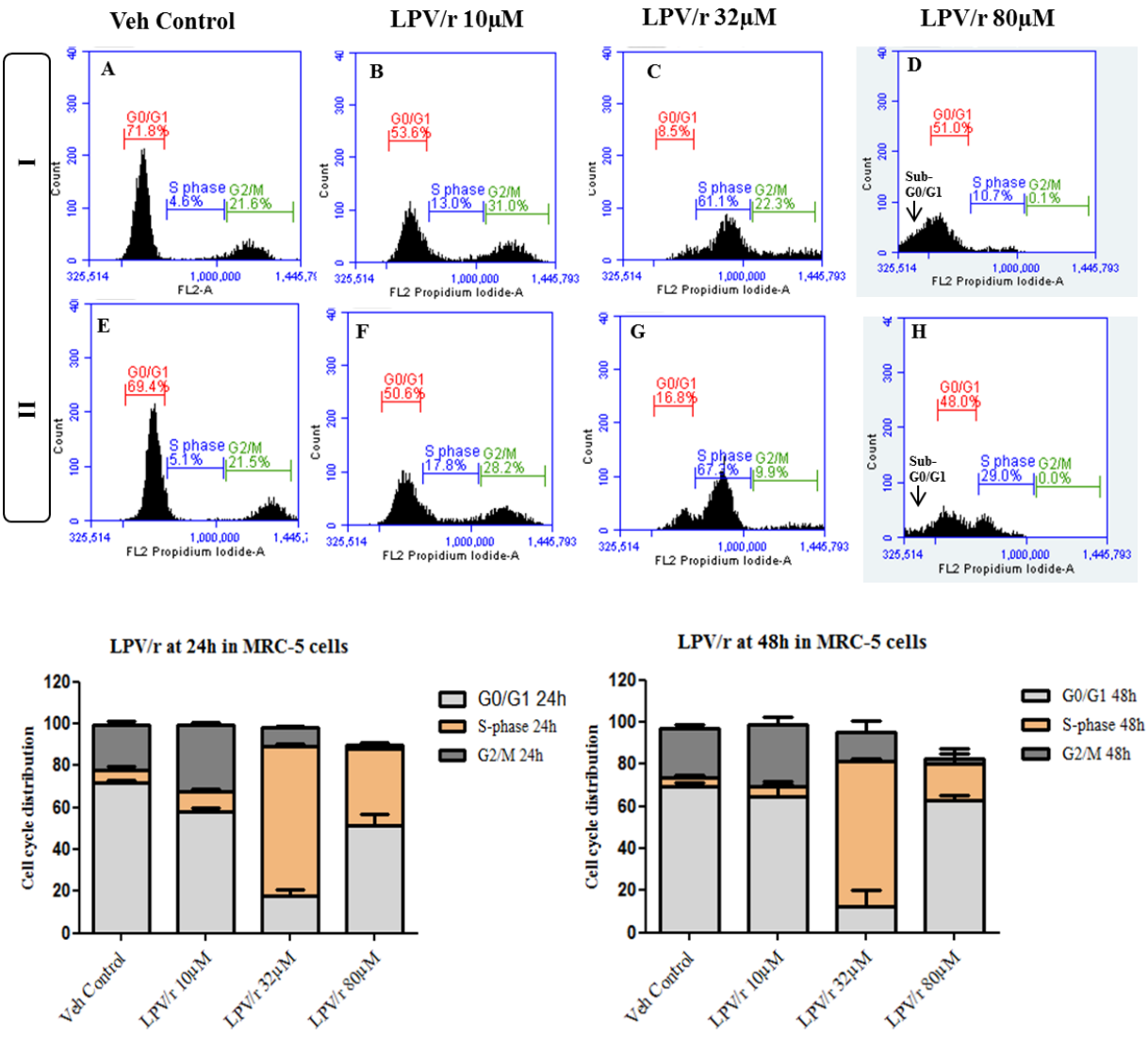

Figure C3.5: The analysis of the cell-cycle interphases in MRC-5 cells treated with (10, 32 and 80) µM LPV/r. The histograms and the bar graphs show an arrest at S phase following 32µM treatment. Cell death is illustrated by the sub-G0/G1 population towards the side-scatter in the histograms.

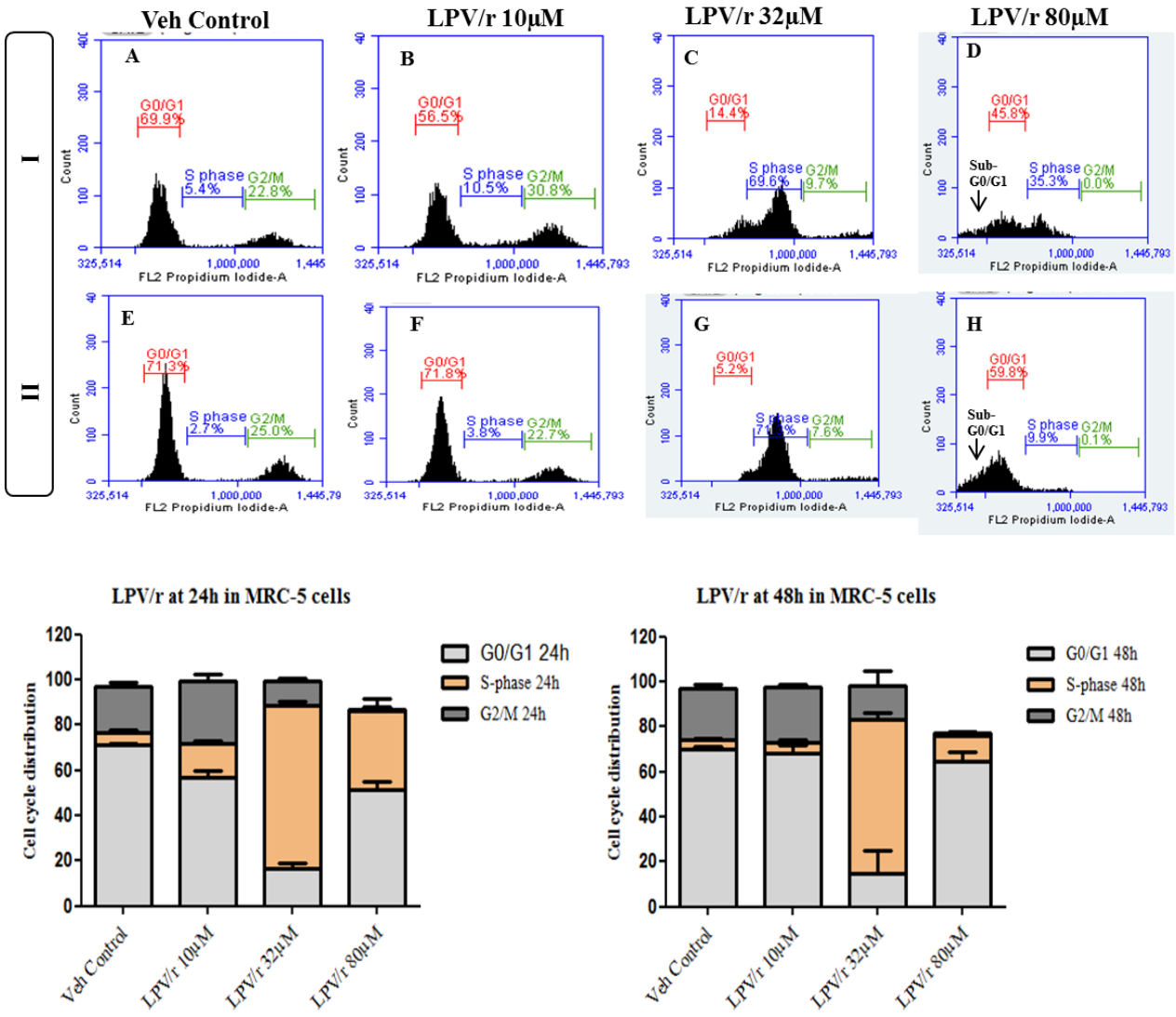

<u>Figure C3.6</u>: The analysis of the cell-cycle interphases in MRC-5 cells treated with (10, 32 and 80) µM LPV/r. The histograms and the bar graphs show an arrest at S phase following 32µM treatment. Cell death is illustrated by the sub-G0/G1 population towards the side-scatter in the histograms.

A549 LPV/r treated

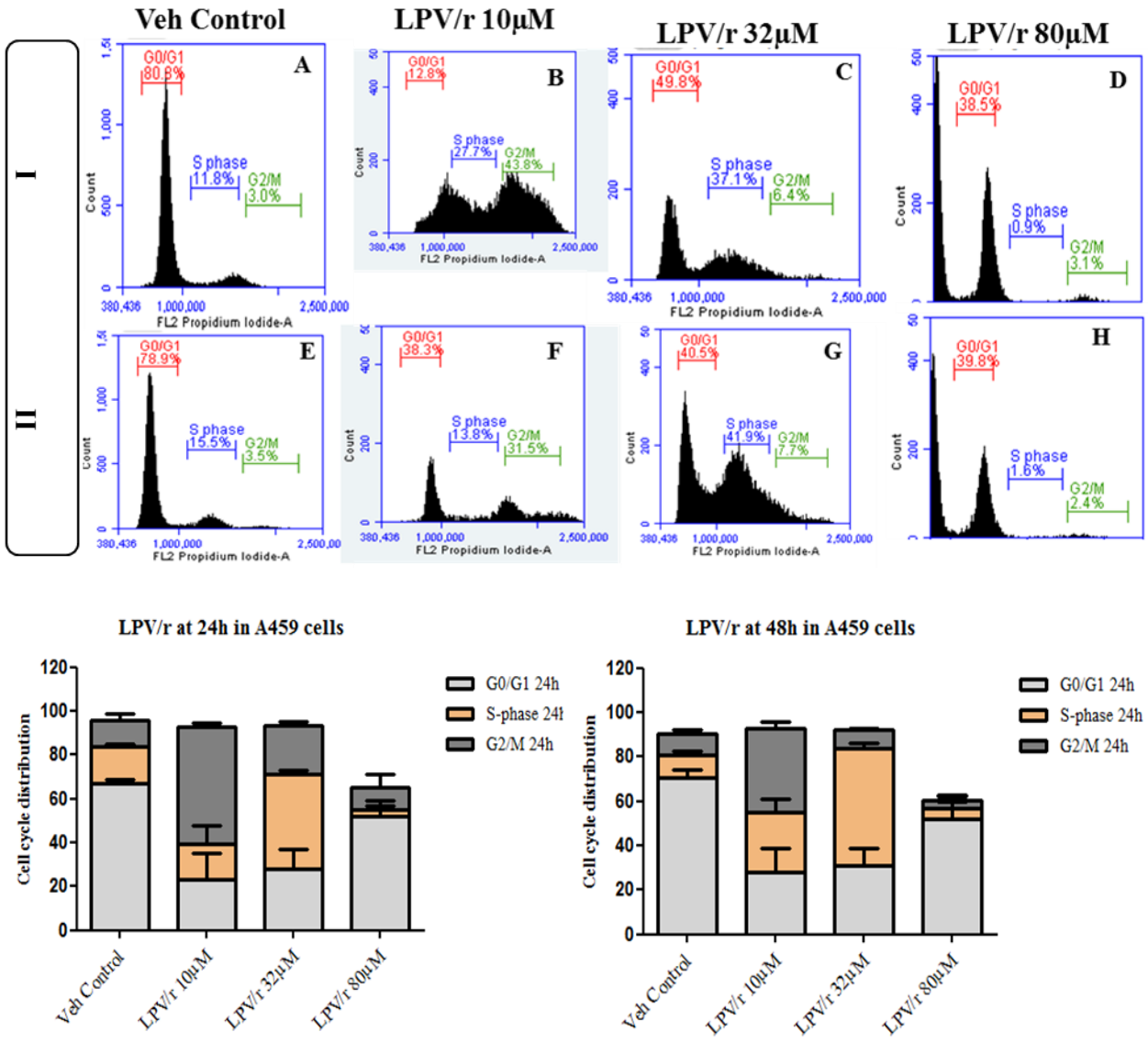

Figure C3.7: The analysis of the cell-cycle interphases in A549 cells treated with (10, 32 and 80) µM LPV/r. The histograms and the bar graphs show an arrest at S phase following 32µM treatment. Cell death is illustrated by the sub-G0/G1 population on the side-scatter in the histograms.

A549 cells LPV/r treated

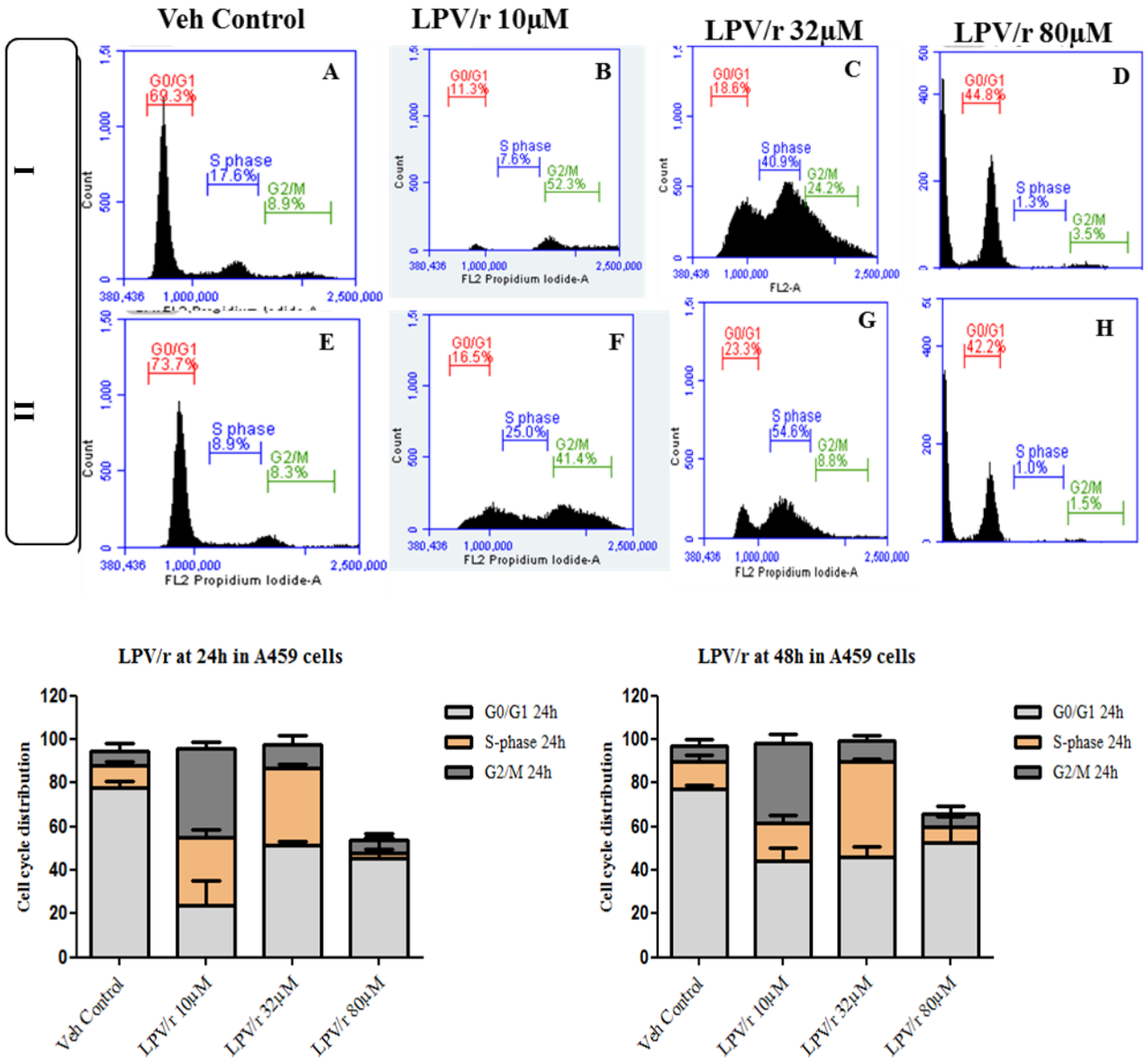

Figure C3.8: The analysis of the cell-cycle interphases in A549 cells treated with (10, 32 and 80) µM LPV/r. The histograms and the bar graphs show an arrest at S phase following 32µM treatment. Cell death is illustrated by the sub-G0/G1 population on the side-scatter in the histograms.

C4) Apoptosis assay by FACS

MRC-5 cells

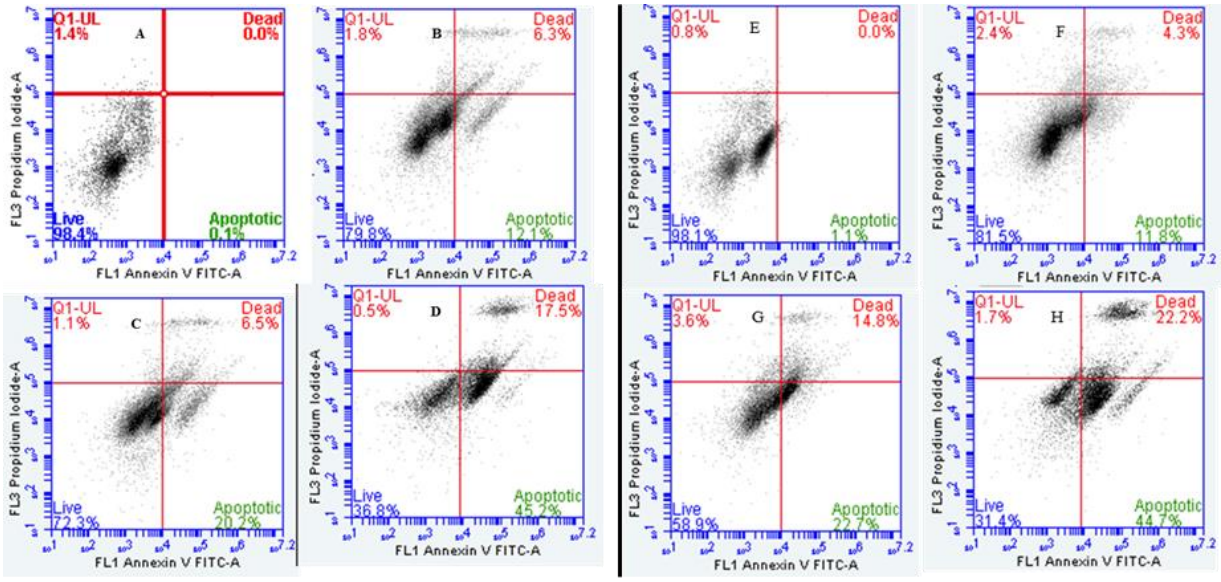

Figure C4.1: MRC-5 cells apoptosis FACS analysis. The cells were treated for 24h (A-D) and 48h (E-H) with; A and E (0.1% methanol-vehicle), B and F CPT as positive control, C and G, 32µM LPV/r and D and H 80µM LPV/r.

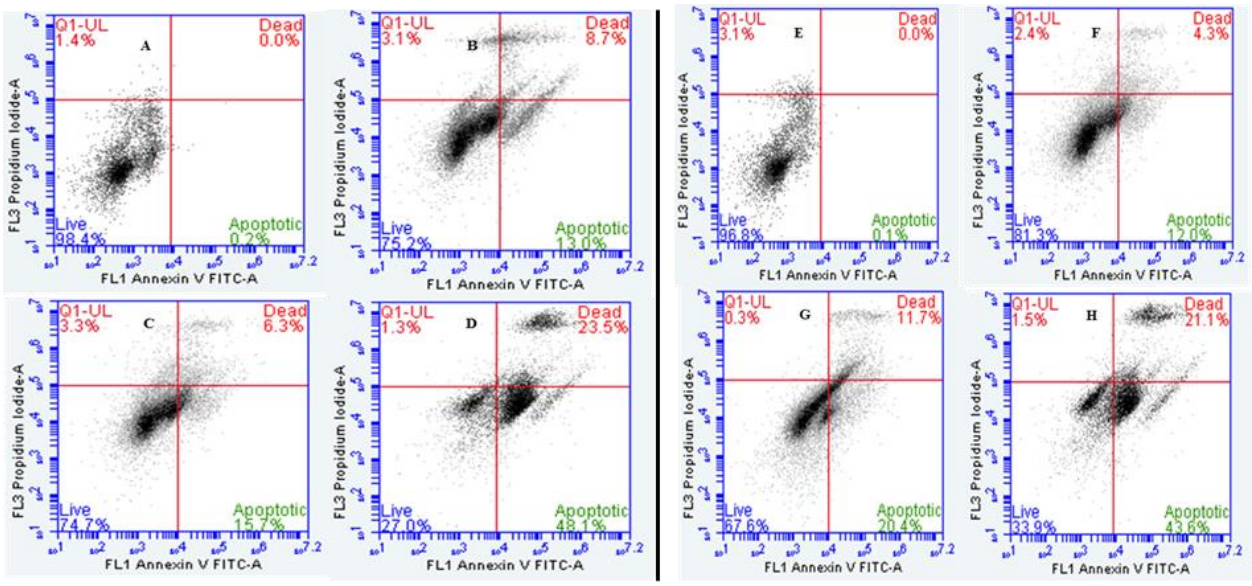

Figure C4.2: MRC-5 cells apoptosis FACS analysis. The cells were treated for 24h (A-D) and 48h (E-H) with; A and E (0.1% methanol-vehicle), B and F CPT as positive control, C and G, 32µM LPV/r and D and H 80µM LPV/r.

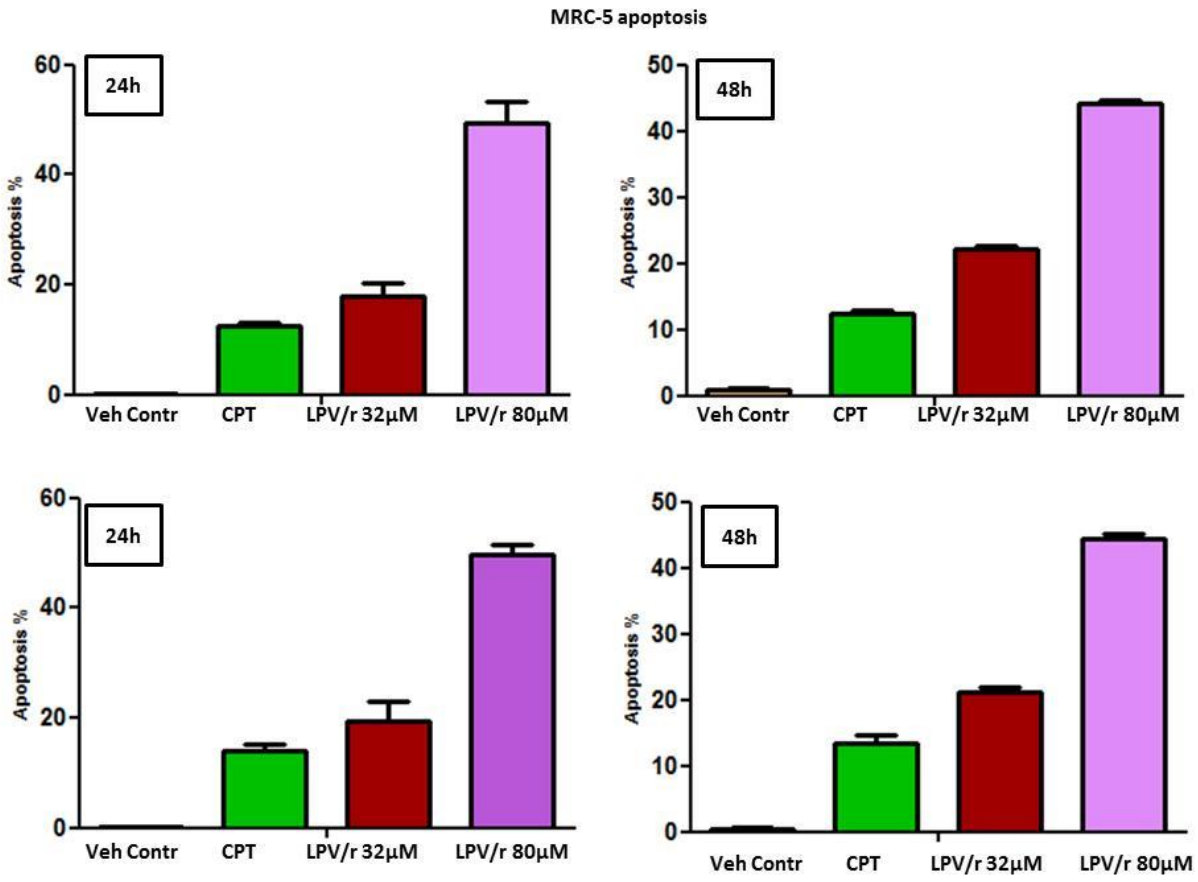

Figure C4.3: MRC-5 cells apoptosis statistical analysis using ANOVA and Tukey's multiple comparison tests. The apoptosis percentage (%) increases with increasing LPV/r concentrations.

LPV/r apoptotic effects in A549 cells

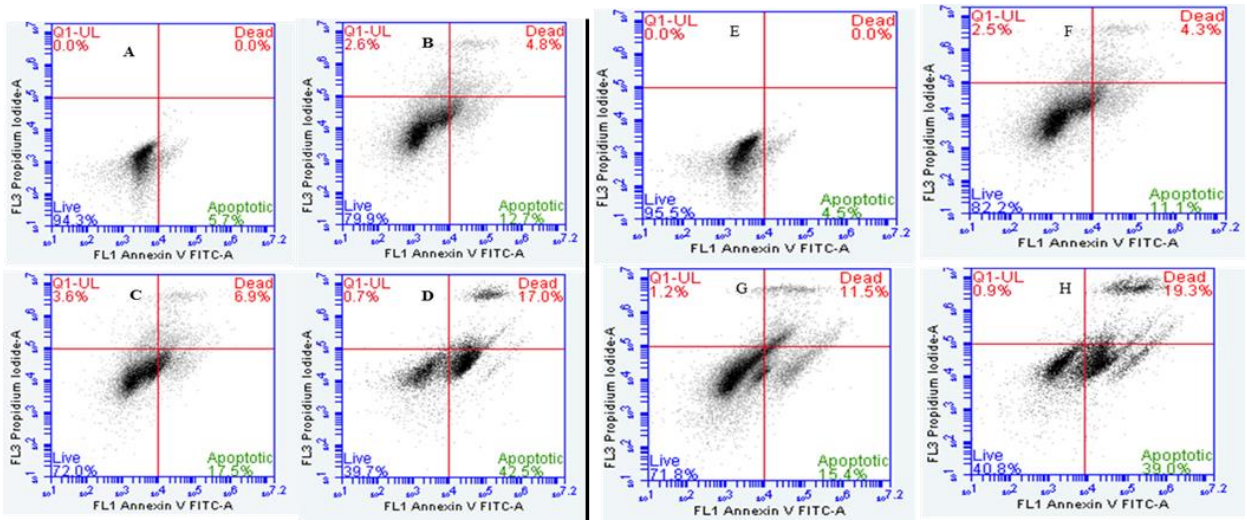

Figure C4.4: A549 cells apoptosis FACS analysis. The cells were treated for 24h (A-D) and 48h (E-H) with; A and E (0.1% methanol-vehicle), B and F CPT as positive control, C and G, 32µM LPV/r and D and H 80µM LPV/r.

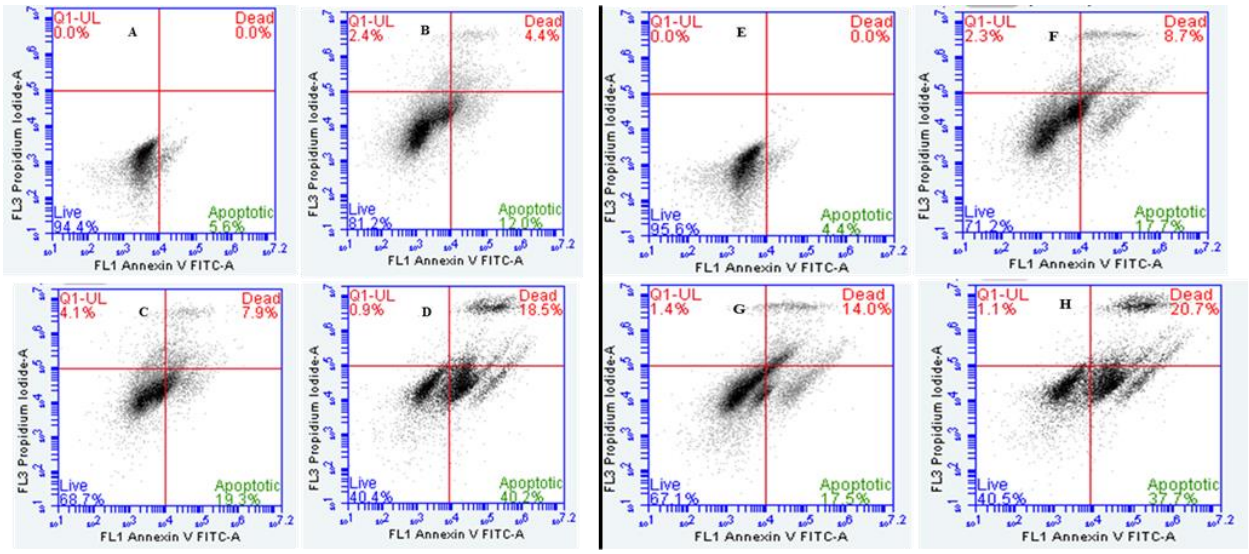

Figure C4.5: A549 cells apoptosis FACS analysis. The cells were treated for 24h (A-D) and 48h (E-H) with; A and E (0.1% methanol-vehicle), B and F CPT as positive control, C and G, 32µM LPV/r and D and H 80µM LPV/r.

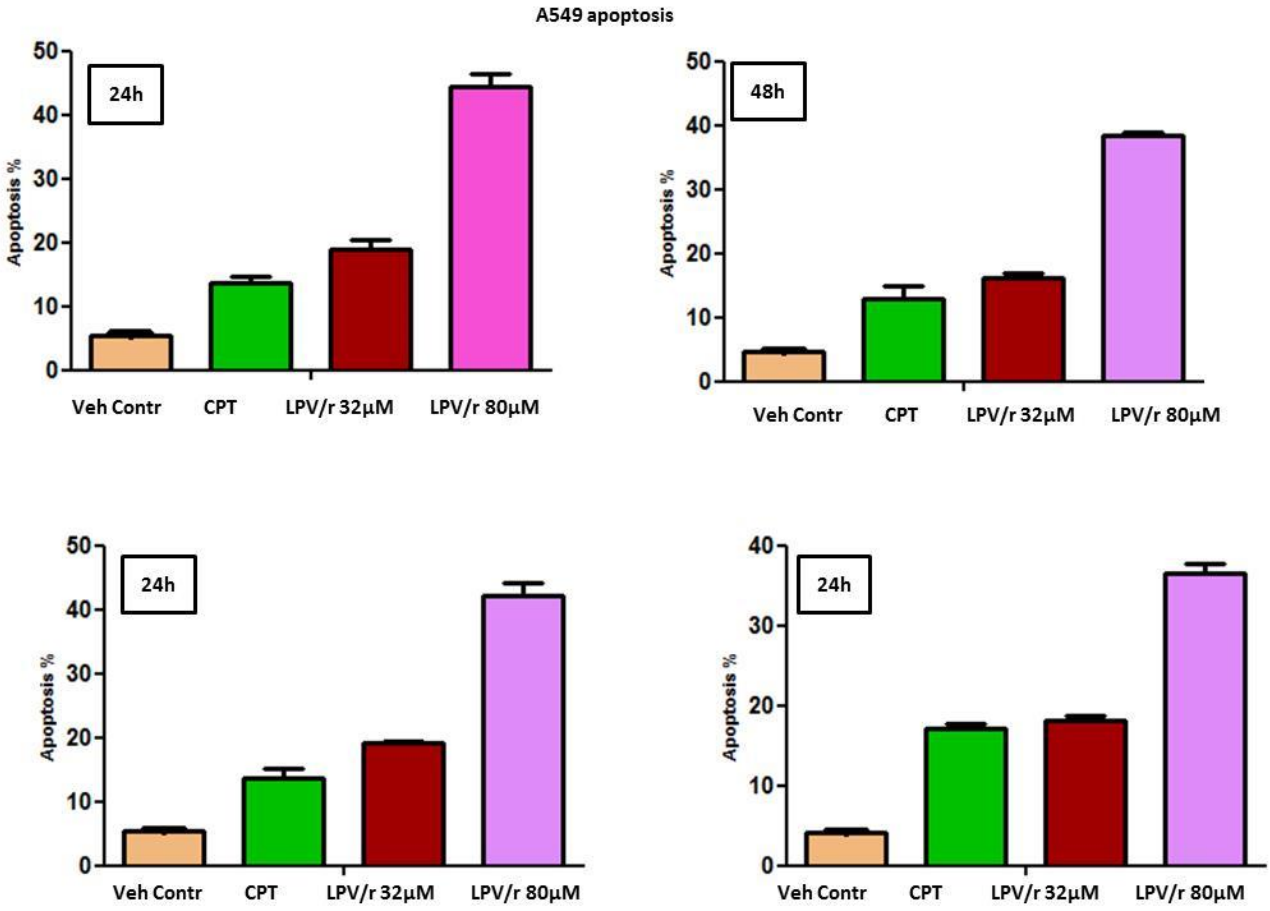

Figure C4.6: A549 cells apoptosis statistical analysis using ANOVA and Tukey's multiple comparison tests. The apoptosis percentage (%) increases with increasing LPV/r treatment.

C5) PCR (Gene) Arrays appendices

	1	2	3	4	5	6	7	8	9	10	11	12
A	ABL1	ANAPC 2	ATM	ATR	AURKA	AURKB	BCCIP	BCL2	BIRC5	BRCA1	BRCA2	CASP3
B	CCNA2	CCNB1	CCNB2	CCNC	CCND1	CCND2	CCND3	CCNE1	CCNF	CCNG1	CCNG2	CCNH
C	CCNT1	CDC16	CDC20	CDC25 A	CDC25C	CDC34	CDC6	CDK1	CDK2	CDK4	CDK5R1	CDK5R AP 1
D	CDK6	CDK7	CDK8	CDKN1 A	CDKN1 B	CDKN2 A	CDKN2 B	CDKN3	CHEK1	CHEK2	CKS1B	CKS2
E	CUL1	CUL2	CUL3	E2F1	E2F4	GADD4 5A	GTSE1	HUS1	KNTC1	KPNA2	MAD2L 1	MAD2L 2
F	MCM2	MCM3	MCM4	MCM5	MDM2	MKI67	MNAT1	MRE11 A	NBN	RAD1	RAD17	RAD51
G	RAD9A	RB1	RBBP8	RBL1	RBL2	SERTAD 1	SKP2	STMN1	TFDP1	TFDP2	TP53	WEE1
H	ACTB	B2M	GAPDH	HPRT1	RPLP0	HGDC	RTC	RTC	RTC	PPC	PPC	PPC

Well	Gene Symbol	GenBank	Gene name
A01	ABL1	NM_005157	C-abl oncogene 1, non-receptor tyrosine kinase
A02	ANAPC2	NM_013366	Anaphase promoting complex subunit 2
A03	ATM	NM_000051	Ataxia telangiectasia mutated
A04	ATR	NM_001184	Ataxia telangiectasia and Rad3 related
A05	AURKA	NM_003600	Aurora kinase A
A06	AURKB	NM_004217	Aurora kinase B
A07	BCCIP	NM_016567	BRCA2 and CDKN1A interacting protein
A08	BCL2	NM_000633	B-cell CLL/lymphoma 2
A09	BIRC5	NM_001168	Baculoviral IAP repeat containing 5
A10	BRCA1	NM_007294	Breast cancer 1, early onset
A11	BRCA2	NM_000059	Breast cancer 2, early onset
A12	CASP3	NM_004346	Caspase 3, apoptosis-related cysteine peptidase
B01	CCNA2	NM_001237	Cyclin A2
B02	CCNB1	NM_031966	Cyclin B1
B03	CCNB2	NM_004701	Cyclin B2
B04	CCNC	NM_005190	Cyclin C
B05	CCND1	NM_053056	Cyclin D1
B06	CCND2	NM_001759	Cyclin D2
B07	CCND3	NM_001760	Cyclin D3

B08	CCNE1	NM_001238	Cyclin E1
B09	CCNF	NM_001761	Cyclin F
B10	CCNG1	NM_004060	Cyclin G1
B11	CCNG2	NM_004354	Cyclin G2
B12	CCNH	NM_001239	Cyclin H
C01	CCNT1	NM_001240	Cyclin T1
C02	CDC16	NM_003903	Cell division cycle 16 homolog (S. cerevisiae)
C03	CDC20	NM_001255	Cell division cycle 20 homolog (S. cerevisiae)
C04	CDC25A	NM_001789	Cell division cycle 25 homolog A (S. pombe)
C05	CDC25C	NM_001790	Cell division cycle 25 homolog C (S. pombe)
C06	CDC34	NM_004359	Cell division cycle 34 homolog (S. cerevisiae)
C07	CDC6	NM_001254	Cell division cycle 6 homolog (S. cerevisiae)
C08	CDK1	NM_001786	Cyclin-dependent kinase 1
C09	CDK2	NM_001798	Cyclin-dependent kinase 2
C10	CDK4	NM_000075	Cyclin-dependent kinase 4
C11	CDK5R1	NM_003885	Cyclin-dependent kinase 5, regulatory subunit 1 (p35)
C12	CDK5RAP1	NM_016408	CDK5 regulatory subunit associated protein 1
D01	CDK6	NM_001259	Cyclin-dependent kinase 6
D02	CDK7	NM_001799	Cyclin-dependent kinase 7
D03	CDK8	NM_001260	Cyclin-dependent kinase 8
D04	CDKN1A	NM_000389	Cyclin-dependent kinase inhibitor 1A (p21, Cip1)
D05	CDKN1B	NM_004064	Cyclin-dependent kinase inhibitor 1B (p27, Kip1)
D06	CDKN2A	NM_000077	Cyclin-dependent kinase inhibitor 2A (melanoma, p16, inhibits CDK4)
D07	CDKN2B	NM_004936	Cyclin-dependent kinase inhibitor 2B (p15, inhibits CDK4)
D08	CDKN3	NM_005192	Cyclin-dependent kinase inhibitor 3
D09	CHEK1	NM_001274	CHK1 checkpoint homolog (S. pombe)
D10	CHEK2	NM_007194	CHK2 checkpoint homolog (S. pombe)
D11	CKS1B	NM_001826	CDC28 protein kinase regulatory subunit 1B
D12	CKS2	NM_001827	CDC28 protein kinase regulatory subunit 2
E01	CUL1	NM_003592	Cullin 1
E02	CUL2	NM_003591	Cullin 2
E03	CUL3	NM_003590	Cullin 3
E04	E2F1	NM_005225	E2F transcription factor 1
E05	E2F4	NM_001950	E2F transcription factor 4, p107/p130-binding
E06	GADD45A	NM_001924	Growth arrest and DNA-damage-inducible, alpha
E07	GTSE1	NM_016426	G-2 and S-phase expressed 1
E08	HUS1	NM_004507	HUS1 checkpoint homolog (S. pombe)
E09	KNTC1	NM_014708	Kinetochore associated 1

E10	KPNA2	NM_002266	Karyopherin alpha 2 (RAG cohort 1, importin alpha 1)
E11	MAD2L1	NM_002358	MAD2 mitotic arrest deficient-like 1 (yeast)
E12	MAD2L2	NM_006341	MAD2 mitotic arrest deficient-like 2 (yeast)
F01	MCM2	NM_004526	Minichromosome maintenance complex component 2
F02	MCM3	NM_002388	Minichromosome maintenance complex component 3
F03	MCM4	NM_005914	Minichromosome maintenance complex component 4
F04	MCM5	NM_006739	Minichromosome maintenance complex component 5
F05	MDM2	NM_002392	Mdm2 p53 binding protein homolog (mouse)
F06	MKI67	NM_002417	Antigen identified by monoclonal antibody Ki-67
F07	MNAT1	NM_002431	Menage a trois homolog 1, cyclin H assembly factor (Xenopus laevis)
F08	MRE11A	NM_005590	MRE11 meiotic recombination 11 homolog A (S. cerevisiae)
F09	NBN	NM_002485	Nibrin
F10	RAD1	NM_002853	RAD1 homolog (S. pombe)
F11	RAD17	NM_002873	RAD17 homolog (S. pombe)
F12	RAD51	NM_002875	RAD51 homolog (S. cerevisiae)
G01	RAD9A	NM_004584	RAD9 homolog A (S. pombe
G02	RB1	NM_000321	Retinoblastoma 1
G03	RBBP8	NM_002894	Retinoblastoma binding protein 8
G04	RBL1	NM_002895	Retinoblastoma-like 1 (p107)
G05	RBL2	NM_005611	Retinoblastoma-like 2 (p130)
G06	SERTAD1	NM_013376	SERTA domain containing 1
G07	SKP2	NM_005983	S-phase kinase-associated protein 2 (p45)
G08	STMN1	NM_005563	Stathmin 1
G09	TFDP1	NM_007111	Transcription factor Dp-1
G10	TFDP2	NM_006286	Transcription factor Dp-2 (E2F dimerization partner 2)
G11	TP53	NM_000546	Tumor protein p53
G12	WEE1	NM_003390	WEE1 homolog (S. pombe)
H01	ACTB	NM_001101	Actin, beta
H02	B2M	NM_004048	Beta-2-microglobulin
H03	GAPDH	NM_002046	Glyceraldehyde-3-phosphate dehydrogenase
H04	HPRT1	NM_000194	Hypoxanthine phosphoribosyltransferase 1
H05	RPLP0	NM_001002	Ribosomal protein, large, P0
H06	HGDC	SA_00105	Human Genomic DNA Contamination
H07	RTC	SA_00104	Reverse Transcription Control
H08	RTC	SA_00104	Reverse Transcription Control

H09	RTC	SA_00104	Reverse Transcription Control
H10	PPC	SA_00103	Positive PCR Control
H11	PPC	SA_00103	Positive PCR Control
H12	PPC	SA_00103	Positive PCR Control

Figure C5.1: The layout of the human cell-cycle PCR Array, each well representing an individual gene. There are 84 genes across the array (A1 to G12), with the H row comprising of the quality controls which include HKG, HGDC, as well as the RTC and PPC. The accession numbers corresponding to the gene names (full) and abbreviations are provided here.

Table C5.1: Gene expression in fold changes in untreated A549 vs MRC-5

Position	Gene Symbol	UniGene	GenBank	**Fold Change**
A01	ABL1	Hs.431048	NM_005157	-2.87
A02	ANAPC2	Hs.533262	NM_013366	-2.64
A03	ATM	Hs.367437	NM_000051	1.07
A04	ATR	Hs.271791	NM_001184	1.55
A05	AURKA	Hs.250822	NM_003600	4.44
A06	AURKB	Hs.442658	NM_004217	14.12
A07	BCCIP	Hs.370292	NM_016567	2.06
A08	BCL2	Hs.150749	NM_000633	1.95
A09	BIRC5	Hs.728893	NM_001168	3.61
A10	BRCA1	Hs.194143	NM_007294	3.84
A11	BRCA2	Hs.34012	NM_000059	4
A12	CASP3	Hs.141125	NM_004346	-3.73
B01	CCNA2	Hs.58974	NM_001237	3.01
B02	CCNB1	Hs.23960	NM_031966	7.62
B03	CCNB2	Hs.194698	NM_004701	14.62
B04	CCNC	Hs.430646	NM_005190	1.21
B05	CCND1	Hs.523852	NM_053056	-10.7

B06	CCND2	Hs.376071	NM_001759	-3541.14
B07	CCND3	Hs.534307	NM_001760	2.38
B08	CCNE1	Hs.244723	NM_001238	3.68
B09	CCNF	Hs.1973	NM_001761	4.08
B10	CCNG1	Hs.79101	NM_004060	-11.63
B11	CCNG2	Hs.13291	NM_004354	-3.23
B12	CCNH	Hs.292524	NM_001239	-1.13
C01	CCNT1	Hs.279906	NM_001240	-1.88
C02	CDC16	Hs.374127	NM_003903	-4.41
C03	CDC20	Hs.524947	NM_001255	2.95
C04	CDC25A	Hs.437705	NM_001789	1.31
C05	CDC25C	Hs.656	NM_001790	3.97
C06	CDC34	Hs.514997	NM_004359	-1.22
C07	CDC6	Hs.405958	NM_001254	5.03
C08	CDK1	Hs.334562	NM_001786	3.76
C09	CDK2	Hs.19192	NM_001798	-1.57
C10	CDK4	Hs.95577	NM_000075	-1.39
C11	CDK5R1	Hs.500015	NM_003885	1.93
C12	CDK5RAP1	Hs.435952	NM_016408	-1.53
D01	CDK6	Hs.119882	NM_001259	-2.16
D02	CDK7	Hs.184298	NM_001799	-1.65
D03	CDK8	Hs.382306	NM_001260	-1.16
D04	CDKN1A	Hs.370771	NM_000389	-16.11
D05	CDKN1B	Hs.238990	NM_004064	1.4
D06	CDKN2A	Hs.512599	NM_000077	-891.44
D07	CDKN2B	Hs.72901	NM_004936	-64.45
D08	CDKN3	Hs.84113	NM_005192	7.46
D09	CHEK1	Hs.24529	NM_001274	1.85
D10	CHEK2	Hs.291363	NM_007194	4.23
D11	CKS1B	Hs.374378	NM_001826	1.73

D12	CKS2	Hs.83758	NM_001827	1.64
E01	CUL1	Hs.146806	NM_003592	-1.12
E02	CUL2	Hs.82919	NM_003591	-3.23
E03	CUL3	Hs.372286	NM_003590	1.66
E04	E2F1	Hs.654393	NM_005225	2.81
E05	E2F4	Hs.108371	NM_001950	1.61
E06	GADD45A	Hs.80409	NM_001924	-10.7
E07	GTSE1	Hs.386189	NM_016426	3.58
E08	HUS1	Hs.152983	NM_004507	-8.11
E09	KNTC1	Hs.300559	NM_014708	4.96
E10	KPNA2	Hs.594238	NM_002266	1.21
E11	MAD2L1	Hs.591697	NM_002358	1.84
E12	MAD2L2	Hs.19400	NM_006341	2.83
F01	MCM2	Hs.477481	NM_004526	1.97
F02	MCM3	Hs.179565	NM_002388	3.07
F03	MCM4	Hs.460184	NM_005914	4.29
F04	MCM5	Hs.517582	NM_006739	3.51
F05	MDM2	Hs.484551	NM_002392	-1.25
F06	MKI67	Hs.689823	NM_002417	3.39
F07	MNAT1	Hs.509523	NM_002431	1.35
F08	MRE11A	Hs.192649	NM_005590	1.78
F09	NBN	Hs.492208	NM_002485	1.09
F10	RAD1	Hs.531879	NM_002853	-4.79
F11	RAD17	Hs.16184	NM_002873	-2.71
F12	RAD51	Hs.631709	NM_002875	1.01
G01	RAD9A	Hs.655354	NM_004584	4.89
G02	RB1	Hs.408528	NM_000321	-2.1
G03	RBBP8	Hs.546282	NM_002894	-1.13
G04	RBL1	Hs.207745	NM_002895	3.46
G05	RBL2	Hs.513609	NM_005611	-1.06

G06	SERTAD1	Hs.269898	NM_013376	-4.5
G07	SKP2	Hs.23348	NM_005983	-3.48
G08	STMN1	Hs.209983	NM_005563	-1.06
G09	TFDP1	Hs.79353	NM_007111	-1.13
G10	TFDP2	Hs.379018	NM_006286	1.16
G11	TP53	Hs.654481	NM_000546	4.32
G12	WEE1	Hs.249441	NM_003390	1.11

Table C5.2: Gene expression fold changes in MRC-5 cells treated with EFV

Position	Gene Symbol	UniGene	GenBank	Fold Change
A01	ABL1	Hs.431048	NM_005157	1.39
A02	ANAPC2	Hs.533262	NM_013366	1.01
A03	ATM	Hs.367437	NM_000051	2.68
A04	ATR	Hs.271791	NM_001184	2.57
A05	AURKA	Hs.250822	NM_003600	1.57
A06	AURKB	Hs.442658	NM_004217	-1.02
A07	BCCIP	Hs.370292	NM_016567	2.36
A08	BCL2	Hs.150749	NM_000633	1.84
A09	BIRC5	Hs.728893	NM_001168	1.72
A10	BRCA1	Hs.194143	NM_007294	2.4
A11	BRCA2	Hs.34012	NM_000059	1.09
A12	CASP3	Hs.141125	NM_004346	-1.45
B01	CCNA2	Hs.58974	NM_001237	1.02
B02	CCNB1	Hs.23960	NM_031966	2.73
B03	CCNB2	Hs.194698	NM_004701	1.01
B04	CCNC	Hs.430646	NM_005190	1.09
B05	CCND1	Hs.523852	NM_053056	-1.09
B06	CCND2	Hs.376071	NM_001759	3.97
B07	CCND3	Hs.534307	NM_001760	1.37
B08	CCNE1	Hs.244723	NM_001238	1.35

B09	CCNF	Hs.1973	NM_001761	1.01
B10	CCNG1	Hs.79101	NM_004060	-1.12
B11	CCNG2	Hs.13291	NM_004354	8.76
B12	CCNH	Hs.292524	NM_001239	7.95
C01	CCNT1	Hs.279906	NM_001240	-1.93
C02	CDC16	Hs.374127	NM_003903	1.59
C03	CDC20	Hs.524947	NM_001255	1.46
C04	CDC25A	Hs.437705	NM_001789	1.41
C05	CDC25C	Hs.656	NM_001790	1.22
C06	CDC34	Hs.514997	NM_004359	1.53
C07	CDC6	Hs.405958	NM_001254	1.4
C08	CDK1	Hs.334562	NM_001786	-1.32
C09	CDK2	Hs.19192	NM_001798	-1.47
C10	CDK4	Hs.95577	NM_000075	1.09
C11	CDK5R1	Hs.500015	NM_003885	1.03
C12	CDK5RAP1	Hs.435952	NM_016408	1.53
D01	CDK6	Hs.119882	NM_001259	2.13
D02	CDK7	Hs.184298	NM_001799	3.16
D03	CDK8	Hs.382306	NM_001260	1.77
D04	CDKN1A	Hs.370771	NM_000389	1.89
D05	CDKN1B	Hs.238990	NM_004064	1.19
D06	CDKN2A	Hs.512599	NM_000077	1.18
D07	CDKN2B	Hs.72901	NM_004936	4.2
D08	CDKN3	Hs.84113	NM_005192	-1.19
D09	CHEK1	Hs.24529	NM_001274	2.28
D10	CHEK2	Hs.291363	NM_007194	1.05
D11	CKS1B	Hs.374378	NM_001826	-1.11
D12	CKS2	Hs.83758	NM_001827	-1.07
E01	CUL1	Hs.146806	NM_003592	1.42
E02	CUL2	Hs.82919	NM_003591	1.36

E03	CUL3	Hs.372286	NM_003590	1.36
E04	E2F1	Hs.654393	NM_005225	1.77
E05	E2F4	Hs.108371	NM_001950	1.34
E06	GADD45A	Hs.80409	NM_001924	1.3
E07	GTSE1	Hs.386189	NM_016426	1.28
E08	HUS1	Hs.152983	NM_004507	2.13
E09	KNTC1	Hs.300559	NM_014708	1.23
E10	KPNA2	Hs.594238	NM_002266	1.19
E11	MAD2L1	Hs.591697	NM_002358	-1.13
E12	MAD2L2	Hs.19400	NM_006341	-1.84
F01	MCM2	Hs.477481	NM_004526	-1.03
F02	MCM3	Hs.179565	NM_002388	2.51
F03	MCM4	Hs.460184	NM_005914	1.83
F04	MCM5	Hs.517582	NM_006739	1.35
F05	MDM2	Hs.484551	NM_002392	3.92
F06	MKI67	Hs.689823	NM_002417	1.16
F07	MNAT1	Hs.509523	NM_002431	1.51
F08	MRE11A	Hs.192649	NM_005590	1.02
F09	NBN	Hs.492208	NM_002485	1.36
F10	RAD1	Hs.531879	NM_002853	-1.2
F11	RAD17	Hs.16184	NM_002873	1.29
F12	RAD51	Hs.631709	NM_002875	2.11
G01	RAD9A	Hs.655354	NM_004584	1.74
G02	RB1	Hs.408528	NM_000321	1.39
G03	RBBP8	Hs.546282	NM_002894	-1.19
G04	RBL1	Hs.207745	NM_002895	2.85
G05	RBL2	Hs.513609	NM_005611	1.42
G06	SERTAD1	Hs.269898	NM_013376	1.88
G07	SKP2	Hs.23348	NM_005983	1.67
G08	STMN1	Hs.209983	NM_005563	-1.12

G09	TFDP1	Hs.79353	NM_007111	1.34
G10	TFDP2	Hs.379018	NM_006286	1.27
G11	TP53	Hs.654481	NM_000546	1.27
G12	WEE1	Hs.249441	NM_003390	1.26

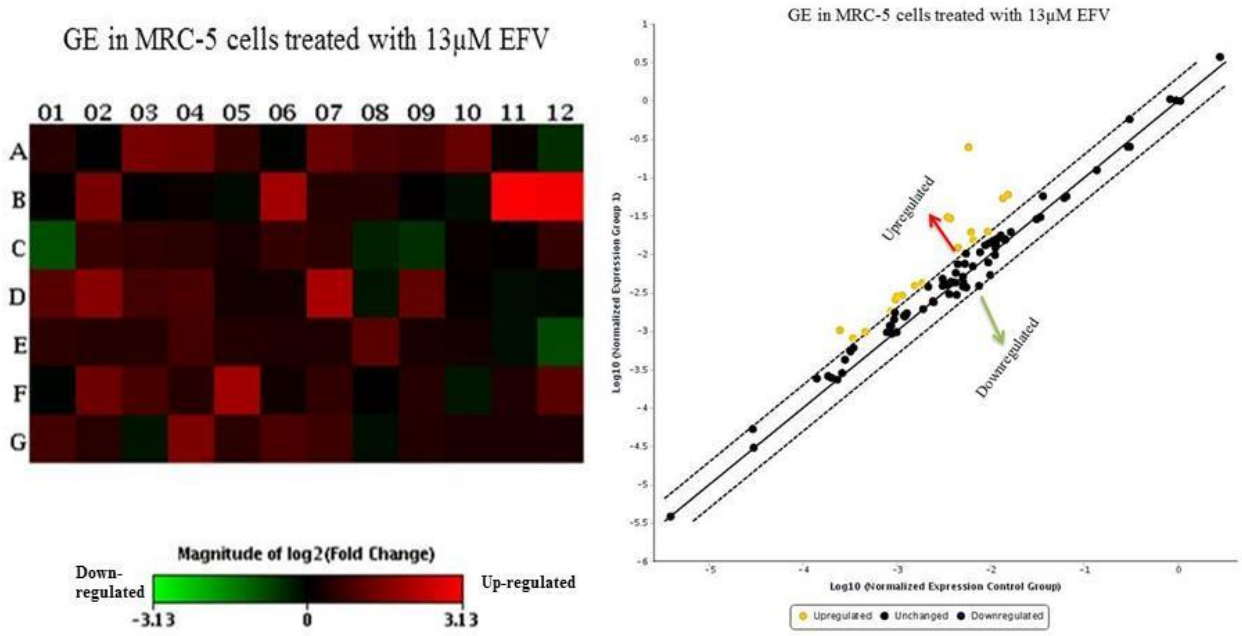

Figure C5.2: The heat map (left) indicating GE in 13µM EFV treated MRC-5 cells. The heat map represents fold changes Fold changes in gene expression are represented between EFV treated *vs* untreated MRC-5 cells. The value of ±3.13 indicates the minimum and maximum change in gene expression across the array. The abundance of the red blocks denotes the up-regulation.

Scatter plot (right) representing gene expression (GE) in 13µM EFV treated MRC-5 cells relative to the untreated control. The scatter plot illustrates the normalized expression of every gene on the array between the treated and untreated groups. The black data points clustered in the region of the solid line show the genes with relatively unchanged expression levels. The up-regulated genes are shown in yellow in the upper left quadrant. No significantly down-regulated genes are depicted in this scatter plot.

Table C5.3: Gene expression fold changes in A549 cells treated with EFV

Position	Gene Symbol	UniGene	GenBank	Fold Change
A01	ABL1	Hs.431048	NM_005157	-1.1
A02	ANAPC2	Hs.533262	NM_013366	-1.28
A03	ATM	Hs.367437	NM_000051	-1.13
A04	ATR	Hs.271791	NM_001184	-3.07
A05	AURKA	Hs.250822	NM_003600	1.02
A06	AURKB	Hs.442658	NM_004217	-4.28
A07	BCCIP	Hs.370292	NM_016567	1.28
A08	BCL2	Hs.150749	NM_000633	1.29
A09	BIRC5	Hs.728893	NM_001168	-1.35
A10	BRCA1	Hs.194143	NM_007294	2.33
A11	BRCA2	Hs.34012	NM_000059	-1.12
A12	CASP3	Hs.141125	NM_004346	2.74
B01	CCNA2	Hs.58974	NM_001237	-1.05
B02	CCNB1	Hs.23960	NM_031966	-1.27
B03	CCNB2	Hs.194698	NM_004701	-2.71
B04	CCNC	Hs.430646	NM_005190	-1.15
B05	CCND1	Hs.523852	NM_053056	1.45
B06	CCND2	Hs.376071	NM_001759	1.04
B07	CCND3	Hs.534307	NM_001760	-1.21
B08	CCNE1	Hs.244723	NM_001238	1.11
B09	CCNF	Hs.1973	NM_001761	-1.15
B10	CCNG1	Hs.79101	NM_004060	2.57
B11	CCNG2	Hs.13291	NM_004354	3.32
B12	CCNH	Hs.292524	NM_001239	1.07
C01	CCNT1	Hs.279906	NM_001240	-1.05
C02	CDC16	Hs.374127	NM_003903	1.76
C03	CDC20	Hs.524947	NM_001255	2.13
C04	CDC25A	Hs.437705	NM_001789	1.03

C05	CDC25C	Hs.656	NM_001790	1.12
C06	CDC34	Hs.514997	NM_004359	1.25
C07	CDC6	Hs.405958	NM_001254	-1.32
C08	CDK1	Hs.334562	NM_001786	-1.43
C09	CDK2	Hs.19192	NM_001798	-1.03
C10	CDK4	Hs.95577	NM_000075	2.43
C11	CDK5R1	Hs.500015	NM_003885	-1.08
C12	CDK5RAP1	Hs.435952	NM_016408	3.14
D01	CDK6	Hs.119882	NM_001259	-1.12
D02	CDK7	Hs.184298	NM_001799	1.32
D03	CDK8	Hs.382306	NM_001260	1.86
D04	CDKN1A	Hs.370771	NM_000389	1.66
D05	CDKN1B	Hs.238990	NM_004064	2.57
D06	CDKN2A	Hs.512599	NM_000077	1.04
D07	CDKN2B	Hs.72901	NM_004936	1.04
D08	CDKN3	Hs.84113	NM_005192	1.35
D09	CHEK1	Hs.24529	NM_001274	1.17
D10	CHEK2	Hs.291363	NM_007194	-2
D11	CKS1B	Hs.374378	NM_001826	1.18
D12	CKS2	Hs.83758	NM_001827	-1.05
E01	CUL1	Hs.146806	NM_003592	-1.15
E02	CUL2	Hs.82919	NM_003591	2.32
E03	CUL3	Hs.372286	NM_003590	1.03
E04	E2F1	Hs.654393	NM_005225	-1.12
E05	E2F4	Hs.108371	NM_001950	-1.93
E06	GADD45A	Hs.80409	NM_001924	1.78
E07	GTSE1	Hs.386189	NM_016426	-1.23
E08	HUS1	Hs.152983	NM_004507	2.21
E09	KNTC1	Hs.300559	NM_014708	-1.33
E10	KPNA2	Hs.594238	NM_002266	-1.25

E11	MAD2L1	Hs.591697	NM_002358	-1.31
E12	MAD2L2	Hs.19400	NM_006341	-5.85
F01	MCM2	Hs.477481	NM_004526	-1.33
F02	MCM3	Hs.179565	NM_002388	-1.25
F03	MCM4	Hs.460184	NM_005914	-3.65
F04	MCM5	Hs.517582	NM_006739	-1.2
F05	MDM2	Hs.484551	NM_002392	1.26
F06	MKI67	Hs.689823	NM_002417	1.11
F07	MNAT1	Hs.509523	NM_002431	1.18
F08	MRE11A	Hs.192649	NM_005590	1.04
F09	NBN	Hs.492208	NM_002485	3.42
F10	RAD1	Hs.531879	NM_002853	2.29
F11	RAD17	Hs.16184	NM_002873	3.3
F12	RAD51	Hs.631709	NM_002875	1.15
G01	RAD9A	Hs.655354	NM_004584	1.41
G02	RB1	Hs.408528	NM_000321	-1.05
G03	RBBP8	Hs.546282	NM_002894	1.13
G04	RBL1	Hs.207745	NM_002895	-3.52
G05	RBL2	Hs.513609	NM_005611	1.3
G06	SERTAD1	Hs.269898	NM_013376	2.76
G07	SKP2	Hs.23348	NM_005983	2.21
G08	STMN1	Hs.209983	NM_005563	-1.08
G09	TFDP1	Hs.79353	NM_007111	1.03
G10	TFDP2	Hs.379018	NM_006286	-1.36
G11	TP53	Hs.654481	NM_000546	1.02
G12	WEE1	Hs.249441	NM_003390	1.12

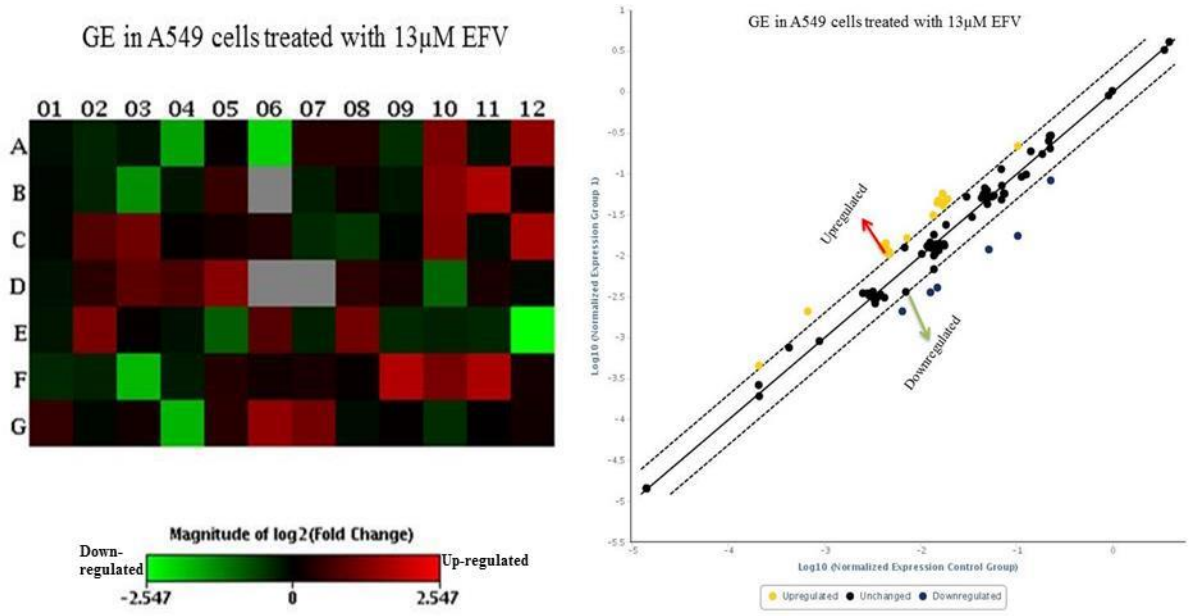

Figure C5.3: The heat map (left) denoting changes in GE in 13µM EFV treated A549 cells relative to untreated. A549 cells. The ±2.547 up/down-regulation indicates the lowest and highest fold changes. The green, red and grey range indicators represent under-expressed, over-expressed and non-detected genes, respectively

The scatter plot (right) representing GE in 13µM EFV treated A549 cells. Unchanged gene expression remains across the solid line in the middle, while the up-regulated and the down-regulated genes fall above (up) and below (down) the dotted lines. Fewer genes are shown to be down-regulated in this scatter plot.

Table C5.4: Gene expression fold changes in MRC-5 cells treated with LPV/r

Position	Gene Symbol	UniGene	GenBank	Fold Change
A01	ABL1	Hs.431048	NM_005157	-2.53
A02	ANAPC2	Hs.533262	NM_013366	-10.78
A03	ATM	Hs.367437	NM_000051	1.06
A04	ATR	Hs.271791	NM_001184	-1.1

A05	AURKA	Hs.250822	NM_003600	-12.82
A06	AURKB	Hs.442658	NM_004217	-11.96
A07	BCCIP	Hs.370292	NM_016567	-1.49
A08	BCL2	Hs.150749	NM_000633	1.79
A09	BIRC5	Hs.728893	NM_001168	-20.68
A10	BRCA1	Hs.194143	NM_007294	-3.03
A11	BRCA2	Hs.34012	NM_000059	-1.21
A12	CASP3	Hs.141125	NM_004346	-4.29
B01	CCNA2	Hs.58974	NM_001237	-17.15
B02	CCNB1	Hs.23960	NM_031966	-21.41
B03	CCNB2	Hs.194698	NM_004701	-17.75
B04	CCNC	Hs.430646	NM_005190	1.1
B05	CCND1	Hs.523852	NM_053056	-8.82
B06	CCND2	Hs.376071	NM_001759	-2.77
B07	CCND3	Hs.534307	NM_001760	-8.22
B08	CCNE1	Hs.244723	NM_001238	-2.83
B09	CCNF	Hs.1973	NM_001761	-14.52
B10	CCNG1	Hs.79101	NM_004060	-3.61
B11	CCNG2	Hs.13291	NM_004354	-2.04
B12	CCNH	Hs.292524	NM_001239	1.11
C01	CCNT1	Hs.279906	NM_001240	-1.91
C02	CDC16	Hs.374127	NM_003903	-2.19
C03	CDC20	Hs.524947	NM_001255	-95.67
C04	CDC25A	Hs.437705	NM_001789	-3.73
C05	CDC25C	Hs.656	NM_001790	-14.32
C06	CDC34	Hs.514997	NM_004359	-2.22
C07	CDC6	Hs.405958	NM_001254	1.51
C08	CDK1	Hs.334562	NM_001786	-27.1
C09	CDK2	Hs.19192	NM_001798	-24.25
C10	CDK4	Hs.95577	NM_000075	-1.52

C11	CDK5R1	Hs.500015	NM_003885	1.09
C12	CDK5RAP1	Hs.435952	NM_016408	-4.41
D01	CDK6	Hs.119882	NM_001259	-3.23
D02	CDK7	Hs.184298	NM_001799	-1.99
D03	CDK8	Hs.382306	NM_001260	-2.08
D04	CDKN1A	Hs.370771	NM_000389	-1.11
D05	CDKN1B	Hs.238990	NM_004064	-2.71
D06	CDKN2A	Hs.512599	NM_000077	-2.66
D07	CDKN2B	Hs.72901	NM_004936	5.17
D08	CDKN3	Hs.84113	NM_005192	-10.13
D09	CHEK1	Hs.24529	NM_001274	-3.68
D10	CHEK2	Hs.291363	NM_007194	-3.46
D11	CKS1B	Hs.374378	NM_001826	-5.66
D12	CKS2	Hs.83758	NM_001827	-5.58
E01	CUL1	Hs.146806	NM_003592	1.09
E02	CUL2	Hs.82919	NM_003591	-1.58
E03	CUL3	Hs.372286	NM_003590	1.01
E04	E2F1	Hs.654393	NM_005225	-4.17
E05	E2F4	Hs.108371	NM_001950	-3.18
E06	GADD45A	Hs.80409	NM_001924	-1.02
E07	GTSE1	Hs.386189	NM_016426	34.3
E08	HUS1	Hs.152983	NM_004507	-2.23
E09	KNTC1	Hs.300559	NM_014708	-3.73
E10	KPNA2	Hs.594238	NM_002266	-12.73
E11	MAD2L1	Hs.591697	NM_002358	-9.71
E12	MAD2L2	Hs.19400	NM_006341	-9.71
F01	MCM2	Hs.477481	NM_004526	-40.79
F02	MCM3	Hs.179565	NM_002388	-14.32
F03	MCM4	Hs.460184	NM_005914	-9.06
F04	MCM5	Hs.517582	NM_006739	-12.3

F05	MDM2	Hs.484551	NM_002392	1.26
F06	MKI67	Hs.689823	NM_002417	-27.28
F07	MNAT1	Hs.509523	NM_002431	-2.28
F08	MRE11A	Hs.192649	NM_005590	-3.84
F09	NBN	Hs.492208	NM_002485	-1.09
F10	RAD1	Hs.531879	NM_002853	-2.33
F11	RAD17	Hs.16184	NM_002873	-1.21
F12	RAD51	Hs.631709	NM_002875	-11.08
G01	RAD9A	Hs.655354	NM_004584	-2.22
G02	RB1	Hs.408528	NM_000321	-1.96
G03	RBBP8	Hs.546282	NM_002894	1.12
G04	RBL1	Hs.207745	NM_002895	-3.48
G05	RBL2	Hs.513609	NM_005611	-1.08
G06	SERTAD1	Hs.269898	NM_013376	-10.78
G07	SKP2	Hs.23348	NM_005983	-9.38
G08	STMN1	Hs.209983	NM_005563	-18
G09	TFDP1	Hs.79353	NM_007111	-5.94
G10	TFDP2	Hs.379018	NM_006286	-2.75
G11	TP53	Hs.654481	NM_000546	1.26
G12	WEE1	Hs.249441	NM_003390	-3.36

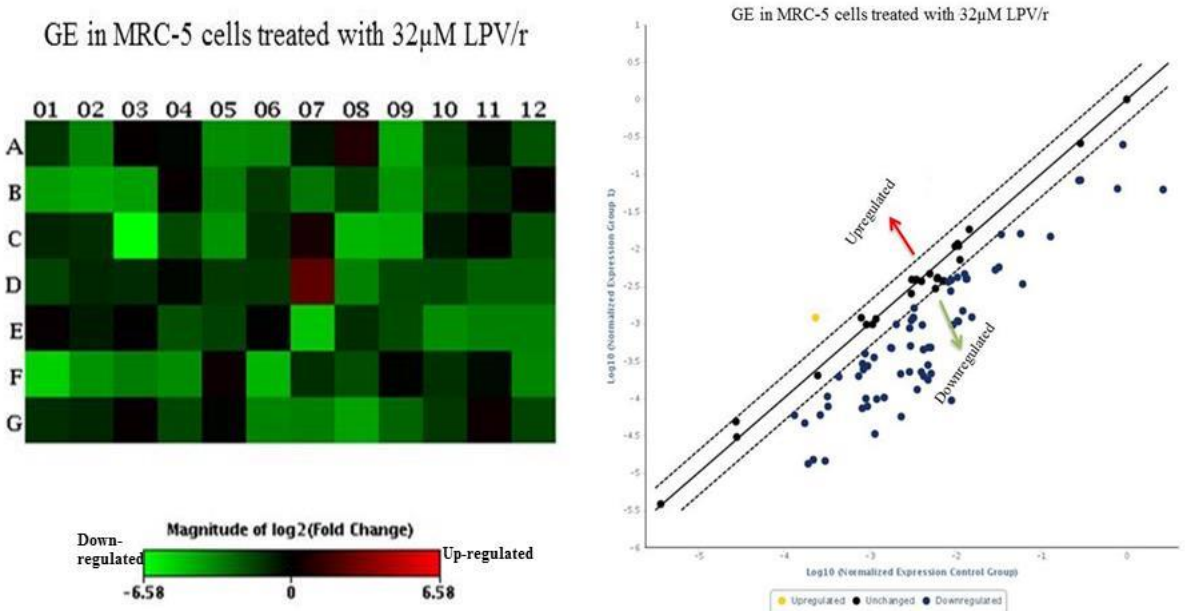

<u>Figure C5.4</u>: The heat map (left) illustrating GE in 32µM LPV/r treated MRC-5 cells relative to untreated MRC5 cells. The log2 value of ±6.58 represents the minimum and the maximum fold changes. The abundance of green blocks indicates the under-expression of most of the genes in response to LPV/r, across the array.

The scatter plot (right) demonstrating GE in 32µM LPV/r treated MRC-5 cells, compared to untreated MRC-5 cells. As reflected in the heat map above, most genes are down-regulated, with data points occurring below the dotted line on the lower right. Genes with unaltered expression are plotted on the solid line in the middle. The dotted lines (upper and lower) represent the ±2 cut-off for the significantly up/down-regulated genes

<u>Table C5.5</u>: Gene expression fold changes in A549 cells treated with LPV/r

Position	Gene Symbol	UniGene	GenBank	Fold Change
A01	ABL1	Hs.431048	NM_005157	-1
A02	ANAPC2	Hs.533262	NM_013366	1
A03	ATM	Hs.367437	NM_000051	4.1
A04	ATR	Hs.271791	NM_001184	1.9
A05	AURKA	Hs.250822	NM_003600	-3.74
A06	AURKB	Hs.442658	NM_004217	-13.3

A07	BCCIP	Hs.370292	NM_016567	2.63
A08	BCL2	Hs.150749	NM_000633	10.38
A09	BIRC5	Hs.728893	NM_001168	-6.34
A10	BRCA1	Hs.194143	NM_007294	-1.54
A11	BRCA2	Hs.34012	NM_000059	-4.18
A12	CASP3	Hs.141125	NM_004346	2.34
B01	CCNA2	Hs.58974	NM_001237	-23
B02	CCNB1	Hs.23960	NM_031966	-45.69
B03	CCNB2	Hs.194698	NM_004701	-44.13
B04	CCNC	Hs.430646	NM_005190	1.12
B05	CCND1	Hs.523852	NM_053056	1.17
B06	CCND2	Hs.376071	NM_001759	2.18
B07	CCND3	Hs.534307	NM_001760	-8.02
B08	CCNE1	Hs.244723	NM_001238	-3
B09	CCNF	Hs.1973	NM_001761	-6.61
B10	CCNG1	Hs.79101	NM_004060	2.42
B11	CCNG2	Hs.13291	NM_004354	3.55
B12	CCNH	Hs.292524	NM_001239	4.71
C01	CCNT1	Hs.279906	NM_001240	2.52
C02	CDC16	Hs.374127	NM_003903	1.98
C03	CDC20	Hs.524947	NM_001255	-13.03
C04	CDC25A	Hs.437705	NM_001789	-3.47
C05	CDC25C	Hs.656	NM_001790	-36.6
C06	CDC34	Hs.514997	NM_004359	1.31
C07	CDC6	Hs.405958	NM_001254	-4.94
C08	CDK1	Hs.334562	NM_001786	-20.31
C09	CDK2	Hs.19192	NM_001798	-3.96
C10	CDK4	Hs.95577	NM_000075	3.17
C11	CDK5R1	Hs.500015	NM_003885	-1.07
C12	CDK5RAP1	Hs.435952	NM_016408	4.52

D01	CDK6	Hs.119882	NM_001259	1.16
D02	CDK7	Hs.184298	NM_001799	1.61
D03	CDK8	Hs.382306	NM_001260	1.62
D04	CDKN1A	Hs.370771	NM_000389	3.15
D05	CDKN1B	Hs.238990	NM_004064	3.13
D06	CDKN2A	Hs.512599	NM_000077	3.24
D07	CDKN2B	Hs.72901	NM_004936	1.11
D08	CDKN3	Hs.84113	NM_005192	-9.34
D09	CHEK1	Hs.24529	NM_001274	-2.61
D10	CHEK2	Hs.291363	NM_007194	-4.61
D11	CKS1B	Hs.374378	NM_001826	-1.5
D12	CKS2	Hs.83758	NM_001827	-3.85
E01	CUL1	Hs.146806	NM_003592	1.7
E02	CUL2	Hs.82919	NM_003591	4.1
E03	CUL3	Hs.372286	NM_003590	3.13
E04	E2F1	Hs.654393	NM_005225	-14.97
E05	E2F4	Hs.108371	NM_001950	1.99
E06	GADD45A	Hs.80409	NM_001924	40.12
E07	GTSE1	Hs.386189	NM_016426	-47.3
E08	HUS1	Hs.152983	NM_004507	23.36
E09	KNTC1	Hs.300559	NM_014708	-4.24
E10	KPNA2	Hs.594238	NM_002266	-1.52
E11	MAD2L1	Hs.591697	NM_002358	-9.34
E12	MAD2L2	Hs.19400	NM_006341	-4.84
F01	MCM2	Hs.477481	NM_004526	-5.22
F02	MCM3	Hs.179565	NM_002388	-4.61
F03	MCM4	Hs.460184	NM_005914	-15.93
F04	MCM5	Hs.517582	NM_006739	-14.66
F05	MDM2	Hs.484551	NM_002392	1.59
F06	MKI67	Hs.689823	NM_002417	-13.12

F07	MNAT1	Hs.509523	NM_002431	-1.78
F08	MRE11A	Hs.192649	NM_005590	-1.25
F09	NBN	Hs.492208	NM_002485	1.81
F10	RAD1	Hs.531879	NM_002853	3.26
F11	RAD17	Hs.16184	NM_002873	5.45
F12	RAD51	Hs.631709	NM_002875	-6.61
G01	RAD9A	Hs.655354	NM_004584	-1.03
G02	RB1	Hs.408528	NM_000321	1.59
G03	RBBP8	Hs.546282	NM_002894	1.87
G04	RBL1	Hs.207745	NM_002895	-2.8
G05	RBL2	Hs.513609	NM_005611	2.88
G06	SERTAD1	Hs.269898	NM_013376	3.4
G07	SKP2	Hs.23348	NM_005983	-1.25
G08	STMN1	Hs.209983	NM_005563	-15.71
G09	TFDP1	Hs.79353	NM_007111	1.1
G10	TFDP2	Hs.379018	NM_006286	-1.09
G11	TP53	Hs.654481	NM_000546	3.4
G12	WEE1	Hs.249441	NM_003390	-1.41

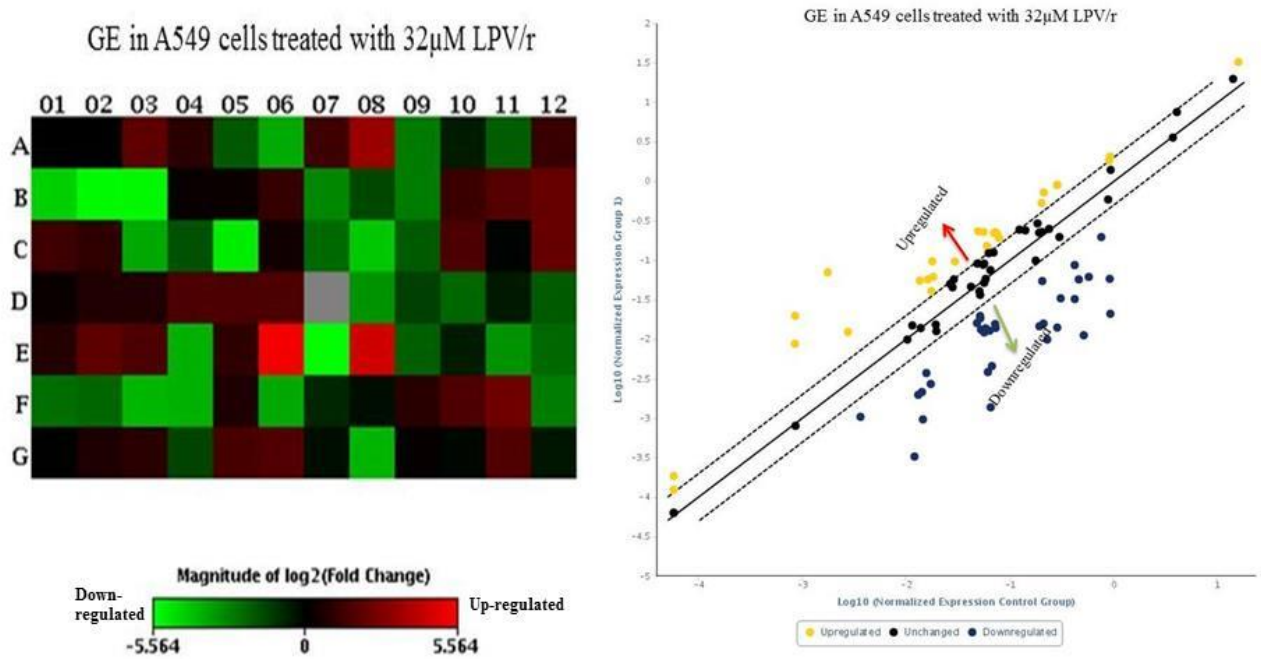

Figure C5.5: The heat map (left) denoting GE in 32µM LPV/r treated A549 cells *vs* untreated A549 cells. Undetectable genes are/is in the grey blocks, while green and red blocks denote down and up-regulated genes, respectively. The log2 value of ±5.564 represents the fold change magnitude.

The scatter plot (right) illustrating GE in 32µM LPV/r treated A549 cells relative to untreated A549 cells. Genes' whose expression remains unchanged are located on the solid middle line, while up and down-regulated genes are positioned above and below the upper and lower dotted lines, which represent the ±2 fold cut-off in expression levels.

C6) RT-qPCR appendices

Table C6.1: The descriptive details of the selected target genes.

Gene symbol	**Description**	**Accession number (GenBank)**
1. MAD2L2	MAD2 mitotic arrest deficient-like 2 (yeast)	NM_006341
2. CASP3	Caspase 3, apoptosis-related	NM_004346

	cysteine peptidase	
3. AURKB	Aurora kinase B	NM_004217
4. GAPDH	Glyceraldehyde-3-phosphate dehydrogenase	NM_002046

In this study, all four genes (three targets and one HKG control) were profiled on 12 cDNA samples, MRC-5: 0.1% methanol at 24h and 48h, 13µM EFV treatment at 24h and 48h, 32µM LPV/r at 24h and 48h. The same was done for A549 cells.

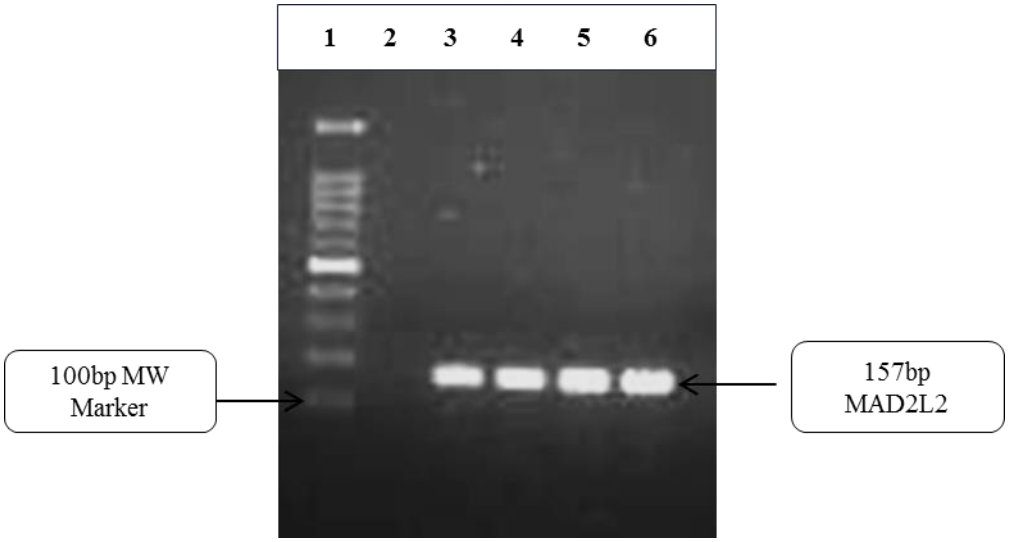

Figure C6.1: **MAD2L2 PCR products**. MAD2L2 inserts represented in lanes 3-6, run parallel to a 100bp molecular weight marker in lane 1.

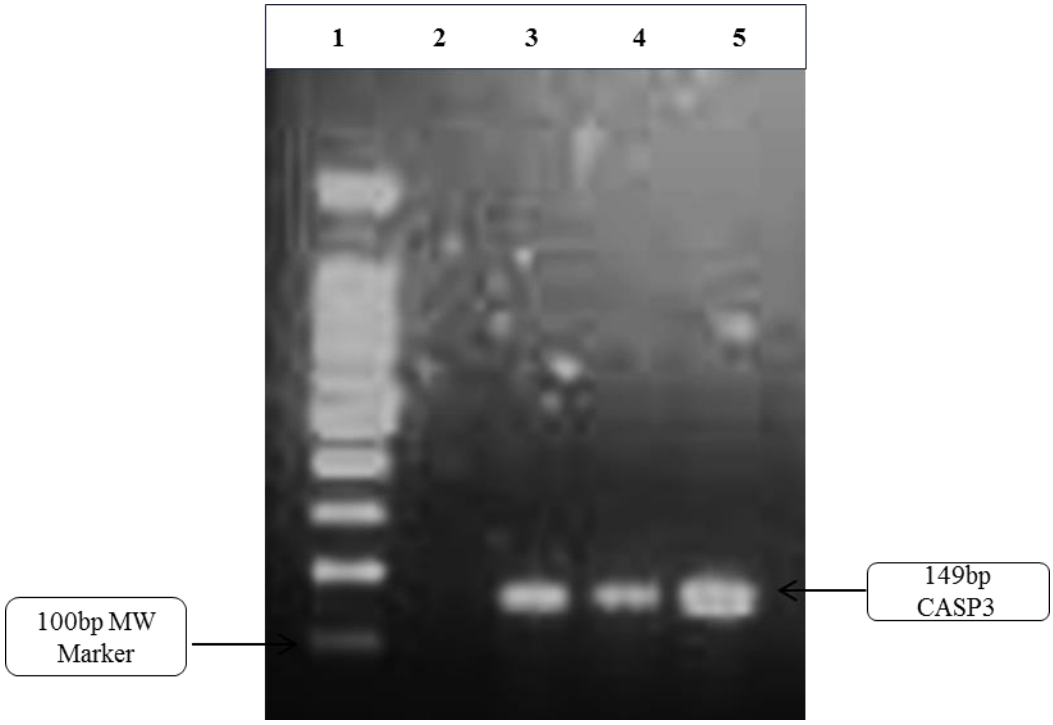

Figure C6.2: **CASP3 PCR products**. CASP3 PCR products illustrated in lanes 3-5, run in parallel to a 100bp molecular weight marker in lane1.

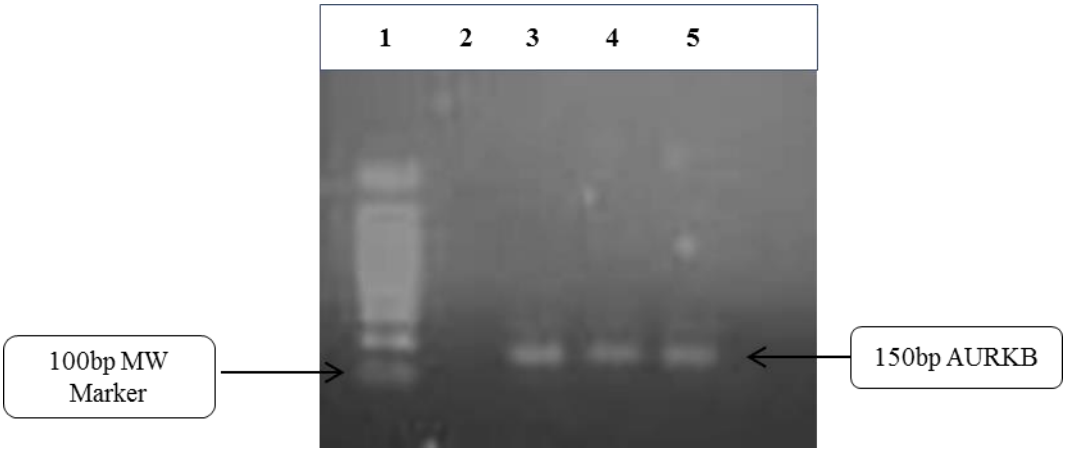

Figure C6.3: **AURKB PCR products**. AURKB amplicons as shown in lanes 3-5, run parallel to a 100bp molecular weight marker in lane1.

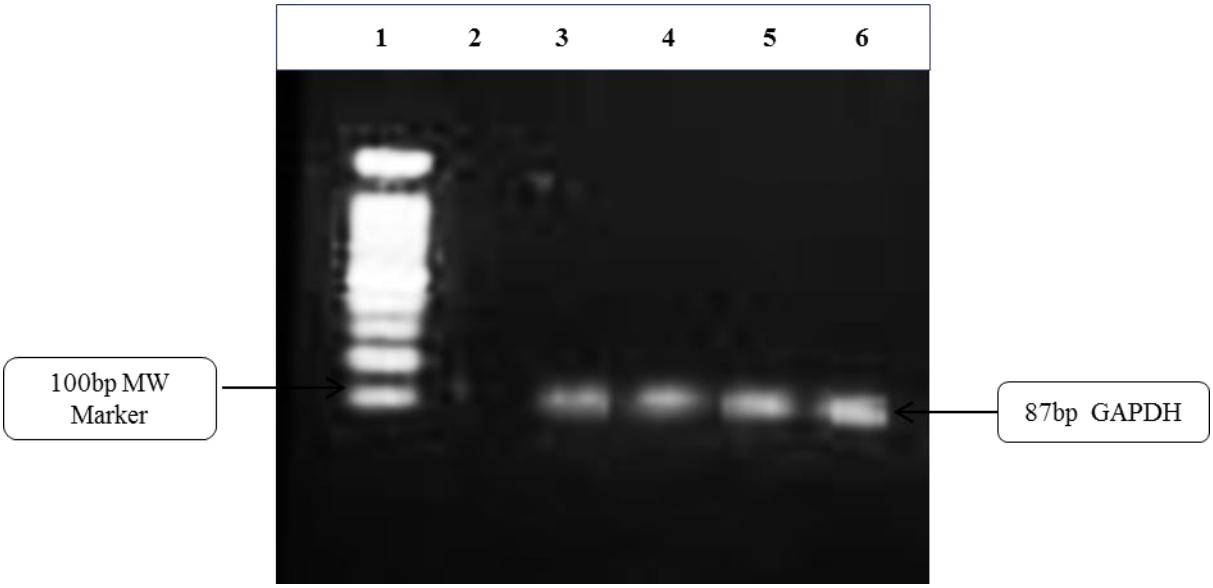

Figure C6.4: **GAPDH PCR products**. GAPDH PCR products as demonstrated in lanes 3-6, run parallel to a 100bp molecular weight marker in lane 1.

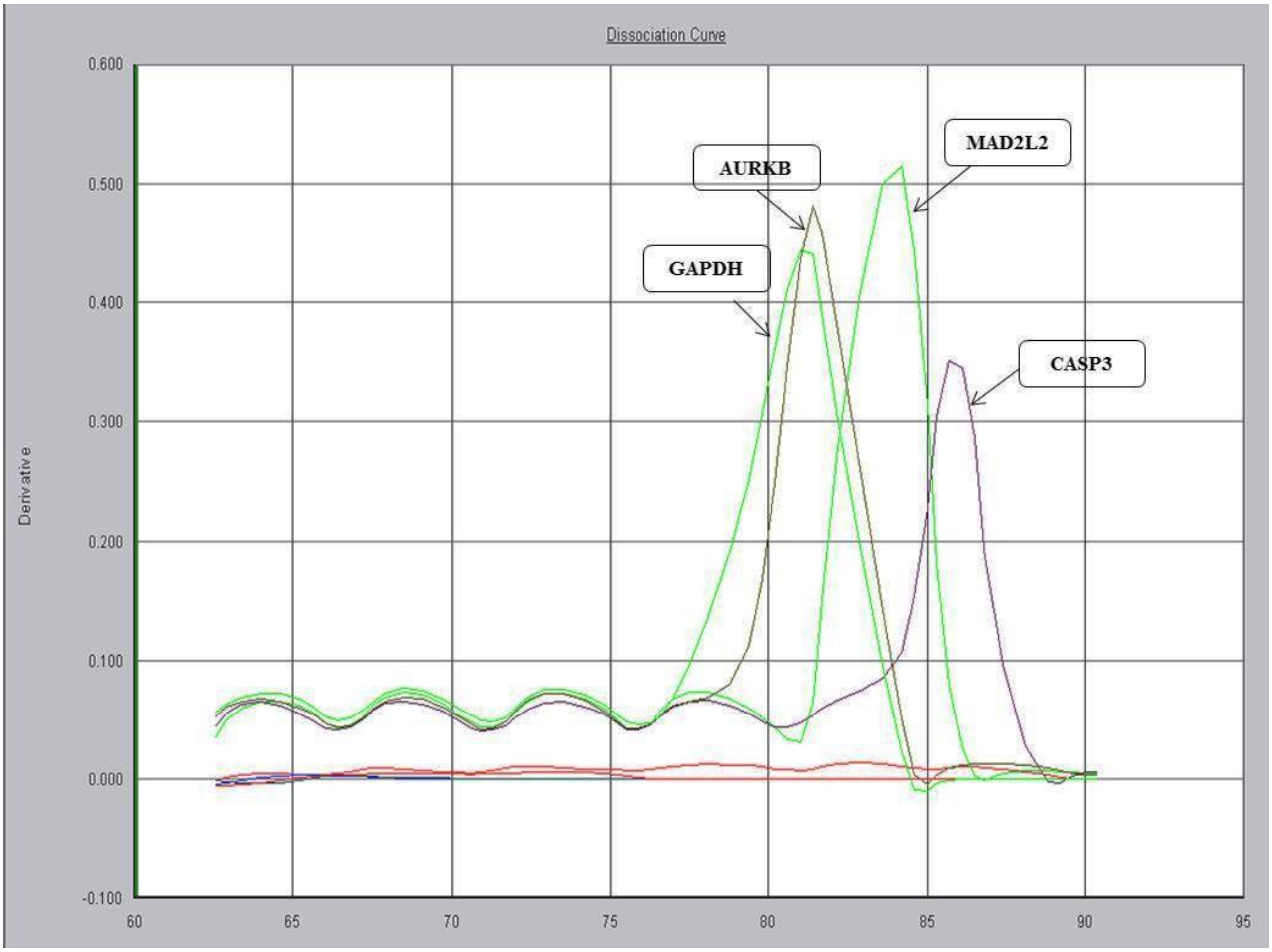

Figure C6.5: **The Melt curves of target genes**. Single peaks show primer specificity, with MAD2L2 (84.2 °C), CASP3 (85.7 °C), AURKB (81.4 °C) and GAPDH (81 °C) melting temperatures. No template controls lack any amplification peaks.

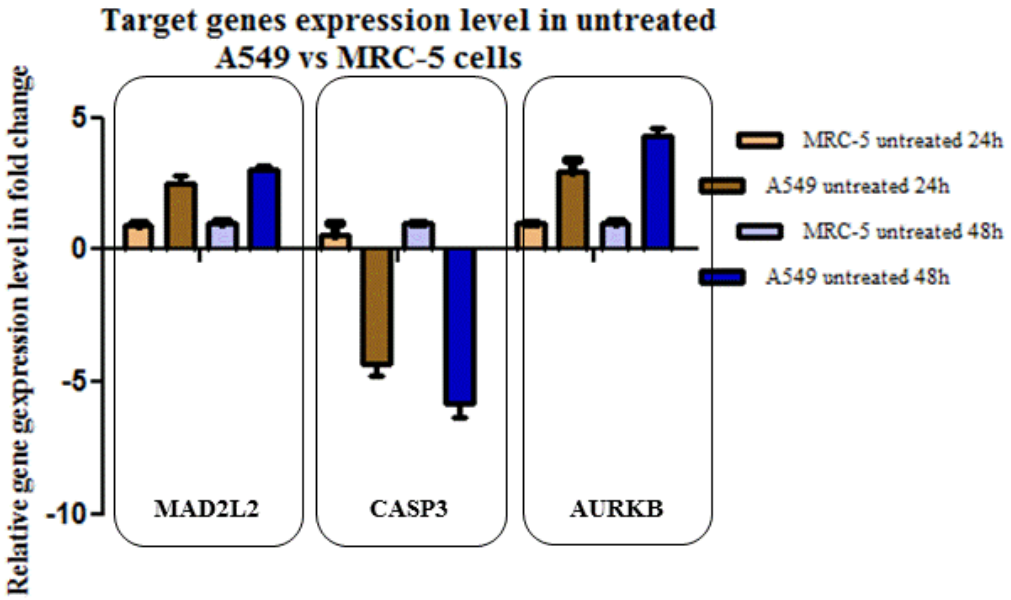

Figure C6.6: Target gene expression level in fold change in untreated A549 *vs* MRC-5 cells. MAD2L2, CASP3 and AURKB gene expression levels were determined in cancer vs normal cells at 24h and 48h

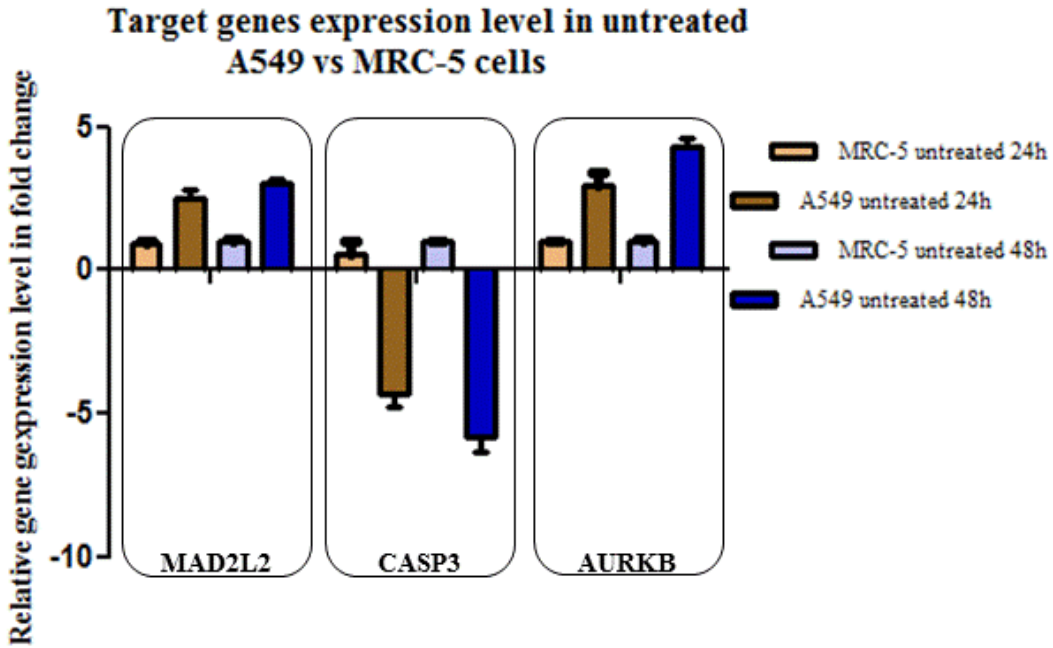

Figure C6.7: Target gene expression level in fold change in untreated A549 *vs* MRC-5 cells. MAD2L2, CASP3 and AURKB gene expression levels were determined in cancer *vs* normal cells at 24h and 48h.

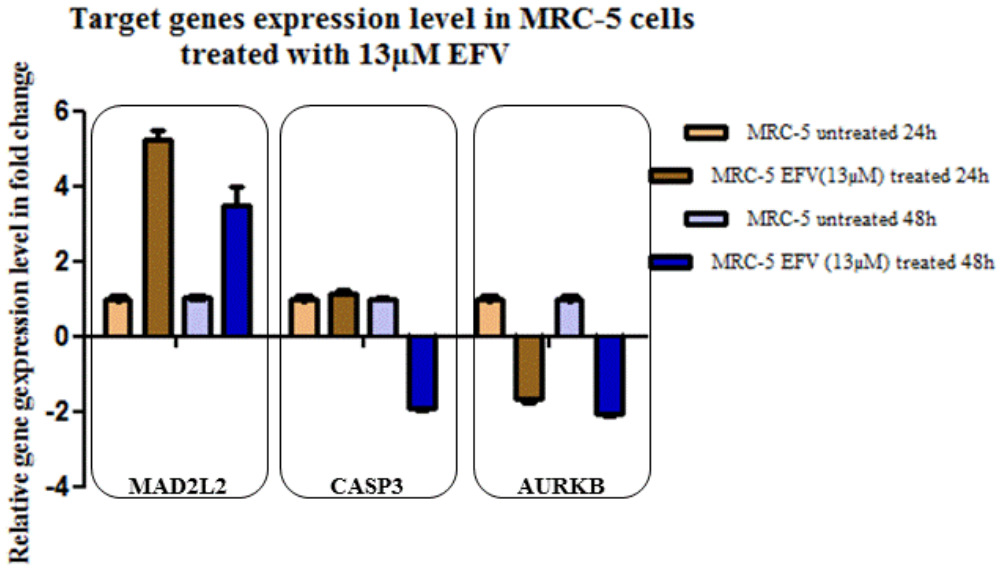

Figure C6.8: Target gene expression level in fold change in EFV treated MRC-5 cells. MAD2L2, CASP3 and AURKB gene expression levels were determined in EFV treated *vs* untreated cells at 24h and 48h.

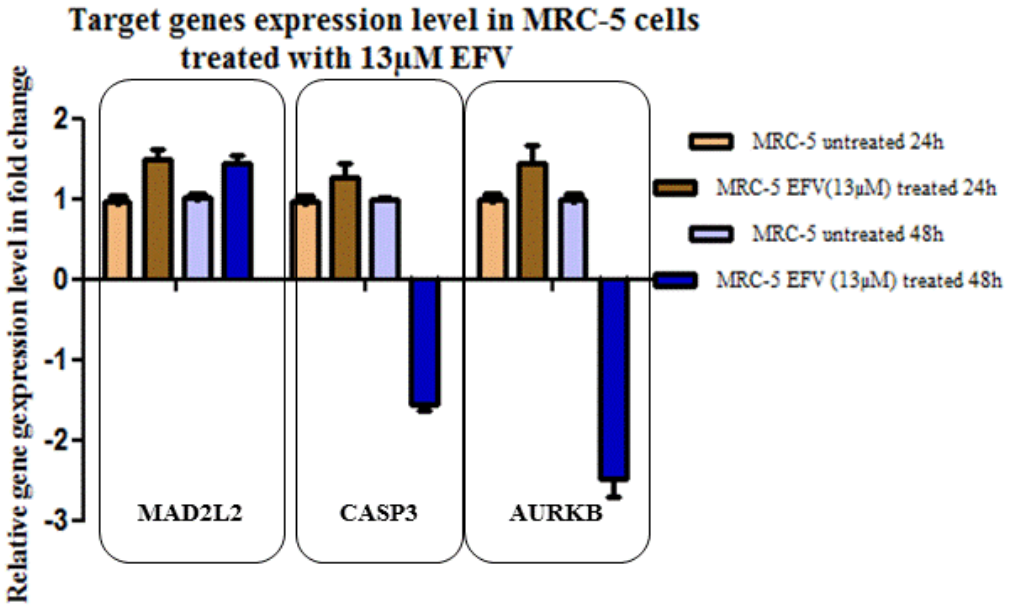

Figure C6.9: Target gene expression level in fold change in EFV treated MRC-5 cells. MAD2L2, CASP3 and AURKB gene expression levels were determined in EFV treated *vs* untreated cells at 24h and 48h.

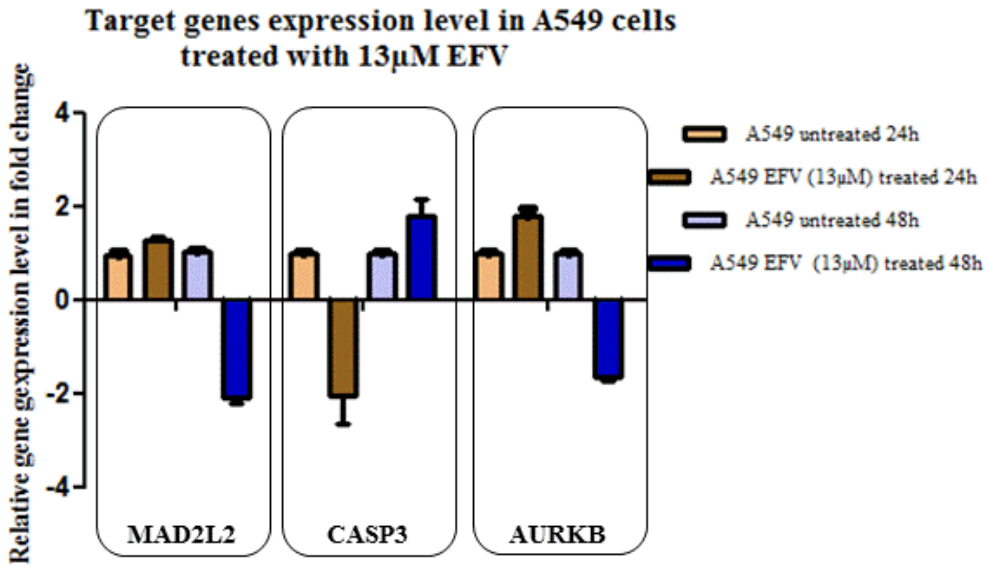

Figure C6.10: Target gene expression level in fold change in EFV treated A549 cells. MAD2L2, CASP3 and AURKB gene expression levels were determined in EFV treated *vs* untreated cells at 24h and 48h.

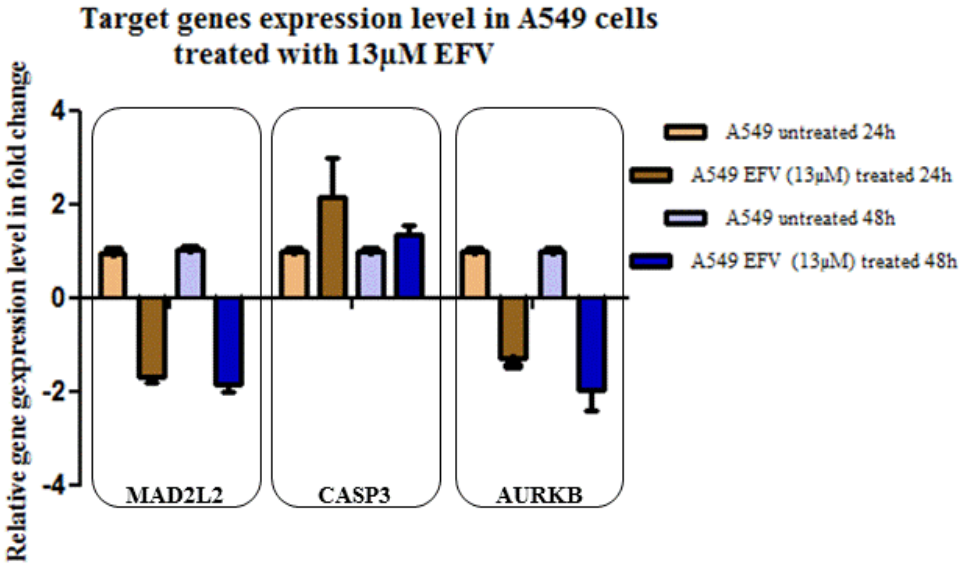

Figure C6.11: Target gene expression level in fold change in EFV treated A549 cells. MAD2L2, CASP3 and AURKB gene expression levels were determined in EFV treated *vs* untreated cells at 24h and 48h.

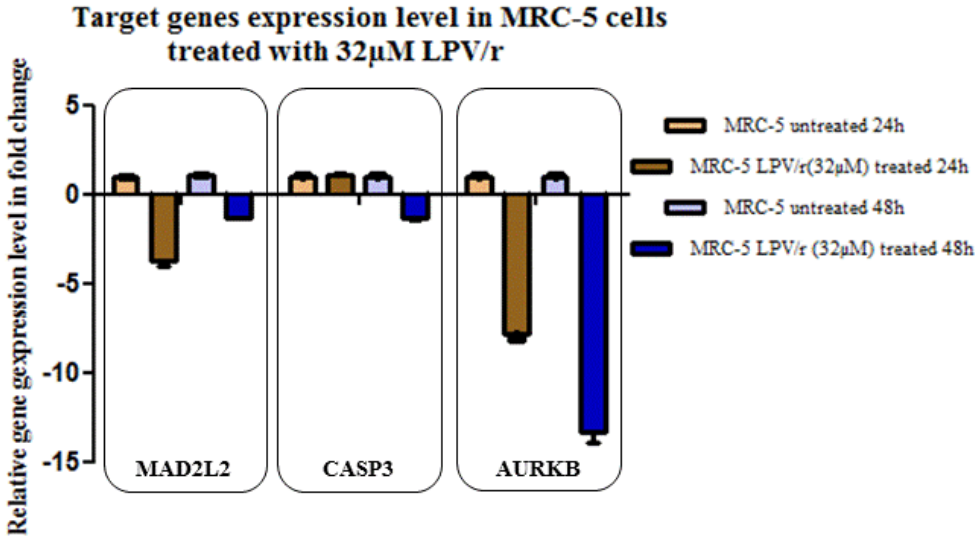

Figure C6.12: Target gene expression level in fold change in LPV/r treated MRC-5 cells. MAD2L2, CASP3 and AURKB gene expression levels were determined in LPV/r treated *vs* untreated cells at 24h and 48h.

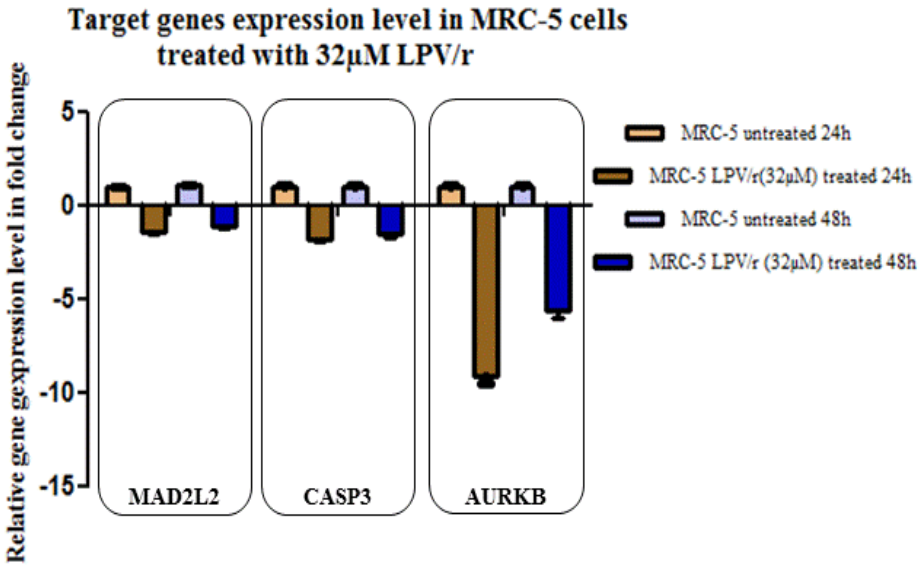

Figure C6.13: Target gene expression level in fold change in LPV/r treated MRC-5 cells. MAD2L2, CASP3 and AURKB gene expression levels were determined in LPV/r treated *vs* untreated cells at 24h and 48h.

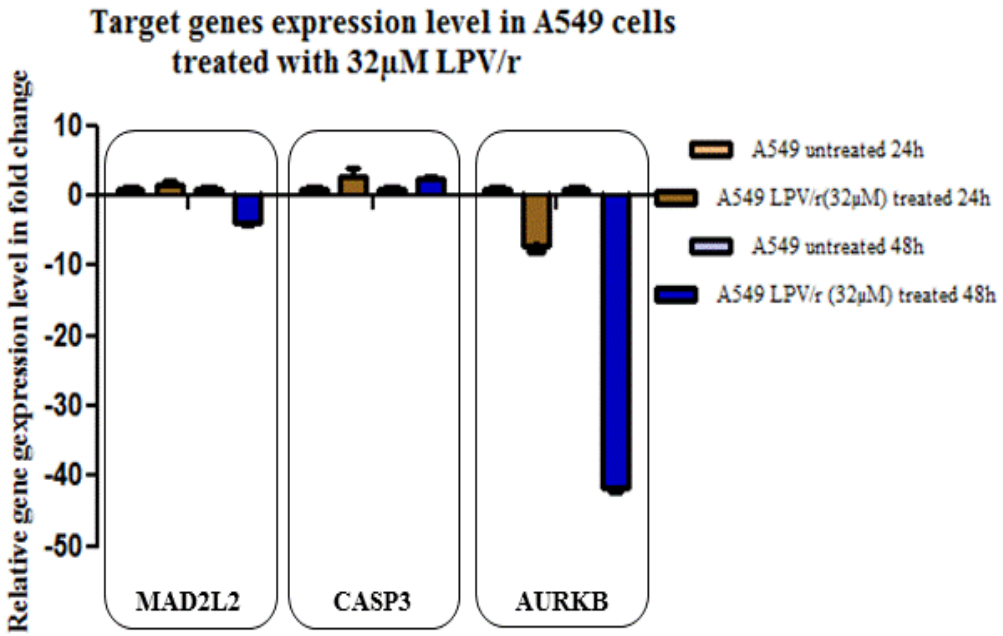

Figure C6.14: Target gene expression level in fold change in LPV/r treated A549 cells. MAD2L2, CASP3 and AURKB gene expression levels were determined in LPV/r treated *vs* untreated cells at 24h and 48h.

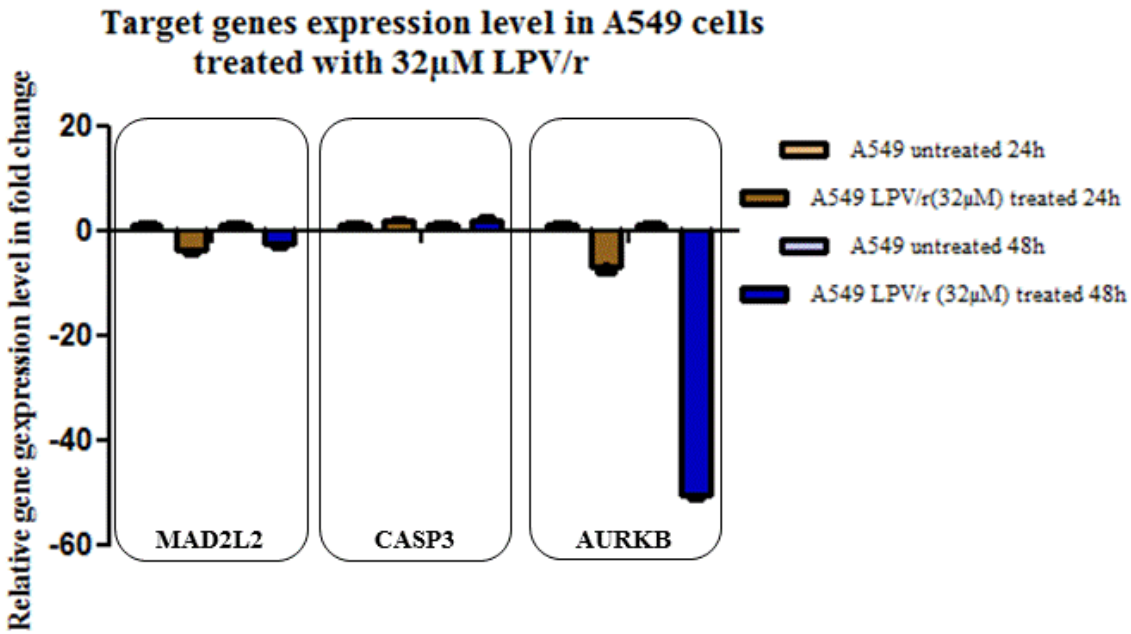

Figure C6.15: Target gene expression level in fold change in LPV/r treated A549 cells. MAD2L2, CASP3 and AURKB gene expression levels were determined in LPV/r treated *vs* untreated cells at 24h and 48h.

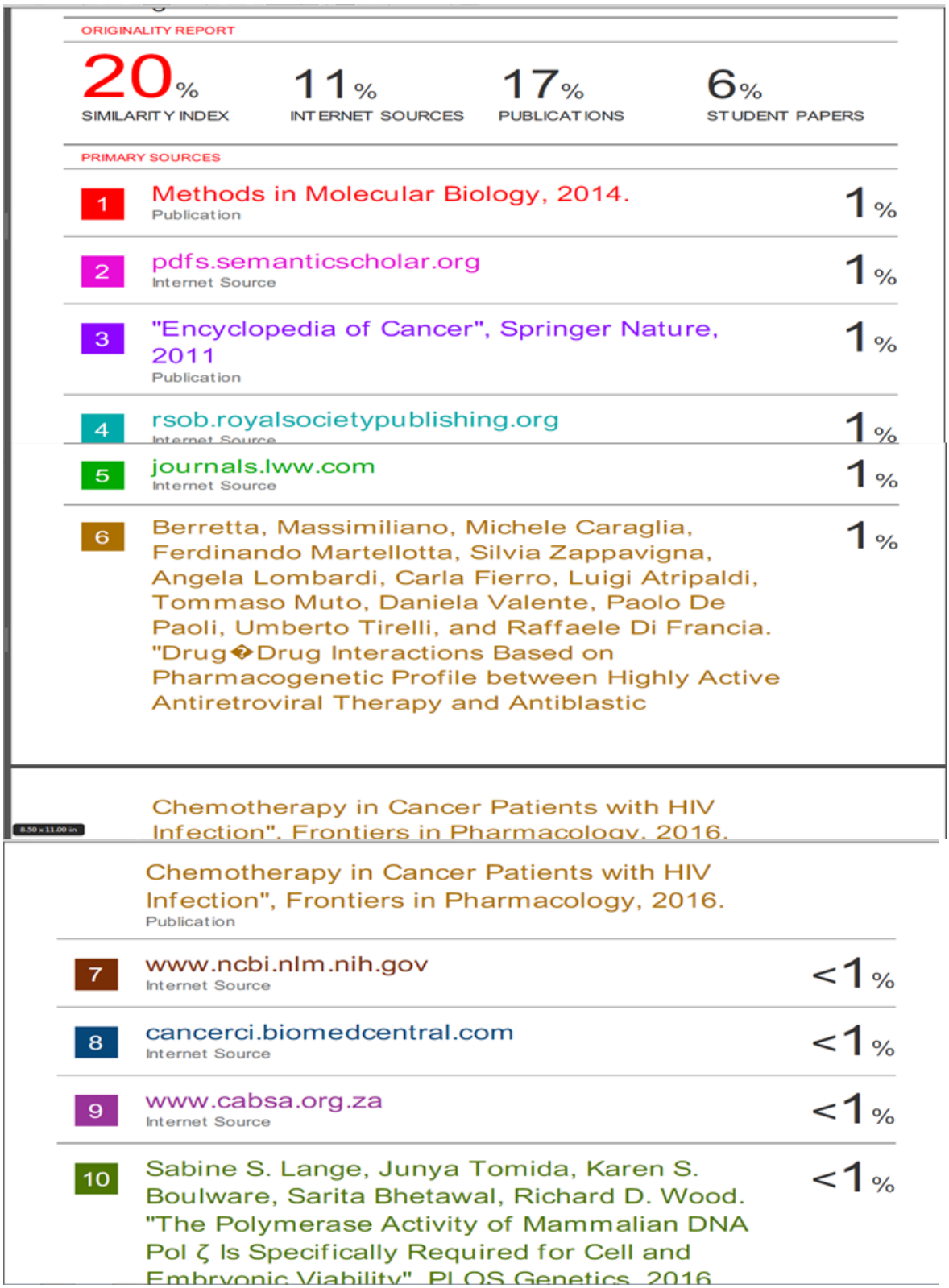

ORIGINALITY REPORT

20%	11%	17%	6%
SIMILARITY INDEX	INTERNET SOURCES	PUBLICATIONS	STUDENT PAPERS

PRIMARY SOURCES

1	Methods in Molecular Biology, 2014. Publication	1%
2	pdfs.semanticscholar.org Internet Source	1%
3	"Encyclopedia of Cancer", Springer Nature, 2011 Publication	1%
4	rsob.royalsocietypublishing.org Internet Source	1%
5	journals.lww.com Internet Source	1%
6	Berretta, Massimiliano, Michele Caraglia, Ferdinando Martellotta, Silvia Zappavigna, Angela Lombardi, Carla Fierro, Luigi Atripaldi, Tommaso Muto, Daniela Valente, Paolo De Paoli, Umberto Tirelli, and Raffaele Di Francia. "Drug–Drug Interactions Based on Pharmacogenetic Profile between Highly Active Antiretroviral Therapy and Antiblastic	1%

Chemotherapy in Cancer Patients with HIV Infection", Frontiers in Pharmacology, 2016.

8.50 x 11.00 in

Chemotherapy in Cancer Patients with HIV Infection", Frontiers in Pharmacology, 2016.
Publication

7	www.ncbi.nlm.nih.gov Internet Source	<1%
8	cancerci.biomedcentral.com Internet Source	<1%
9	www.cabsa.org.za Internet Source	<1%
10	Sabine S. Lange, Junya Tomida, Karen S. Boulware, Sarita Bhetawal, Richard D. Wood. "The Polymerase Activity of Mammalian DNA Pol ζ Is Specifically Required for Cell and Embryonic Viability", PLOS Genetics, 2016	<1%